The Evolution and Geometry of the outer parts of the Small Magellanic Cloud

A Thesis submitted for the degree of *Doctor of Philosophy*

Edinburgh University 1989.

This Thesis is an account of work carried out at the University of Edinburgh between October 1985 and December 1988. It consists entirely of my own work, except where specifically indicated in the text. Some of the results presented in Chapters II, III and IX have been submitted for publication in the *Mon.Not.R.astr.Soc*, under the joint authorship of M.R.S. Hawkins (Papers I and II) and K.Gyldenkerne (Paper I). In addition preliminary results from Chapter IX were presented at the de Vaucouleurs meeting, 'Le Monde des Galaxies' (Paris, April 1988).

Department of Astronomy
University of Edinburgh
Blackford Hill

December 1988.

καί πλατύς επάνου ο ουρανός
γιά νά διαβάζεις μόνος σου
τήν απεραντοσύνη.

Οδυσσέας Ελύτης

Acknowledgements

I very much appreciate the help and support of my supervisors, especially of Dr. M.R.S. Hawkins, also Drs M.T. Brück, R.D. Cannon, M.J. Smyth and R.S. Stobie, to whom I offer my grateful thanks.

I also wish to thank all those who have helped me with useful suggestions and stimulating discussions: S.Beard, P.Brand, K.C.Freeman, K.Gyldenkerne, N.Heyden-Dumpleton, M. & E. Kontizas, H. MacGillivray, D.Morgan, H.Pedersen, N.Ramamani, J.A.Sellwood, M.Shaw, S.Tritton, M.Yates.

I am also most grateful to the U.K. Schmidt Telescope Unit, the COSMOS and STARLINK groups, and the ROE photographic laboratories, for their valuable help, as well as to the staff and astronomers of the 1.5m Danish Telescope at La Silla (Chile) and the Anglo-Australian Telescope (Siding Spring) for their much appreciated collaboration.

My most sincere thanks are also due to Mary Smyth for kindly checking the present manuscript.

Finally, I am indebted to the University of Edinburgh for the award of the 'University of Edinburgh Studentship' during the years 1985-1988, and to the Science and Engineering Research Council for the allocation of travel grants.

Abstract

The purpose of this study is to achieve an improved and more complete understanding of the structure and evolutionary history of the Small Magellanic Cloud, the second nearest galaxy to our own.

The study was focused on the northeastern and west/southwestern outer parts of the SMC, including populations at projected distances larger than 2.2 kpc from the centre of the SMC. These regions have scarcely been studied in detail in the past.

The observational material consisted of good quality B and R photographic plates taken with the U.K. Schmidt Telescope in Australia, digitised by the COSMOS automatic microdensitometer and calibrated by a series of CCD photometric sequences obtained at the European Southern Observatory (with the 1.5m Danish Telescope) and at the Anglo-Australian Observatory (with the 4m Telescope).

Colour-magnitude diagrams were constructed over the whole of the area measured. The analysis of the properties of these diagrams resulted in (a) establishing the population synthesis in the outer parts of the SMC as a function of position with respect to the centre, and (b) probing the geometrical structure (in three dimensions) of these outlying regions of the SMC, which led to the discovery of a significant line-of-sight depth in the NE outer parts.

A study of the carbon star population in the SMC outer regions was also conducted, using UKST prism plates. The carbon stars were used as probes of the intermediate-age populations in the outer parts of the SMC.

TABLE OF CONTENTS

Chapter I: *Introduction and aims of the thesis* ..... 1.

Chapter II: *The CCD photometry* ..... 12.

II.1 The observations ..... 12.

II.2 Reductions of the 1.5m Danish Telescope observations. ..... 17.

II.3 The reduction of the AAT observations ..... 28.

Chapter III: *The photographic photometry* ..... 36.

III.1 The photographic plate material ..... 36.

III.2 The COSMOS measurements ..... 38.

III.3 Pairing and calibration of the plates ..... 44.

III.4 Discussion and Conclusions ..... 46.

.1 Accuracy of the derived magnitudes ..... 46.

.2 Completeness of the sample ..... 50.

.3 Field effects ..... 55.

.4 Conclusions ..... 59.

Chapter IV: *Construction of the CMDs* ..... 60.

IV.1 Introduction ..... 60.

IV.2 Back/foreground removal ..... 69.

IV.3 The colour-magnitude diagrams ..... 73.

IV.4 The distance modulus ..... 75.

IV.5 Reddening ..... 77.

Chapter V: *The metal abundance* ..... 84.

V.1 Introduction ..... 84.

V.2 The metal abundance of the SMC: a review ..... 85.

V.3 Methods of metallicity determination from CMDs ..... 88.

V.4 Metal abundance in the SMC outer regions ..... 93.

V.5 Discussion of the metallicity of the SMC outlying regions ..... 100.

Chapter VI: *The age distribution* ..... 106.
VI.1 Introduction ..... 106.
VI.2 The main sequence stars ..... 106.
.1 Main sequence chronology ..... 106.
.2 The ms luminosity function ..... 112.
.3 Radial distribution of stellar populations younger than 1-2 Gyr .. 114.
VI.3 The clump/horizontal branch ..... 124.
.1 The core helium burning stars ..... 124.
.2 The clump/HB in the outer regions of the SMC ..... 127.
.3 The radial distribution ..... 129.
.4 Age distribution from the clump/HB properties ..... 134.
VI.4 The subgiant branch ..... 145.
VI.5 The absence of blue horizontal branch stars in the SMC 'halo' ... 146.

Chapter VII: *Carbon Stars* ..... 148.
VII.1 Introduction ..... 148.
VII.2 The significance of CS as age indicators ..... 149.
VII.3 Field carbon stars in the outer parts of the SMC ..... 150.
VII.4 The radial distribution and LF of the CS ..... 159.

Chapter VIII: *Discussion of the stellar content and evolution of the SMC outer regions* ..... 165.
VIII.1 Outline of the conclusions on the stellar content of the SMC outer regions ..... 165.
VIII.2 Population synthesis: comparison with previous studies ..... 166.
VIII.3 The chemical evolution of the SMC ..... 171.
.1 The age-matallicity relation ..... 171.
.2 Modelling the AMR in the SMC ..... 174.
.3 Conclusions ..... 179.
VIII.4 The 'disk' and 'halo' components in the SMC outer regions .... 180.

Chapter IX: *Geometry of the SMC outer regions* ..... 182.
IX.1 Introduction ..... 182.
IX.2 The method ..... 183.
IX.3 The results ..... 186.
.1 The mean clump magnitude ..... 186.
.2 The clump size ..... 191.
IX.4 Discussion ..... 197.
.1 Interpretation of the observations ..... 197.
.2 The morphology of the tidally disrupted NE area of the SMC .... 200.
IX.5 Summary and conclusions ..... 204.

Chapter X: *General Conclusions* ..... 207.

Appendix A: *Colour-magnitude diagrams* (Figures) ..... 209.

Appendix B: *Carbon stars* (lists and finding charts) ..... 229.

List of References ..... 241.

CHAPTER I : INTRODUCTION AND AIMS OF THE THESIS

At the beginning of the twentieth century, astronomical interest in the Magellanic Clouds was stimulated by the discovery of a large number of cepheid variables in the Small Magellanic Cloud (SMC) by Mrs. Leavitt (1908). Harlow Shapley was one of the principal cosmographers of the Magellanic Clouds in the first part of the century and lay the foundations of the research in the Clouds in subsequent years.

'The Magellanic Clouds, because of their proximity, offer exceptional opportunities for detailed studies of nebulae as stellar systems.' (E. Hubble 1936).

'The Magellanic Clouds are a Gateway to the Sidereal Universe' (H. Shapley 1956).

'The Magellanic Clouds are like a well-stocked laboratory for the study of star birth and evolution.' (B.J. Bok 1966)

The study of the SMC is of particular interest to the present day astronomer, as it was eighty years ago, mainly because of two important characteristics, besides its proximity:

(i) *It is the archetype of Magellanic irregular galaxies (IBm).* As described by Hubble (1926) such galaxies 'lack both dominating nuclei and rotational symmetry'. According to de Vaucouleurs (1959), irregular galaxies are 'normal disk-like systems', a statement which still holds today (e.g. Gallagher & Hunter 1984; Hunter & Gallagher 1986). Irregular galaxies are thus defined by their lack of organised optical structure (de Vaucouleurs & Freeman 1972) and they are apparently less evolved (high gas-to-total mass fraction and moderately low metallicities) than most spiral galaxies. Therefore, they provide a different sort of system in which to study the processes of galaxy evolution. Although the organisation of star formation (SF) in irregular galaxies is still an open question, it has become clear that *local* processes play an extremely important role in their evolution.

(ii) *It is a member of a dynamically interacting system of galaxies.* The SMC is the less massive –and hence presumably the most severely affected– member of the triple interacting system consisting of our Galaxy and the two Magellanic Clouds. Kerr (1965;

1971) was one of the first to point out the significance of this interaction. He suggested that 'the Large Magellanic Cloud (LMC) and the SMC should be regarded as forming one system' and that they 'may be separating' from each other at the present time. He also considered the probable distortion of the thin central gaseous equatorial disk of our Galaxy by the Magellanic Cloud tidal effects. However, as Bok emphasized in his 1966 review, the tidal effects of the Galaxy upon the Magellanic Clouds should also be considered. This aspect has been the subject of ardent debate during the past decade.

In principle, the study of the stellar content and geometry of the SMC can provide us with clues about the effect of the tidal interaction with the LMC and the Galaxy on the gas and star dynamics, and the subsequent effect on the evolutionary history of the SMC.

The structure of the SMC

It has been suggested that the complex kinematical behaviour of neutral hydrogen (HI) and associated young objects in the SMC is caused by the tidal field of the Large Magellanic Cloud (LMC) (e.g. Songaila *et al.* 1986). In a series of recent papers Mathewson and his collaborators (1984; 1986; 1988) have claimed that the SMC is in the process of 'irreversible disintegration' (see also Chapter IX), due to a recent close encounter with the LMC. The Magellanic Stream, a narrow band of HI gas extending along a great circle from the Magellanic Clouds past the South Galactic Pole approaching the Galaxy (Wannier & Wrixon 1972), is thought to consist of material drawn from the SMC by the LMC and then extended by the tidal effect of the Galaxy (Fujimoto & Murai 1984; Murai & Fujimoto 1986). The relative positions of the Galaxy, the Magellanic Clouds and the Magellanic Stream are shown in Fig.1, along with the Magellanic Clouds orbits favoured by the Murai and Fujimoto models.

A problem thought to be related to the complex geometry of the SMC resulting from these interactions, is the great controversy regarding the distance modulus of the SMC, the latter being of particular importance for the calibration of the distance scale. This question will be addressed in Chapters IV and IX.

The complicated structure of the SMC was interpreted by de Vaucouleurs & Freeman (1972) as showing spiral features, emerging from one end of the asymmetrical Bar

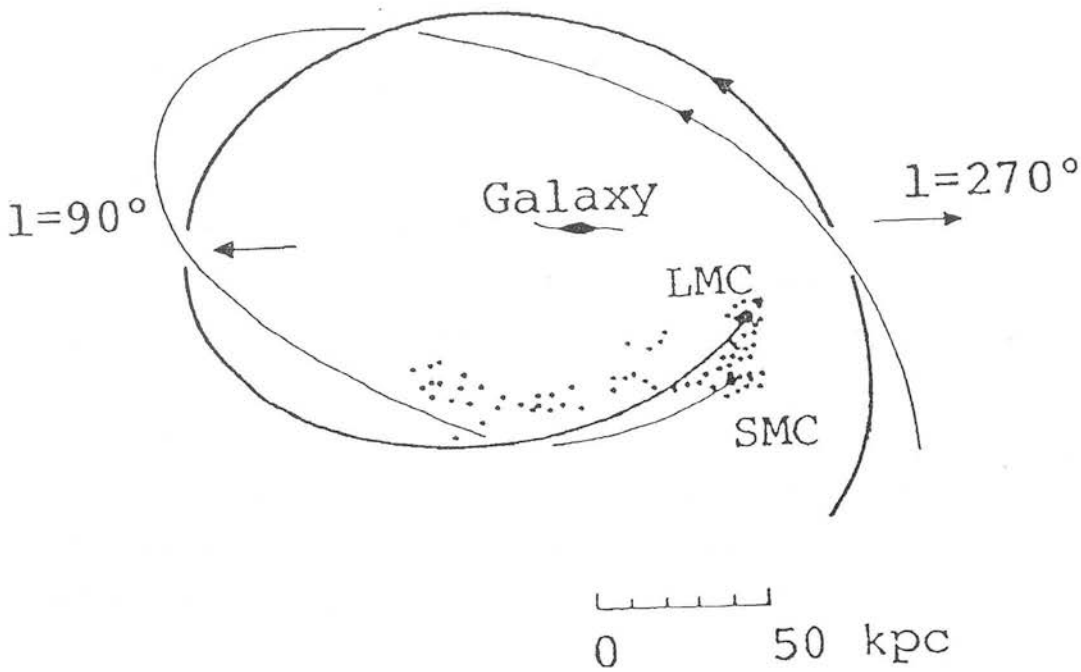

Figure 1: The relative positions in the sky of the Galaxy, the Magellanic Clouds and the Magellanic Stream. The orbits suggested by Fujimoto and Murai (1984) are superimposed.

(Fig.2a). Brück (1982) proposed a similar though simpler classification of the SMC main features, based on their stellar content (Fig.2b). Several years ago Johnson (1961) interpreted the optical and radio observations of the SMC as showing an elliptical component, like a Fornax-type dwarf galaxy, a view adopted again by Brück (1980) for the old population.

The population synthesis of the SMC

'The Magellanic Clouds must be regarded as mixtures of stellar population types' (Thackeray 1958). Nowadays, it is known that the SMC includes objects covering a wide range of ages from more than 10 billion years ago to the present time. It is not however clear that the stellar content of the SMC can be broken up into well-defined 'groups' or distinct populations. In our Galaxy (and in spirals in general) the division between different types of population (Pop.I and II) coincides with a kinematical and spatial distinction (disk and halo, respectively). In the SMC no such well-defined divisions have been established: it is not obvious that there is a kinematic equivalent of the galactic halo, or that objects of demonstrably different ages display strong differences in spatial distribution. In other words stars of different ages seem to be well-mixed spatially and kinematically (Aaronson 1986), with the exception of the clumpy distribution of the youngest stars (which is expected, given the sporadic nature of the star formation processes in such a low mass galaxy). The division that is adopted in the following review of the SMC stellar content is only for convenience and no presumptions are made at this stage regarding the continuity or rate of evolution in the SMC.

(i) The older stars are represented by the RR-Lyrae variables (Graham 1975; 1984) and two old populous star clusters, Lindsay 1 ($\tau \simeq 10^{10}$ yr) and NGC121 ($\tau \simeq 12 \times 10^9$ yr). As was extensively discussed by Stryker and her collaborators (1985) and Olszewski *et al.* (1987), the RR-Lyrae variables can be as young as 10-12 Gyr and their mere existence in the SMC does not necessarily indicate ages of the order of those of galactic globular clusters (14-16 Gyr). On the basis of the number density of RR-Lyraes in the SMC general field, Frogel (1984) estimated that the old metal-poor population accounts for approximately 6% of the total mass of the SMC (which is comparable to the ratio of spheroidal to disk mass in our Galaxy within the solar circle). However, it is only during the past three years that a handful of deep colour-magnitude diagrams of field

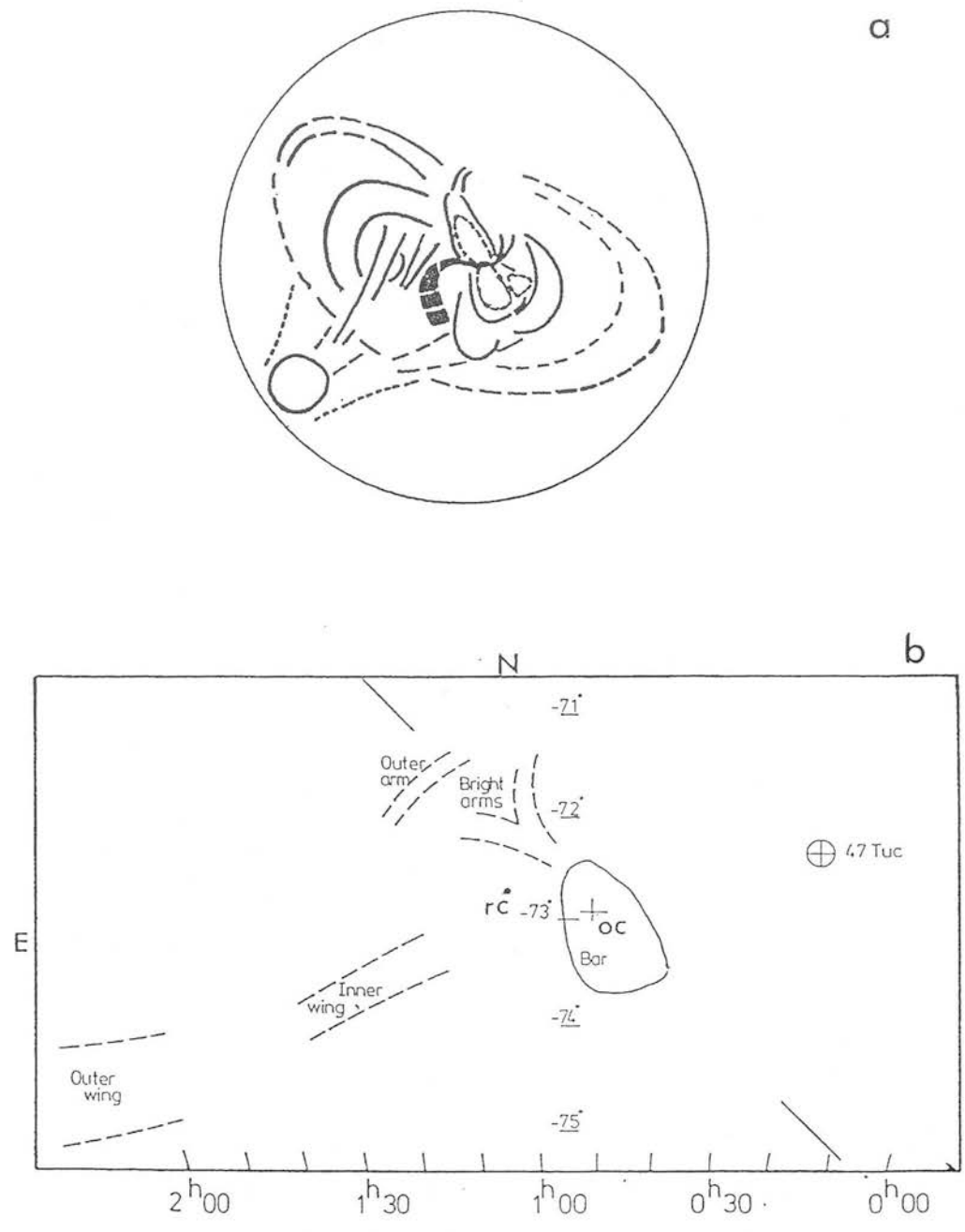

Figure 2: the structure of the SMC according to (a) de Vaucouleurs & Freeman (1972) and (b) Brück (1982). The position of the major axis is taken from the former study. **OC** marks the position of the optical centre of the SMC and **DC** the dynamical (rotational) centre.

stars in the SMC have become available, thus permitting a more detailed study of the SMC older populations. These CMDs reach faint enough magnitudes for the main sequence turnoff region of a 10-12 Gyr old population to be detected and suggest that there is a significant contribution to the stellar content of the SMC from stars in this age-range, although a deep luminosity function study is required to put this conclusion on a quantitative basis. Interestingly, no trace of a blue horizontal branch has been found in the SMC and the horizontal branch has the 'short, red' morphology, thought to characterise an old disk population rather than a halo population, in the sense that these terms are used in our Galaxy.

The distribution of the old population in the SMC does not seem to display any strong central concentration (Graham 1975; 1984) and appears to belong to a flattened rather than a spheroidal system, according to the study of Frogel (1984). Brück (1980,1982), on the other hand, has indicated that the older stars have a more extended distribution than the younger ones –reviewed in the next two paragraphs– and that a purely exponential disk could not account for the observed star-count profiles. As she pointed out the older stars in the SMC do not necessarily form a 'corona-like' three-dimensional structure.

(ii) The intermediate age population (between 2 and 8 Gyr). It was believed –till a few years ago– that the dominating field population of red giants in the SMC was formed during this period (Butcher 1977; Brück 1982), along with the majority of globular-like clusters (e.g. Westerlund & Danziger 1985), as well as the numerous carbon stars (Blanco & McCarthy 1983). This picture of a 'young' galaxy has been extensively challenged recently, by the deep CMD referred to in the previous paragraph. Brück (1982) described this population as an 'old disk', giving to the term 'disk' an evolutionary rather than a geometrical sense.

(iii) The young populations include blue and red supergiants and stellar associations ($\leq 5 \times 10^7$ yr) inhabiting the 'Bar', 'Arms' and 'Wing' (see Fig. 2), and an older group (of the order of a few 10^8 yr or less) exemplified by cepheid variables and blue globular clusters, found in the 'outer Arm', 'outer Wing' and 'Bridge' (Fig.2b; Brück 1982; Stryker 1984).

The discovery of protostars in the SMC (e.g. Gatley, Hyland & Jones 1982) shows that there is a current mode of star formation in the SMC.

It is worth recalling here Bok's (1965) concluding remark in his classic review of the astronomical knowledge on the SMC gathered in the first half of the century: 'In all likelihood Population II stars determine the gravitational and rotational properties of the SMC, and the spectacular Population I component represents only the frosting on a beautiful cake'.

The evolution of the SMC

Has the star formation history of the SMC been continuous, possibly with small variations in time, or has it proceeded 'violently' in global bursts? This vital question –which is connected both with the low mass of the SMC and with its interaction with the LMC and the Galaxy– has not yet been satisfactorily answered. One of the main qualitative arguments in favour of the 'global burst' hypothesis is the apparent existence of distinctive age groups in the SMC, with the formation of each group having started apparently simultaneously all over the SMC (Westerlund & Danziger 1985). According to Westerlund & Danziger, any evolution controlled by density waves (as in spiral galaxies) or by stochastic SF processes (as in low mass disk galaxies), should have moved around in a more-or-less systematic way, not have started everywhere at the same time. They thus concluded that one or more major (global) SF bursts must have taken place during the history of the SMC, and they attributed these tentative global SF events to the influence of external forces namely the dynamical interaction of the SMC with the LMC and the Galaxy.

This argument, although attractive at first sight, suffers from a serious hiatus: other Magellanic-type irregulars, which are *isolated*, show evidence of similar population synthesis to the SMC (see Hunter & Gallagher 1986). Consequently, the explanation must be sought in the way in which SF is organised within low mass galaxies, rather than in external factors. Moreover, it is not yet proved observationally that there *are* distinct populations in the SMC, i.e. that there have been discrete SF events followed by periods of reduced SF activity. In addition, Westerlund's argument essentially depends on the timescale with which stochastic SF propagates across the galaxy. This timescale may well be much smaller (see e.g. Hunter & Gallagher 1986) than the age of the intermediate and old populations, which therefore would appear to have formed 'simultaneously' all over the SMC. Note that the youngest populations show a rather clumpy distribution, as previously mentioned, indicating local bursts of SF. Some aspects of these

problems will be addressed in Chapter VIII.

Other arguments in favour of global discontinuities in the star formation rate in the SMC have been proposed in the past:

• Untill very recently, the large number of carbon stars discovered in the SMC (Blanco, McCarthy & Blanco 1980; Blanco & McCarthy 1983) was interpreted as the result of a major global star formation event in the SMC a few Gyrs ago (which is roughly the age of the carbon stars). Recent progress in the theoretical understanding of the formation of carbon stars explains the numbers of carbon stars in the SMC without invoking an increase in the star formation rate in the past (Mould 1986; see Chapter VII).

• The age distribution of star clusters seems to peak at intermediate ages and was also interpreted as favouring the hypothesis of a major star formation burst a few Gyr ago (review by Westerlund & Danziger 1985), although the observational evidence was characterised as *weak* by van den Bergh (1984). In principle the age distribution of star clusters is an excellent guide to the star formation history of a system. In practice, however, the interpretation of such a distribution is complicated by a number of largely unknown factors: i.e. the rate and conditions of formation and the processes and rate of destruction of clusters in the SMC (and in Magellanic Irregulars in general; see Bhatia & Hatzidimitriou (1988) and Hatzidimitriou & Bhatia (1988) for an aspect of the complexity of the problem) as well as the luminosity function of clusters. Therefore, it can be misleading to apply conclusions from the age distribution of star clusters to the populations of the general field.

• The age–metallicity relation in the SMC, which will be discussed extensively in Chapter VIII, possibly indicates an enhancement of the SF rate a few Gyr ago. However, it will be seen that this interpretation of the phenomenon is by no means unique.

• From a study of global properties of the SMC, Rocca-Volmerange and her collaborators (1981; also Lequeux 1984) concluded that star formation in the SMC has been continuous, probably with a slightly decreasing rate in the past. This does not exclude local bursts, or small amplitude and small duration variations of the SFR. It must be emphasised that they based their conclusion on the assumption that the simple 'close-box' evolution is applicable for the SMC, which is not confirmed by the observations

(see Chapter VIII).

Dopita (1985) inferred –from the present day heavy element abundance and abundance ratios in the SMC– that a continuous SF rather than a violent early star burst, followed by a period of less violent and continuous SF, characterises the Magellanic Clouds. Dennefeld & Tammann (1980), as well as Kennicutt & Hodge (1986) concluded that the current SF rate in the SMC is higher than the average past rate, but this effect can be attributed to localised bursts of star formation activity. From the above short review it is obvious that a great deal of work needs to be done regarding the evolution of the SMC.

The aims and content of the present study

The great majority of detailed studies related to the analysis of the stellar content and geometry of the SMC have been limited to the 'main body' of the SMC including areas where relatively recent star formation has taken place. As was previously mentioned the star clusters of the SMC have been used as a tool for investigating the evolution of the SMC. Due to the uncertainties inherent in this method (see previous paragraph), we turn to the study of the stellar content of the general *field* in the SMC, which is technically a more difficult task, since the interpretation of the properties of a not *a priori* known mixture of generations of stars is far from trivial. It is not therefore surprising that very few detailed studies of the stellar content in the SMC general field exist to date. In a series of relatively recent publications (Brück & Marsoglu 1978; Hawkins & Brück 1982; Hawkins & Brück 1984; Brück *et al.* 1985) the stellar content of the SMC outer regions ('halo') was investigated on the basis of colour-magnitude diagrams, and with a limiting visual magnitude of 21. More recently, a number of studies of SMC clusters lying in the SMC periphery were conducted by various authors using deep CCD imaging. In most cases nearby SMC fields were also observed (see Chapter VIII for details). All the existing CMDs cover on the whole less than one square degree of the SMC periphery and are mostly within 2-2.5 kpc from the SMC centre, while the SMC 'halo' as defined by Brück (1982) extends over as many as 90 square degrees on the sky and to distances $\sim$ 5-6 kpc from the SMC centre.

In the present study, a total area of 48.5 square degrees was scanned in B and R using good quality UK-Schmidt telescope photographic plates, measured with the COS-

MOS automatic microdensitometer and calibrated using CCD photometric sequences obtained during two observing runs.

The *ESO/SERC* survey Fields 28 (centred on 0^h00^m, $-75^o00'$ (1950)) and 52 (centred on 1^h44^m, $-70^o00'$ (1950)) were selected for the study. The selection of these fields was determined by two factors: Firstly, they are symmetrically situated along the main body major axis of the SMC (de Vaucouleurs & Freeman, 1972) towards the SW and NE respectively (Fig.2). Secondly, they are suitable for application of automated methods of plate measurement, owing to the lack of extended overdense regions and of large numbers of star clusters in them. Moreover, Field 52 does not include the 'Wing' which complicates additionally the picture in the southeastern areas.

Colour–magnitude diagrams were constructed over the whole of the scanned area reaching the tidal limit of the SMC, with a limiting magnitude of $B = 21^m.5$. The analysis of these CMD has the purpose of:

• improving by a factor of 50 the areal coverage of the SMC's outer regions achieved by the previous CMD studies;

• studying the contribution of different generations of stars to the stellar content of the SMC periphery and the positional change of their mixture, thus improving our insight into the evolutionary processes in the SMC in these largely unresearched areas;

• examining the spatial distribution of the SMC stars in the outer regions, with the two-fold aim of: (i) determining the *depth* and *inclination* of the SMC
(ii) investigating the probable influence of the LMC on the shape of these outer regions of the SMC.

In Chapter II, the CCD observations obtained are presented.

In Chapter III, the photographic photometry over the 48.5 square degrees of the sky is described and the accuracy of the resulting data-set evaluated.

In Chapter IV, the CMDs are presented and the basic distance modulus and reddening scales –necessary for their interpretation– discussed.

In Chapter V, the metal abundance range in the outer regions of the SMC is derived, on the basis of these CMDs, and the metallicity gradient in the SMC periphery examined.

In Chapter VI, the age range of the populations present in the SMC field is examined

quantitatively and their relative contribution as a function of distance from the SMC central part analysed.

In Chapter VII, the carbon star population in these outer regions of the SMC is examined.

In Chapter VIII, the conclusions from the study of the stellar content of the SMC peripheral regions are summarised and their implications for the history of the SMC evolution discussed.

In Chapter IX, the three-dimensional distribution of the SMC stars in the outer regions studied is presented and the possible effect on it of the dynamical interaction with the LMC discussed.

Finally, in Chapter X, the conclusions of the study are summarised and some directions for future work outlined.

1 The observations

The CCD observations were obtained during the nights of the 26, 27/10 and 1/11/1986 using the ESO-CCD camera mounted on the 1.5m Danish telescope at La Silla, Chile. This camera employs an RCA CID53612 chip which is a thinned, buried channel, back-side-illuminated device (Pedersen 1985). Its active area consists of 320 by 512 pixels, with a pixel size of 30 microns, which corresponds to 0.47 arcsec on the sky, at the Cassegrain focus of the telescope. The characteristics of the CCD used are summarised in Table 1 (information from the ESO Technical Report on the La Silla CCD detectors, June 1986). All CCD frames were observed in the B and R wavebands and some in V as well, using Johnson B, V and Gunn R filters.

In order to ensure a satisfactory coverage of magnitudes and to be able to detect sensitivity variations on the *UKST* photographic plates (see Chapter III), a number of CCD frames were obtained at several positions on each of the *ESO/SERC* survey Fields 28 and 52; 7 on the former and 6 on the latter. In each case three of them were short exposures of regions with brighter stars, while the rest were longer exposures of regions with acceptably good distributions of fainter stars (down to a B magnitude of 21.5). The distribution of the positions of the CCD frames on the photographic plates is indicated in Fig.1. Table 2 contains a compilation of the observational details.

For the definition of the zero point of the CCD frames, a series of short exposures of *BVR* photoelectric standard stars in E-regions 1 and 2 (Graham 1982) and in the LMC/SMC general field (Menzies *et al.* 1980) were obtained (Table 3). Some of the standards were observed several times each night, as a monitor of the stability of the photometric conditions during the observing run. Calibration exposures were also taken each night, comprising bias frames and flat fields (see section 2) All three nights were photometric with seeing between 1 and 1.5 arcsec.

An additional region was observed in Field 52 with the 4m Anglo-Australian

Type: RCA SID 53612

Serial Number: J 587BT-21B

Format: 512 × 320 pixels

Image size: 15.6 × 9.8 mm

Conversion factor: 17 electrons/ADU at gain 50

Noise level: 70 electrons at gain 50 (slow readout)

Linearity: saturation limited by AD converter at gain 50 (290,000 electrons).

Full well capacity: 400,000 electrons.

Blemishes: three hot areas, one hot column. The output amplifier produces light affecting the lower left corner of the CCD.

Dark current: 120 electrons/pixel/hour at 150K.

Cosmic Rays: Low sensitivity to cosmic rays.

Charge transfer: 150–200 ADU of preflash needed.

Relative quantum efficiency: 65% at 7000 Å.

Table 1: The characteristics of the CCD chip used for the observations with the 1.5m Telescope.

Name	RA (1950)			DEC (1950)			Filter	T (sec)	χ
F52R4	01	22	50	−71	32	09	B	300	1.574
							R	120	1.615
F52R1	01	25	23	−71	03	12	B	1200	1.588
							R	900	1.538
F52R5	01	25	39	−71	08	20	B	120	1.655
							R	60	1.667
F52R2	01	46	02	−70	20	49	B	120	1.322
							R	60	1.322
F52R6	01	46	38	−70	15	16	B	1800	1.342
							R	900	1.329
F52R3	01	57	14	−68	22	30	B	900	1.321
							R	900	1.344
F52R7	01	57	36	−68	20	47	B	120	1.374
							R	60	1.367
F28R1	00	20	18	−75	22	16	B	1200	1.441
							R	900	1.449
F28R5	00	21	50	−75	21	52	B	300	1.483
							R	60	1.475

Table 2: The CCD observations.

Column 1: The first three characters of the identification of each frame is the number of the ESO/SERC survey field in which it is located. The last number corresponds to the numbering in Fig.1.

Column 5 gives the integration time in seconds for each frame.

Column 6 gives the airmass through which the frames were observed.

Name	RA (1950)			DEC (1950)			Filter	T (sec)	χ
F28R2	00	30	03	−72	48	21	B	120	1.631
							R	60	1.644
F28R6	00	30	34	−72	51	10	B	1200	1.555
							R	900	1.515
F28R3	23	41	00	−75	55	00	B	900	1.507
							R	900	1.526
F28R4	23	44	29	−72	49	31	B	120	1.600
							R	60	1.609
F28R7	23	45	01	−72	46	08	B	1800	1.517
							R	600	1.561

Table 2: continued.

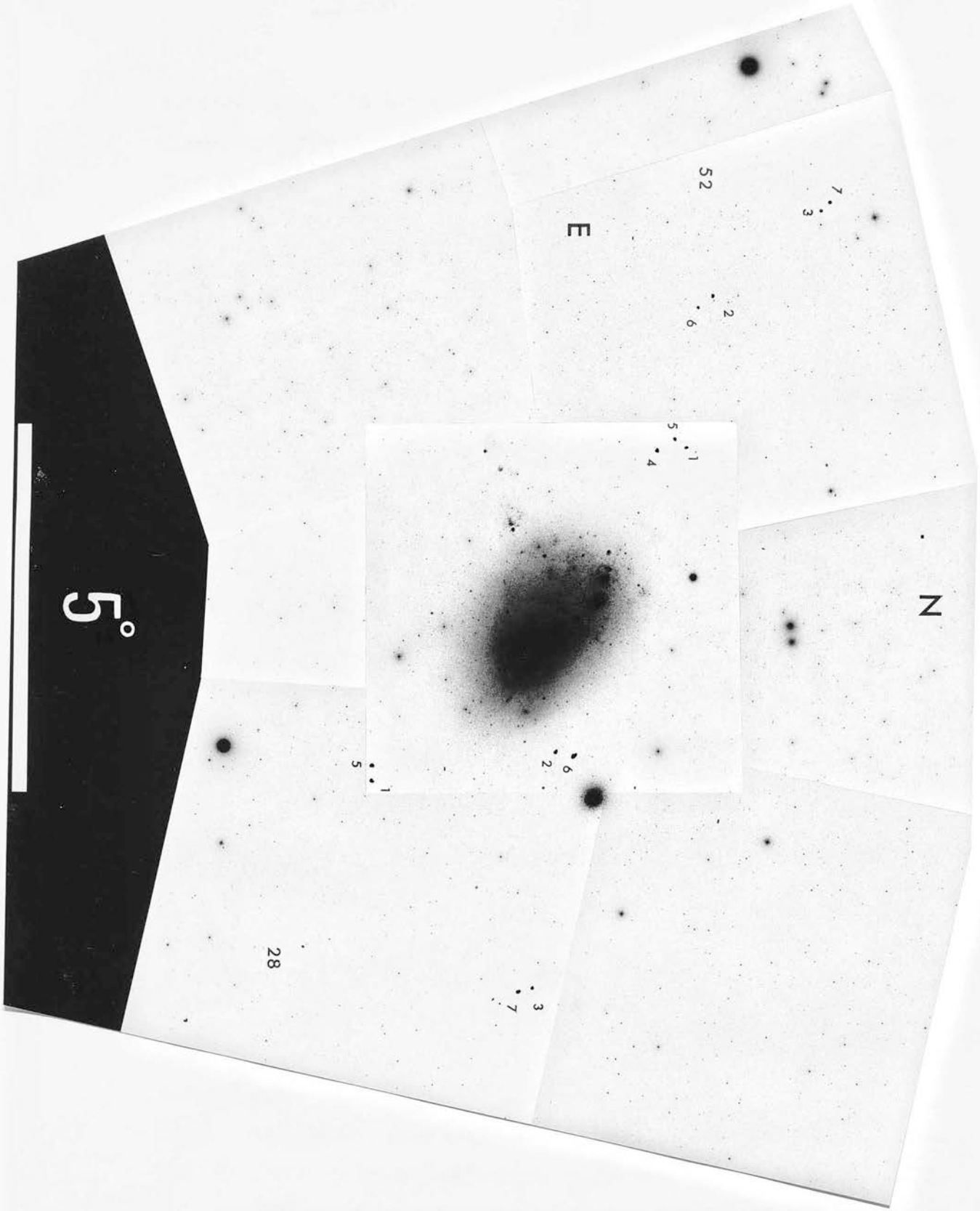

Figure 1: The location of the CCD frames with respect to the central part of the SMC.

Telescope during CCD service imaging on the night of the 31/1/1987, using a newly commissioned lower readout noise RCA chip (AAO RCA *5, type SID501ES) at prime focus (Robertson & Stathakis 1987; Robertson 1987). The CCD format was again 320 columns by 512 rows and the pixel size 0.5 arcsec. The KPNO B, V and R interference filters were used for the observations. Dome flat fields were obtained through each filter and the 8 standard stars used for the determination of the zero point were taken from Landolt (1983). The night was photometric and the seeing around 1.5 arcsec.

2 Reductions of the 1.5m Danish Telescope observations

The CCD frames were reduced through standard procedures, using the ASPIC package in the STARLINK software collection.

Bias: First of all the readout electronic 'bias level' was subtracted from all frames. The bias level is the offset value added to the signal from the CCD before it is converted to digital values. This permits keeping the zero light level at a positive value and avoiding feeding the A/D converter with negative values. The bias level was determined by taking the so-called bias frames at zero length exposure time and with the shutter closed. There was no appreciable variation of the bias level across the chip, therefore subtraction of a constant mean value, around 200 analogue digital units (ADU), was considered adequate and was extracted from the overscanned columns in each frame.

Flat fields: The sensitivity of the CCD chip is not uniform. The differences from pixel-to-pixel most commonly arise from imperfections introduced during the manufacturing process such as variations in pixel size across the array (Mackay 1986) as well as quantum efficiency changes, i.e. changes in the ratio of output e^- to input photons. These non-uniformities are strongly dependent on the wavelength of the incoming photons; the longer λ ones penetrate more deeply into the silicon substrate and are thence more seriously affected by the non-uniformities. Apart from these effects intrinsic to the CCD, vignetting and distortions within the telescope introduce a curvature to the global sensitivity of the chip. In order to correct for all these sensitivity variations each 'science' exposure is divided by a similar exposure, taken through the *same* imaging optics as the object frame. This is the so-called flat field, and it is taken on a uniformly emitting

No	Star	RA(1980)		DEC(1980)		V	B–V	V–R	Ref.	n
1	6193	1	00.5	−71	39	9.780	0.344	–	1	4
2	6222	1	00.9	−71	39	7.751	1.120	0.581	1	6
3	6997	1	07.5	−73	07	9.098	0.915	0.478	1	19
4	7187	1	09.4	−73	03	7.146	0.078	0.038	1	3
5	8501	1	22.4	−44	47	9.855	0.736	0.402	2	3
6	E218'	4	03.1	−44	31	9.502	0.587	0.328	2	3
7	25842	4	03.2	−44	32	8.478	0.727	0.409	2	3
8	25966	4	04.2	−44	43	8.032	1.608	0.923	2	4
9	32533	4	58.9	−66	14	9.806	0.533	0.305	1	9
10	35183	5	17.5	−68	29	9.153	0.141	0.075	1	9

Table 3: The standard stars used to calibrate the the CCD observations with the 1.5m Danish Telescope.

Column 2: The HD numbers of the standards (for star no.6, the E-region number is given instead).

Column 8: Reference 1: Menzies *et al.* 1980. Errors of the order of 0.005 mag. Reference 2: Graham (1982). Errors of the order of 0.001 mag.

Column 9: Number of observations of each star.

source, for example on the twilight sky, or on a uniformly illuminated section of the inside of the dome, or on a 'blank' patch of the sky. In the present observations the flat fields were obtained by exposing through the various filters on the twilight sky. The 'dome flats' are very easily controllable but often cause an overcorrection to the science frames, due to the large difference of the effective temperature between the night sky and the light inside the dome whether this is scattered sunlight or comes from the tungsten lamps in the dome. The 'blank' flats are better, but require very long exposures to give statistically meaningful results, therefore they are very costly in terms of observing time. The obtained flat fields were well reproducible from night to night and displayed sensitivity variations of a few percent, reaching values as high as 10% for the R filter, as one would expect according to the previous discussion. In each band the available flat fields were bias subtracted, normalised to unity and then coadded to produce the final 'master' B, V and R flats. Subsequently all programme frames were divided by the appropriate flat fields; no considerable residual structure was shown on the resulting corrected science frames. The importance of correct flat-fielding is demonstrated in a succinct discussion by Shaw (1988): Briefly, by effectively removing the pixel non-uniformities, the photon-count errors –which define the absolute lower limit of the accuracy achievable by a CCD– become dominant for a much larger range of signal values than in the raw frames.

The thinning of the CCD chip usually creates variations of the thickness of the silicon substrate, which in turn can cause the formation of *interference fringes* on the frames, for wavelengths of the order of the Si layer thickness (if the wavelength band is contaminated by strong night emission, which is often the case in the red). However, no inteference-fringe structure was apparent on any of the frames, not even on the long-exposure (900s) R frames.

The *dark current* of the CCD is due to thermally created photons within the Si substrate, registered as signals. It was very low across the whole chip (~ 0.002 ADU/sec/pixel) and was not taken into account, since the stellar photometry routines applied a local sky background.

There was excess emission leaking into the bottom of each frame, most noticeable on long exposures. This region, as well as the various cosmetic defects of the chip such as

hot spots and cold columns, was avoided in the reductions.

The cosmic ray events are generally distinguishable from stellar images by their sharper profiles, their images extending over 1-2 pixels only. Their removal was not crucial for the reductions, since –even if some were wrongly identified as stars– the probability of their occurence on the same position in both the B and R exposures, and therefore of their being included in the final catalogue, is minimal. On the other hand, cosmic–ray images were avoided when evaluating the background in the photometry routines.

The calibration of the CCD exposures was accomplished by direct transfers from the standard stars observed (Table 3). The colour equations were taken from the standard ESO-CCD figures:
$B = b + 0.014(B - V)$ and $R = r + 0.047(V - R) + 0.029(B - V)$, where b, r are the instrumental magnitudes. These equations are very stable and more accurate than can be measured without a dedicated colour equation run. However, exposures of programme frames were generally taken only through the B and R filters, while the application of the given colour equations required both $V - R$ and $B - R$ colours. To overcome this problem, a relation between $B - R$ and $V - R$ established from all BVR photoelectric standards in the Graham E-regions was used:

$V - R = (0.358 \pm 0.004).(B - R)$, for $(B - R) < 1.5$ and
$V - R = (0.350 \pm 0.002).(B - R)$, for $(B - R) \geq 1.5$.

The relation was very tight and did not introduce any significant errors to our photometry. It is worth noting that identical transformations can be obtained using model atmospheres (e.g. VandenBergh & Bell 1985; Bell & Gustaffson 1978; see also Chapter V). The colour equations now become:

$$B = b + 0.009(B - R) \quad (1)$$

$$R = r + 0.035(B - R) \quad (2)$$

The observations of the standard stars did not cover a large enough range in zenith distance to allow an independent determination of the extinction coefficients. Therefore the La Silla mean extinction corrections, C_B and C_R for the standard (Johnson) B and

R passbands respectively were applied to bring all the stars to the same airmass:

$C_B = 0.215 - 0.022(B - R)$, and

$C_R = 0.091$.

To reduce the errors introduced by this approximation, all programme frames were observed near the average airmass of the standard stars, therefore any extinction differences are mostly incorporated in the zero point.

The standard stars

As mentioned before, the standard stars were observed with very short exposure times (1 to 3 sec) in order to avoid saturation, which occurs at 16383 ADU, although linearity is already affected above a level of 9000 counts per pixel. The time accuracy of the shutter of the camera for 1 sec exposures was very satisfactory and did not introduce any significant errors (i.e larger than $\sim 0.003^m$) in the resulting magnitudes; this was verified by observing one of the fainter standards with 1, 3, and 5 sec exposures. The charge transfer efficiency of the CCD is less than 100%; there is a threshold charge level below which any input charge to a particular pixel either fails to be detected, or is registered in a completely non-linear fashion. So the exposure time must be long enough for the sky-background level to contribute sufficiently to the recorded flux, to overcome the charge transfer threshold (Jørgensen & Hansen 1983; Walker 1984; Pedersen 1985). As a result, the quality of exposures with low background levels –as is the case with the observations of standard stars– suffers from distortion of the stellar image contours (to the right and upward). For this reason, preflashing is essential for short-exposures, in order to raise the sky background level above the charge transfer threshold. For technical reasons preflashing could not be successfully applied during the observing run. Long enough exposures of the bright standards could only be obtained with significant defocusing of the telescope, a procedure which has proved unsatisfactory in the past, because of serious subsequent problems with the aperture used for the photometry. However, it has been found (e.g. Pedersen 1988, private communication) that defocusing is essential in order to determine the colour equations for a particular CCD, as the few pixels covered by a focused standard star are hardly representative of the whole chip.

The observations of standard stars were reduced with a digital aperture photometry routine APERASP. Each frame was displayed on the ARGS TV monitor and a circular

cursor was used to define the area containing the stellar image and a nearby region of sky. The summed intensities within these areas were then subtracted from each other and a magnitude index (APERMAG) was calculated, normalised to the local sky background intensity. The procedure was repeated several times to achieve a more representative evaluation of the sky contribution. In all cases the aperture was centred so as not to include any other images, or defective pixels. The count-statistics error of the resulting magnitude varies from 0.1 to 1.0 %, depending on the size of the aperture applied and of course the magnitude of the star. Growth curves of this instrumental magnitude APERMAG, versus the aperture size (see Fig.2 for an example) showed that an aperture of 40 pixels in diameter (corresponding to 18.8 arcsec) centred on the stellar image included essentially all of the recorded flux and still produced a stable enough magnitude. However, an aperture of this size would not be practicable for the programme stars, because of their proximity to each other and the essentially lower signal-to-noise ratio. An aperture size of 10 pixels in diameter appeared to be more suitable for the programme frames. The possibility of applying a 10-pixel aperture to the standard stars is now investigated. The images of these stars, as previously mentioned, suffer from charge transfer threshold effect. In order to quantify this effect on the resulting magnitudes, the difference of the instrumental magnitudes derived with aperture sizes 40 and 10 pixels in diameter, was examined for all standard stars and all long-exposure programme stars for which an aperture of size 40 was applicable. The 40-10 aperture corrections in both categories of stellar images are identical, within the errors. Actually, for the 14 short-exposure standard stars,

$$B_{40} - B_{10} = 0.131 \pm 0.008, \tag{3}$$

$$R_{40} - R_{10} = 0.120 \pm 0.005, \tag{4}$$

while for the 5 long-exposure programme stellar images,

$$B_{40} - B_{10} = 0.15 \pm 0.03, \tag{5}$$

$$R_{40} - R_{10} = 0.11 \pm 0.01. \tag{6}$$

Fig.3 shows the resulting correlations between the corrections and the magnitudes for the standard stars. The above analysis demonstrates that even the magnitudes of the faintest of the observed standard stars were hardly affected by the charge transfer inefficiency. Having thus established the correctness of the aperture-10 instrumental

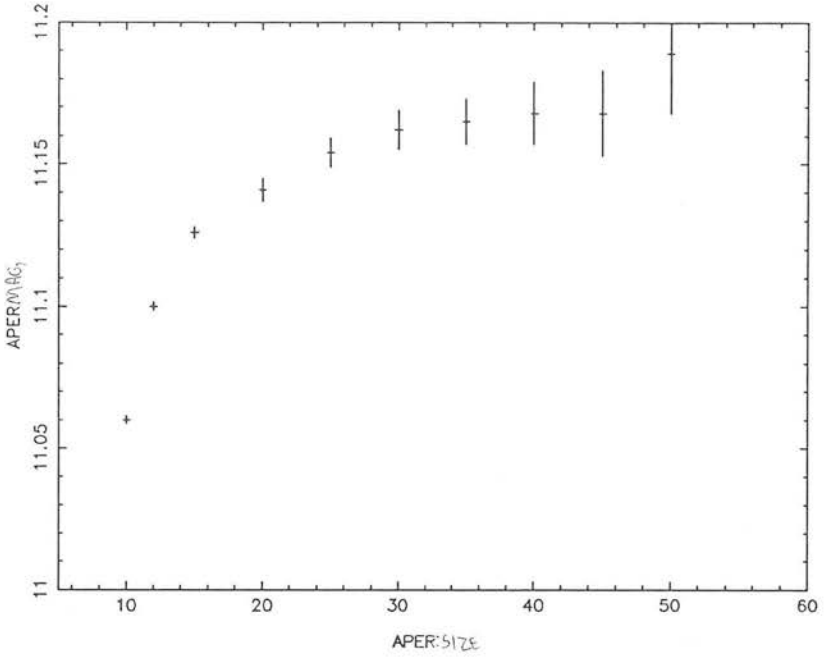

Figure 2: Example of the growth curve for the magnitude (APERMAG) of a standard star. The size of the (circular) aperture is given in pixels.

Fig.3a

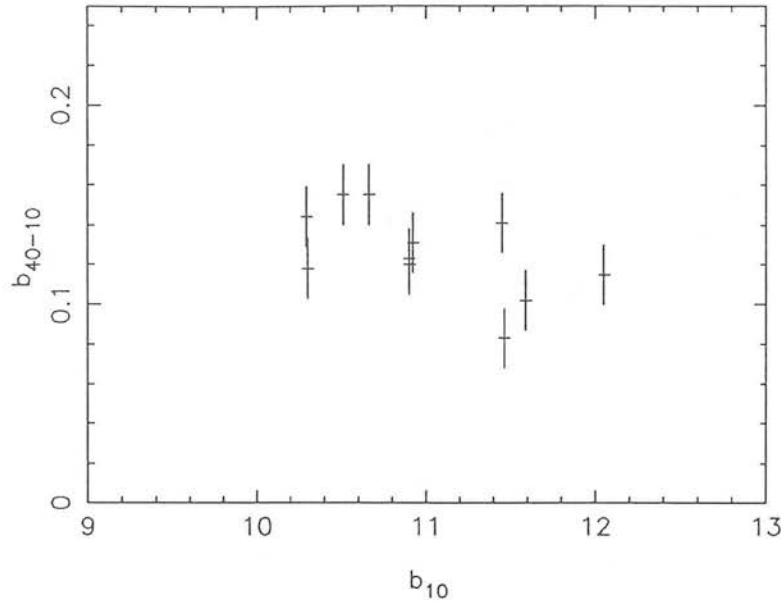

Fig.3b

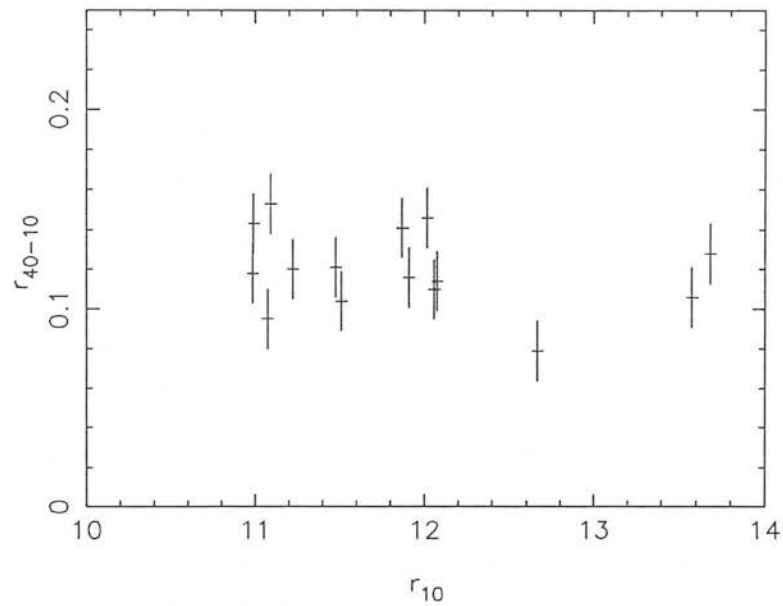

Figure 3: The 40–10 aperture correction versus magnitude for the observations of the standard stars.

magnitudes of the standards, the appropriate colour equations and extinction coefficients were applied in order to zero-point the instrumental photometry by comparison with the photoelectric magnitudes of the same stars. The resulting zero points (terms ZB_1 and ZR_1 in eq (7), (8) below) were determined with an accuracy ± 0.03 in B and ± 0.02 (standard errors) in R. No systematic deviations were noticed for any particular night, which confirms that there was little variation in extinction during each night and from night to night. Fig.4a gives the relation of $B' = B - 0.009(B-R) - 0.215\chi$ versus B_{40} and Fig.4b that of $R' = R - 0.035(B-R) - 0.091\chi$ versus R_{40}.

The programme stars

The stars on the programme frames were reduced using a two dimensional Gaussian profile fitting routine (GAUMAG in the ASPIC package), rather than aperture photometry, which was also applied –as will be discussed later on– to zeropoint the Gauss-fit photometry. Because of the possibility of structural changes of the images across the CCD frame a Gaussian profile with 6 free parameters was chosen, the parameters being the height, base, centre x,y and radii (i.e. the dispersion) R_x,R_y . Briefly, the GAUMAG routine takes a small area of adjustable size around each star (the predefined coordinates are used as initial values for fitting the centre of the Gaussian) and fits a two-dimensional Gaussian function (with background) to estimate its magnitude. The star profile is in the form,

$I = I_o e^{-d^2} + base,$

where $d = [(x/R_x)^2 + (y/R_y)^2]^{1/2}$, and I_o the height of the Gaussian. The output magnitude is given as $GAUMAG = 30 - 2.5log(\pi I_o R_x R_y)$. The size of the half-width of the fitted Gaussian was used as a discriminant between stars and galaxies (Stobie *et al.* 1985) or contaminated images. Stars lying very close to the edge of a frame and high rms fits were also excluded. The internal accuracy of the derived instrumental magnitudes decreases with magnitude, but remains smaller than 0.01^m.

The reason for choosing a fitting routine for the programme stars instead of the aperture photometry used for the reduction of the standard stars is the much better accuracy achievable with a fitting routine for the lower signal-to-noise images. Fig 5 shows the consistency between the two routines (APERMAG and GAUMAG) for the stellar images in the CCD frame F52R1.

Fig.4a

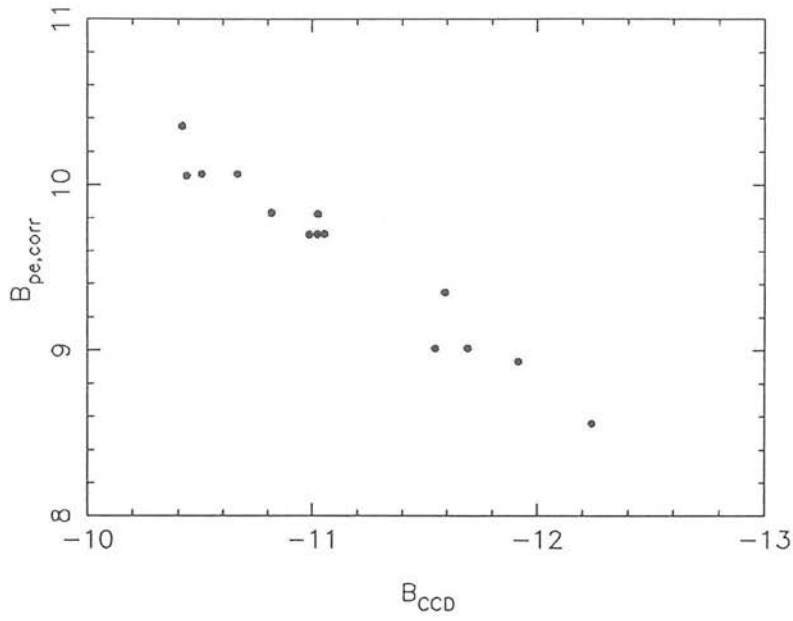

Fig.4b

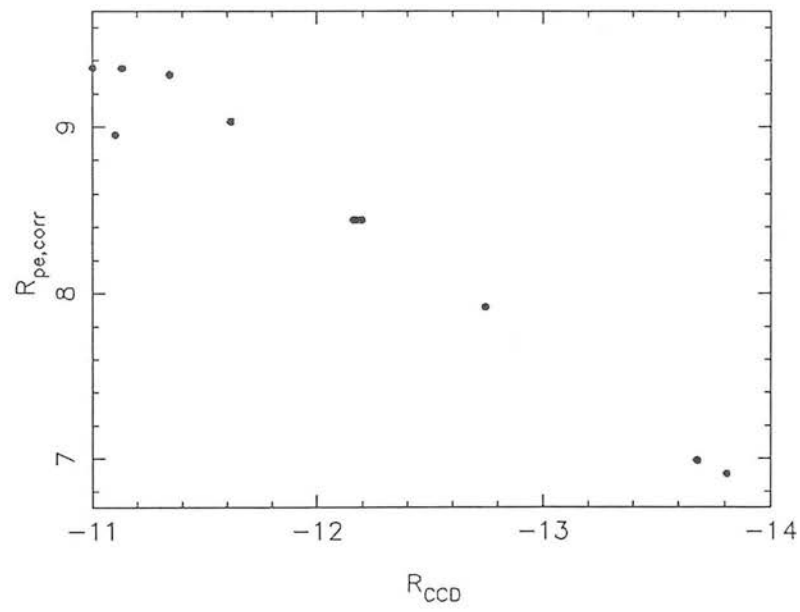

Figure 4: The CCD calibration curves in B (a) and R (b). The instrumental magnitude APERMAG (derived with an aperture of a diameter of 40 pixels) are plotted against the standard magnitudes of the stars, after taking into account the colour equations of the CCD and the difference in zenith distance of each observation.

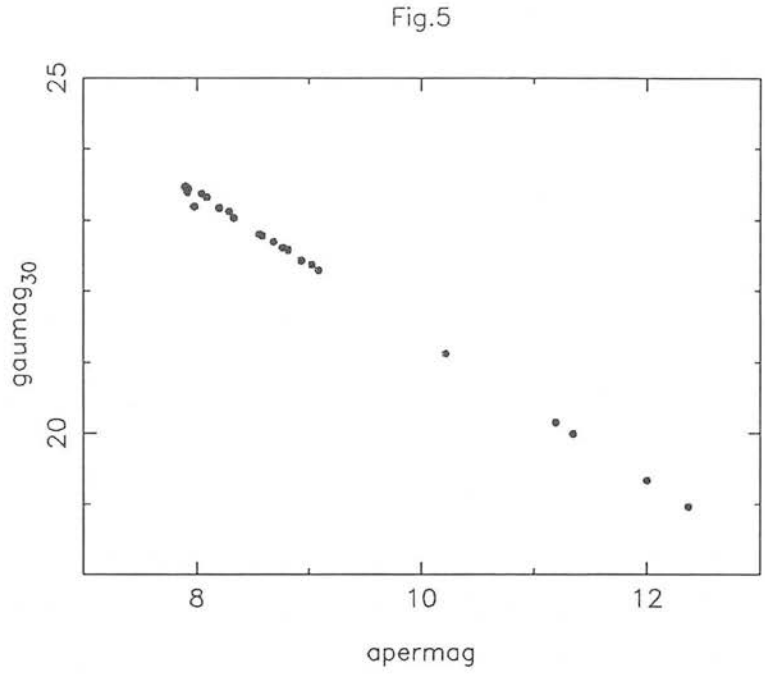

Figure 5: Comparison between the instrumental magnitudes derived with the two routines APERASP and GAUMAG (stars from the frame F52R1 are used, as an example).

The Gaussian fitted magnitudes were calibrated (ZB_2, ZR_2 terms in eq.(7), (8)) by the aperture-10 photometry of the brighter stars in each frame. The terms ZB_2 and ZR_2 are variable from frame to frame. This effect can be of the order of several hundredths of a magnitude and is mainly caused by the non-matching of the Gaussian profile to the true stellar image profile (Walker 1984) in conjunction with seeing variations. For this reason ZB_2 and ZR_2 were individually determined for each frame, with an accuracy better than 0.01 mag in most cases (see Table 4). The internal uncertainties in the above transfers amount to less than one hundredth of a magnitude, thus slightly raising the overall standard error.

The final calibration equations applied to the programme stars were the following :

$$B = B_{gau} + 0.009(B-R) + 0.215\chi + 2.5logT + ZB_1 + ZB_2 \quad (7)$$

$$R = R_{gau} + 0.035(B-R) + 0.091\chi + 2.5logT + ZR_1 + ZR_2 \quad (8)$$

where $ZB_1 = 20.85 \pm 0.03$, $ZR_1 = 20.69 \pm 0.02$, B and R are the standardised calibrated magnitudes, B_{gau} and R_{gau} are the Gaussian-fitted magnitudes, χ is the airmass at which the programme star was observed and T the exposure time in sec. Taking all sources of random error into account, the overall accuracy of the calibration of the CCD photometry is ± 0.033 in B and ± 0.024 in R. Table 5 gives a list of the numbers and B and R magnitudes of the measured stars in each one of the regions listed in Table 2, while Fig.6 gives finding charts for the same stars.

3 The reduction of the AAT observations

The same procedure as described in Section 2 was applied to the reduction of the programme frames from the AAT CCD (region F52R4 in Table 2 and Fig.6). The calibration equations provided by J.G. Robertson (1987) and the $B-R$ vs.$V-R$ relation previously mentioned were applied. Subsequently the Gaussian-fitted magnitudes were zero-pointed. The final calibration equations were

$$B = -0.73 + B_{gau} + 0.141(B-R), \quad (9)$$

$$R = -1.62 + R_{gau} - 0.005(B-R), \quad (10)$$

with an accuracy of ± 0.022 in B and ± 0.034 in R.

Region	ZB_2	ZB_2
F28R1	31.330 ± 0.008	31.317 ± 0.002
F28R2	31.314 ± 0.005	31.301 ± 0.004
F28R3	31.241 ± 0.002	31.221 ± 0.005
F28R4	31.497 ± 0.002	31.211 ± 0.008
F28R5	31.268 ± 0.004	31.352 ± 0.001
F28R6	31.269 ± 0.015	31.335 ± 0.013
F28R7	31.266 ± 0.005	31.238 ± 0.005
F52R1	31.359 ± 0.006	31.333 ± 0.004
F52R2	31.373 ± 0.004	31.250 ± 0.003
F52R3	31.310 ± 0.010	31.350 ± 0.002
F52R4	31.351 ± 0.004	31.347 ± 0.003
F52R5	31.293 ± 0.007	31.352 ± 0.008
F52R6	31.285 ± 0.003	31.271 ± 0.001
F52R7	31.313	31.346

Table 4: The APERMAG – GAUMAG correction for each CCD frame.

no	B	R	no	B	R	no	B	R
	F28R1							
1	19.91	18.53	4	20.77	19.31	34	20.60	19.15
2	20.85	18.43	5	20.59	18.69	35	19.63	18.45
3	17.06	16.12	6	21.20	19.02	36	20.40	19.12
4	20.21	18.91	7	21.07	19.60	37	19.91	18.45
5	18.42	16.45	8	18.32	16.14	38	20.02	18.77
6	18.73	17.50	9	20.52	19.00	39	20.15	18.95
7	20.66	20.16	10	20.12	18.87	40	19.06	17.40
8	20.31	19.12	11	20.79	19.48	41	20.32	19.01
9	21.11	20.37	12	20.64	19.20	42	20.44	19.22
10	20.45	19.21	13	18.89	18.37	43	20.56	19.14
11	20.66	19.64	14	20.46	19.00	44	20.83	19.99
12	20.02	18.73	15	20.27	18.88	45	20.85	20.72
13	20.73	20.75	16	20.04	18.80			
14	19.84	18.34	17	20.29	19.44		**F28R3**	
15	21.30	20.21	18	20.09	19.28	1	20.71	19.35
16	20.28	19.00	19	20.19	19.04	2	20.43	18.10
17	21.48	21.08	20	18.69	16.98	3	18.13	17.70
18	21.32	20.73	21	20.42	18.95	4	21.26	20.22
19	18.48	17.17	22	20.61	19.05	5	20.44	19.65
20	20.10	19.00	23	20.45	19.13	6	17.01	15.99
21	18.83	17.76	24	20.43	18.87	7	15.34	14.50
22	20.42	19.06	25	18.82	16.77	8	22.99	19.61
23	22.13	19.54	26	20.32	19.04	9	21.93	20.52
24	21.45	21.09	27	18.56	18.86			

Table 5: The CCD photometric sequences. The stars are identified in Fig.6.

no	B	R	no	B	R	no	B	R
25	21.86	21.41	28	20.28	18.89		**F28R4**	
26	22.08	20.06	29	19.62	18.00	1	17.20	16.49
			30	19.97	18.78	2	17.04	16.50
	F28R2		31	19.37	17.63	3	20.05	19.30
1	20.07	19.13	32	18.89	17.11	4	19.68	19.64
2	21.25	20.62	33	20.09	18.99	5	19.93	19.21
6	20.14	19.29	6	21.43	20.52		**F52R2**	
7	18.95	17.65	7	21.37	20.22	1	19.03	17.60
8	19.51	18.67	8	22.01	21.32	2	19.10	17.07
9	19.03	18.33	9	19.66	18.62	3	19.26	18.28
10	19.71	18.34	10	20.31	19.03	4	18.72	17.13
11	21.93	20.63	11	21.00	20.11	5	19.91	18.61
			12	21.13	20.51	6	20.49	19.30
	F28R5		13	21.25	20.04	7	17.54	16.46
1	18.85	17.70	14	17.27	15.97	8	19.72	18.60
2	17.54	16.10	15	21.68	20.82	9	21.15	20.05
3	14.85	13.25	16	21.41	20.28	10	21.03	20.97
4	17.98	16.77	17	21.60	20.19	11	21.60	19.12
5	19.48	17.88	18	22.19	19.27	12	20.78	10.76
			19	18.40	16.84	13	21.74	21.10
	F28R6		20	20.74	20.43	14	20.11	18.88
1	16.03	14.66	21	20.96	20.51	15	19.85	18.50
2	16.30	15.13	22	21.04	20.99	16	21.52	20.98
3	15.88	14.76	23	19.98	18.74	17	21.90	19.43
4	13.09	15.56	24	16.24	15.20			

Table 5: continued.

no	B	R	no	B	R	no	B	R
			25	21.61	21.28		**F52R3**	
	F28R7		26	21.81	21.03	1	21.30	20.47
1	15.81	14.50	27	21.45	21.20	2	21.31	19.02
2	15.10	13.92	28	20.64	20.35	3	21.24	20.31
3	17.05	16.07	29	21.78	21.22	4	18.55	18.00
4	15.99	14.55	30	19.89	18.38	5	20.62	19.84
			31	20.47	19.59	6	21.55	19.43
	F52R1		32	20.26	19.04	7	19.89	18.23
1	19.57	17.94	33	20.92	18.47	8	21.92	19.88
2	21.01	19.66	34	20.35	18.94	9	16.55	15.79
3	19.71	18.50	35	22.11	20.87	10	21.98	21.17
4	21.00	20.82	37	20.86	19.45			
5	17.43	16.60						
	F52R4		23	20.19	18.67	46	20.92	20.58
1	20.57	19.17	24	21.93	20.77	47	14.41	12.96
2	21.90	21.68	25	20.80	20.58	48	15.49	14.42
3	19.95	18.67	26	21.72	21.38			
4	21.78	21.68	27	21.49	21.38		**F52R5**	
5	21.40	21.18	28	22.10	20.78	1	13.88	12.96
6	21.92	21.58	29	20.17	18.77	2	17.23	16.08
7	19.87	17.77	30	18.92	17.87	3	17.59	15.86
8	19.79	18.27	31	21.42	21.08	4	17.27	15.45
9	22.03	21.58	32	21.92	19.47	5	13.19	12.21
10	21.30	21.08	33	21.12	18.67	6	17.09	15.64

Table 5: continued.

no	B	R	no	B	R	no	B	R
11	21.47	21.48	34	21.45	20.17			
12	21.22	20.88	35	21.89	21.78		**F52R6**	
13	21.78	20.98	36	20.80	20.58	1	14.77	13.39
14	22.00	21.07	37	18.95	17.67	2	16.28	14.40
15	21.52	21.18	38	19.45	19.58			
16	21.72	21.38	39	20.30	18.67		**F52R7**	
17	22.05	20.77	40	21.63	21.18	1	17.56	15.93
18	20.95	19.67	41	21.32	20.98	2	14.71	14.03
19	21.60	21.38	42	21.27	21.28	3	17.80	16.87
20	19.80	18.87	43	21.67	20.98			
21	18.59	17.07	44	21.93	21.48			
22	22.03	21.58	45	20.77	20.78			

Table 5: continued.

Figure 6: Finding charts for the CCD sequences

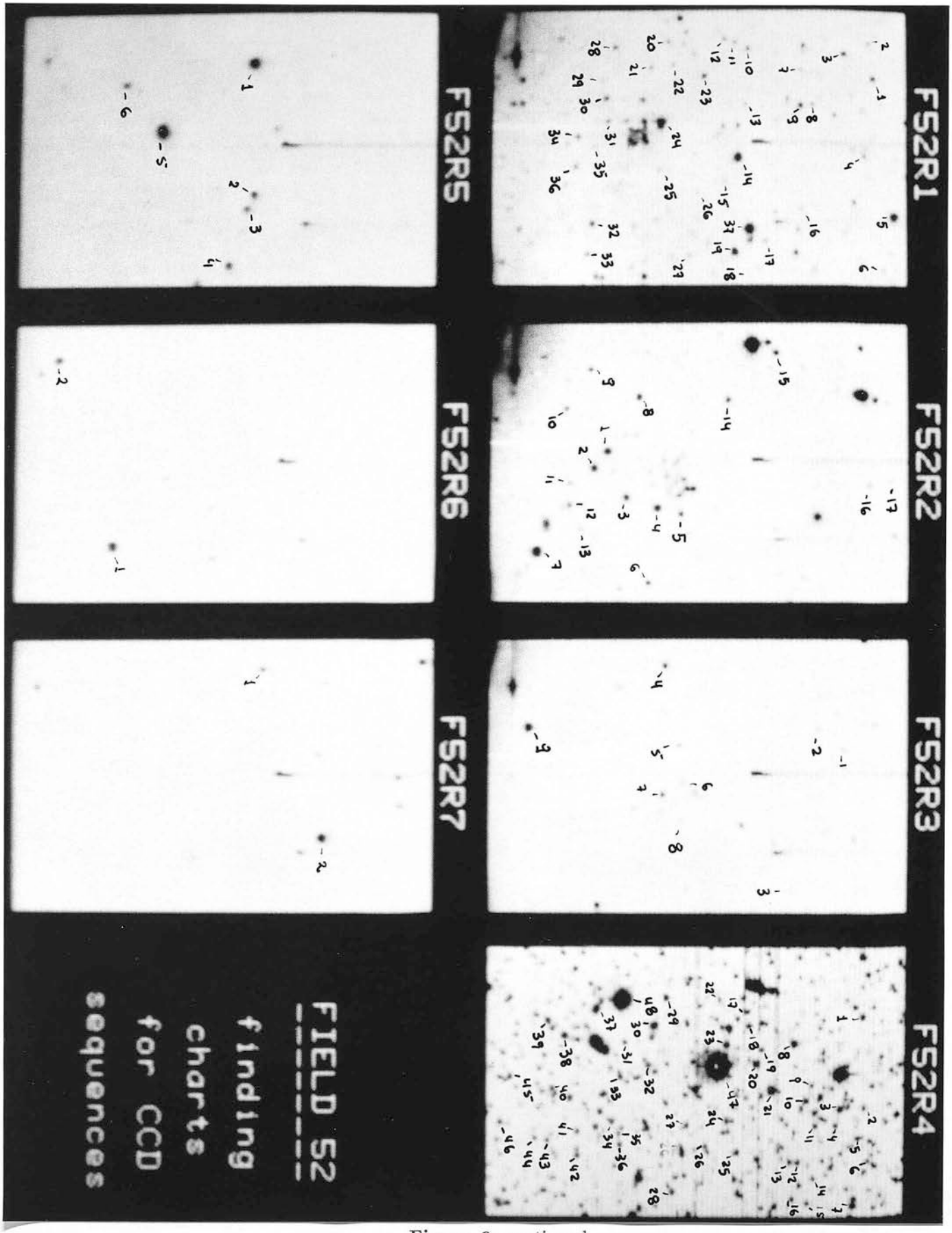

Figure 6: continued

1 The photographic plate material

The photographic plates used in this study were taken with the 1.2m UK Schmidt Telescope (UKST) at Siding Spring Observatory in Australia. As mentioned in Chapter I, there are two sets of plates, the first centred on the ESO/SERC survey Field 52 and the second on Field 28. Each set comprised of three 'blue' and three 'red' plates; the standard combination of IIIaJ emulsion with a GG395 filter was used for the blue (J) plates and a IIIaF/RG630 combination for the red (R) plates. The correlation of these passbands to the standard Johnson photometric system is discussed in Section 3.

It is desirable to use as many plates as possible for each colour and Field, in order to improve the accuracy of the photographic photometry through the pairing process (Section 3) and to reduce any position dependent systematic errors across the face of the plates (Section 4.3). At the time of the study, three good quality plates were available in each colour (in Field 28 there were additional plates in J, but only three were finally used in order to ensure comparability of the data set with that for Field 52). Table 1 summarises the characteristics of the plate material used.

The image quality on the plates was acceptably good, the grades of the plates ranging from α to β (non-survey grading system) and from A to C (survey grades). One of the red plates (R10510) showed significant haze halos in the upper NE corner. The plate was originally included in the set of plates processed by COSMOS –in the absence of a possible substitution. However, it was subsequently rejected –along with R7220– because of significant systematic errors in the photometry (Section 4).
All exposures were sky-limited, the exposure time ranging from 60-80 min for the J plates and from 90 to 115 min for the R plates, depending on the actual batch of photographic plates used.
The actual filters used for the various exposures of the same type were not identical. Their serial numbers are also given on Table 1. However, the variations of the optical thickness between different filters (of the same type) were too small to create any detectable differences in the photographic photometry

Plate No	Date UT	Emulsion	Filter	Grade
Field 52				
J2566*	1976.7	IIIaJ	GG395/1	AI2
J3671	1977.9	IIIaJ	GG395/1	BE2
J1825	1975.8	IIIaJ	GG395/1	AIF3
R10640*	1986.0	IIIaF	RG630/4	aT
R10516	1985.8	IIIaF	RG630/4	a
R10510	1985.9	IIIaF	RG630/4	bH
Field 28				
J3675*	1977.9	IIIaJ	GG395/1	AI3
J1935	1975.9	IIIaJ	GG395/1	BUX2
J9553	1984.7	IIIaJ	GG395/8	aI
R9587*	1984.8	IIIaF	RG630/4	aH
R9600	1984.8	IIIaF	RG630/4	a
R7220	1981.8	IIIaF	RG630/3	CIU6

Table 1: List of the photographic plate material used in the study. *Columns 1–4* are self-explanatory. In *Column 5* the quality of the plates is described using the UKSTU grading system. The plates used as master-plates are followed by an asterisk.
E: emulsion fault; **F**: fogging; **I**: image size $> 35\mu$; **U**: underexposed; **UX**: although underexposed, no obvious difference from the survey plate; **H**: haze halos (affecting only the brightest stars); **T**: trail

(D.Morgan, private communication).

The plates were taken between October 1975 and January 1986. During this period several changes in the operation of the telescope and the plate processing took place (UKSTU Handbook, Appendix 4, 1983); of these only the introduction in 1982 of nitrogen flushing the plate holder during an exposure should affect significantly the quality of the plates; all three J plates in Field 52, two J plates and one R plate in Field 28 were taken earlier than 1982. The nitrogen-flushing technique improves both the large scale and the point-to-point variations in plate uniformity (Dawe, Coyte & Metcalfe 1984). Such variations tend to increase the effective extent of the vignetted region (see below) and are caused by differential desensitisation of the emulsion across the photographic plate, due to moist air trapped between the flat filter and the curved plate. The extent of the effect on each plate depends on the exposure time and the air humidity on the particular night when the exposure was taken.

Apart from this desensitisation effect, other plate non-uniformities include the geometrical vignetting of the plates (which obviously affects the edges of a plate), differential atmospheric extinction for observations made at high airmass (which is manifested by a North-to-South variation), changes of image structure across a plate (caused by differential refraction) and finally variations due to plate fogging, zodiacal light and stray light, which are negligible in the plates of Table 1. The composite effect of all these non-uniformities on the photographic photometry is examined in Section 4.

2 The COSMOS measurements

The COSMOS machine

The COSMOS plate scanner is a high-speed, flying-spot scanning microdensitometer which can digitise photographs of up to a maximum size of $287 \times 287 mm^2$. In the present case a pixel size of 16 microns was used for the digitisation, with a scanning spot of FWHM size of 32 microns. The selected pixel size extracts 90 percent of the image information on the photograph. The basic information stored for each pixel –along with its coordinates– is the 16-bit transmission value, which provides a measure of the emulsion density. This is converted to an intensity using a Baker density curve obtained

from the 16 densitometer spots or the step wedge at the edge of each plate. COSMOS functions in three different modes (e.g. Stobie 1986). The *threshold mapping* mode (TM) was applied to the present data. In this mode, only information on pixels above a local density level are output. The value of this intensity threshold is a compromise between losing information on faint objects and on the other hand outputting too many noise pixels. In the present case, the intensity cut off was chosen so as to ensure detection of images down to the plate limit. Subsequently, the image pixels are passed serially through a software pattern analyser (Thannish *et al.* 1984) which determines which pixels are connected together to form a coherent image and calculates a number of parameters for each image: (a) the centroid x and y coordinates (1st order moments of the object pixel distribution) with an accuracy of $\sim$ 3 microns; (b) a photometric parameter defined as $COSMAG = -2.5log\Sigma I$ where ΣI is the sum of the intensities above the sky background of the pixels within the image area (zeroth-order moments); (c) a number of parameters connected with image classification and derived from the higher order moments. The one of relevance here is the ellipticity of the image, i.e. the ratio of the minor to the major axis of an ellipse uniquely defined by the normalised and centralised second order moments.

A limitation of this technique (Stobie 1986) is that the analysis is based on the presumption that each object is isolated, i.e. it does not distinguish overlapping objects and therefore it is only appropriate for low density regions of the sky. A new 'deblending' software package has been recently developed (S. Beard, H.T.MacGillivray & Q.Parker private communication), which aims at remedying this problem. The quality of the resulting deblended images had not been meticulously tested before the present measurements were performed. The properties of the deblending process and its potential usefulness for the present study are examined in the following subsection.

Mostly original photographic plates were scanned by COSMOS. In some cases (survey plates) glass copies had to be used. However, according to Stobie *et al.* (1984) the effective degradation and information loss in the copying process are minimal: The copying does reduce the dynamic range and therefore there is a cut off in usable images at high density levels, but in practice, the useful density range is not set by the photographic plate but by COSMOS itself (McGillivray & Stobie 1984). Furthermore, as a

copy has normally a sky-background density lower than the original plate, the measuring machine noise is likely to be less important in the copy measurements (Stobie *et al.* 1984).

Finally, it must be pointed out that the instrumental magnitude $COSMAG$ used in all following discussions was not corrected for the local sky value. This practice was avoided because the field variation can be erroneously estimated in the field-correcting routine by nearby bright objects (stars, nebulae, galaxies) and certainly in the case of the SMC there is an intrinsic field variation due to the galaxy itself.

The deblending software:

This software was designed so as to deblend the images on the large fields of the UKST plates, without consuming unacceptably high CPU time; it does not apply a complex profile fit, as is customary in other routines used for example for photometry of stars in globular clusters (e.g. DAOPHOT or ROMAPHOT routines). Briefly, the routine re-thresholds each image at eight intensity levels, such that $I_n = I_{thresh} \times C^n$, where C is the *areal profile parameter*, $n = 1, ..., 7$ and $I_{thresh} = (1 + x/100).I_{sky}$ (x the *percentage cut*, here 10%). Whenever the peak of an initially unresolved object falls within one of the threshold zones, it is separated from the blended image. In this way an initially multiple image is resolved into at least some of its constituents. The areal profile parameter governs the spacing between the successive threshold levels used for areal profile calculation and deblending. A small value would increase the efficiency of resolving faint merged images, but would miss close multiple images. A large value of C on the other hand would split even close doubles, but some merged images would be missed, because the probability of both peaks lying between adjacent levels would have risen. Here, the value of $C = 1.07$ was used, which has been empirically found to give the best results for UKST photographic plates (McGillivray private communication); the resulting efficiency of the achieved deblending will be examined in the next subsection. A number of other parameters also regulate the deblending capacity of the software (Q.Parker 1988): the minimum and maximum area an image can have before deblending is attempted (here $A_{min} = 8$ pixels and $A_{max} = 60,000$ pixels), the blend area cut and the maximum deblending level (here set at its maximum value, 8).

In connection with the present study, the crucial characteristic of the software is the

way in which the various pixels are assigned to one or the other of the deblended images: The decision is made by using the areal profile to fit a Gaussian to each image and then extrapolating that Gaussian to the fainter threshold. It must be emphasised that the image parameters are calculated from the actual pixel positions and intensities, not from Gaussian profiles. The software assigns *whole* pixels to one or other of the images. This procedure can be expected to cause systematic errors in the derived instrumental magnitudes.

The application of the deblending software on the present data-set

The initial COSMOS output from the photographic plates was processed through both the old non-deblending and the new deblending software. The results were compared with both the stellar images on the original plates and the CCD sequences (presented in Chapter II).

For the particular combination of deblending parameters used here (as described in the previous subsection), these comparisons yielded the following conclusions:

(i) Images closer to each other than 6 arcsec (peak-to-peak) are not separated by the deblending routine.

(ii) The halos and diffraction spikes of very bright stars are often split by the 'deblender' into many low surface density images (mimicking the images of faint galaxies) in a random way. However, these spurious images having 'random' coordinates are almost entirely excluded through the pairing process of the plates (Section 3).

(iii) Not all multiple images are deblended. The efficiency of the deblending is shown in Fig.1, as a function of the 'true' number density of stars (detected on the photographic plates and the CCD frames). For number densities of less than $\sim$ 7 per square arcmin, more than $\sim$ 95% of the images are separately detected by the deblending software. Obviously a percentage of these are essentially multiple images. For densities higher than $\sim$ 10 images per square arcmin the efficiency of the deblending decreases rapidly.

(iv) The 'non-deblending' software gives comparable results with the 'deblending' one for number densities of the order of 7-10 per square arcmin or less (see Fig.2).

(v) The magnitudes of *deblended* images were compared with the CCD photometry results. The available sample of stars with independent CCD photometry, which are resolved on the CCD frames but not on the initial COSMOS measurements, can be

Fig.1

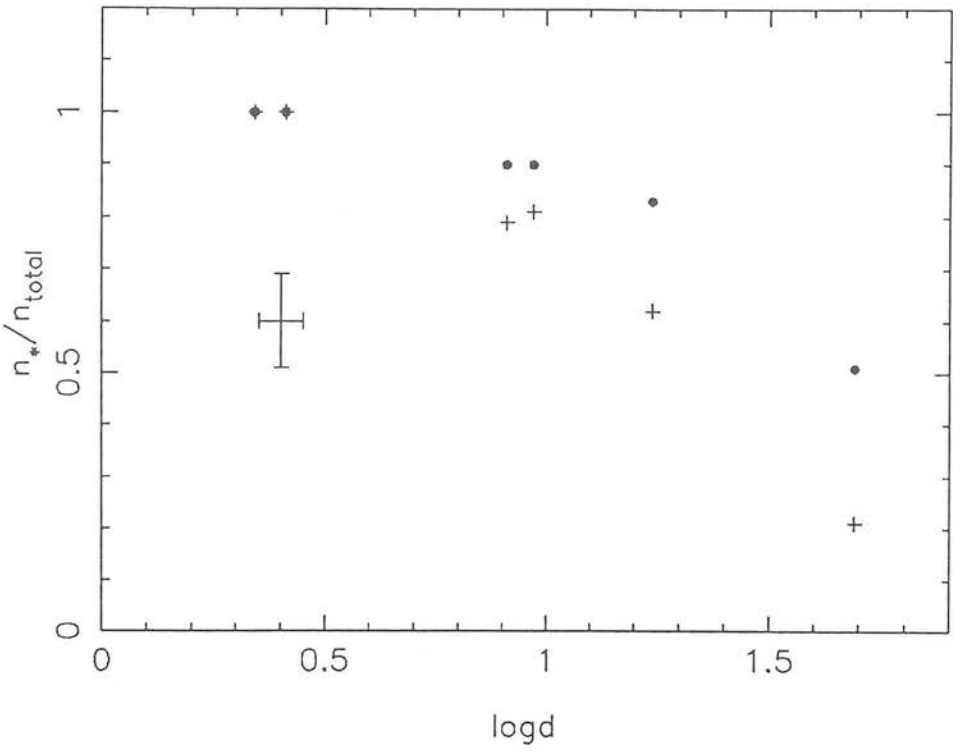

Figure 1: Percentage of images detected by the deblending software (crosses), compared with the 'true' number of stars detected on the photographic plate (by eye), as a function of the surface density of the latter. The filled circles show the percentage of single images among the 'deblended' stars.

Fig.2

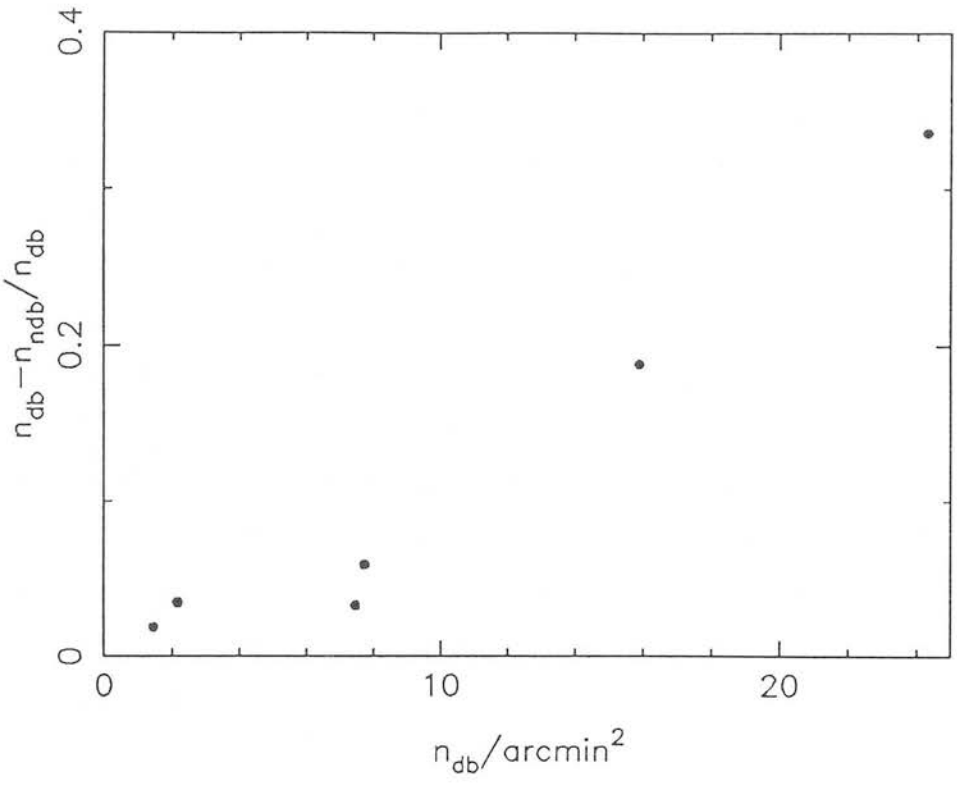

Figure 2: Comparison of the numbers of images detected by the *deblending* software (n_{db}) and the *non-deblending* software (n_{ndb}) as a function of the true surface number density of stellar images σ). As an example, the results from plate J2566 are shown.

'deblended' by the new software, is rather small. However, the following conclusions could be reached:

• For magnitude differences between the deblended stars of the order of 2 mag or less, the intrinsically fainter star is assigned a systematically fainter magnitude by several hundredths of a magnitude, depending on the actual magnitudes, the magnitude difference and the distance between the deblended stars.

• For magnitude differences greater than $\simeq 2^m.5$, the effect is reversed with the fainter image appearing systematically brighter. This effect can be as high as 0.3-0.4 mag.

In view of the outcome of these tests, it was decided that for the purposes of the present study, the improvement in the deblending of overlapped images is outbalanced by the systematically erroneous magnitudes assigned to the deblended images. In any case, the deblending software only starts to give significantly different results from the old software for number densities higher than $\sim$ 10 per square-arcmin. The study was confined to regions with densities lower than the above limit.

In Field 28, a strip of a total area of 8 square degrees at the eastern edge of the photographic plates was not measured at all, because of the large CPU time and storage space required. This strip included an extended high density region of the SMC main body, as well as the galactic globular cluster 47 TUC. On the whole 20 square degrees on each of the Field 28 plates and 28.5 square degrees on the Field 52 ones were processed through *COSMOS*.

3 Pairing and calibration of the plates

The software used for the analysis of the *COSMOS* data has been extensively described by Hawkins (1983; 1984). The same pairing procedure was adopted for the combination of the *COSMOS* data sets in each filter and field. Briefly, a master plate was chosen and a least-squares rotation, translation and scale-change transformation was evaluated from the positions on this plate to each one of the other plates. The nearest image on the secondary plate to the transformed position was then chosen as a provisional pair. If no pair was found, the image was discarded. The best quality plates were chosen as master plates. On the first pairing the data set was typically reduced by 8% (e.g. from the

original number of 380000 images detected on plate $J2566$, approximately 30000 were lost when matched with $J3671$ images) mainly due to plate limit effects and various types of spurious images being eliminated (Section 4). An average of 3% of the images per plate was lost for the remainder of the pairings (depending on the quality of the plate), resulting in a final data set of 320000 images in Field 52 and 180000 images in Field 28 (note that the F52 measurements cover an area 35% larger than the F28 ones). Following the application of the pairing process all magnitudes were reduced to the same relative scale (Hawkins 1983). The relation between IIIa-J/GG395 magnitudes and standard Cousins B magnitudes was obtained from comparison of photographic magnitudes with CCD sequences converted to the standard Cousins system and is given by the following equation: $B - B_j = 0.25(B_j - R) + constant$ (M.Hawkins private communication).

The final conversion to B and R magnitudes was achieved with the aid of the CCD sequences described in the previous section and of a photometric sequence near the cluster L1 in Field 28 established by Gascoigne (unpublished) and kindly made available to me by M.T. Brück. There are also other photoelectric sequences in both Fields 28 and 52 (near the clusters NGC416, 419, 458, 47TUC and Kron3), but in all cases they are located in the denser regions of the Fields which were not included in the present study. The correlation of $COSMAG$ to true magnitude is known to be nonlinear (e.g. MacGillivray & Stobie 1984). For the fainter stars ($B > 18$) the images are unsaturated and the machine and photometric magnitudes are reasonably well-fitted by a straight line of slope near unity, implying that an approximately correct density-intensity relation has been adopted. At brighter magnitudes the core of the image becomes saturated and the slope changes. Finally for very bright images ($B < 10$, not considered here) the slope steepens again as the halo of the image rises above the threshold surface brightness and contributes to the image magnitude. This complexity of shape requires that reliable standards be available over the whole range of interest on a plate. This requirement was fulfilled by the CCD photometric sequences (Chapter II) obtained, for the magnitude range of $14 < R < 20$ and $15 < B < 21.5$.

A simple fourth-order least squares polynomial fit was applied for the conversion of $COSMOS$ instrumental magnitudes ($COSMAG$) to standard magnitudes in the BVRI photometric system. Fig.3 shows a typical example of the final calibration line (the

converted COSMAG versus the standard magnitudes). The rms scatter around the mean line was $0^m.11$ in B and $0^m.13$ in R in Field 28 and 0.12 and 0.11 respectively in Field 52. The fact that the curve is quite accurately a straight line indicates that the adopted simple polynomial fit for the calibration of *COSMOS* magnitudes was an adequately good approximation for the magnitude-range $15 < B < 21.5$. For stars brighter than $\sim 15^m$ the calibration is not esssentially correct, given the small number of calibrating stars in this section of the curve.

4 Discussion and conclusions

In this section, we examine the accuracy of the photographic magnitudes, the level of completeness of the resulting data-base and finally the absence of significant systematic trends in the photographic calibration. All these points are crucial for the reliability of the use of the colours and magnitudes (R vs $B - R$ CMDs), for the detection of geometrical features, metallicity changes and changes in the population synthesis in the outer regions of the SMC.

4.1 Accuracy of the derived magnitudes

The total error of a magnitude is a combination of the errors originating in the photographic plate, the microdensitometer and the algorithms. In order to estimate the random errors in the derived photographic magnitudes, the rms variation for the magnitude measurement of a single image on an individual plate was calculated. Fig.4 shows the distribution of the rms variation in three different magnitude ranges for each of the two fields and filters. The 'tail' of the error distribution includes non-normally distributed errors, mainly caused by variables, flawed or wrongly paired images and diffuse galaxies. The peak of the distribution is therefore considered as a close enough estimate

Figure 3

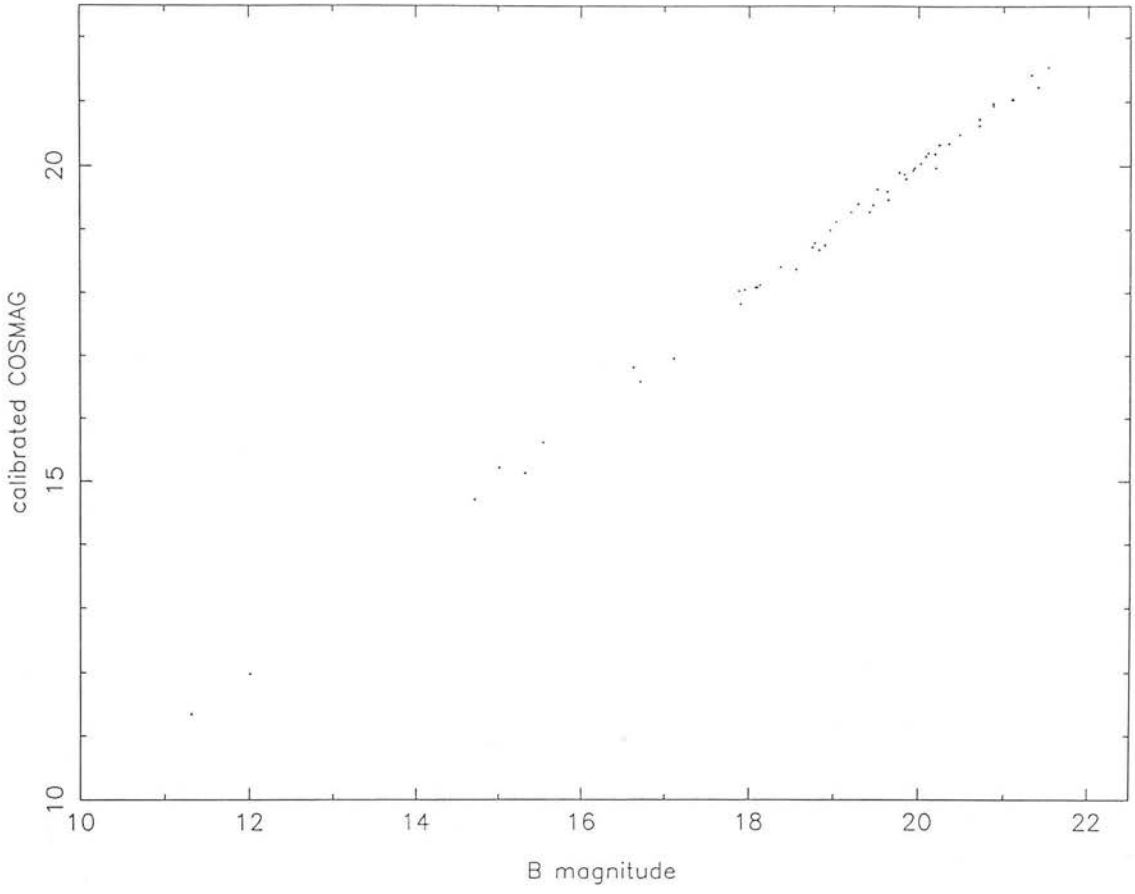

Figure 3: The calibration of COSMAG in B and R using the stars of Table 5 of Chapter II and the Gascoigne photometry sequence in Field 28. The y-axis gives the transformed COSMAG, $f_4(COSMAG)$, where f_4 is the 4th order polynomial used to describe the original COSMAG vs. magnitude curves.

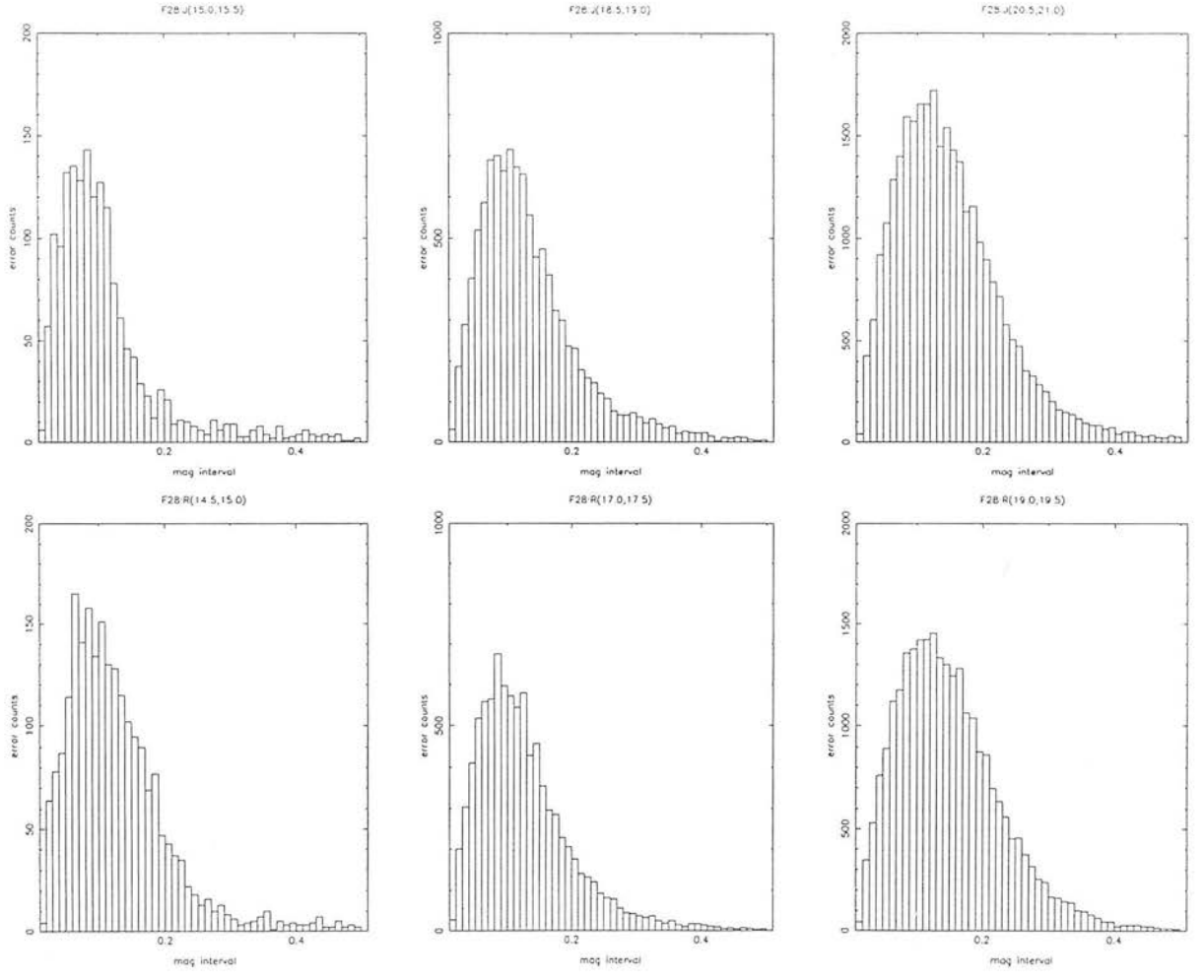

Figure 4: Distribution of the rms magnitude variation in three different magnitude in B and R: (a) Field 28; (b) Field 52.

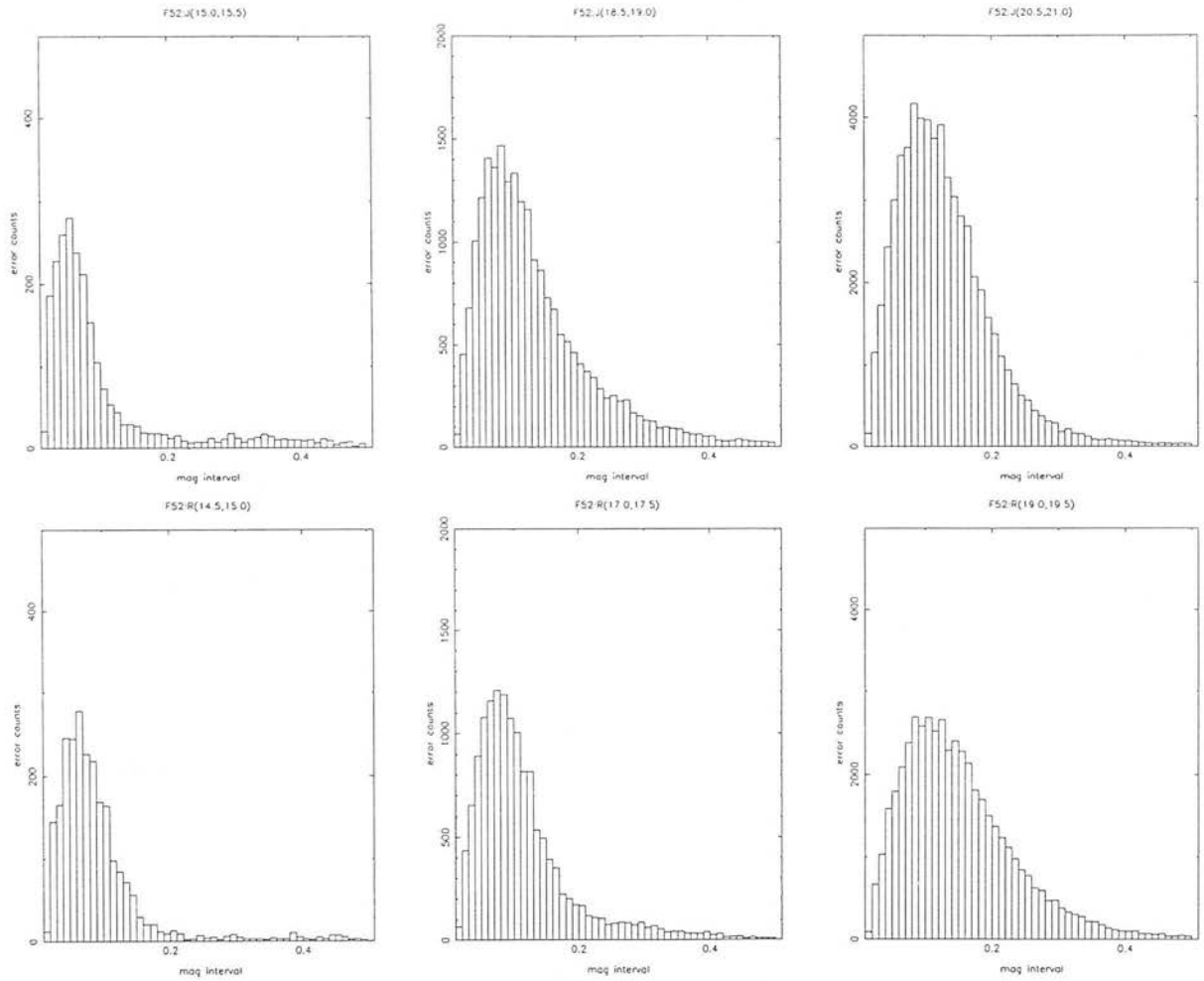

Figure 4: continued.

of the Gaussian error of the measurement of a single image in each case. This error is only weakly dependent on magnitude ranging from 0.09 for the brighter magnitudes to 0.12 for the fainter ones. Obviously, the standard error for the magnitude of each star calculated from n plates is given by the above values divided by $\sqrt{n}$. There is no significant difference in the error distributions in the two different fields, which is important for the reliability of comparisons between their corresponding colour magnitude diagrams in the subsequent chapters). Fig.5 shows the dependence of the total mean error (including the non-Gaussian tail of the error distributions) as a function of magnitude in B_J and R in both Fields.

4.2 Completeness of the sample

The plate pairing process removed spurious images, but also rejected a significant number of faint images due to the different limiting magnitudes of the various plates, adjacent images which were merged into one image on one plate but resolved on another, images which were not paired due to random errors in their coordinates, variable objects and finally, when pairing J and R plates, objects of extreme colour at faint magnitudes.

All the above introduce incompleteness to the final catalogue. To investigate the nature and significance of this incompleteness, the distribution of unmatched and matched images as a function of magnitude, position on the plate and image ellipticity was examined. As a representative example, Fig.6 presents the results from the pairing of plates $J2566$ and $J3671$. As expected, the bulk of unmatched images are very faint (peak around $B = 22$). There is also a slight preference for the loss of highly elliptical images (mostly spurious or multiple images). There is no significant position dependence of the distribution of unmatched images brighter than $B = 21.0$. However the surface distribution of the matched and unmatched images shows a drop in the percentage of faint ($B > 21$) unmatched images in the innermost regions (Table 2), which can be understood in terms of the high surface density of images there. On the whole the incompleteness is around 3% for images brighter than $B = 21$, but rises sharply for fainter images.

In the innermost regions there was a high percentage of overlapped (multiple) images.

Fig.5a

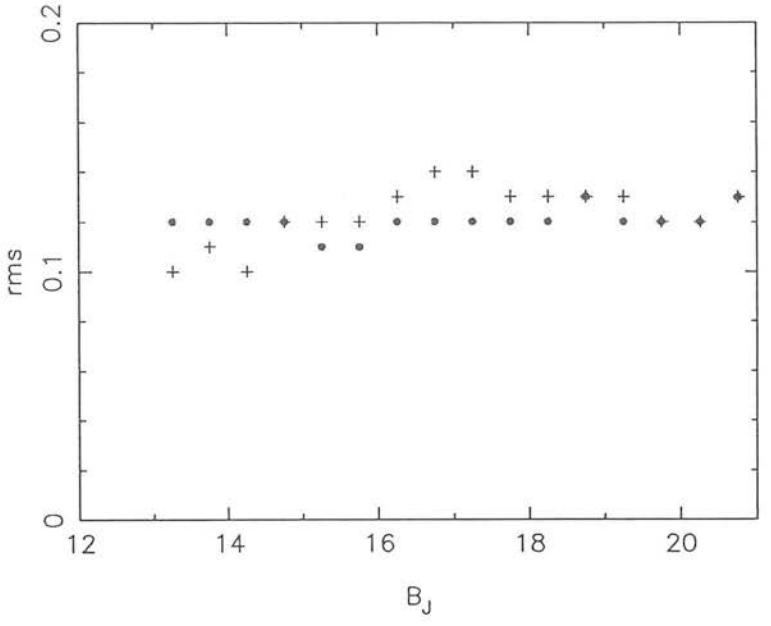

Fig.5b

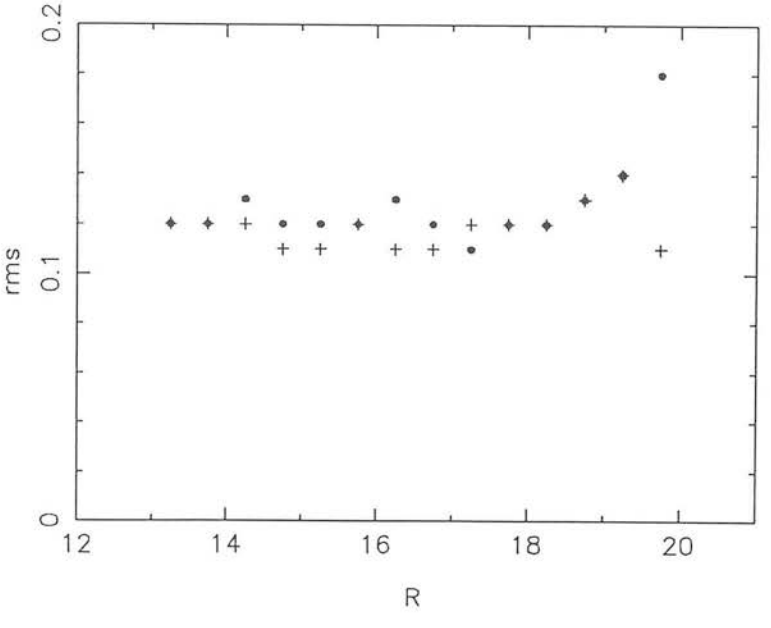

Figure 5: The derived mean errors (including non-Gaussian errors) of the photographic photometry, as a function of magnitude (•: Field 28; +: Field 52) B_J (a) and R (b).

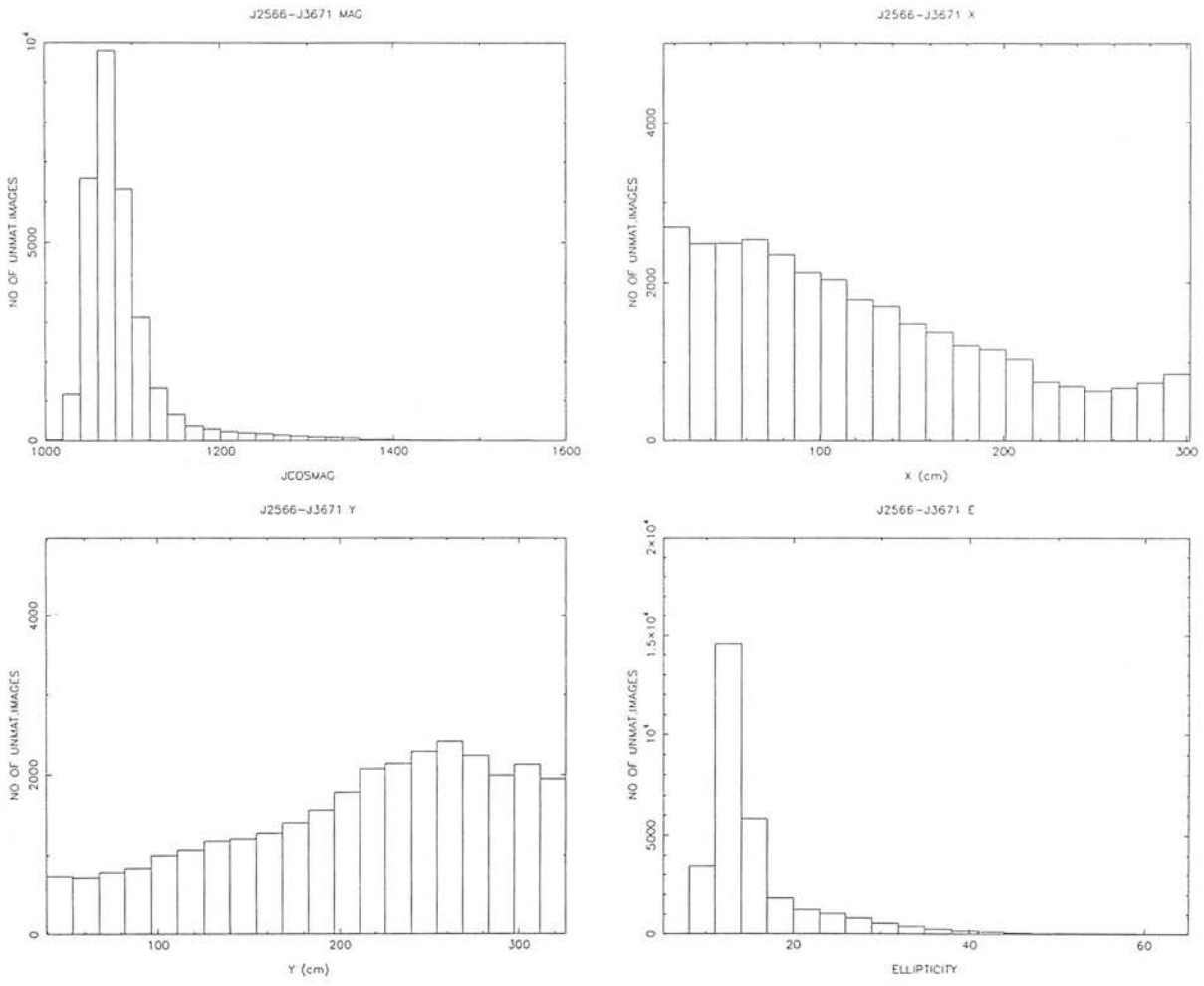

Figure 6a: Example of the distribution of unmatched images as a function of magnitude, position on the plate and ellipticity, for the pairing of the plates J3671 and J2566.

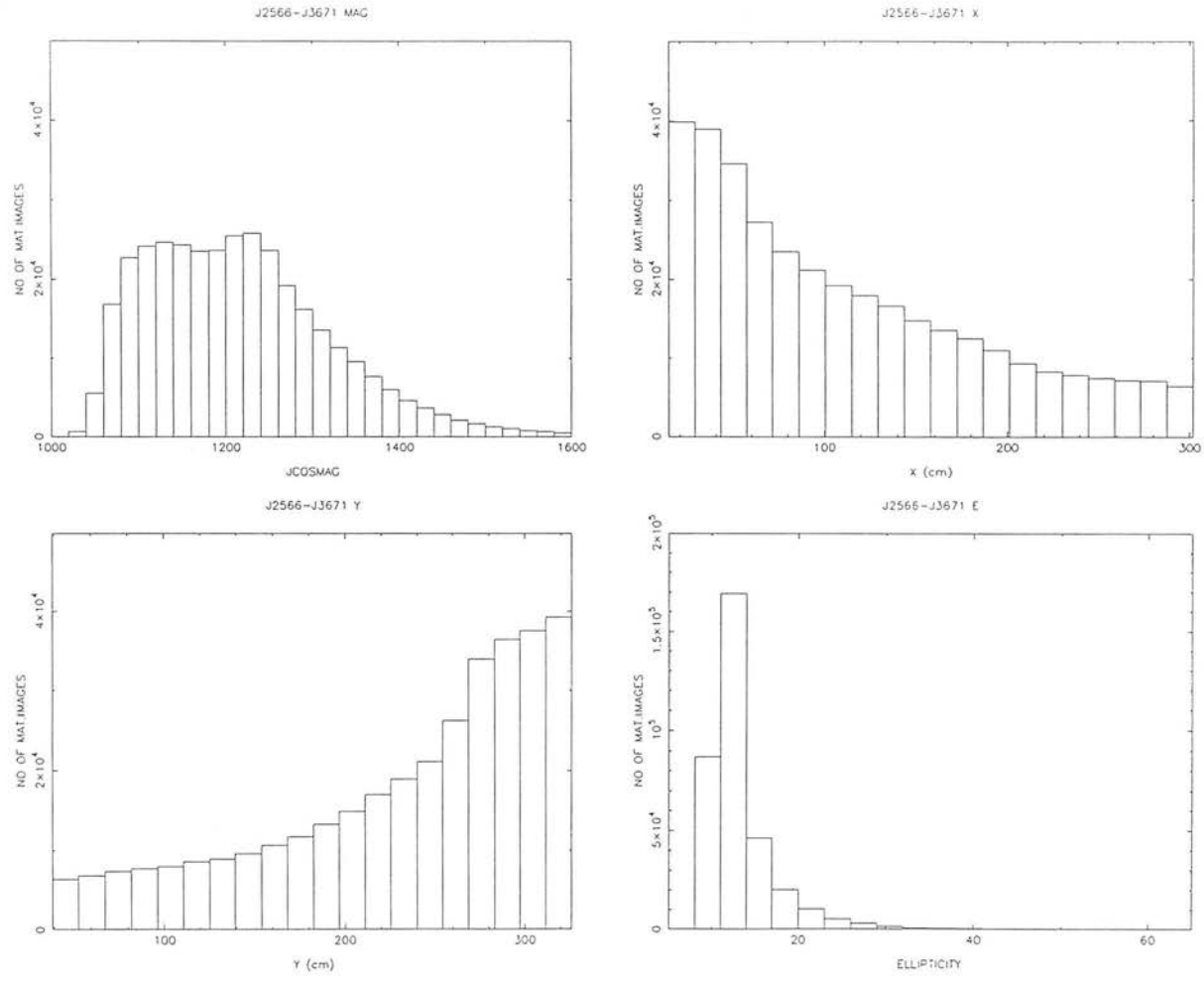

Figure 6b: as in (α) for matched images.

$B < 21.5$					$B > 21.5$					
							$\leftarrow x$			
1	3	2	3	2:	40	41	38	32	21:	y
2	2	2	3	3:	37	40	37	33	33:	$\downarrow$
3	2	2	2	3:	39	43	38	34	35:	
2	2	2	2	2:	39	40	41	37	39:	
5:	4:	2:	2:	3:	42:	44:	42:	39:	39:	

Table 2: Projected space distribution of the percentage of unmatched images from the pairing of plates J2566 and J3671, for $B < 21.5$ and $B > 21.5$. The arrows indicate increasing distance in the x and y direction away from the central dense regions.

For a surface density of 20 images/sq.arcmin, only 60% of the images were single, while this number falls to 20% for densities around 40 images/square arcmin. However, in the less dense regions (surface density smaller than 10 images/square arcmin) to which this study is confined, the percentage of multiple images is small (between 2 and 5%), and most of them are unpaired. So the additional incompleteness induced from this effect is hardly significant for low and moderate surface densities.

Fig. 7 shows the counts of matched images from all J and R plates in the two fields. In principle it is possible to derive the onset of significant incompleteness from the observed fall-off in counts at faint magnitudes, which does not occur in this case for magnitudes brighter than $B \simeq 21.2$. The counts presented in Fig.7 display features which cannot be attributed to incompleteness effects: the histograms corresponding to the J plates show a significant peak in the measures for $B \simeq 20$ and the field 52 histograms show less well defined peaks, which cannot be attributed to higher errors in the F52 measurements, as can be seen from Fig.4. It will be shown in the following chapters that the observed peaks in the B_J histograms are due to the large number of clump giants in the outer regions of the SMC, while the larger dispersion in the F52 distributions is a result of the large line-of-sight depth of the SMC towards the NE side.

4.3 Field effects

One of the factors which are important in determining the accuracy of the photographic photometry is whether it is valid to assume that the same magnitude calibration applies over the whole area measured. Factors such as changes of image structure across a photographic plate (caused by differential refraction), geometrical vignetting, and sensitivity variations in the emulsion of the plate (see Section 1), can all affect the magnitude calibration and give rise to systematic errors of the order of several tenths of a magnitude which can occur over an individual plate. The errors rise sharply near the edges of the plate -as one would expect. Table 3 gives a typical example of residuals between mean magnitudes from all F52 J plates and plate $J2566$ as a function of position on the plate. The procedure for correcting for field effects of this type is based on a position-dependent calibration process that is described in detail by Hawkins (1983; 1984). However, global effects affecting all plates cannot be removed by this method

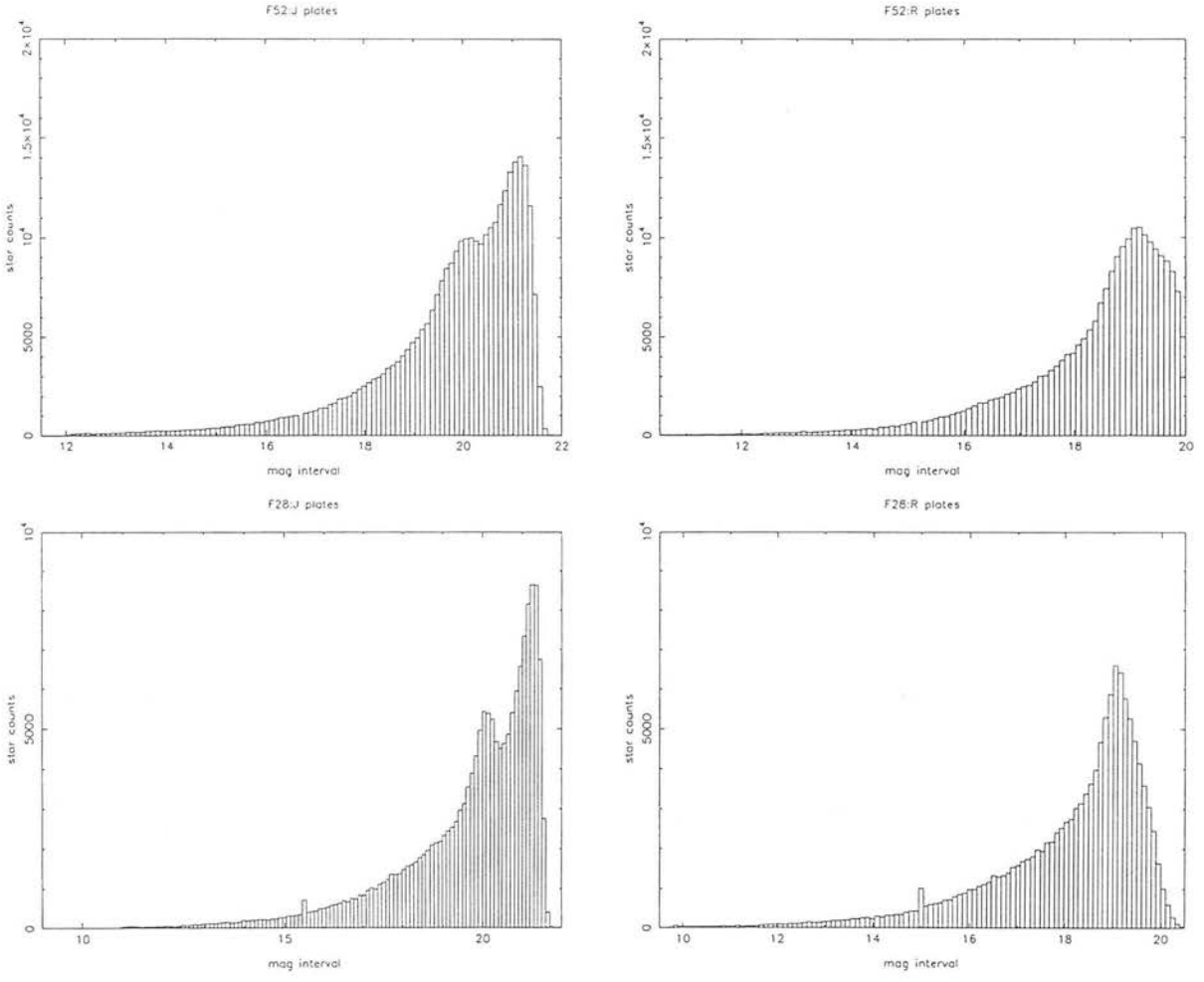

Figure 7: Number counts of matched images from all J and R plates in Field 28 & 52.

Bright images, $12 < B < 17$															
−8	−5	−2	1	5	6	7	6	3	7	7	7	9	9	6	11
−6	−3	0	3	5	3	5	8	6	6	8	14	13	8	7	8
−6	−3	2	3	3	4	5	7	8	6	10	12	6	7	8	9
−6	−1	2	3	5	4	2	5	4	5	4	8	6	5	8	7
−3	1	0	0	0	2	0	4	1	2	4	6	6	7	8	8
0	5	−1	1	1	3	1	4	3	5	4	7	5	7	7	8
−4	−1	0	2	0	4	0	4	4	5	4	7	8	9	10	9
−4	−1	1	1	1	4	2	4	4	3	2	7	9	9	11	10
−4	−1	0	0	2	3	1	5	1	4	2	5	5	7	9	11
−3	−2	0	2	3	2	3	3	3	1	2	3	6	7	7	8
−1	−1	0	2	0	2	0	0	0	−1	0	−2	4	4	6	7
−3	0	0	1	1	2	1	0	−3	−3	0	3	2	5	4	4
−3	−3	0	0	0	−1	−4	−5	−5	−3	−1	0	1	3	1	2
−5	−4	−3	−4	−1	−3	−6	−7	−8	−3	−3	−4	−1	0	0	−1
−3	−6	−7	−4	−6	−8	−11	−10	−6	−8	−7	−5	−4	−2	−4	−4
6	−7	−9	−10	−8	−14	−12	−13	−10	−11	−7	−7	−6	−5	−6	−7

Table 3: Residuals in 0.01 mag spaces, between the mean magnitude from all plates of Field 52 and plate J2566, as a function of position. The figures give mean residuals for 1.8cm–squares over the Field.

Faint images, $17 < B < 21.5$															
−6	−2	0	3	3	5	6	6	4	5	4	6	5	5	3	2
−5	−2	0	3	4	5	5	5	4	5	6	8	6	5	3	1
−7	−3	0	3	3	2	4	6	5	4	6	7	4	3	4	3
−5	0	0	2	3	4	4	3	2	3	2	5	2	3	4	4
−3	0	0	2	2	3	2	3	2	3	3	2	2	3	4	6
−1	2	1	2	3	3	4	3	3	4	3	4	4	3	4	4
−3	0	0	2	3	4	4	4	4	5	5	4	6	6	6	5
−3	0	2	3	3	3	4	4	4	4	3	4	6	7	7	6
−2	0	1	3	3	4	4	5	4	6	5	5	5	6	7	7
−2	0	1	4	4	4	4	4	4	4	4	4	5	6	5	7
−2	0	1	3	3	4	3	3	3	3	2	4	4	5	4	6
−3	0	1	2	3	3	3	2	2	2	2	2	4	5	4	5
−3	−1	0	1	1	2	1	0	1	0	2	2	2	4	2	2
−3	0	−2	0	0	0	0	−1	−1	0	0	1	0	1	0	0
0	−4	−5	−4	−4	−3	−4	−3	−2	−1	−1	−1	−1	−1	−1	−2
−4	−4	−9	−8	−7	−6	−6	−5	−5	−3	−3	−4	−5	−4	−3	−5

Table 3: continued.

and we therefore rely on the CCD standards to set limits to such effects. As indicated in Chapter II, the observed CCD sequences were well distributed over the plates, thus allowing any major systematic trends in the magnitudes across any individual plate to be detected. Even before applying the previously mentioned corrections, no systematic errors significantly larger (i.e. more than 2σ) than the errors expected from the inaccuracy of the zero point determination of the CCD sequences were detected across the plates, with the possible exception of plates $R10510$ and $R7220$ which were subsequently removed from the final data set. It is worth mentioning at this point that both the geometrical vignetting and significant desensitisation –if present– affect the edges of a plate, generally within 30-50 arcmin. No regions so close to the edges of the plates were included in the data analysis described in the following chapters.

4.4 Conclusions

An area of 48.5 square degrees on the sky, covering the northeastern and southwestern outer regions of the SMC, was studied with the use of 1.2m UK Schmidt telescope photographic plates, taken through B_J and R filters. The plates were measured with the *COSMOS* microdensitometer and calibrated with CCD photometric sequences. The resulting magnitudes and colours were checked for accuracy (standard errors from all plates ± 0.07 in B and ± 0.10 in $B-R$), completeness ($\geq 95\%$) and absence of significant systematic errors due to field effects. They can thus be used reliably for the construction of colour magnitude diagrams covering the entire area and subsequently for the determination of the stellar population and geometrical structure of the outer regions of the SMC.

1 Introduction

The data-set consisting of the B and R magnitudes of 550,000 stellar images in the northeastern and southwestern outer regions of the SMC (Fields 52 and 28 respectively), were used for the construction of colour-magnitude diagrams (R vs. $B-R$; hereafter CMDs) over the whole area of 48.5 square degrees measured (Chapter III).

The areas of the two Fields were divided into square regions of 0.87 square degrees each. A CMD including all images with $R \leq 20.5$ and $B-R \geq -1.0$ was then constructed for each of these areas. In addition to this 'coarse grid' of CMDs, a finer grid with a unit cell of 0.22 square degrees was also considered, in order to provide a more detailed picture of the surface distribution of the various populations in the SMC. Figure 1 shows the grids overlayed on the 'maps' of two Fields derived from the COSMOS measurements (including only the 1000 brightest images in each Field). Table 1 gives the right ascension and declination (1950) of the centres of each 'cell' for both the coarse and the fine grid, along with the projected distances, r_{oc} and r_{dc}, of these centres from the *optical* and *dynamical* centres of the SMC, respectively. The optical centre ($RA = 00^h51^m$, $DEC = -73^o$, 1950) was defined by de Vaucouleurs (see e.g. de Vaucouleurs & Freeman 1972) as the centre of the smoothed elliptical isodensity contours of bright stars. The dynamical (or rotational centre; $RA = 01^h02^m12^s$, $DEC = -72^o53'02''$, 1950) was suggested by Hindman (1967) as the centre of the HI rotation curve and it is displaced by ~ 50 arcmin to the East of the optical centre. According to Brück (1978; 1980) the optical centre represents the centre of the youngest populations while the dynamical centre that of the older ones. In the following, both centres will be used for reference in the study of the radial distribution of the various properties of the stellar populations in the SMC periphery.

In Section 2 the procedure of removing from the CMDs the contribution of the Galactic foreground and of background galaxies is analysed; in Section 3 the 'cleaned' CMDs are presented and their main features briefly described; in Sections 4 & 5 the distance and reddening scales for the SMC are discussed and the values adopted for the

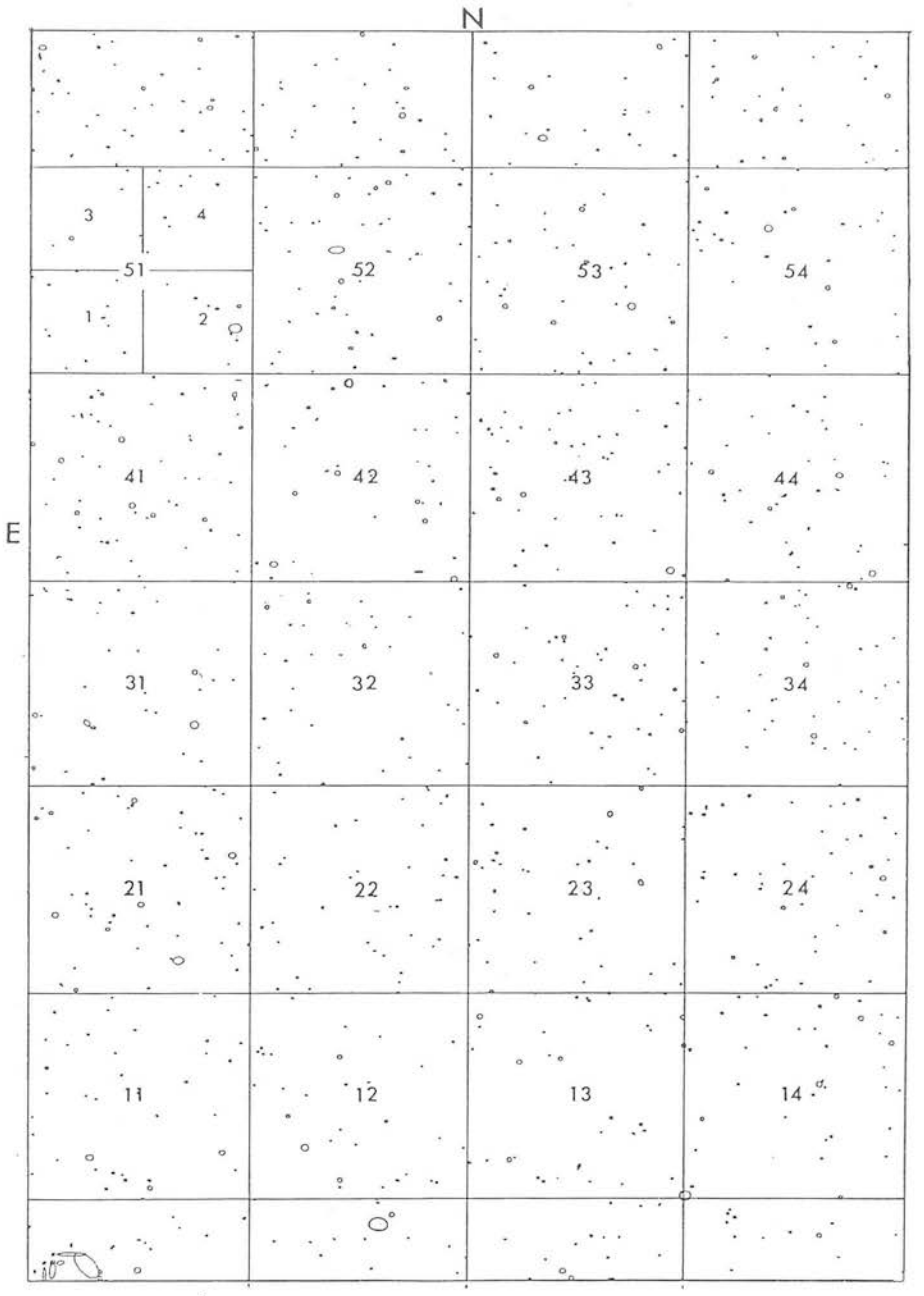

Figure 1a: A COSMOS map of the 1000 brightest images in the scanned area in Field 28. The 'coarse' and 'fine' grid used for the CMDs are also shown, together with the numbering of the cells, which is used throughout the following chapters.

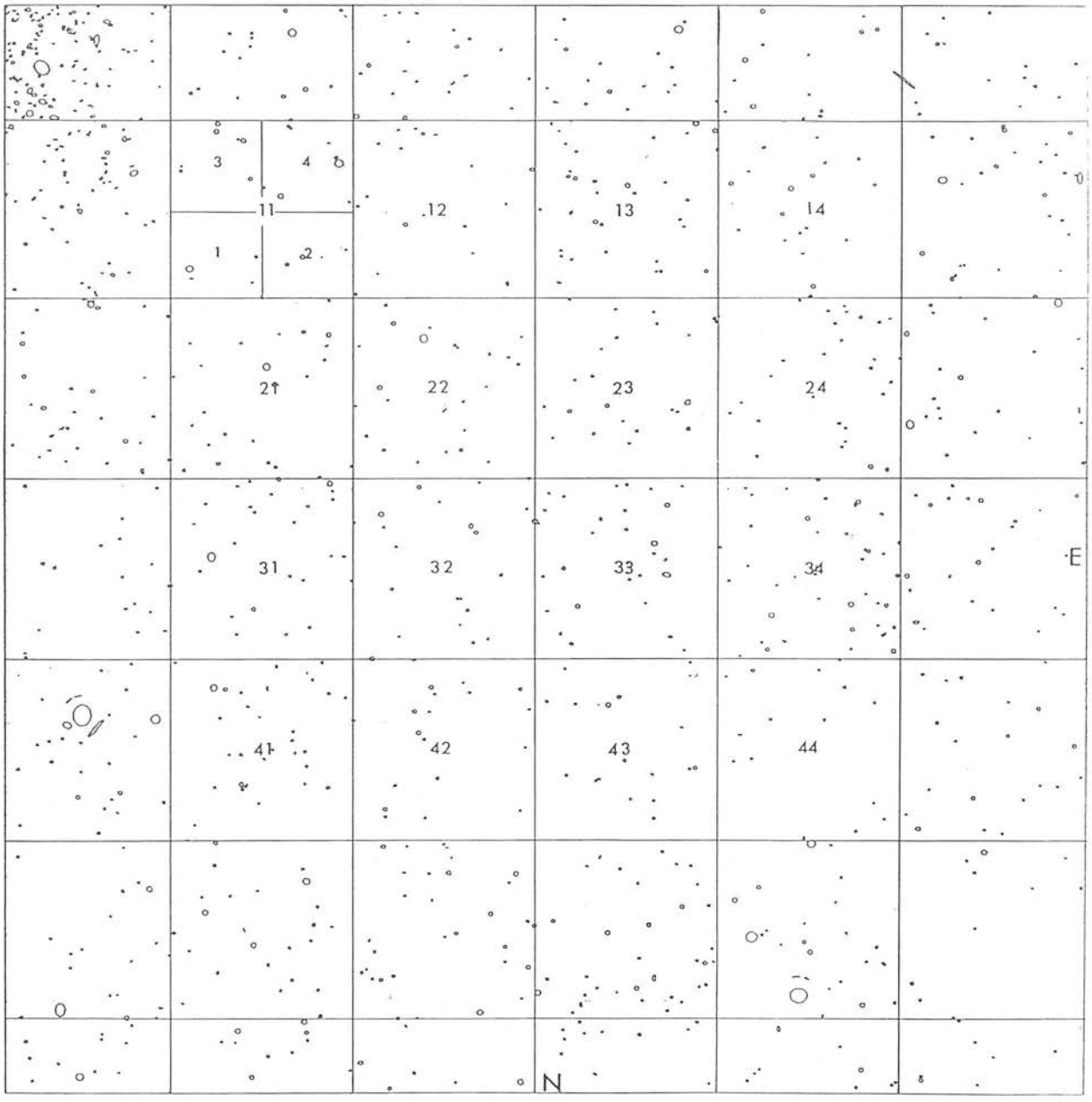

Figure 1b: As in Fig.1a, but for Field 52.

Region	RA (1950)			DEC (1950)			r_{oc}	r_{dc}
51	00	13	35.5	−73	9	37	2.72	3.56
52	00	00	43.3	−73	11	18	3.65	4.48
53	23	47	50.8	−73	09	58	4.58	5.41
54	23	35	2.9	−73	05	38	5.51	6.34
41	00	14	22.2	−74	05	25	2.81	3.60
42	00	00	45.8	−74	07	12	3.72	4.52
43	23	47	09.0	−74	05	47	4.63	5.44
44	23	33	37.6	−74	01	11	5.55	6.37
31	00	15	14.6	−75	01	14	3.18	3.88
32	00	00	48.6	−75	03	08	4.00	4.74
33	23	46	22.1	−75	01	37	4.87	5.63
34	23	32	02.1	−74	56	43	5.75	6.53
21	00	16	13.8	−75	57	02	3.75	4.34
22	00	00	51.7	−75	59	03	4.47	5.13
23	23	45	29.2	−75	57	26	5.26	5.96
24	23	30	14.4	−75	52	12	6.08	6.81
11	00	17	21.1	−76	52	47	4.44	4.94
12	00	00	55.3	−76	54	57	5.07	5.64
13	23	44	29.0	−76	53	13	5.77	6.40
14	23	28	12.1	−76	47	36	6.53	7.20

Table 1a: Field 28.

Column 1: number of the grid-cell (see Fig.1a).

Column 4: projected radial distance of the centres of the grid-cells from the optical centre of the SMC.

Column 5: the same for the dynamical centre.

Region	RA (1950)			DEC (1950)			r_{oc}	r_{dc}
511	00	17	01.8	−73	22	40	2.48	3.31
512	00	10	31.3	−73	24	17	2.95	3.78
513	00	16	34.5	−72	54	48	2.52	3.35
514	00	10	14.4	−72	56	22	2.98	3.81
411	00	18	01.1	−74	18	25	2.66	3.43
412	00	11	08.1	−74	20	08	3.10	3.88
413	00	17	30.6	−73	50	32	2.53	3.33
414	00	10	49.2	−73	52	12	2.99	3.80
311	00	19	07.7	−75	14	10	3.12	3.77
312	00	11	49.3	−75	15	59	3.50	4.19
313	00	18	33.4	−74	46	18	2.86	3.57
314	00	11	28.1	−74	48	04	3.27	4.00
521	00	03	59.8	−73	25	08	3.41	4.24
522	23	57	27.9	−73	25	13	3.88	4.70
523	00	03	53.4	−72	57	12	3.44	4.27
524	23	57	32.0	−72	57	17	3.90	4.74
421	00	04	13.8	−74	21	02	3.55	4.33
422	23	57	19.1	−74	21	07	4.00	4.79
423	00	04	06.6	−73	53	04	3.45	4.26
424	23	57	23.6	−73	53	10	3.91	4.73
321	00	04	29.5	−75	16	57	3.90	4.61

Table 1a: continued.

Region	RA (1950)			DEC (1950)			r_{oc}	r_{dc}
322	23	57	09.1	-75	17	03	4.31	5.04
323	00	04	21.4	-74	49	00	3.70	4.45
324	23	57	14.3	-74	49	05	4.13	4.90
211	00	20	23.0	-76	09	53	3.76	4.30
212	00	12	36.0	-76	11	50	4.08	4.66
213	00	19	44.1	-75	42	02	3.42	4.02
214	00	12	11.9	-75	43	55	3.77	4.41
221	00	04	47.3	-76	12	52	4.42	5.05
222	23	56	57.9	-76	12	58	4.79	5.45
223	00	04	38.1	-75	44	55	4.15	4.81
224	23	57	03.7	-75	45	01	4.54	5.23
111	00	21	48.8	-77	05	32	4.50	4.94
112	00	13	29.3	-77	07	38	4.77	5.26
113	00	21	04.5	-76	37	43	4.12	4.61
114	00	13	01.7	-76	39	45	4.41	4.95

Table 1a: continued.

Region	RA (1950)			DEC (1950)			r_{oc}	r_{dc}
11	02	04	34.1	−68	06	31	2.54	2.00
12	01	54	35.1	−68	10	02	3.18	2.78
13	01	44	33.7	−68	11	18	3.94	3.64
14	01	34	32.2	−68	10	17	4.76	4.52
15	01	24	32.8	−68	07	01	5.61	5.42
21	02	05	26.7	−69	02	10	3.33	2.68
22	01	55	02.3	−69	05	52	3.84	3.31
23	01	44	35.2	−69	07	12	4.49	4.05
24	01	34	07.8	−69	06	08	5.23	4.86
25	01	23	43.0	−69	02	42	6.01	5.71
31	02	06	24.0	−69	57	51	4.18	3.48
32	01	55	32.0	−70	01	44	4.60	3.98
33	01	44	36.7	−70	03	08	5.15	4.62
34	01	33	41.3	−70	02	01	5.81	5.34
35	01	22	48.7	−69	58	24	6.53	6.13
41	02	07	26.7	−70	53	30	5.06	4.33
42	01	56	04.4	−70	57	35	5.41	4.75
43	01	44	38.4	−70	59	03	5.89	5.29
44	01	33	12.3	−70	57	53	6.47	5.94
45	01	21	49.5	−70	54	05	7.12	6.65
51	02	08	35.4	−71	49	06	5.96	5.21
52	01	56	39.9	−71	53	24	6.26	5.56
53	01	44	40.3	−71	54	57	6.68	6.03
54	01	32	40.5	−71	53	43	7.19	6.61
55	01	20	44.4	−71	49	43	7.78	7.25

Table 1b: Field 52.

Region	RA (1950)			DEC (1950)			r_{oc}	r_{dc}
121	01	57	13.3	−68	23	19	3.16	2.69
122	01	52	09.9	−68	24	31	3.51	3.10
123	01	56	57.2	−67	55	25	2.85	2.47
124	01	52	00.0	−67	56	36	3.23	2.90
221	01	57	47.6	−69	19	08	3.89	3.30
222	01	52	31.2	−69	20	24	4.17	3.64
223	01	57	30.1	−68	51	13	3.52	2.98
224	01	52	20.3	−68	52	27	3.83	3.35
321	01	58	25.1	−70	14	57	4.69	4.03
322	01	52	54.3	−70	16	17	4.92	4.31
323	01	58	05.9	−69	47	02	4.28	3.66
324	01	52	42.5	−69	48	21	4.54	3.96
131	01	47	06.1	−68	25	10	3.88	3.51
132	01	42	02.0	−68	25	14	4.26	3.94
133	01	47	02.3	−67	57	14	3.62	3.34
134	01	42	04.4	−67	57	17	4.03	3.79
231	01	47	14.1	−69	21	04	4.48	4.00
232	01	41	56.9	−69	21	08	4.82	4.38
233	01	47	10.0	−68	53	07	4.16	3.73
234	01	41	59.5	−68	53	11	4.53	4.14

Table 1b: continued.

Region	RA (1950)			DEC (1950)			r_{oc}	r_{dc}
111	02	07	17.5	−68	19	11	2.61	1.99
112	02	02	15.9	−68	21	32	2.86	2.32
113	02	06	49.2	−67	51	23	2.21	1.67
114	02	01	53.7	−67	53	41	2.51	2.06
211	02	08	17.6	−69	14	47	3.45	2.75
212	02	04	40.7	−70	58	40	3.65	3.00
213	02	07	46.9	−68	46	59	3.02	2.36
214	02	02	39.1	−68	49	23	3.24	2.65
311	02	09	23.2	−70	10	23	4.33	3.60
312	02	03	54.8	−70	12	59	4.49	3.79
313	02	08	49.7	−69	42	35	3.88	3.17
314	02	03	28.5	−69	45	07	4.06	3.39
331	01	47	22.9	−70	17	00	5.19	4.62
332	01	41	51.3	−70	17	04	5.48	4.95
333	01	47	18.4	−69	49	02	4.82	4.29
334	01	41	54.2	−69	49	06	5.14	4.65
411	02	10	34.9	−71	05	57	5.22	4.48
412	02	04	51.2	−71	08	41	5.35	4.64
413	02	09	58.2	−70	38	11	4.77	4.03
414	02	04	22.4	−70	40	50	4.91	4.21

Table 1b: continued.

subsequent interpretation of the CMDs are given.

2 Back/foreground removal

In Figure 2 two examples of the resulting coarse–grid CMDs are shown. As would be expected, there is a significant contribution to the SMC CMDs from foreground galactic stars and from background galaxies. The most distant areas studied here, lying more than 5.6 kpc away from the SMC optical centre, have CMDs which show no evidence of any contribution from SMC stars. Their mean number density is 4050 ± 350 objects per square degree, or, taking into account the incompleteness factor of $\sim 95\%$ (Chapter III), ~ 4260 objects per square degree.

It should be mentioned at this point that the outermost regions in Field 52 – presumably consisting only of back/foreground objects– have systematically fewer stars by $\sim 10\%$ than the corresponding regions in Field 28. A large part of this effect is due to the different galactic latitudes of the two Fields ($b = -47^o$ for the centre of Field 52 and $b = -40^o$ for Field 28); however some contribution to the effect can be expected from a probably different degree of completeness in the faint magnitude regime for the two Fields.

As an independent check on the completeness of the data-set, we compare this value of the back/foreground surface number density with the one expected from the predicted contribution of galactic stars and background galaxies. In the direction of the SMC and for $B_{lim} \simeq 21.2$, the expected number density of galactic stars is 3100 ± 300 per square degree. This value was derived by interpolation from the predictions of Galactic models by Ratnatunga & Bahcall (1985). Using the Jarvis & Tyson (1981) galaxy count study in the northern hemisphere, a number of ~ 880 galaxies per square-degree was estimated for the above magnitude limit, with an expected uncertainty of 30%. On the other hand, Shanks *et al.* (1984) give a higher value of ~ 1300 galaxies for the same magnitude limit, from counts at the south galactic pole. The difference between the two values (which happen to be extreme cases in the bibliography; see Ellis, 1987 for a review) can be attributed partly to the higher obscuration in the lower galactic latitude fields studied by Tyson & Jarvis. As a rough estimate, the mean of these values was adopted,

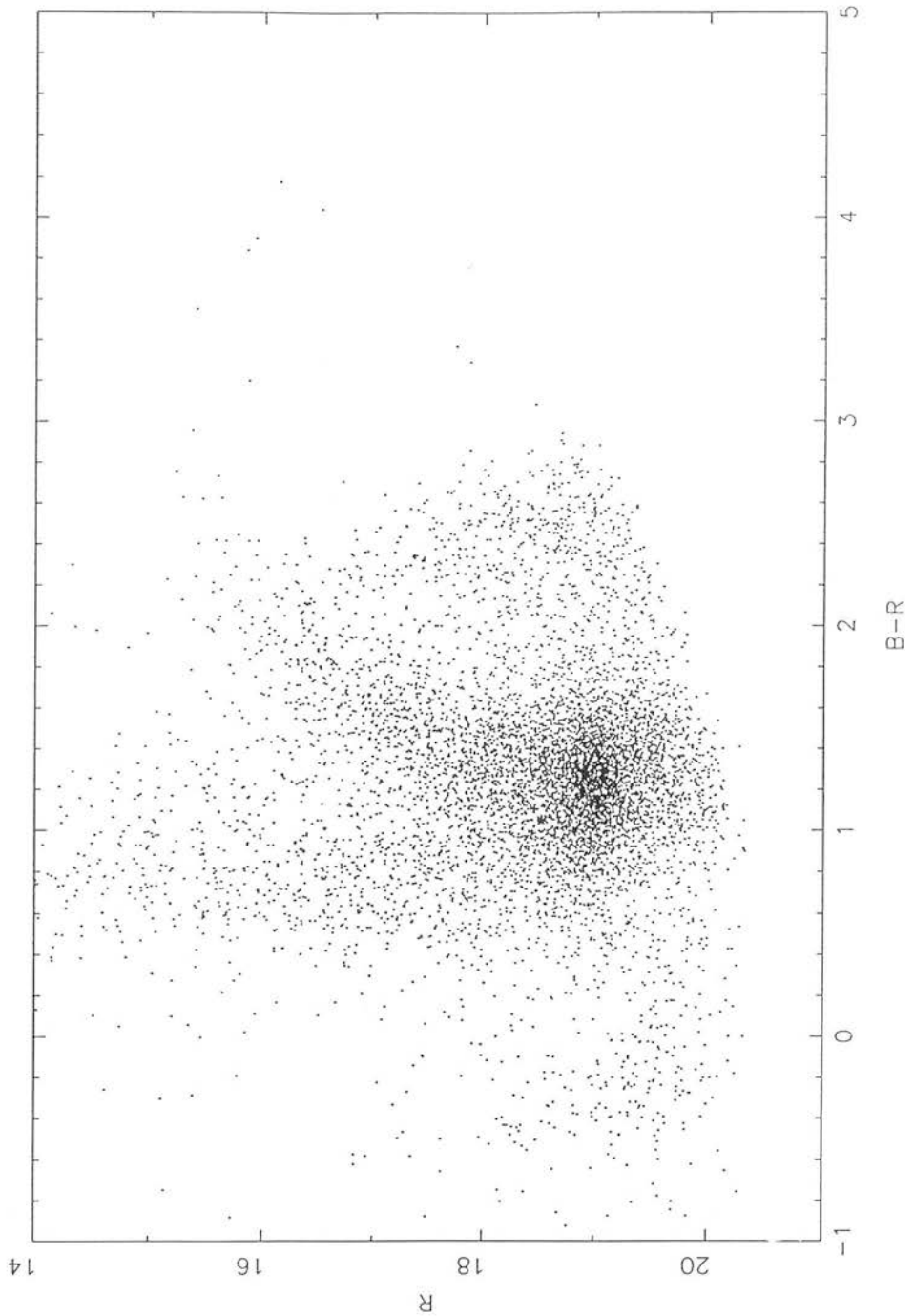

Figure 2a: CMD from region 41 in Field 28, without back/foreground subtraction.

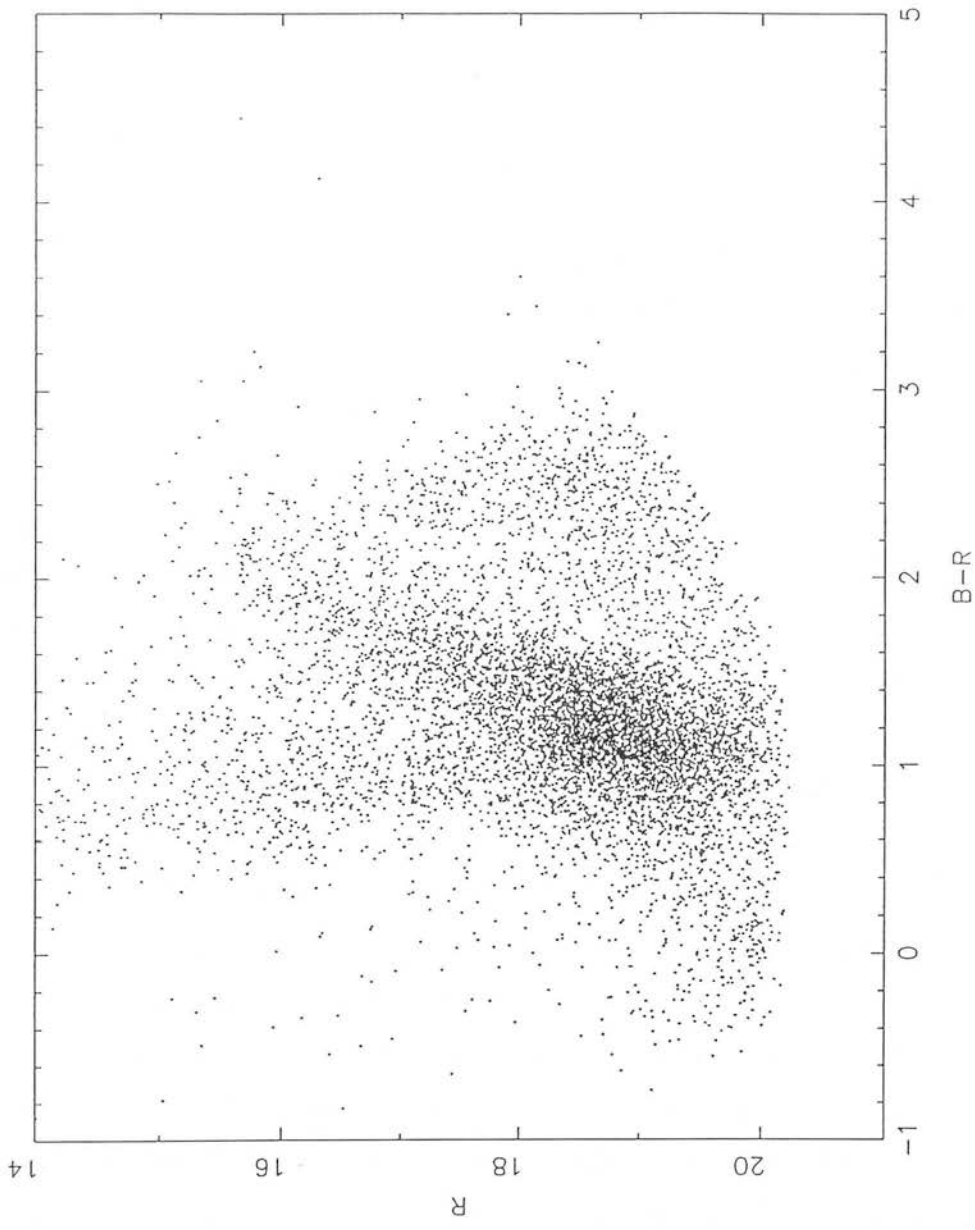

Figure 2b: CMD from region 11 in Field 52, without back/foreground subtraction.

i.e. $\sim$ 1100 galaxies per square degree. Therefore the total expected back/foreground contribution per square degree amounts to $\sim 4280 \pm 470$ objects, which agrees very well within the errors with the previously mentioned densities observed in the remote areas, in both Fields.

Assuming that the outermost regions in the two Fields consist purely of back/foreground objects, their CMD was 'subtracted' from the SMC CMDs, in order to remove the back/foreground contribution from them. The procedure followed was the normal one of looking for nearest neighbour stars in the two CMDs (e.g. Hesser *et al.*, 1987). For each star in the comparison field CMD, the nearest match to it in $(R, B-R)$ was found in the SMC field CMD and then both stars were removed from their lists, as long as the separation on the CMD given by $d = ({d_R}^2 + {d_{B-R}}^2)^{1/2}$ was less than a prescribed radius D. The selection of the value of D was made in such a way as to compensate for the following two opposing factors: (i) if D is of the order of the observational error (corresponding to a 'radius' of $\simeq \pm 0.1$ around each point on the CMD), a significant number of points remain unremoved from the CMD, due to randomly higher observational errors, or real variations in the distribution of points on the CMD. The latter effect is pronounced in the areas of the CMD with low densities of points. (ii) If D is too large (> 0.6) distortions can be caused at the low density edges of the CMD, due to the anticipated fluctuations of the total number of back/foreground objects.
After several trials the value of $D = 0.15$ was selected. A residual scatter is still present in the resulting diagrams (Fig.2), but this cannot be avoided in view of the relatively large intrinsic fluctuations in the back/foreground. In principle, the different degree of crowding in the SMC and back/foreground fields can cause an overestimate of the back/foreground contribution in the most crowded fields. This effect is magnitude-dependent and is not easily quantifiable. However, the crowding is relatively small in the regions we have considered here (see Chapter III) and this effect should be negligible.

Another factor that influences the back/foreground removal is the difference in galactic latitude between the back/foreground region and each of the SMC regions. In Field 52 the galactic latitude is higher (in absolute value) in the back/foreground region, therefore the background contribution in the innermost area is underestimated by a few %. The opposite is the case in Field 28. Although a correction for this effect is

possible in principle, it has not been attempted because the random variations of the back/foreground itself are significantly larger than this effect. Nevertheless, care was taken to select the reference back/foreground fields as near the mean latitude in each Field as possible.

3 The colour-magnitude diagrams

All the back/foreground subtracted coarse–grid CMDs in Fields 28 & 52, which include significant numbers of SMC stars, are presented in Appendix A. Three features are noteworthy in these CMDs:

(i) *the main sequence (ms)*, extending to $R_{ms} \simeq 18.0$ in the innermost regions. The bright end of the ms fades away with distance from the SMC centre and finally disappears below the limiting magnitude;

(ii)*a densely populated clump/horizontal branch (HB)*, around $R \sim 19.0$ and $B-R \sim 1.1$, present on all diagrams where SMC stars are detectable;

(iii)*a well-defined red giant branch* (RGB), approximately centred at its base with respect to the clump. The RGB becomes less well delineated in the outer regions. A red and bright extension of the RGB can be seen in some of the diagrams and can be identified with an *asymptotic giant branch* in the Aaronson & Mould (1982) sense.

There is also some evidence for the existence of a *subgiant branch*, as a separable extension toward fainter magnitudes of the clump/HB.

For comparison, Fig.3 presents a composite colour-magnitude diagram, for $R < 20.0$, of all intermediate and old SMC clusters for which accurate observations have been made in the past, permitting the determination of their ages with the ms isochrone–fitting method (see Chapter VI). These clusters cover an age range from 1.8 Gyr to 12 Gyr and have metallicities [Fe/H] (see Chapter V) between -0.9 and -1.4 dex; the CMD of an LMC cluster of higher metallicity ($[Fe/H] = -0.5$) and of age comparable to the youngest SMC cluster in the sample, is also included in the Figure. A comparison of this composite CMD with the CMDs of the SMC northeastern and southwestern outer regions (Appendix A) shows a remarkably good agreement of the main features of the CMD and their location on the diagram. A detailed discussion of these CMDs in terms

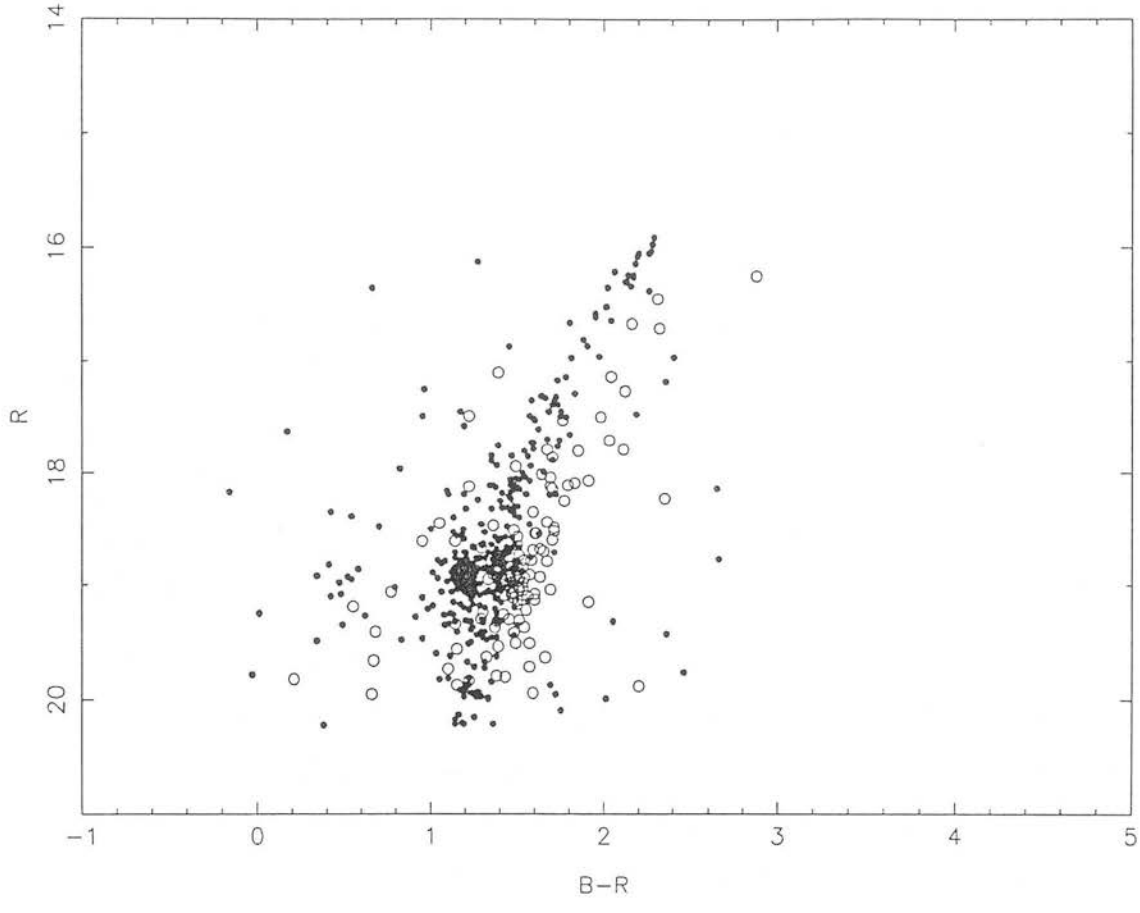

Figure 3: Composite CMD of the SMC clusters (filled circles) NGC411, L113, Kron3, NGC121, L1 and an LMC cluster NGC1651 (open circles; Mould, Da Costa & Crawford 1986).

of metallicity and age will be presented in Chapters V and VI respectively.

4 The distance modulus

The determination of the distance scale is essential for the interpretation in terms of age and metal abundance of the CMDs presented in the previous Section. During the past decade, the distance modulus (hereafter d.m.) of the SMC has been a source of controversy, with reported values ranging from $(m-M)_o = 18.62$ (de Vaucouleurs 1978) to $(m-M)_o = 19.47$ (Sandage & Tammann 1981).

Part of the discrepancy between results derived from the application of different distance indicators, may be due to the effect of the metal defficiency of the SMC with respect to the LMC and the Galaxy on the zero point of the young distance indicators in particular. Moreover, the large line-of-sight depth of the SMC that has been suggested by several researchers (see Chapter IX) can cause additional complications, since the d.m. may be a strong function of the position of the objects examined with respect to the SMC centre.

Table 2 gives a compilation of relatively recently derived values for the SMC d.m. based on primary distance indicators as reviewed by de Vaucouleurs (1978), i.e. novae, cepheids, RR-Lyrae and horizontal branch stars, A & B supergiants and eclipsing binaries. The values cluster about two means of $(m-M)_o = 18.80 \pm 0.13$ and 19.10 ± 0.16. The two values are customarily referred to as the short and long distance scale respectively. Both values were generally considered equally plausible, however recent studies of SMC star clusters seem to require the smaller distance scale (Mould *et al.* 1984 (L113); Rich *et al.* 1984 (Kron 3); Da Costa & Mould 1986 (NGC 411); Olszewski *et al.* 1987 (Lindsay 1)). In addition a recent study of intermediate age core helium burning stars (clump/HB stars) in Magellanic Cloud clusters by Seidel, Da Costa & Demarque (1987) supports the adoption of the short d.m. for both the Clouds. They show that the long d.m. leads to physical inconsistency, in the sense that the observed masses of the clump/HB stars in the clusters would appear to be larger than the masses of their predecessors of the main sequence turnoff region. The discrepancy is removed when the short d.m. is applied.

Indicator	d.m.	source
novae	18.95 ± 0.25	de Vaucouleurs 1978
cepheids	19.01 ± 0.25	de Vaucouleurs 1978
	18.95	Eggen 1977
	19.11 ± 0.07	Visvanathan 1985
	19.05 ± 0.06	Laney & Stobie 1986
	18.93 ± 0.05	Welch *et al.* 1987
	18.97 ± 0.07	Caldwell & Coulson 1986
	18.86 ± 0.27	Mathewson *et al.* 1986
	19.47	Sandage & Tammann 1981
	19.24	Feast 1984
RR-Lyraes	18.85	Graham 1975
	18.83	de Vaucouleurs 1978
	18.58	de Vaucouleurs 1978
AB	18.65	Divan 1976
Supergiants	19.0 ± 0.1	Ardeberg & Maurice 1979
	19.1 ± 0.1	Azzopardi 1982
	19.2	Humphreys 1979
O-stars	18.7[1]	Garmany *et al.* 1987
	19.1[2]	Garmany *et al.* 1987
eclipsing	18.85 ± 0.10	Dworak 1974
binaries	18.62 ± 0.22	Dworak 1974
	18.84	Gaposchkin 1970

Table 2: Review of d.m. evaluations for the SMC. *Notes* 1: ZAMS fitting, 2: spectroscopic parallax.

Further arguments concerning the SMC distance rely on the relative modulus of the two Clouds, which fixes the SMC 0.3-0.5 mag behind the LMC, based on cepheids (Feast 1984; Laney & Stobie 1986), RR-Lyrae variables (Graham 1984) and carbon stars (Blanco, McCarthy & Blanco 1980). Recent work on the zero points of these indicators consistently led to the short scale for the LMC. The revised cepheids d.m. is now 18.47 ± 0.15 (Feast & Walker, 1987); Walker (1985), Blanco & Blanco (1986) and Walker & Mack (1988) derive a similar LMC modulus from the apparent magnitudes of LMC RR-Lyraes.

In the following, the short distance modulus scale is adopted for the SMC. However, due to the complicated geometry of this galaxy, the relative d.m. for each region under examination will be separately derived, using the mean magnitude level of the clump/horizontal branch stars (see Chapter IX).

5 Reddening

The reddening to the outer regions of the SMC has to be evaluated before an interpretation of the CMDs is attempted.

Review

The mean interstellar extinction to SMC objects, as measured by the colour excess $E(B-V)$, has been the subject of numerous investigations.

The interstellar extinction is generally determined either from the reddening of individual stars by means of spectroscopy and photometry, or from background galaxy counts in the direction of the SMC. In the first case, there may be a systematic bias towards low values of the extinction (for magnitude limited samples), since the brightest and presumably less reddened stars, i.e. stars in the near side of the SMC, are oversampled (Israel 1984). An additional source of error is the role of metallicity on the intrinsic colour curves used to derive the colour excesses (Welch *et al.* 1987), which is not yet well-established. In the second case, the derived extinction values are usually overestimated due to count-incompleteness in the crowded star fields, an additional source of error being galaxy clustering. Nonetheless, there is generally good agreement between the values of $E(B-V)$ towards the SMC derived by the different methods.

Part of the reddening to SMC objects is intrinsic to the SMC and part of it is due to the galactic foreground. Table 3 presents a compilation of the values for the colour excess $E(B-V)$ proposed by several authors during the past three decades. The mean value amounts to $E(B-V) = 0.060 \pm 0.022$. The foreground (Galactic) contribution to this value can be determined separately (values followed by an asterisk in Table 3) and is estimated around $E(B-V) = 0.034 \pm 0.017$. Therefore, the interstellar extinction intrinsic to the SMC is $E(B-V) = 0.026 \pm 0.028$.

Differential reddening

An important aspect of the reddening towards the SMC objects is the surface distribution of the interstellar extinction values. Interestingly, there is no evidence of differential reddening across the SMC, with the possible exception of the SMC 'dusty' core. From a study of SMC supergiants, Florsch *et al.* (1981) detected no gradient in interstellar extinction along the axis of the SMC; in particular, they emphasized that the reddening did not appear to increase at the southernmost end of the SMC Bar, where the observed supergiants were systematically fainter than elsewhere in the Bar. Caldwell & Coulson (1985) examined the positional dependence of the reddening within the SMC, based on the individual reddenings of SMC cepheids. They also found no evidence of any large-scale gradient or segregation of values. However, there is evidence of higher absorption in the dusty core of the SMC Bar, defined by the dark nebulae concentration (Hodge 1974).

Adopted reddening value

From all the above it can be safely deduced that a reddening value of $E(B-V) = 0.06$ is applicable over most of the SMC inner regions. Unfortunately, there exist no studies of the interstellar extinction to individual stars in the outer regions of the SMC, which are of interest in the present study. Certainly, the value previously mentioned can serve as an upper limit to the possible colour excess in $B-V$ in the outlying areas of the Cloud. Furthermore, it can be plausibly assumed that these regions lying well away from the main body of the SMC, and outside the outer contour of the SMC neutral hydrogen (HI) distribution (see Mathewson & Ford 1984), are unlikely to be affected by any reddening internal to the SMC. Therefore, the extinction previously mentioned due to the Galactic foreground is a plausible estimate (or at least the lower limit)

Method	E(B-V)	source
cepheids	0.054 ± 0.004	Caldwell & Coulson 1985
	0.078 ± 0.041	Feast 1984
	0.054 ± 0.015	van Genderen 1983
	0.069 ± 0.005	Crampton & Greasley 1982
	0.30^{1}	Madore 1982
Supergiants	0.056 ± 0.014	Azzopardi 1981
	0.08	Harris 1981
	0.019 ± 0.004	McNamara & Feltz 1980
	0.04 ± 0.01*	Lee 1977
	0.07 ± 0.04	Azzopardi & Vigneau 1977
	0.044 ± 0.033*	Azzopardi & Vigneau 1977
	0.024 ± 0.021*	Hesser & Davis-Philip 1976
	0.030 ± 0.004*	Crawford & Snowden 1975
	0.21	Osmer 1973
	0.12 ± 0.01	Butler 1972
	0.06 ± 0.05	Dachs 1970
	0.07 ± 0.05*	Dachs 1970
	0.02	Gascoigne 1969
	0.05	Hodge & Wright 1969
	0.06 ± 0.01	van den Bergh & Hagan 1968
	0.05	Walraven & Walraven 1964
	0.06	Arp 1960
	0.10	Feast *et al.* 1960
	0.01*	Arp 1958
galaxy counts	0–0.03	Burstein & Heiles 1982
other	0.04 ± 0.02	Carney *et al.* 1985.
	$0.033 \pm 0.01*$	Nandy *et al.* 1979
	≥ 0.020*	Mathewson & Ford 1970

Table 3: Review of SMC reddening. The values followed by a (*) refer to Galactic foreground extinction. [1]: this result was strongly criticised by Feast 1984).

for the IS extinction towards the SMC outlying regions, i.e. the colour excess $E(B-V) = 0.034$. On the other hand, the Burstein & Heiles (1982) maps also imply a colour excess of $E(B-V) = 0.0 - 0.03$ mag in the SMC outer regions. A uniform reddening in both Fields 28 and 52 with $E(B-V) = 0.03$ will be adopted.

The colour excess $E(B-R)$ and the reddening A_R can be derived easily using the galactic extinction law of Whitford (1958). As shown by Nandy (1984) the extinction curve for the SMC is identical with that of the Solar Neighbourhood, in the near infrared and optical wavebands. Therefore, using Whitford's law, the values $E(B-R) = 0.045$ and $A_R = 0.07$ are obtained for the SMC outlying regions.
As pointed out previously, there is no evidence of differential reddening in the SMC inner regions, and it would appear reasonable to assume that this is also the case in the outer regions where the intrinsic SMC extinction is negligible. This leaves only the variations of the foreground extinction across the SMC. No such variations larger than 0.01 in $E(B-V)$ are implied by the Burstein and Heiles maps. Unfortunately individual reddenings are available only for stars in the West of the Bar, near the Galactic globular cluster 47TUC.

An independent estimate of the reddening to the stars in the regions examined here can be obtained from the position of the zero-age main sequence (ZAMS) in the colour-magnitude diagrams of the regions for which the location of the ZAMS can be at least approximately defined. Regions 4.1 in Field 28 and 1.1 in Field 52 were the only ones suitable for this purpose; i.e. they have statistically significant numbers of stars apparently on the unevolved main sequence. A straightforward comparison of the observed ZAMS with the theoretically predicted one requires a knowledge of the d.m. and metallicity of the stars involved. Assuming Z=0.004 and Z=0.001 (see Chapter V) and $(m-M)_o = 18.85$ for the Field 28 region and $(m-M)_o = 18.75$ for the Field 52 region (see Chapter IX), the location of the corresponding ZAMS from the revised Yale isochrones (Green, Demarque & King 1987) is demonstrated in Fig.4a&b, superimposed on the CMDs of the two regions. Although the scatter of the observational points is large, a comparison of the outer envelope (bluewards) of the ms stars in the CMDs, presumably defining the ZAMS, with the theoretical locus suggests that there is no significant reddening present in any of the regions examined. However, there is some

indication of a zero-point difference of the order of 0.08mag in $B - R$ between the two Fields, the Field 52 ZAMS apparently being systematically bluer. As will be seen in Chapter V, this effect is also present in the colour of the red giant branch. The effect could be accounted for by a combination of metallicity, reddening and d.m. differences, or a systematic error in the photometric calibration (it lies within the range of possible systematic error stated in the previous Chapter). The problem cannot be resolved without independent measurement of the reddening and metallicities of individual stars in the two Fields.

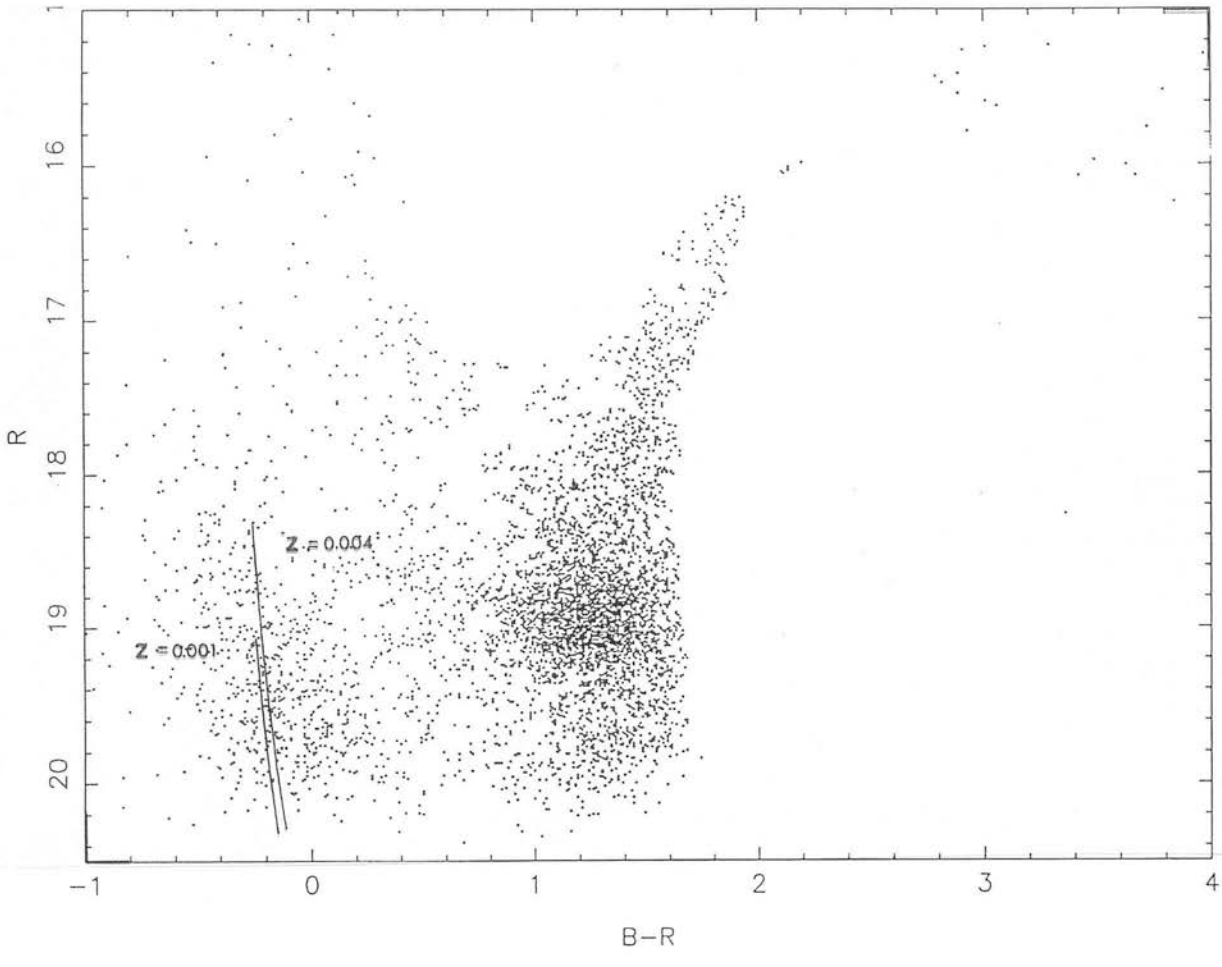

Figure 4a: The CMD of region 41 in Field 28, with the ZAMS locus (from the revised Yale isochrones) superimposed, for two metallicities [Fe/H]=0.001 and 0.004 and for d.m.=18.85.

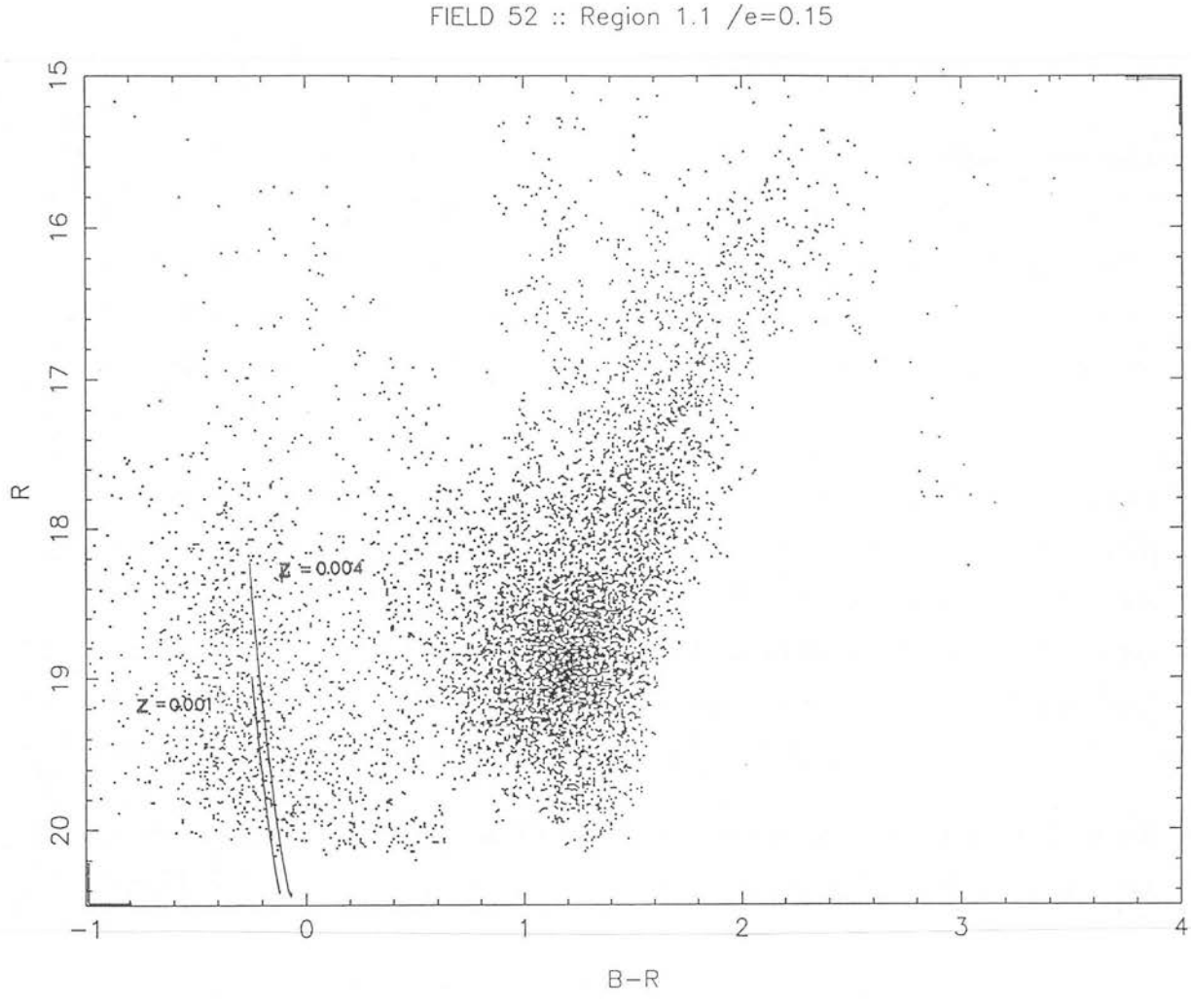

Figure 4b: As in Fig.4a, but for region 11 in Field 52, with a d.m. of 18.75 (see Chapter IX).

1 Introduction

In this Chapter the metal abundance of the SMC populations prevailing in the outer parts of the SMC is discussed. In the absence of any spectrophotometric study of SMC stars in these regions, the metallicity determination has to rely on the characteristics of the colour-magnitude diagram and particularly of the red giant branch, as well as on comparisons with the metallicity of stars and clusters of various ages in other regions of the Cloud.

Section 2 reviews our present knowledge on the metallicity of the SMC; in Section 3 various empirical or semi-empirical methods of metallicity determination from a CMD are briefly described and in Section 4 the most well-established of these methods are applied to the CMD of Chapter IV to estimate the mean metal abundance and the metallicity range in the SMC outer regions. In Section 5 the results are discussed and the positional dependence of metal abundance in the SMC periphery is examined.

Notation: In the following the classical notation for metallicity will be used: $[Fe/H] = \log[n(Fe)/n(H)]_* - \log[n(Fe)/n(H)]_\odot$, where $n(Fe)$ signifies the number density per unit volume of iron atoms, and $n(H)$ of hydrogen atoms; it is however common to consider the iron abundance as representing that of all elements heavier than ^{12}C and therefore [Fe/H] is used as a measure of the 'metallicity' of the star. The subscript $\odot$ denotes solar abundance. This comparison with the solar abundance is also a comparison with that of the Population I stars of the Galaxy. The ratio n(Fe)/n(H) is usually symbolised by Z. In the following the solar abundance will be taken as $Z_\odot = 0.02$.

2 The metal abundance of the SMC: a review

The SMC is deficient in metals with respect to the Galaxy and the LMC. Although this is a well–established fact, the actual chemical composition values for SMC stars of different ages remains largely unexplored.

Few detailed analyses of the metal abundance of individual stars in the SMC exist to date. Table 1 (enlarged and updated version of Table I by Théverin 1987) summarises the existing observational data on the metallicity of various SMC objects, from a variety of methods: high and medium dispersion spectroscopy of individual blue and red supergiants, low resolution spectroscopy of cepheids, giants and RR-Lyrae variables, HII regions, supernova remnants and planetary nebulae, and finally photometric studies –usually through narrow-band filters– of individual stars and star clusters (including integrated photometry and spectroscopy in the latter case). The most accurate method is high dispersion spectroscopy, which has been applied up to now only to supergiants. Metallicities derived from early type supergiants should be given less weight because these stars often show variability and the physics in their atmospheres is not well understood. Only 5 late type supergiants, the study of which does not suffer from similar uncertainties, have been observed at high dispersion to date. The resulting metallicities show a rather large scatter and range from $[Fe/H] = -0.8$ to -0.3 dex. The statistics are obviously very poor, to allow the derivation of any further conclusions on the metallicity scatter in the SMC youngest population. Low resolution spectrophotometry has yielded metallicities for a much wider range of SMC objects, including young PopI-type stars (Cepheids, young RR-Lyraes, late type supergiants), as well as old stars including RR-Lyraes and red giants. In a recent low dispersion spectrographic study of 34 SMC red supergiants, Richtler & Seggewiss (1987; 1988) report a large range of metallicities for these Population I objects, from $[Fe/H] = -0.5$ to -2.0.

It has been generally noticed that metallicities derived photometrically differ systematically from those derived spectroscopically. It must be mentioned here that according to Geisler (1984; 1986; also Nissen *et al.* 1985; Leep *et al.* 1987; Hesser *et al.* 1987) the relatively abundant elements such as Ne, Mg, Si and S are significantly enhanced relative to Fe in metal deficient stars (like Pop.II stars in the Galaxy and SMC stars).

Objects	[Fe/H]	age	method	source
AB supergiants				
HD7583	-1.0	vy	1	Przybylski 1972
HD7583	-0.3 ± 0.2	vy	1	Wolf 1972
HD5045	≤ -0.6	vy	1	Osmer 1973
HD7099	≤ -0.6	vy	1	Osmer 1973
HD7583	-1.0	vy	1	Przybylski 1972
FG supergiants				
AZV-369	-0.4 ± 0.2	vy	1	Foy 1981
AZV-369	-0.7 ± 0.2	vy	1	Spite & Spite 1987
AZV-121	-0.4 ± 0.2	vy	1	Théverin & Foy 1986
AZV-140	-0.8 ± 0.2	vy	1	Spite & Spite 1987
AZV-197	-0.6 ± 0.24	vy	1	Spite & Spite 1987
	-0.6 ± 0.1	vy	2	Smith 1980
	[-0.5—2.0]	vy	2	Richtler & Seggewiss 1987
Cepheids				
	-0.5	y	2′	Harris 1981
	-0.6	y	2′	Pel 1984
RR-Lyraes				
	-1.8 ± 0.2	$\geq$ 10Gyr	2	Butler *et al.* 1982

Table 1: Review of metallicity determinations in the SMC. *Column 3* gives the age of the objects: vy=younger than a few 10^7 yr; y=younger than a few 10^8yr. *Column 4*: 1: high and medium dipersion spectroscopy, 2:low dipersion spectroscopy and photometry(2′), 3: isochrone fitting, 4: from CMD metallicity indicators, 5:integrated photometry.

Objects	[Fe/H]	age	method	source
Red giants				
	-1.63 ± 0.31		2,3	Suntzeff *et al.* 1986
field ms stars				
	-1.7	10Gyr	3	Stryker *et al* 1985
	-0.79		4	Bolte 1987
Star clusters				
NGC419	≥ -1.0	1.2 ± 0.5 Gyr	5	Hardy & Durand 1984
NGC416	≥ -1.0	2.5 ± 0.7 Gyr	5	Hardy & Durand 1984
L113	-1.4	5 Gyr	4	Mould *et al* 1984
Kron 3	-1.3 ± 0.3	8 Gyr	2,4	Rich *et al.* 1984
NGC330	-1.4	12×10^{6}*	1	Spite & Spite 1987
	-1.8 ± 0.2		2	Richtler & Nelles 1983
NGC411	-0.9 ± 0.3	1.8 ± 0.3 Gyr	4	Da Costa & Mould 1986
L1	-1.2 ± 0.1	11 ± 1 Gyr	4	Olszewski *et al.* 1987
NGC121	-1.4 ± 0.1	12 ± 2 Gyr	2,4	Stryker *et al.* 1985
NGC152	-0.76	0.8 Gyr	3	Hodge 1981

Table 1: continued. Note:* from Carney *et al.* 1985.

Thus one should not equate [Fe/H], which is measured spectroscopically, with the overall metal abundance [M/H], which is derived from the photometric indices, for such stars. Such a possibility would tend to reconcile the discrepancy previously mentioned.

Although more data are needed to improve the statistics, it seems plausible from the accumulated evidence that the metal abundance in the SMC –among objects of similar ages– may not be uniform. As Richtler and Seggewiss put it 'the broad metallicity distribution of young stars contradicts a simple evolutionary scenario and either invokes infall processes (see Chapter VIII) or requires local mixing'.

The metal abundance shows a systematic trend towards lower values as the age of the objects studied increases, reaching the value of $[Fe/H] = -1.8$ for RR-Lyraes (Butler 1982 *et al.*). The change of metallicity among groups of different ages yields information about the chemical evolution history of the SMC. The chemical enrichment history of the SMC will be further discussed in Chapter VIII.

3 Methods of metallicity determination from CMDs

A number of properties of the colour magnitude diagram of a coeval population (such as a star cluster) can be used as abundance indicators. It is well known from studies of globular clusters CMDs, that the Red Giant Branch (RGB) becomes redder and fainter in (R, B-R) as [Fe/H] increases. This effect can be understood theoretically in a family of old stellar populations in which age and helium abundance are held fixed and only metallicity is varied. As emphasised by Sandage (1982), the *photospheric* parameter [Fe/H] is related to the metal abundance that determines the envelope opacity of a star. Evolved models (e.g. Sweigart & Gross 1978) show that $(B-V)_{o,g}$ (and $\Delta V_{1.4}$) are sensitive functions of the mix of metals that determines the envelope opacity. Given that $(B-V)_{o,g}$ correlates well with $[Fe/H]_{photospheric}$, it follows that this parameter measures in some gross way the required Z (interior).
However, a quantitative theoretical prediction of the dependence would depend on the rather arbitrarily chosen value of the 'mixing length' parameter, which decides the extent of the convective envelope, which in turn determines the temperature and hence the colour of the red giant.

Several, not entirely independent from each other, methods have been proposed to calibrate the RGB colour and morphology as a function of metallicity: the slope, S, of the line joining the HB/RGB intersection point with the point on the RGB with $V = V_{HB} + 2.5$; the intrinsic (dereddened) colour $(B-V)_{o,g}$, of the subgiant branch at the level of the HB; the magnitude difference in V, $\Delta V_{1.4}$, between the HB level and the RGB at $(B-V)_o = 1.4$. In practice, the calibration of these quantities is carried out using clusters of 'known' abundance. There are some difficulties associated with the use of these indicators. Any observed colour, such as $(B-V)_g$, must be corrected for reddening, which has to be independently determined; a sparsity of stars on the RGB may affect the determination of some of the indicators.

In the following, the most recently calibrated metallicity indicators on a CMD are described.

(i) The colour of the RGB at the magnitude of the core helium burning stars, $(B-V)_{o,g}$: (Notation: the subscript 'o' signifies dereddened values) It has been known since the early 1950s that the giant branch colour at the horizontal branch level varies with [Fe/H]. A calibration by Butler (1975) gave $(B-V)_{o,g} = 0.139[Fe/H]_{Butler} + 0.97$, which agrees approximately with the calculations of Bell & Gustaffson (1975) which give $\partial(B-V)_{o,g}/\partial[Fe/H] = 0.23$, based on the RGB models of Rood (1972). Sandage (1982) gives the correlation $(B-V)_{o,g} = 0.180[Fe/H] + 1.10$ (1) for Galactic globular clusters. The dependence is well determined and shows very little scatter. Sandage's result agrees well with Butler's calibration if the zero-point difference between the two metallicity scales is taken into account.
In the (R, B–R) plane, eq.(1) can be written as $(B-R)_{o,g} = 0.29[Fe/H] + 1.72$ (2), using transformations from the (V, B-V) to the (R, B-R) plane from the model atmospheres of Bell & Gustaffson (1978).

The application of this calibration of the metallicity indicator $(B-V)_{o,g}$, to Magellanic Cloud clusters (or field regions) was criticised by Gustafsson, Bell & Hejlesen (1977), since it has been based on the CMDs of Galactic globular clusters. They argued that this sort of relation should only be applicable to stars of similar ages, or more precisely of similar masses to those in Galactic globular clusters. However, as pointed out by Mateo and Hodge (1985), eq.(1) is valid for clusters (or populations) older than

$3 - 5 \times 10^8$ yr, since in these cases $(B-V)_{o,g}$ approaches a constant value with increasing age and therefore any horizontal displacement of the RGB base for ages older than 3×10^8 yr is primarily due to variations in [Fe/H]. As shown from a grid of theoretical RGB models by Vandenbergh (1984), the $(B-V)_{o,g}$ depends only on the HB absolute visual magnitude and metallicity and not on the helium abundance or on the CNO/Fe ratio (which is known to affect the absolute visual magnitude of the main sequence turnoff point). Another essential assumption made when applying eq.(1) is that Sandage's globular cluster calibration correctly describes this displacement $\delta(B-V)_{o,g}$ in terms of [Fe/H]. This assumption is forced on us due to the lack of any observational relation for young populations.

Based on the same principle is the procedure followed by Da Costa, Mould & Crawford (1985; hereafter DMC) for the determination of the metallicity of Magellanic Cloud clusters. They used the models of Janes & Demarque (1983; hereafter JD) to determine the differential relation $\partial(B-V)_{o,g}/\partial[Fe/H] = 0.32$ (3), or, using the same model-atmospheres transformations as before, $\partial(B-R)_{o,g}/\partial[Fe/H] = 0.5$ (4). This relation can be used to find the metallicity of a cluster (or of a field population) relative to any Galactic cluster (of similar age, or of any age if the object is older than $3 - 5 \times 10^8 yr$, as previously stated) with a known metallicity.

(ii) The metallicity dependence of the height $\Delta V_{1.4}$ of the RGB: The secondary metallicity indicator $\Delta V_{1.4}$ correlates very closely with decreasing metal abundance (Sandage & Wallerstein 1960). Sandage (1982) gave an empirical law for the correlation (in his Fig.2(a)), which can be simply expressed as
$\Delta V_{1.4} = -0.81[Fe/H] + 1.32$ (5).

(iii) The slope parameter S: An alternative to method (ii) is the slope parameter S (Hartwick 1968), which is independent of reddening and of the colour of the RGB. However, as pointed out recently by Bell & Gustaffson (1983), the calibration of the S–metallicity relation shows large scatter, mainly due to the difficulty of determining the intersection of the HB and the subgiant branch, aggravated by the common paucity of stars in the bright end of the RGB.

Bell & Gustafsson (1983) presented a calibration of the various metallicity indicators

based on CMDs of Galactic globular clusters. They concluded that ΔV and $(B-V)_{o,g}$ are the more useful tools for giving the metallicity for a cluster. They fitted non-linear curves to the calibration data, however their claimed deviation from linearity is rather small and the proposed curvature was determined essentially by two points; it was therefore not considered essential to use these non-linear calibrations in the following.

(iv) The parameter $(B-V)_{-1}$: Hodge (1982) proposed a semiempirical relation, based on a composite of various theoretical models (Kinahan & Härm 1975; Ciardullo & Demarque 1977; Gustaffson *et al* 1977; Flower *et al* 1980), which were scaled and zero-pointed from the characteristics of well-defined CMDs of Galactic globular clusters. The parameters used were the reddening corrected colour of the RGB at $M_V = -1$, $(B-V)_{-1}$, and the absolute visual magnitude of the ms 'top', MS_L (which is easier to determine on a cluster CMD than the ms turnoff; it is the usually well defined limit of the thick population of blue stars above the ms). The three parameters (MS_L, $(B-V)_{-1}$, Z) are interdependent, with $(B-V)_{-1}$ being strongly dependent on Z, and MS_L moderately dependent on it. Fig.1 is a reproduction of Hodge's semiempirical model.

(v) Grids of theoretical isochrones: Interpolation of the positions unknown metallicity giants within the corresponding RGB grid taken either from theoretical isochrones, or from loci of well studied globular clusters, can yield an estimate of the metallicity of a given giant. The method, recently adopted by Suntzeff *et al.* (1986) suffers from the following sources of error:

1. The range of age among the stars (in the case of a non-coeval CMD)
2. The uncertainties inherent in the interpolation procedure
3. The uncertainty as to whether a given star is on the first ascent GB, or on the asymptotic GB.

(vi) Other metallicity indicators: Two other approaches to the determination of the metal abundance from the CMD of a cluster (or a coeval population), which are not yet well established, are the following: The first, put forward by Dickens & Sweigart (1978), relies on discontinuities on the RGB luminosity function (caused when the H-shell passes through the composition discontinuity produced by the deep inward penetration of the convective envelope during the subgiant branch phase) and is

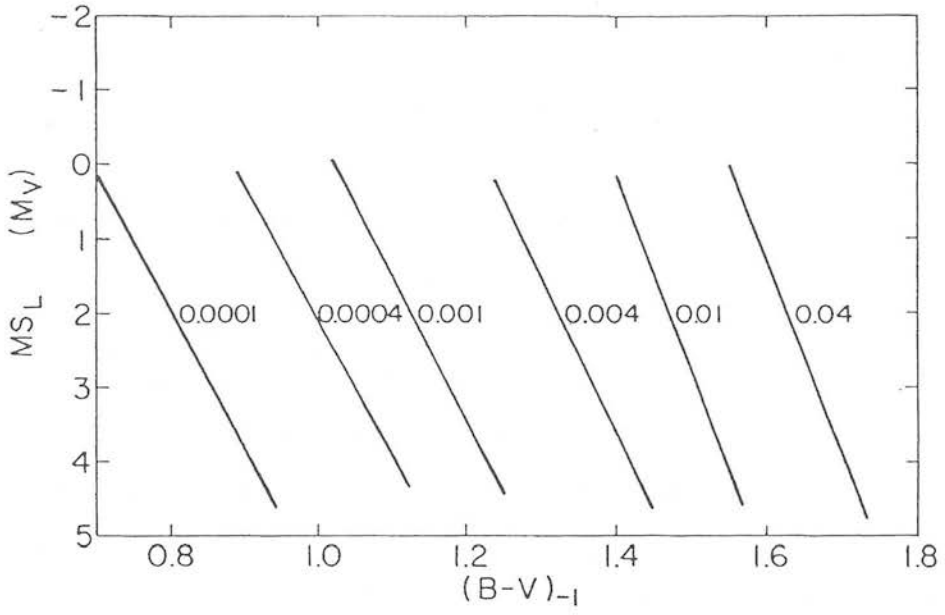

Figure 1: The Hodge (1982) semiempirical model for the determination of the metallicity of a coeval population.

applicable only to well observed populous old clusters and obviously not to non-coeval populations, because of loss of contrast from the superposition of different ages. The second, proposed by Flower, Jones & Clemson (1983), correlates the metallicity of intermediate-age clusters to the magnitude difference between the faintest core-helium burning red giants and the brightest ms stars. However, the age sensitivity of this metallicity indicator must be important, and therefore it is inapplicable for the case of a mixture of noncoeval populations of not well known ages. The large scatter of the true d.m. among the stars further invalidates the method.

4 Metal abundance in the SMC outer regions

The empirical methods of metal abundance determination described in the previous section are based on the CMDs of *star clusters*. The application of these methods to non-coeval populations, such as those presumably comprising the outer parts of the SMC, can only yield upper and lower limits for the metal abundance range. The interpretation of the results can be further complicated by the presence of a wide –and not *a priori* known– range of ages in the stellar fields studied, as well as the claimed significant line-of-sight depth of the SMC (see Chapter IX). An attempt was made to apply to the SMC field CMD all the well-established metallicity indicators reviewed in the previous section. In all cases, in order to improve the statistics and the accuracy of the evaluation of the metallicity indicator, the 'coarse' grid of CMDs was used, i.e. each CMD corresponds to an area of 0.88 square degrees on the sky.

Application of the metallicity indicator (i): The colour of the RG/subgiant branch at the level of the HB/clump, $(B-R)_g$, was estimated for each of the CMDs in Appendix A, and corrected for reddening with the use of the colour excess estimate derived in Chapter IV. The determination of $(B-R)_{o,g}$, though straightforward, suffers from several uncertainties: There is a large scatter in the RG/subgiant branch caused by a combination of (a) the observational errors in R and $B-R$, (b) the statistical removal of the back/foreground objects from the SMC CMDs, the effect being most noticeable in the more sparsely populated bright end of the RGB (which however is not critical for the determination of $(B-R)_g$), (c) the actual range in metallicity and age among the

SMC field stars, and (d) the intrinsic range in the distance modulus, especially in Field 52 (Chapter IX).

The 'clumpiness' of the horizontal branch (Chapter VI), which appears almost centred on the RG locus, obliges us to interpolate the value of $(B-R)_g$ from the colours of the brighter RGB and fainter subgiant branch. The induced uncertainty is more important in Field 52 where the magnitude range of the clump giants is significantly increased. In Table 2 the estimated values of $(B-R)_g$ accompanied by the corresponding dereddened values $(B-R)_{o,g}$ are presented. The mean value is given in each case, followed by the upper and lower limits within which $(B-R)_{o,g}$ lies (not the standard error). The bluest limit of these estimates may have been overestimated (i.e. too blue) because of the inclusion of asymptotic GB stars, which cannot be separated from first ascent red giants, for which the metallicity indicators are calibrated. This eventually leads to an underestimate of the low metallicity limit and the deduced mean metal abundance denotes a somewhat metal–poorer population. A quantification of the effect will not be attempted here. The values for the metal abundance given in columns 4 & 5 of Table 2 were derived using Sandage's calibration (eq.(2)) and the JD/DMC calibration (eq.(4)) respectively. In the latter case the well-observed SMC cluster NGC121 was used as the comparison cluster. The metallicity of NGC121 is $[Fe/H] = -1.4 \pm 0.1$, derived from a multiplicity of methods and $(B-R)_{o,g}^{N121} = 1.28$ (Stryker *et al.* 1985). The applicability of eq.(2) & (4) is safeguarded by the absence of any significant populations younger than 3×10^8 yr, in the regions of interest (see Chapter VI).

Both methods give identical results within the errors. There is a small but systematic difference between the values of metal abundance in Field 28 & 52. This difference arises from an offset of 0.07 in $(B-R)_g$ between the two Fields, which is of the same magnitude and sign as the effect noticed in the reddening evaluation, in Chapter IV. In both cases a zero point difference in the photographic photometry would be the most straightforward explanation. However, a genuine metallicity difference cannot be excluded at this stage.

Application of the metallicity indicator (ii): The application of this method suffers from larger uncertainties than the previous one, because it involves the less well-populated bright end of the RGB, which can be more seriously affected by the back/foreground removal procedure. The calibrated indicator $\Delta V_{1.4}$ was transformed to its equivalent

Region	$(B-R)_{o,g}$	$[Fe/H]_{Sandage}$	$[Fe/H]_{JD/DMC}$
Field 28			
41	1.35 ± 0.20	-1.27 ± 0.69	-1.26 ± 0.40
31	1.32 ± 0.21	-1.38 ± 0.72	-1.32 ± 0.42
51	1.39 ± 0.20	-1.14 ± 0.69	-1.18 ± 0.40
32	1.35 ± 0.20	-1.27 ± 0.69:	-1.26 ± 0.40:
52	1.44 ± 0.21:	-0.96 ± 0.72:	-1.08 ± 0.42:
21	1.30 ± 0.17:	-1.45 ± 0.59:	-1.36 ± 0.34:
42	1.30 ± 0.20:	-1.45 ± 0.69:	-1.36 ± 0.40:
411	1.34 ± 0.20	-1.31 ± 0.69	-1.28 ± 0.40
Field 52			
11	1.32 ± 0.23	-1.38 ± 0.79	-1.32 ± 0.46
12	1.28 ± 0.20	-1.52 ± 0.69	-1.40 ± 0.40
13	1.31 ± 0.20:	-1.41 ± 0.69:	-1.34 ± 0.40
21	1.26 ± 0.17	-1.58 ± 0.59	-1.44 ± 0.34
22	1.25 ± 0.17	-1.62 ± 0.59	-1.46 ± 0.34
23	1.25 ± 0.17:	-1.62 ± 0.17:	-1.46 ± 0.34:
31	1.30 ± 0.19	-1.45 ± 0.65	-1.36 ± 0.34
32	1.27 ± 0.19	-1.55 ± 0.65	-1.42 ± 0.38
113	1.34 ± 0.20	-1.31 ± 0.69	-1.28 ± 0.40

Table 2: Determination of the metal abundance range in the outer regions of the SMC. *Column 1* qives the identification number of each region (Chapter IV); *Column 2* gives the dereddened value of $(B-R)_{o,g}$; *Columns 3 and 4*, the derived mean metal abundance using the Sandage calibration and the JD/DMC calibration, respectively. The values following the $\pm$ sign denote lower and upper limits (not errors).

$\Delta R_{2.22}$ in the (R, B-R) plane. The reddening corrected quantity $\Delta R_{2.26}$ was evaluated from the CMDs of the regions 5.1 in Field 28, and 1.1 ,1.2 & 3.1 in Field 52. These are the only CMDs for which $\Delta R_{2.26}$ can be derived without extrapolation. Subsequently, ΔR was transformed to the equivalent ΔV and eq.(5) was applied. The resulting estimates of [Fe/H] appear in Table 4. The indicator $\Delta R_{2.22}$ was also independently calibrated using the (R, B-R) CMDs of well observed Magellanic Cloud clusters with 'known' metallicities (Table 3). All of these clusters have ages greater than 0.9 Gyr and are therefore suitable for the calibration. The resulting calibration curve appears in Fig.2 and the corresponding relation can be expressed as:
$\Delta R_{2.22} = -0.61[Fe/H] + 2.3$ (6). However, this relation shows large scatter due to the small number of available data. The corresponding estimates for [Fe/H] appear in Table 3 (column 4).

Both calibrations (5) & (6) yield similar results for [Fe/H], which are comparable with those derived from the application of indicator (i), with the exception of the apparently higher metallicity derived for the Field 52 regions. This discrepancy could be accounted for by a combination of the poor statistics in both the number of regions examined and the number of stars at the bright end of the RGB, which are additionally scattered in Field 52 due to geometrical effects.

Application of the indicator (iii): Although the application of this method involves large uncertainties as already pointed out (section 3), it is independent of zero-point, or, reddening discrepancies. Unfortunately, in the present case the determination of S would require significant extrapolation of the RGB towards brighter and redder magnitudes, and was not attempted.

Application of the indicator (iv): This method requires the evaluation of both MS_L and of $(B-V)_{-1}$. In the case of the noncoeval CMD studied here, only an estimate of the magnitude of the ms 'top' for the youngest population present in each region can be obtained. The transformation of $MS_L(V)$ and $(B-V)_{-1}$ to the $(R, B-R)$ plane is accomplished as in the previous cases, by using the Bell & Gustaffson (1978) model atmospheres. The equivalence $(B-V)_{-1} \Leftrightarrow (B-R)_{-1.6}$ was used as an initial value, which was subsequently iteratively corrected for in each case. The resulting estimates for $(B-V)_{-1}$ and the lower limit of $MS_L(V)$ for the youngest populations are given in

Cluster	$\Delta R_{2.26}$	$[Fe/H]$	τ_9	source
LMC				
NGC1777	2.70	-0.7 ± 0.5	0.9	Mateo & Hodge 1985
NGC2213	2.60	-0.6 ± 0.2	1.3	Da Costa *et al.* 1985
H4	2.60	-1.0 ± 0.1	2.5	Mateo & Hodge 1986
SMC				
NGC411	2.60	-0.9 ± 0.3	1.8	Da Costa & Mould 1986
NGC121	3.00	-1.4 ± 0.1	12	Stryker *et al.* 1985
L113	2.80	-1.4 ± 0.2	5	Mould *et al.* 1984
Kron3	2.99	-1.2 ± 0.2	8	Rich *et al.* 1984

Table 3: Calibration of the indicator (iii) using Magellanic Cloud clusters. *Column 4* gives the age of each cluster in billion years.

Region	$\Delta R^o{}_{2.26}$	$[Fe/H]_1$	$[Fe/H]_2$
Field 28			
51	3.1 ± 0.2	-1.23 ± 0.18	-1.33
Field 52			
11	3.0 ± 0.3	-1.04 ± 0.27	-1.08
12	3.0 ± 0.3	-1.04 ± 0.27	-1.08
31	2.9 ± 0.3	-0.97 ± 0.30	-1.05

Table 4: Metal abundance from indicator (ii). *Column 1* gives the identification number for the regions studied; *Column 2* is the estimated value of $\Delta R_{2.26}$ after taking into account the reddening; *Column 3* gives the metal abundance derived from eq.(5) and *Column 4* gives the metal abundance as estimated from the calibration in Fig.2.

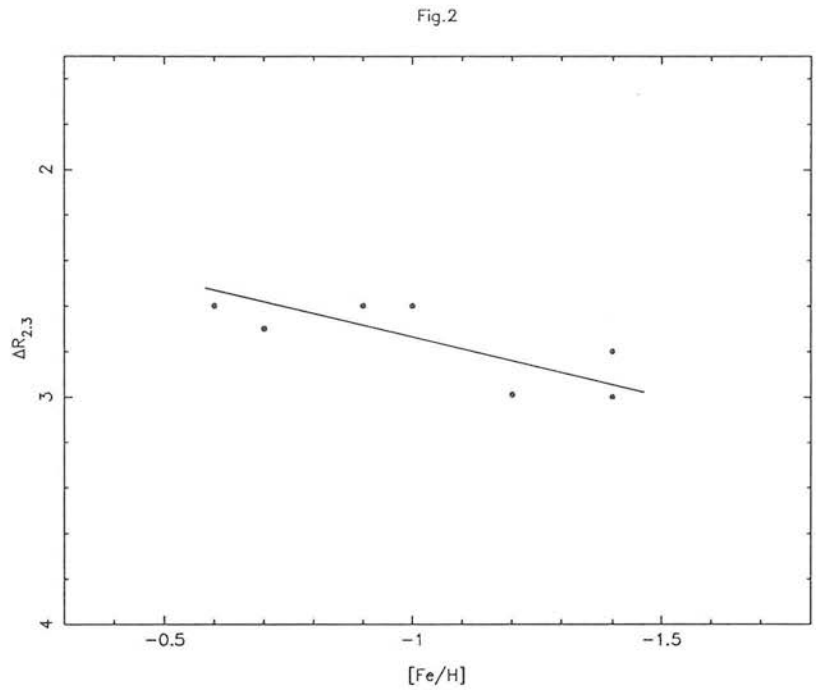

Figure 2: Calibration of the metallicity indicator $\Delta V_{1.4}$ transformed into the (R, B–R) plane (data from Table 3).

Table 5. The apparent magnitude of the ms 'top' is transformed to its equivalent absolute value, using the d.m. determinations of Chapter IX. Using Fig.1, the corresponding upper metallicity limit for the youngest population in each region was derived. Only the regions nearest to the SMC main body were included. As will be seen in Chapter VI, the decrease of $MS_L(R)$ (and of its equivalent $MS_L(V)$) with projected distance from the SMC centre, does not necessarily signify an increase of the age of the younger populations present in the region. Therefore the values of the metal abundance given on Table 5 should not be interpreted necessarily as decreasing with distance. It is more useful to derive the overall metal abundance range: In both Fields 28 and 52, the $(B-V)_{-1}$ is in the range 1.1 ± 0.1. This sets the upper and lower limit to the possible metal abundance for an age range from 0.3 to 12 Gyr known to be present in these fields (see Chapter VI). The corresponding $MS_L(M_V)$ would be in the range $\sim 0. - \sim 3.$ respectively (from the Yale isochrones). Then, according to the calibration in Fig.1 the metallicity of the younger population of $\sim 3 \times 10^8$ yr is ~ -0.7 and of an old population $\sim 10 - 12$ Gyr, around -1.8. These limits agree very well with the results from the application of the other metallicity indicators, given in Table 1.

5 Discussion of the metallicity of the SMC outlying regions

Mean metallicity and metallicity range:

In the absence of detailed metallicity studies of field stars in the outer regions of the SMC considered here, the colour of the RGB was used in the previous Section to derive the range in metal abundance and to investigate its positional dependence across the Cloud. All methods applied yielded comparable values for [Fe/H]:

In Field 28, $[Fe/H] = -1.26 \pm 0.36$, and

in Field 52, $[Fe/H] = -1.30 \pm 0.35$ (8).

The values following the $\pm$ signs denote the maximum range in metallicity as derived from the CMDs and not the standard deviation around the mean metallicity. The range indicated includes the scatter induced by the observational errors in the photometry and the back/foreground removal procedure, the uncertainties of the calibration of the

Region	$(B-R)_{-1.6}$	$(B-V)_{-1}$	$R_{max}(MS_L)$	M_V	$[Fe/H]_{min,y}$
Field 28					
51	1.72 ± 0.16	1.11 ± 0.16	18.2	-0.5	-0.90
41	1.66 ± 0.15	1.07 ± 0.10	18.2	-0.5	-0.85
31	1.64 ± 0.17	1.06 ± 0.11	18.2	-0.5	-0.80
Field 52					
11	1.78 ± 0.20	1.15 ± 0.13	17.8	-0.9	-0.70
12	1.67 ± 0.20	1.08 ± 0.13	18.8	0.13	-0.90
21	1.70 ± 0.20	1.10 ± 0.13	18.8	0.13	-0.90
22	1.62 ± 0.17	1.04 ± 0.11	18.8	0.18	-1.30
31	1.72 ± 0.22	1.11 ± 0.14	19.0	0.27	-0.80

Table 5: Results from the application of the metallicity indicator (iv). *Column 4* gives the apparent magnitude of the top of the main-sequence, after transforming from the (R, B–R) to the (V, B–V) plane using model atmospheres. *Column 5* gives the corresponding absolute magnitudes using the d.m. derived in Chapter IX (averaged for the coarser-grid regions, and corrected for the V passband). *Column 6* gives the metallicity values derived by interpolation from Fig.1, using the data in columns 3 and 5. These values are lower limits of the metallicity of the younger populations present in each area.

metallicity indicators themselves and finally the range in distant modulus and age among the stars used to estimate the values of the metallicity indicators.

Therefore the metal abundance in the areas studied lies between ~ -0.9 and ~ -1.7, which agrees very well with the metallicity range of stars and clusters in the SMC older than several 10^8 yr of age (Table 1).

Suntzeff *et al.* (1986) reported a mean metallicity of $[Fe/H] = -1.60 \pm 0.32$ (s.d.) for a proper motion selected sample of SMC 'halo' giants located in a field near the SMC cluster NGC121 (dominant age larger than 10 Gyr, according to Stryker *et al.* 1985). They claimed that the intrinsic metallicity spread is $\sim$ 0.25dex, after removing the contribution of the observational errors and the possible age range among the stars. Although no attempt is made to derive the 'true' metallicity range from the present data, due to several unquantifiable factors previously mentioned, the metallicity range reported here does not contradict the conclusions of Suntzeff *et al.*.

The positional dependence of metallicity:

Although it has been debated that there is significant scatter of the metal abundance –the source of which is yet to be clarified– among the young, population I objects of the SMC (section 2), there is no evidence of a *positional* metal abundance gradient across the SMC analogous to that found in spiral galaxies. For example, Harris (1981) based on the metal abundances of cepheid variables, found no correlation between abundance and location in the SMC; Pagel and his collaborators (1985) reached the same conclusion from a study of HII regions in the SMC. However, little is known about the positional dependence of metallicity among the older populations of the SMC, extending to larger distances from the SMC centre. Blanco & McCarthy (1983) found evidence for a possible *increase* of metallicity towards the periphery of the SMC, based on the surface distribution of the ratio of the numbers of carbon stars to M giants; as they emphasize 'this effect, if true, is valid only for the epoch when the red giants were formed (i.e. a few Gyrs ago) and not necessarily at the present time', which is -however- the case in the study by Pagel *et al.* just mentioned. However, the C/M effect can be also attributed to a mean age gradient (see Chapter VII).

On the basis of the present data it is not possible to distinguish between the metal-

licities of different age-groups. Therefore, a positional abundance dependence would refer to the mean metallicity of all age-groups present and would be the result of the combination of the 'age-mixture' at different distances from the SMC central part, the chemical evolution history and finally any original chemical composition inhomogeneities in the SMC. Fig.3 a&b show the $< [Fe/H] >$ as a function of radial distance, r_{oc}, from the SMC optical centre, for Field 28 and 52 respectively. Because the SMC does not possess spherical symmetry, a better representation of the situation can be achieved by replacing r_{oc} with the total number of SMC stars per square degree in each region (Fig.3 c&d). It can be concluded from these figures that **there is no positional dependence of the estimated mean metallicity** within the errors of measurement, in either Field, for $r_{oc} \geq 2.6 Kpc$. In Field 52 the regions with $r_{oc} < 2.6 kpc$ appear to have marginally higher mean metallicities. As will be seen in the following Chapter, this can be attributed to the presence of a significant young population ($\tau < 4 \times 10^8$ yr), which according to Table 1 and the conclusions of the previous section is more metal rich.

The implications of the present conclusions for the chemical evolution of the SMC will be discussed in the next chapter, in connection with the age distribution of the stars in these outer regions of the SMC.

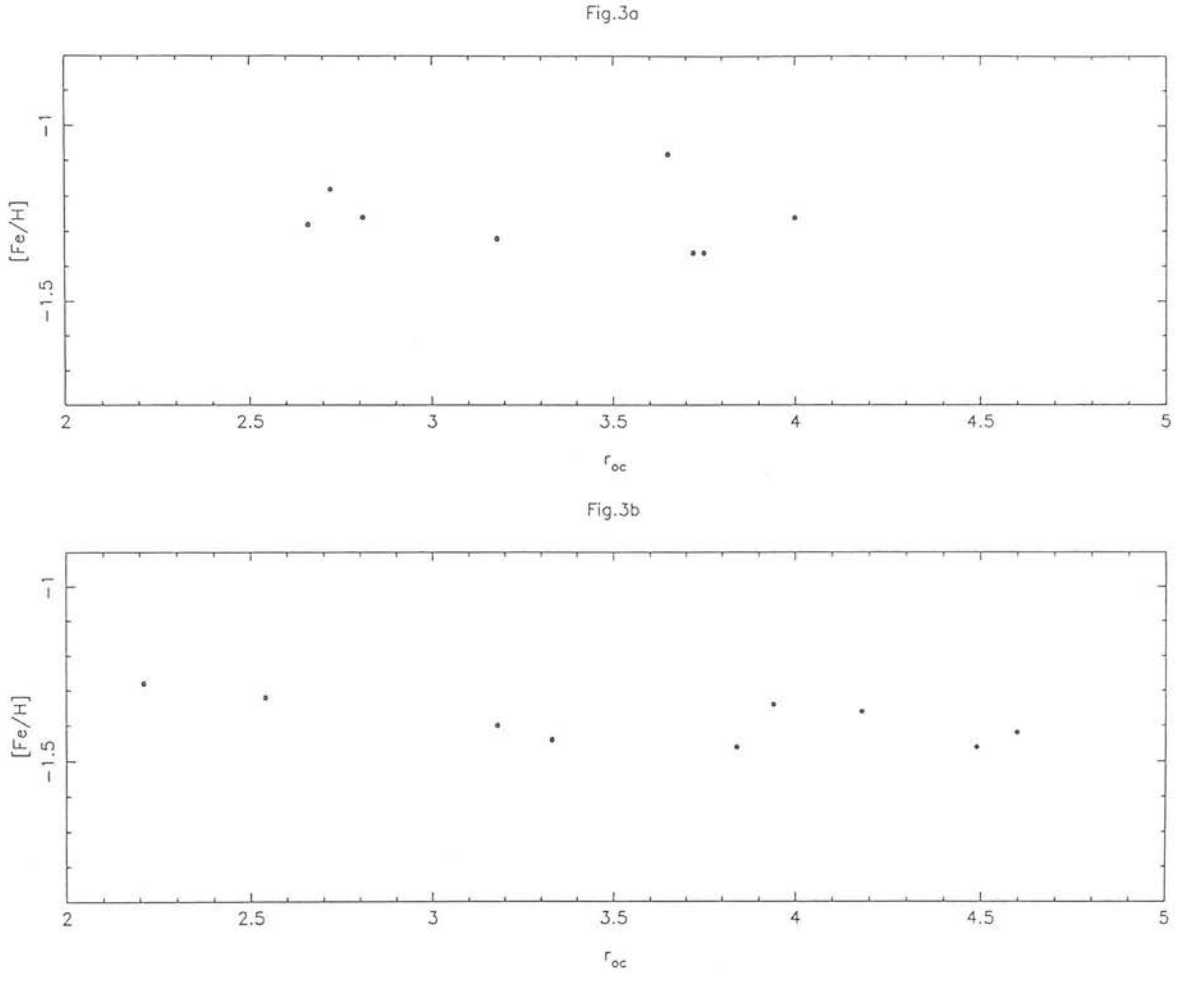

Figure 3: The radial distribution of the derived mean metallicity with respect to the optical centre of the SMC: (a) in Field 28, (b) in Field 52.

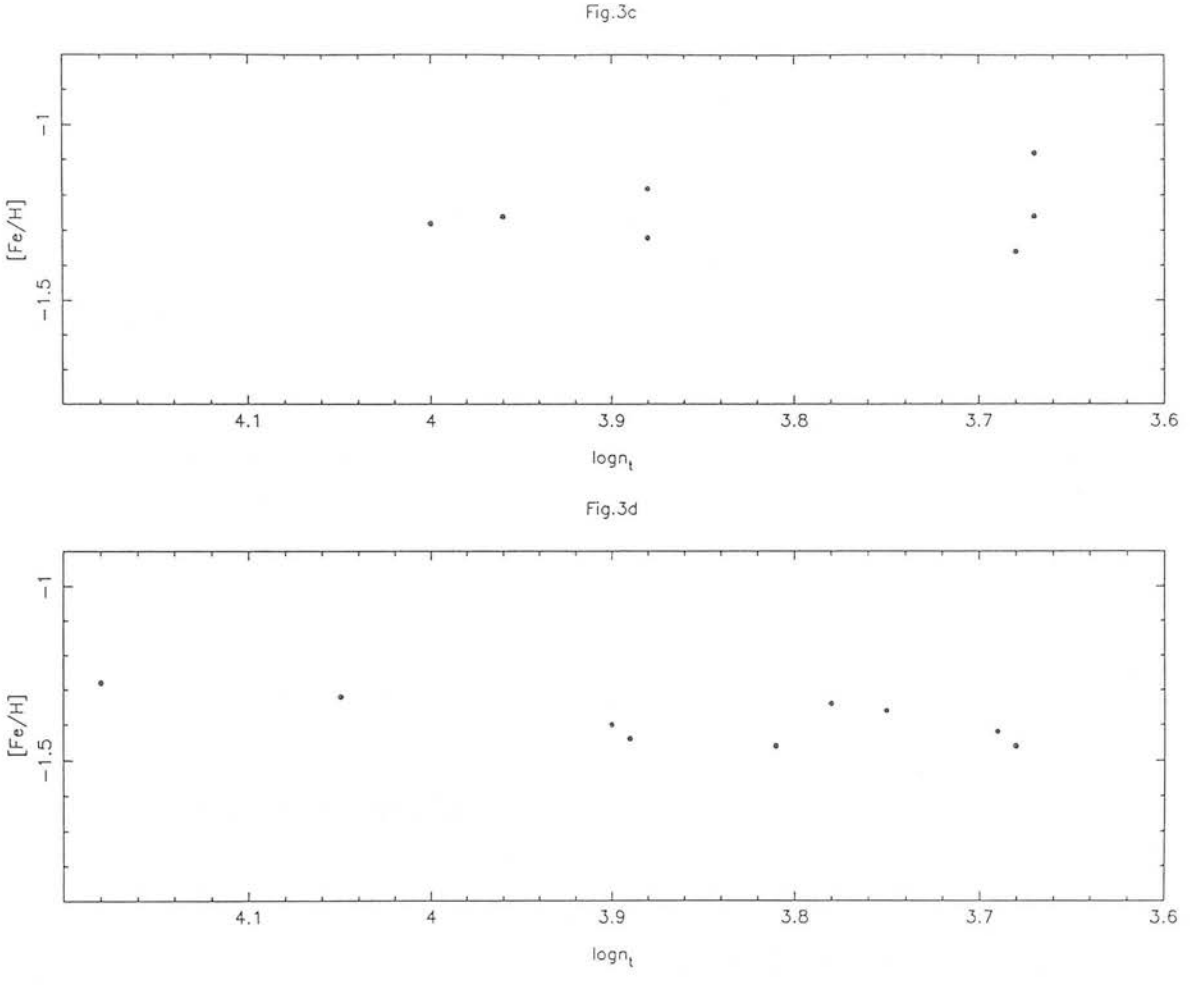

Figure 3: continued. The distribution of the derived mean metallicity as a function of the logarithm of the number star density in each region: (c) in F28, (d) in F52.

1 Introduction

In this chapter, the population synthesis of the outer regions of the SMC is examined on the basis of the CMDs constructed in Chapter IV. The interpretation –in terms of age– of the CMD of a non-coeval population is far from trivial. In the following, several characeristic features of the CMDs are studied for this purpose. The relative contribution of stars of different ages will be examined, along with their radial distribution with respect to the SMC central parts.

In Section 2 the main sequence stars detected in the CMDs are studied; in Section 3 the horizontal branch stars and in Section 4 the subgiant branch stars. Finally, in Section 5 the possible existence of blue horizontal branch stars in the field is discussed.

2 The main sequence stars

2.1 Main sequence chronology

The characteristics of the main sequence (hereafter ms) of a star cluster (or a coeval population in general) are often used to derive the age of the cluster. The ms–chronology is one of the principal tools of the study of stellar populations and it is achieved by comparing the observed colour-magnitude diagram with theoretical isochrones constructed from the evolutionary tracks of individual stars. In particular the location of the ms turnoff point (i.e. the region in the Hertzsprung–Russell (HR) diagram where the stars deviate from their core-hydrogen-burning locus) is a direct measure of the age. From consideration of the luminosity functions associated with such isochrones Da Costa, Mould & Crawford (1985) suggested that the best feature to use to date clusters (or coeval populations) in the age range of a few Gyr is the 'tip' of the ms, i.e. the point on the isochrone where (rapid) evolution to the red begins. The reason for this is that the

blueward jump in the isochrones at the point of core-H-exhaustion makes the definition of the turnoff difficult for these ages. For older populations a better procedure is to try to fit the shape of the entire locus, between the slightly evolved ms stars and the 'subgiant branch' (Hodge 1983). Hodge has produced a self-consistent age-calibration system based on ms characteristics, by interpolating between various sets of theoretical isochrones.

In practice, several uncertainties affect this method of age determination: (i) the observational errors in the magnitudes and colou rs, (ii) errors in the adopted values of the distance modulus, the reddening and metal abundance, (iii) uncertainties in the theoretical models, e.g. in stellar interior opacities, in the simple convection theory usually employed and in the neutrino production (VandenBergh 1982) and finally (iv) errors arising from the transformations between the theoretical bolometric luminosities and temperatures and the corresponding observed magnitudes and colours (Carney 1980). An additional problem is the effect of *convective overshooting*: Stars in the mass range corresponding to the upper ms of a cluster/coeval population of a 1-a few Gyr have convective cores. As shown by Maeder & Mermilliod (1981), the ms lifetime of such stars and the luminosity they reach before evolving to the red depend on the extent to which the ms evolution is prolonged by the internal mixing that arises from overshooting outside the convective core. Failure to allow for this effect would cause the cluster/coeval population age to be underestimated. According to the models of Maeder & Mermilliod, for a composition of $Z = 0.03$ and $Y = 0.27$ and ages $\sim 10^9$ yr, the apparent tip of the ms is brighter by 0.3 mag if mixing up to one half of the pressure scale height at the edge of the core occurs. This can lead to underestimation of the age by almost 40%. Unfortunately, no predictions for the lower metallicities in the SMC exist to date. However, it must be kept in mind that since the ages that will be discussed on the basis of the ms in the following, reach 1-2 Gyr, the actual values suggested by the isochrone fitting may have been underestimated by a significant amount.

In the following, the set of the revised Yale isochrones (Green, Demarque & King 1987) will be used for convenience since they are given in the B–R plane and exist in computerised form. The use of the more closely spaced grid in the age-metallicity plane of the VandenBergh isochrones (1985) yields essentially identical ages for the same metal

abundances with the Yale isochrones, at the level of precision dictated by the present data.

For the CMDs of Chapter IV, a mixture of populations of different ages and metallicities comprise the detected main sequence. Therefore the previous techniques can only be partially applied, to provide limits for the younger populations present. The limiting magnitude of $R \sim 20$ restricts the detectability of the ms to populations younger than 1–2 Gyr of age (for the short d.m.), as can be deduced from a comparison with the Yale isochrones for a range of metallicities $0.0001 < Z < 0.004$ (Chapter V). In the best populated ms observed (Field 52 region 113), the brightest ms stars apparently reach $R \simeq 17.6$ which corresponds to an age of $\sim 3 \times 10^8$yr. In Fig.1a&b, the 0.15, 0.5, 1 & 2 Gyr isochrones for Z=0.0001 and Z=0.001 are superimposed on the CMDs of region 411 in Field 28 and region 113 in Field 52. On the other hand, application of the Hodge–calibration of the ms turnoff and the magnitude of the brightest blue stars on the ms in terms of age, yield similar age-limits. For the brightest blue stars around R=17.6, an age of 2×10^8 yr is suggested, while for the limiting value of $R \simeq 20$ the derived age limit is ~ 1 Gyr.

Study of the deep AAT CMD (Fig. 2). The observational details are given in Chapter II. Although this CMD includes a small sample of stars, its interpretation is important, as it is the only existing deep CMD in Field 52. The AAT field lies ~ 2.2 kpc from the SMC optical centre and displays a well–defined ms reaching as bright as $R \sim 20.4$, a well-delineated subgiant branch and a red horizontal branch at $< R > \sim 18.8$ and $1.0 < B - R < 1.4$.

The age of the youngest population present can be derived using the methodology of the previous paragraph. The 2 Gyr isochrones for $[Fe/H] = -1.0$ and $[Fe/H] = -0.75$ are superimposed in the CMD, assuming the short d.m. $(m - M)_o = 18.7$ and a reddening of $E(B - V) = 0.03$. The 2 Gyr isochrone with $[Fe/H] = -1.0$ fits the data reasonably well. Although the completeness at magnitudes fainter than $R \sim 21.5$ drops significantly, there is evidence of the presence of older ms stars. For comparison, a 10 Gyr isochrone is also given with $[Fe/H] = -1.7$. However, a complete sample down to at least 2 mag from the turnoff would be needed to define the age and metallicity of the older populations present.

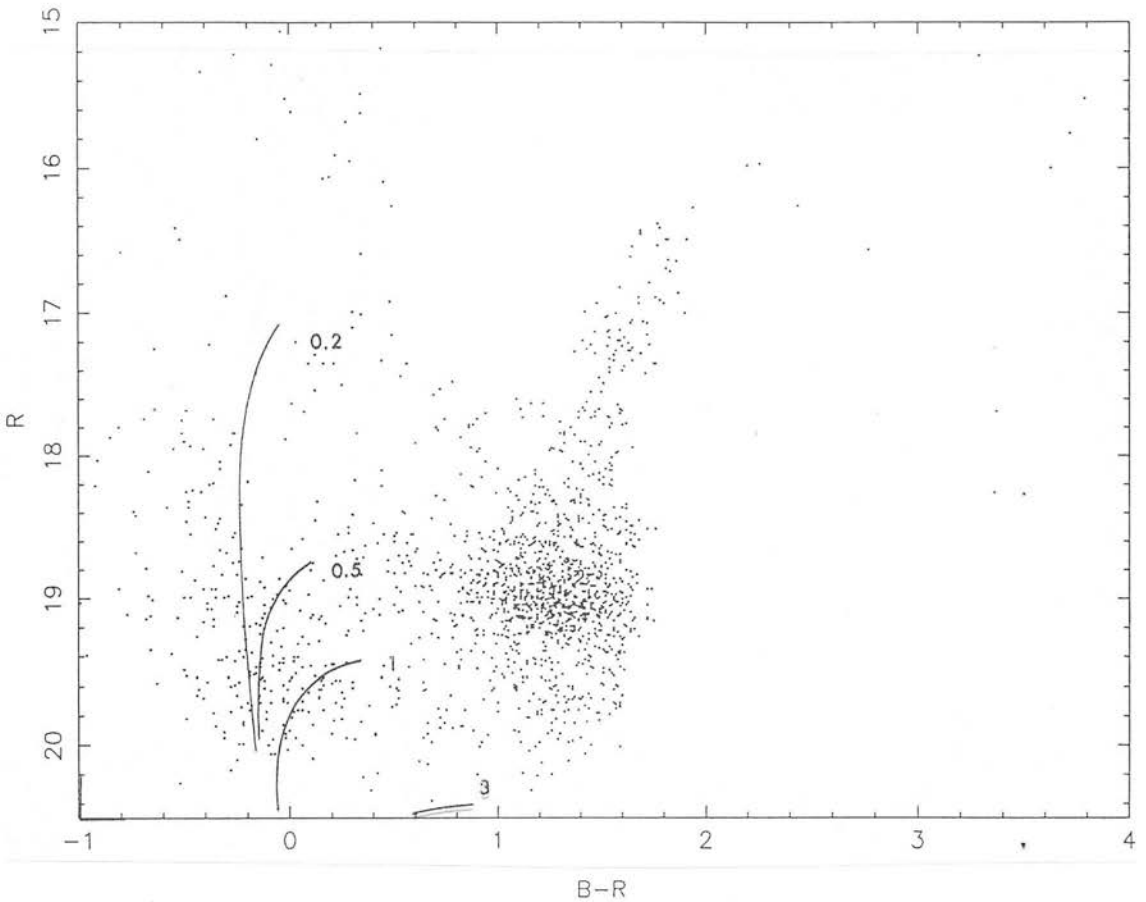

Figure 1a: The CMD in region 411 in Field 28, with the Yale isochrones of 0.2, 0.5, 1 and 3 Gyr superimposed (Y=0.3, Z=0.001).

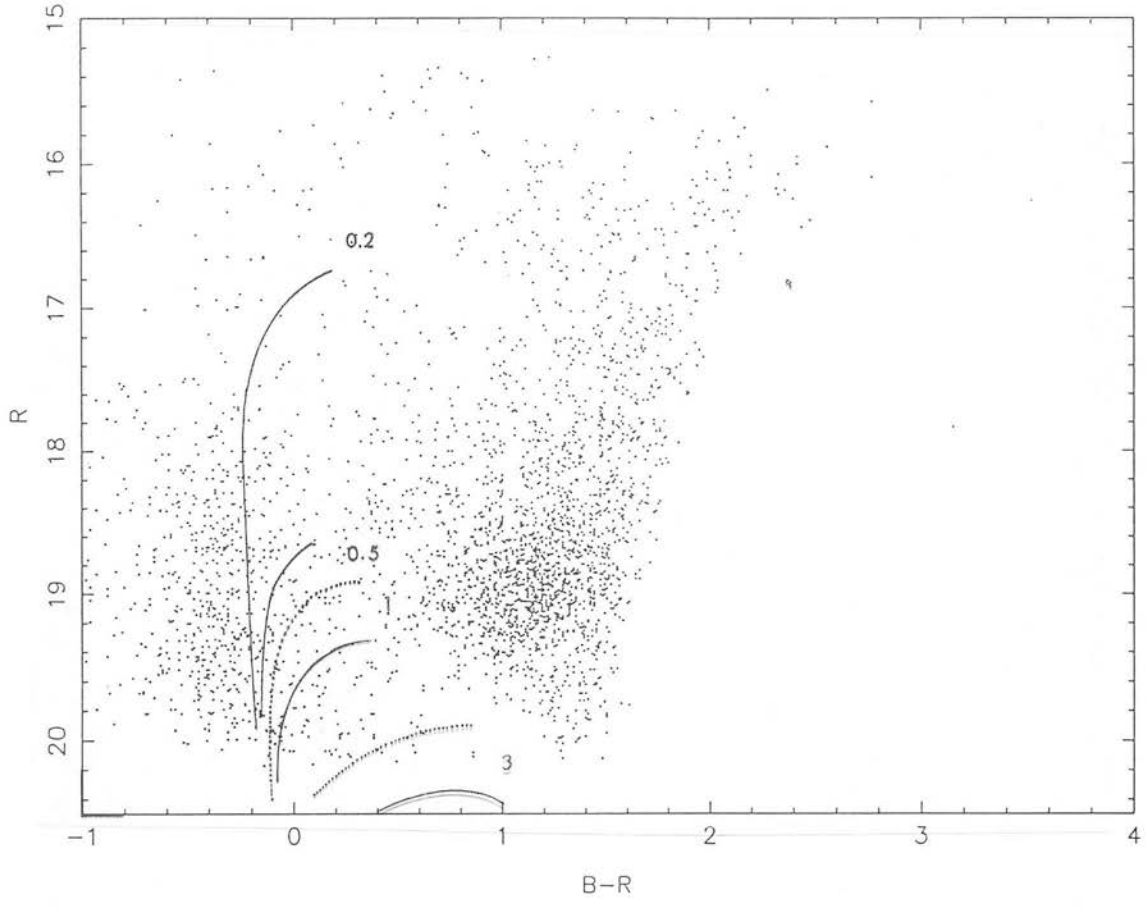

Figure 1b: as in Fig.1a, for the region 113, in Field 52. The dotted curves correspond to the 0.2 and 0.5 Gyr isochrones for Z=0.0001

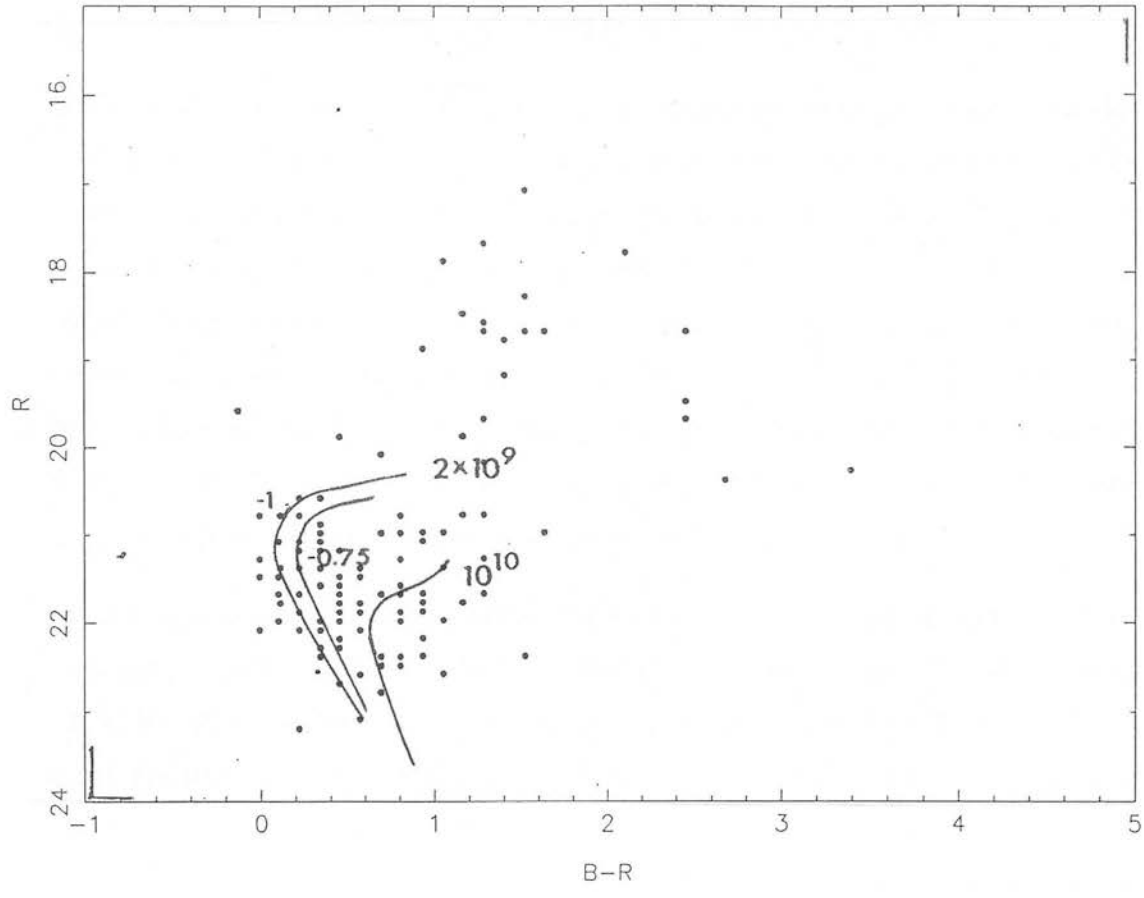

Figure 2: The CMD from the CCD observations with the 4m-AAT. The 2 Gyr Yale isochrones are superimposed for [Fe/H]=-1.0 and -0.75, as well as the 10 Gyr isochrone for [Fe/H]=-1.7.

It would appear plausible that at least some of the ms stars observed in the CMDs of Chapter IV near the magnitude limit of $R = 20$ mag belong to the top of the ms of this 2 Gyr population.

2.2 The ms luminosity function

In view of the decreasing total numbers of stars present in the CMDs as projected distance from the SMC centre increases, the interpretation of the apparent 'top' of the observed main sequence in each case in terms of the age of the youngest population present in the region becomes meaningless, without taking into account some normalisation with respect to the diminishing total number of stars on the CMD. A comparison between the luminosity functions of the ms in the various regions in Field 52 and Field 28 can offer some insight into the population synthesis of these younger SMC stars and clarify whether the observed ms can be simply scaled on to each other or whether there are genuine differences in the mixture of populations comprising them.

The logarithmic luminosity function $\log \Phi_R$ for the ms, was determined for all regions with at least 80 stars (Table 1, col.5) in the magnitude range $20 > R > 16$ and $-1. < B - R < 0.5$ (for the back/foreground subtracted fine–grid CMDs). The luminosity function Φ_R is defined by $dN = \phi(R)dR$, where dN is the total number of stars within the magnitude range $R - dR$ and $R + dR$. Here, $dR = 0.1$ mag, i.e. of the order of the observational error in R. A comparison of these LF (see Fig.3 for representative examples) shows them to agree well with each other within the errors (which are presumed to be described by pure Poisson number-count statistics). Note, however that this conclusion holds only for the relatively well-populated ms considered in this analysis. Moreover, there are two groups of LF in Field 52, which appear to deviate significantly from the mean locus defined by the other regions though statistically the significance of the difference is marginal considering the observational errors. The first of these groups includes the less dense regions, which apparently display a steeper ms-LF than the rest. The second is exemplified by the best-populated main sequence in the Field (region 113) and shows a broad 'bulge' in the LF between the 18th and 19th magnitude, presumably caused by the presence of a younger population in this region (see next section).

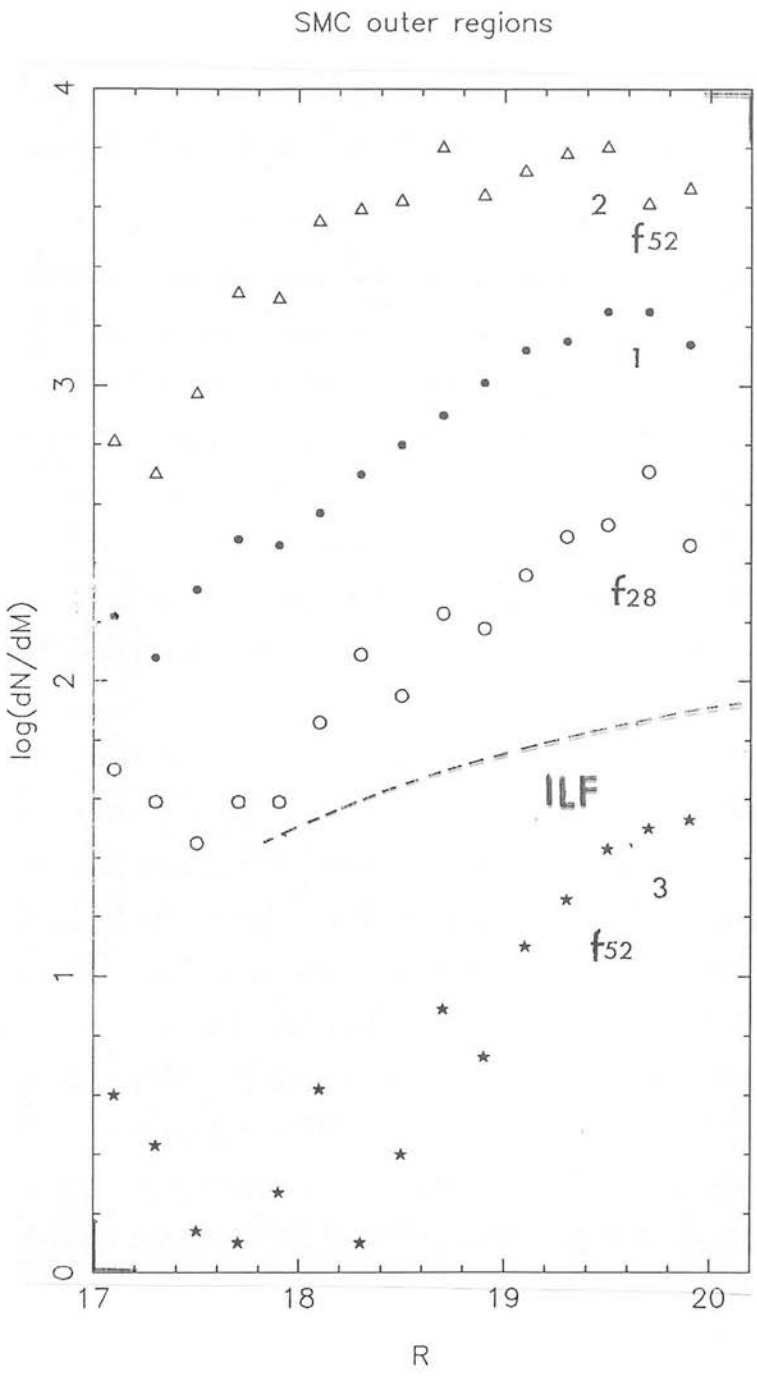

Figure 3: Examples of representative main sequence luminosity functions (from 0.22 square–degree regions) for Fields 28 and 52 (curve 1: most of the LF follow this curve which is identical within the errors with the LF for F28; curve 2 corresponds to the innermost area in Field 52, and curve 3 to the outer most areas). The dashed-line is Salpeter's initial luminosity function. Arbitrary offsets were applied along the log axis.

In Fig.3, Sandage's initial LF (ILF; Sandage 1957) is also shown. From the slope of the ILF it is clear that the observed LF cannot be attributed to coeval populations and that a superposition of star formation periods is implied.

There is no clear evidence of the presence of an evolutionary turnoff along the LF. There are however discontinuities which may indicate evolutionary deviations; nevertheless, the superposition of different ages should be expected to bury the effect of a turnoff by reducing the detection contrast. Some of the LFs show discontinuities between the 18th and 19th magnitude and –as mentioned previously– region 113 in Field 52 shows a detectable change of the LF-shape in this magnitude range. Although the reality of the occurence of a ms turnoff in this area cannot be claimed, an attempt was made to investigate whether the brighter and fainter ms stars (younger and older respectively) can be spatially separated, assuming that a turnoff does exist. If there was a turnoff around $R = 19$ mag, it would correspond to an age of $\sim 5 - 6 \times 10^8$ yr, according to the Yale isochrones (see Fig.1) as well as from the Hodge (1983) calibration. The ratio γ of the number of ms stars brighter than $R = 19$ mag to the number of ms stars fainter than that, was determined for each region in Fields 28 and 52. Table 1 (cols 6,7) gives the resulting values. Fig.4a&b shows the dependence of this ratio on the projected distance r_{oc} from the SMC centre. Only regions with at least 20 stars in the ms region were considered in this exercise. As would be expected from the agreement of the ms luminosity functions in Field 28, there is no evidence of a radial dependence of the ratio in the W/SW outer regions of the SMC studied. On the contrary, in Field 52 the ratio increases sharply in the innermost regions examined and it levels away to a constant value for distances larger than ~ 3.2 kpc. This indicates that in the innermost regions of Field 52 there is a population younger than $\sim 5 \times 10^8$ yr which does not appear in Field 28 and drops off 'faster' than the populations older than 5×10^8 yr. This younger population at the SW edge of Field 52 can be identified with the edge of the 'outer arm' which is known to possess such a population (Brück 1982).

2.3 Radial distribution of stellar populations younger than 1-2 Gyr

Already in the previous paragraph an aspect of the surface distribution of the younger populations in the SMC northeastern and southwestern outer regions

Region	n_t	n_{cl}	n_{sub}	n_{ms}	n'_{ms}	γ
511	2106	1311	138	120	93	0.22
512	1797	1064	105	41	26	0.36
513	2012	1275	109	16	10	-
514	1606	927	72	14	11	-
521	1208	577	35	7	7	0
523	1121	518	31	12	5	-
411	2512	1514	161	273	170	0.38
412	2112	1302	134	67	46	0.31
413	2427	1368	133	323	218	0.32
414	2121	1274	129	90	61	0.32
421	1406	740	41	17	10	0.41
422	967	421	13	3	3	-
423	1415	727	39	12	9	0.25
424	995	421	18	7	6	0.14
311	1774	1125	83	33	29	0.14
312	1566	905	47	19	10	0.47
313	2274	1433	140	149	91	0.39
314	1943	1206	103	34	25	0.26
321	1156	560	44	11	4	-
322	1086	466	13	8	5	0.37
323	1355	693	64	12	10	0.17
324	1069	442	15	6	5	0.17
211	1035	466	23	6	5	0.17
212	1124	515	23	5	1	-
213	1347	722	60	14	11	0.21
214	1268	634	31	15	10	0.33

Table 1a: Field 28; the total number of SMC stars in each CMD (n_t), the number of clump/HB stars (n_{cl}), of subgiants (n_{sub}), of main sequence stars with $R < 20$ (n_{ms}) and of ms stars with $19 < R < 20$ (n'_{ms}). *Column 7* gives ratio $\gamma = (n_{ms} - n'_{ms})/n_{ms}$.

Region	n_t	n_{cl}	n_{sub}	n_{ms}	n'_{ms}	γ
111	2753	1586	160	207	137	0.51
112	2258	1295	108	81	60	0.35
113	3763	1811	168	756	369	1.05
114	2580	1588	141	113	84	0.34
121	1958	1076	105	85	73	0.16
122	1830	909	77	80	66	0.21
123	2197	1155	103	112	92	0.22
124	1954	989	61	105	84	0.25
211	1857	982	71	48	43	0.12
212	1749	915	92	68	58	0.17
213	2109	1189	108	47	35	0.34
214	2074	1120	104	73	59	0.24
221	1611	801	49	56	50	0.12
222	1367	667	33	41	33	0.24
223	1935	1026	84	67	56	0.20
224	1542	777	46	66	54	0.22
131	1618	803	71	65	35	0.37
132	1314	596	35	40	34	0.18
133	1623	809	50	67	49	0.37
134	1478	706	47	52	43	0.21

Table 1b: Field 52 (as in Table 1b).

Region	n_t	n_{cl}	n_{sub}	n_{ms}	n'_{ms}	γ
231	1198	555	33	25	18	0.39
232	1057	389	9	11	7	-
233	1388	663	34	42	35	0.20
234	1109	486	13	19	12	-
331	985	378	42	10	5	-
333	1177	466	41	31	18	-
311	1239	614	48	21	13	-
312	1319	626	67	18	10	-
313	1594	849	102	24	17	0.41
314	1478	744	51	31	29	0.07
321	1112	514	28	17	8	-
322	1138	509	64	16	10	-
323	1345	676	48	36	25	0.36
324	1334	584	40	36	23	0.56
413	1079	465	41	9	8	-
414	1092	464	35	17	6	-

Table 1b: continued.

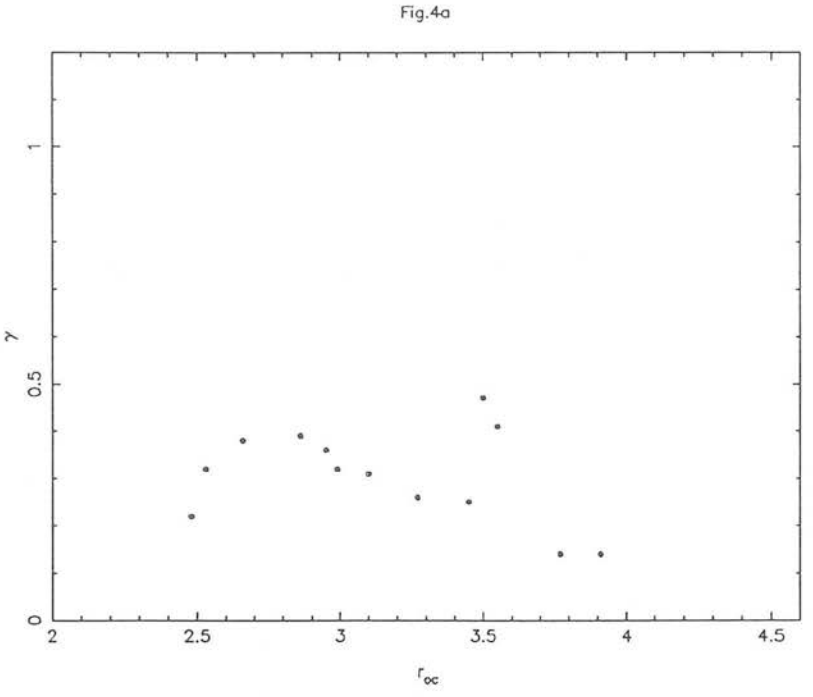

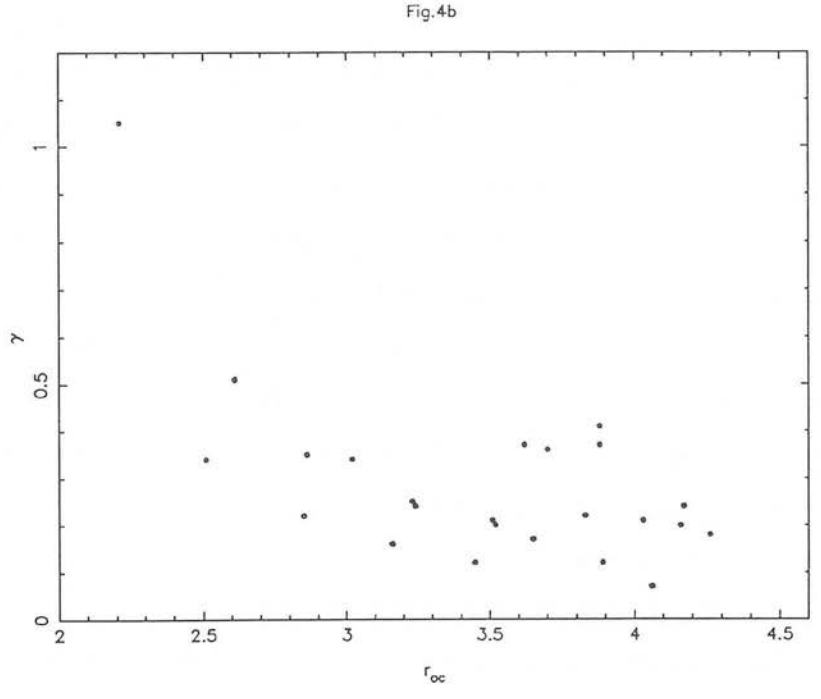

Figure 4: The ratio of ms stars brighter than R=19 to those fainter than this limit, as a function of radial distance r_{oc} from the SMC centre, in Field 28(a) and Field 52(b).

(with $r_{oc} > 2.2$ kpc) was examined. Here the radial distribution of all ms stars on the CMDs will be investigated. As was shown in Section 2.1, these stars belong to populations younger than 1-2 Gyr. Fig.5 presents the distribution of the number of ms stars in the 0.22–square–degree regions, n_{ms}, as a function of radial projected distance from the SMC optical centre, in Fields 28 (a) and 52 (b). The values of n_{ms} are given in Table 1. In Fig.5(c&d) the total density of SMC stars in each region is used instead of the distance r_{oc}. The reasons for presenting this distribution were discussed in Chapter V. For comparison, the same distributions of Fig 5(a&b), but with respect to the dynamical centre of the SMC, are given in Fig.6 (a & b). In all cases, there is a significant difference between the distributions in Fields 28 and 52. Even beyond the distance where -according to the discussion in the previous section- the youngest ($\tau \leq 5 \times 10^8$ yr) populations drop off, there is a much steeper decrease of the ms–stars' number density in Field 28 than in Field 52. The effect is also obvious in the luminosity functions of the less dense regions in Field 52, seen in the previous section. Four factors could account for this effect:

(i) a genuine persistence of the populations younger than 1-2 Gyr to larger distances in the NE than in the SW outlying regions of the SMC.

(ii) the distance modulus difference between the stars in the two Fields, which is investigated in detail in Chapter IX, could cause an overestimate of the numbers of ms stars counted in the Field 52 regions, where the d.m. is shorter by ~ 0.2 mag on the av erage. Therefore, by counting stars down to the same limit in both fields, older, or less massive, main sequence stars are included in the lower d.m. regions, thus increasing n_{ms}. The effect can be corrected, by adjusting the limiting magnitude of the counts according to the mean d.m. in each region (as determined in Chapter IX). This correction however is only indicative, because of the significant dispersion around the mean d.m. in the NE (Chapter IX). The resulting corrected curves are superimposed in Fig.5(c&d). It can be readily seen that this effect cannot account for the differences between the n_{ms} distributions in the two fields.

(iii) a significantly erroneous estimate of the back/foreground subtracted from the CMD. However, as can be seen in Fig.2 (Chapter IV) there is no significant contribution from back/foreground stars in the area of the SMC main sequence locus. Moreover, the difference in galactic latitude on the foreground star density, which was discussed in

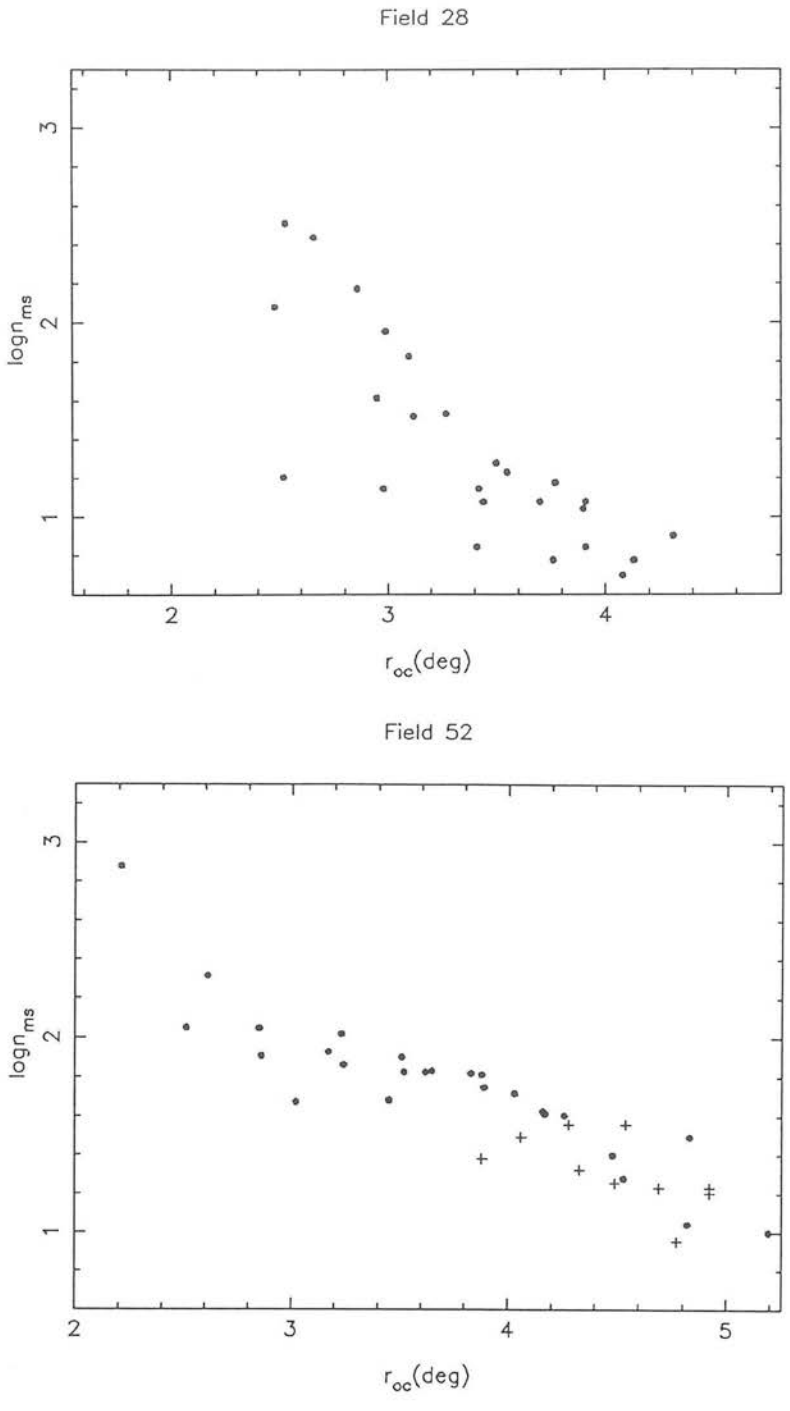

Figure 5: The radial distribution with respect to the optical centre of the surface number density of main sequence stars ($R \leq 20$) for Field 28(a) and Field 52(b; the + refer to the regions with significantly different d.m.; see Chapter IX).

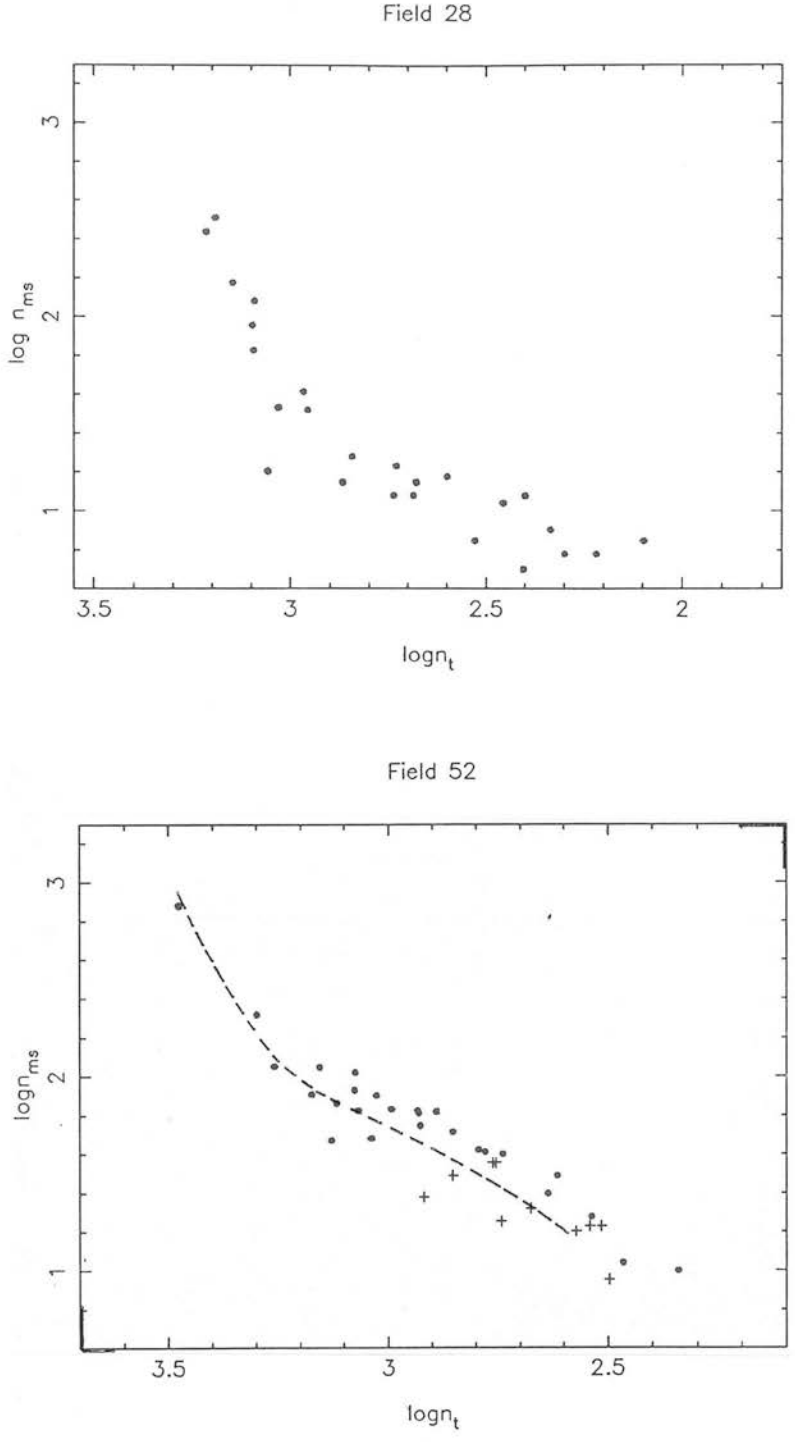

Figure 5(c,d): as in Fig.5(a,b), but the distribution given with respect to the logarithm of the total surface number density of SMC stars, in Field 28 (c) and in Field 52 (d). The dashed line corresponds to the values corrected for the geometrical effect (see text). The correction is negligible in Field 28.

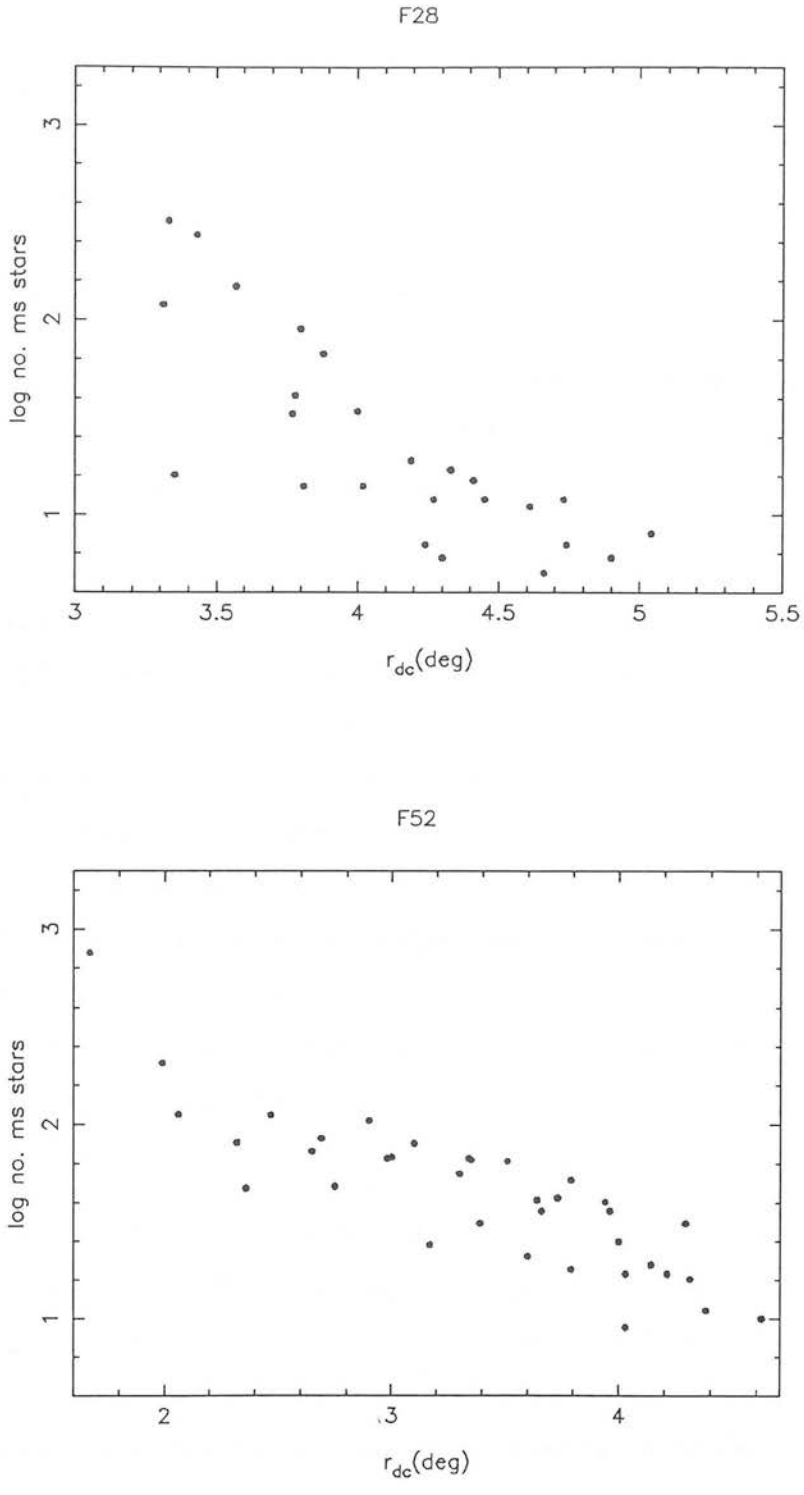

Figure 6: The radial distribution with respect to the dynamical centre of the surface number density of main sequence stars ($R \leq 20$) for Field 28(a) and Field 52(b).

Chapter IV, should have the effect of flattening rather than steepening the curve in Field 28 (and the other way round in Field 52).
(iv) significant incompleteness at faint magnitudes in Field 28. According to the discussion in Chapter III, there is no evidence of such an effect, down to $R = 20$.
Therefore, the first of these factors causes at least most of the difference between the n_{ms} distributions in the two Fields.

An inspection of Fig.5 shows that the decrease of the surface density of stars younger than $\sim$ 1 Gyr with radial distance cannot be realisically fitted with a single exponential curve, especially in Field 52, a conclusion already reached by Brück (1982) on the basis of star counts.

Following this discussion it can be concluded that :
• In Field 28, the number of stars younger than 1-2 Gyr decrease more rapidly than it does in Field 52, with increasing distance from the SMC centre.
• In Field 52 there is a contribution to the ms stars from a population younger than $\sim 5 \times 10^8$ yr, presumably originating in the 'outer arm' and disappearing at a distance of $\sim$ 3 kpc from the optical centre.
• In Field 52, the top of the ms of a 1-2 Gyr population persists to distances as large as $\sim$ 5 kpc from the optical centre.
• The presence of a turnoff of a 2 Gyr population is shown in the deep CMD observed with the 4m AAT in Field 52 (see also Chapter VIII).

This difference between the distribution of the younger intermediate-age populations in the NE and SW outer regions of the SMC was also suggested by the number density contours produced by Brück (1980) as well as by the detection of a 2 Gyr population in the field near the star cluster L113 (Mould, Da Costa & Crawford 1984), which lies $\sim$ 4 kpc to the east of the optical centre (northwards of the 'Wing' but to the south of the southern edge of Field 52). The implications of this result will be discussed in Chapter VIII.

3 The clump/horizontal branch

A conspicuous feature of the CMD in both F28 and F52 is the presence of a high concentration of stars almost centred at the base of the red giant branch, and reminiscent of the well-known 'clump', characteristic of the CMDs of young and intermediate age populations like galactic open clusters and many clusters in the Magellanic Clouds.

3.1 The core helium burning stars

Cannon (1970) identified the 'clump' stars with stars powered by a helium burning core and a hydrogen burning shell. They are thus the higher mass equivalents of the horizontal branch stars observed in the CMDs of older populations (as in globular clusters). This identification was verified by the theoretical models of Faulkner & Cannon (1973; hereafter FC). The principle of the clump formation is quite simple: stars with masses $\leq 2.25 M_{\odot}$ have electron–degenerate cores and the helium burning begins in them only when the core reaches a fixed critical mass, which is nearly independent of the total mass of the star, as well as of its metallicity. The helium–core behaves almost like an independent star (Faulkner & Iben 1966) of fixed mass, hence the constancy in luminosity of the clump giants, provided that most of the luminosity of the star comes from the He–core. For high helium abundance Y however the H-burning shell is the main energy source. In this case, semiconvection must be taken into consideration for the interpretation of the situation.

Although the observed 'clump' in most clusters possesses no apparent structure, the theoretical models show that it is in fact almost a vertical sequence in the CMD, running parallel to the Hayashi fully-convective boundary: stars with masses in excess of $\sim 1 M_{\odot}$ do not describe extended blueward loops in the HR diagram during He-core burning (like 'normal' HB) and remain close to the giant branch showing a very small change in $logT_{eff}$ during this phase (FC; Hirshfeld 1980). The transition from the vertical morphology of the clump to the horizontal morphology of the 'normal' HB, presumably occurring at masses $< 1 M_{\odot}$, is not well understood either observationally or theoretically.

The luminosity and size of the 'clump'. In the original models of FC it was found that the displacement of the clump magnitude with age, for ages between $3 - 5 \times 10^8$yr and 2×10^9yr (this being the whole range of ages studied by FC), is appreciably smaller than the clump size itself. The 'clump size', i.e. the spread in magnitude among the members of a single clump, was calculated by FC to be $\Delta log L/L_\odot = 0.25$. They also emphasized that the clumps of clusters younger than $\sim 5 \times 10^8$ yr (i.e. with red giant masses $> 2.25 M_\odot$) showed a progressive brightening with age. This effect can be understood by the fact that such massive red giants do not have sufficiently degenerate cores to cause a helium flash, thus the reason for constancy in luminosity (i.e. the existence of a critical value for the He-core mass before the He-flash begins) is removed. However, a retardation of evolution takes place, which gives rise to a clump–like feature, the mean luminosity of which depends on mass and hence on age. In a series of recently published models (Vandenbergh 1985; Seidel, Demarque & Weinberg 1987, hereafter SDW) the evolution of the clump stars has been investigated in more detail, and the dependence of the luminosity and size of the clump on chemical composition (Z), helium abundance (Y), helium-core mass (M_c) and total mass (M_t) was explored. For ages between 1 and 10 Gyr (total mass of clump giants between 0.7 and 0.9 $M_\odot$) the total difference in mean clump luminosity suggested by SDW is $\delta \log(L/L_\odot) \sim 0.03$, which is evidently much smaller than the size of the clump itself. This is in agreement with the empirical conclusion known since the first systematic study of the clump by Cannon (1970) mentioned previously. Recent results on Magellanic Cloud clusters confirm this (Olszewski *et al.* 1987; Olszewski 1988; Mateo & Hodge 1985).

The dependence of the mean luminosity level of the clump on metallicity is difficult to assess observationally –especially for the low metallicities appropriate for the SMC intermediate and old populations– because of the paucity of well observed star clusters in the SMC. A study of galactic open clusters tabulated by Cannon (1970) did not yield any evidence of such a dependence, but they have higher metallicities, and it is not clear that this result can be extrapolated to the low metallicity objects of the SMC. The models by SDW were evaluated only for Z=0.01 and Z=0.001, of which values only the latter can be used (as an upper limit) for the SMC outer regions (see Chapter V). Moreover, the metallicity changes found in these regions are much smaller –if at all present– than the metal abundance difference between the two sets of the SDW models.

However, an upper limit to the possible variations of clump luminosity due to metallicity changes, can be obtained on the basis of these models. An inspection of the SDW tracks indicates that in the age range of interest, the change in metallicity from 0.01 to 0.001 causes a clump luminosity variation between $\sim +0.05$ and ~ -0.05, depending on the values adopted for Y and M_c. Therefore, no obvious systematic trend of the clump luminosity with metallicity can be established.

Sandage (1982) deduced from the luminosities and metallicities of RR-Lyraes in Galactic globular clusters that there is a strong correlation between metallicity and HB luminosity. As Cannon (1983) pointed out, there is no proof that this necessarily applies globally: 'Even if the rule does apply to those clusters with RR-Lyraes, it may not be valid to use a simple linear interpolation for the metal rich globulars like 47TUC that do not contain such stars' or for the younger globular-like clusters in the Magellanic Clouds.

The *clump size*, i.e. the finite spread in luminosity of the clump stars (of a coeval population), is caused by the evolution of the clump giants from their 'zero-age' locations. Using the evolutionary tracks of clump red giants by SDW, the clump size can be determined from the luminosity range of the section on the isochrone where the stars spend most of their time. The resulting 'size' is $\Delta R \simeq 0^m.3$, but the maximum possible size reaches $\Delta R \simeq 0^m.5$–$0^m.6$ (see also Seidel, Da Costa & Demarque 1987, hereafter SDD). These values confirm the early observational conclusion of FC, mentioned previously. The clump size as predicted by the models depends on all four parameters (M_c, M_t, Z, Y). For the values of M_t (0.7-1.0) and Z (= 0.001) appropriate for the intermediate and old populations of the SMC of interest here, this dependence is negligible, with the exception of a few particular combinations of the four parameters for which the difference in size of the clump can change by ~ 0.05 in $logL/L_\odot$, for the above range in total clump-star mass M_t. However, in the neighbourhood of $\sim 10^{10}$ yr, there is an indication of a transition to a horizontal morphology, and a decrease of the clump size (in magnitude). Empirical data both from the CMDs of open galactic clusters and of well-observed Magellanic Cloud clusters show no dependence of the size of the clump on either age or metallicity, in the range 0.5 – 10 Gyr.

It should be mentioned at this point that, as shown by SDD, the colour of the clump

predicted by the SDW models do not seem to fit well the observed clumps of Magellanic Cloud clusters. The discrepancy is attributed to the assumed value for the mixing length in the models. Moreover, as demonstrated by Sweigart & Gross (1976), the colour of core–helium burning stars with masses below 0.9 $M_{\odot}$ is very sensitive to total mass, with the model predictions becoming rapidly hotter as the total mass decreases, i.e. a small uncertainty in the model mass leads to a large uncertainty in colour.

To summarise, both empirical data and theoretical predictions agree that for cluster ages between ~0.5 and 10 Gyr:
(i) the mean clump luminosity is approximately constant with age and metallicity, any variations being much smaller than the clump size itself;
(ii) the (full) size of the clump is smaller than 0.6 mag and displays little change with age or metallicity;
(iii) the point of transition from the 'vertical' clump to the HB morphology depends mainly on M_t (and hence on age) and apparently occurs in the neighbourhood of 10^{10} yr.

3.2 The clump/HB in the outer regions of the SMC

The fine grid CMDs are considered in the following discussion. The 'clump' region on the CMD is defined here by the limits $18 < R < 20$ and $0.6 < B - R < 1.8$. The large adopted range of magnitudes is dictated by the large clump size in some of the F52 regions (Chapter IX).

The contribution of the younger populations to the observed clump.
In Section 2 it was shown that the ms stars detected on the CMDs span a range of ages from a few 10^8yr to probably $\sim 1 - 2 \times 10^9$yr and that the younger of these stars ($\tau \leq 5 \times 10^8$yr) diminish much faster with projected distance from the centre than the older ones.

The extent to which the number density of stars in the observed 'clump' can be interpreted as originating in the young and intermediate–age populations for which ms stars are detected on the CMDs will now be investigated. For this purpose, the number of stars in the 'clump', n_{cl} (Table 1), is compared with the number of stars in the faint

end of the ms within the magnitude limits $19 \leq R \leq 20$, n'_{ms} (Table 1). Region 113 in Field 52 which shows the most well-populated ms, is used for this comparison as a limiting case. The total number of clump stars in this region is $n_{cl} = 1811$ while the number of ms stars is $n'_{ms} = 369$. Notice that n_{cl} includes red giants that are not on the clump phase, due to the large magnitude range adopted for its evaluation as previously mentioned. As will be seen in Section 4 (see also Table 1) the maximum contribution of subgiants to this number is $n_{sub} = 168$ of which $\sim 50\%$ are actually higher error clump stars. Assuming an approximately uniform LF along the giant branch for the considered magnitude range the RGB contribution is ~ 80. Therefore, the clump stars in the region are $\simeq 1640$ and the ratio of lower ms to clump stars becomes $\simeq 0.22$. This value is an upper limit for the CMDs in the outer regions in both Fields and decreases rapidly with distance (for the next most populous ms, the ratio is only $\simeq 0.10$) to reach negligibly small values, as would be expected from the surface distribution of the ms stars discussed in Section 2. The expected ratio for coeval populations with ages in the range $\sim 5 \times 10^8$ yr to 13×10^8 yr varies from ~ 0.7 to ~ 1.0 respectively. These values were derived from counts in the CMDs of well-observed open galactic clusters (NGC 7789, 1245, 752, 2158, 6940, 2360, 2477 from the Publs.D.Dunlop Obsy. 1970) and intermediate age LMC clusters (NGC 2213 from Da Costa *et al* 1985; NGC1777 from Mateo & Hodge 1985). Therefore, even in the innermost area studied here, in Field 52, stars younger than ~ 1 Gyr can only account for at most 30% of the observed clump stars, while in the rest of the regions studied, the difference is at least of one order of a magnitude. This conclusion becomes evident when comparing the surface distribution of the number densities of ms and clump stars (see Section 3.3).

A 'normal' horizontal branch or a 'vertical' clump?

Although the transition between these two morphologies is not well established, as discussed previously, it is empirically known that the former is a characteristic of globular like (old) clusters, while the latter of intermediate age clusters. The oldest known SMC cluster, NGC121, possesses a short red HB. It is interesting to examine the morphology of the clump/HB observed in the CMD of the SMC outlying regions. For this purpose, the spread in $\log T_{eff}$ for the clump/HB stars was calculated for each region, from the observed dispersion of the clump/HB colour, $\sigma(B-R)$. Only clump giants with R magnitude within ± 0.25 mag from the median R (see Chapter VI) were included in

the calculation. On average, in both Fields, $\sigma(B-R) = \pm(0.22 \pm 0.03)$ (Table 2). The positional variations of $\sigma(B-R)$ are discussed in Section 3.3. The observational errors in $(B-R)$ can account for $\sim \pm 0.1$ of the scatter in this magnitude range. Some additional scatter is introduced by the back/foreground–removing routine, particularly in the more sparsely populated areas of the clump. Both this scatter as well as that introduced from the inclusion of first ascent giants and subgiants in n_{cl} are minimised by considering a relatively shallow (i.e. smaller than the full width of the clump in R; see Chapter IX) strip of $\Delta R = 0.5$ mag around the median magnitude of the clump stars, but still wide enough to obtain statistically meaningful results. The fact that the densest regions –where both of these effects should be minimised– do not show any tendency towards lower values of $\sigma(B-R)$ indicates that at least some of the observed scatter is due to a genuine temperature range among the clump/HB stars. Assuming that the observational scatter can be square–added to the intrinsic $\log T_{eff}$ scatter, it is estimated that the scatter in the clump colour due to the spread in temperature is $\sim \pm 0.19$. Evidently, this value should be treated as an upper limit (although probably a good approximation for the densest regions) and corresponds to total temperature scatter of $\Delta \log T_{eff} \simeq 0.04$. By comparison with the models of SDW, it becomes obvious that the temperature range previously estimated is significantly larger than the one expected for clump stars. The presence of a genuine HB component was also suggested by Brück *et al.* (1985). The above discussion implies that there is a *horizontal branch* component among the core-helium burning giants in the outer regions of the SMC studied here, and therefore a significant, *old* (probably $\sim 10^{10}$yr or more) population is present among the field stars.

3.3 The Radial Distribution

The clump/HB stars span the whole range of ages of the populations present in the studied areas. The radial distribution of n_{cl} with respect to the SMC optical centre is shown in Fig.7(a&b), while Fig.7(c&d) give the distribution with respect to r_t. The decrease of n_{cl} with r_{oc} is better defined in Field 52 than in Field 28, which may indicate that spherical symmetry with respect to the O.C. is a better approximation in F52 (see also Brück 1978). This does not seem to be the case in F28.

Field 28	$\sigma(B-R)$	n_s	Field 52	$\sigma(B-R)$	n_s
511	0.20	608	111	0.22	640
512	0.21	491	112	0.21	489
513	0.20	614	113	0.25	778
514	0.21	423	114	0.23	656
411	0.24	767	121	0.23	383
412	0.22	647	122	0.22	301
413	0.23	649	123	0.22	405
414	0.19	590	124	0.20	359
421	0.23	316	211	0.23	365
422	0.31	100	212	0.21	257
423	0.24	308	213	0.22	420
424	0.29	80	214	0.23	398
311	0.22	555	221	0.22	278
312	0.20	440	222	0.24	202
313	0.22	704	223	0.20	328
314	0.20	608	224	0.21	241
321	0.24	192	311	0.26	200
322	0.29	123	312	0.28	210
323	0.24	263	313	0.20	278
324	0.30	111	314	0.20	262
211	0.27	135	323	0.28	209
212	0.28	172	324	0.29	176
213	0.23	303	131	0.22	219
214	0.23	259	133	0.21	262
			134	0.24	191
			233	0.23	187

Table 2: The dispersion in colour of clump/HB stars (*Col.2*), included in a strip of ± 0.25 mag around the median R magnitude of the clump stars (given in Chapter IX). *Column 3* gives the number of clump/HB stars in this strip.

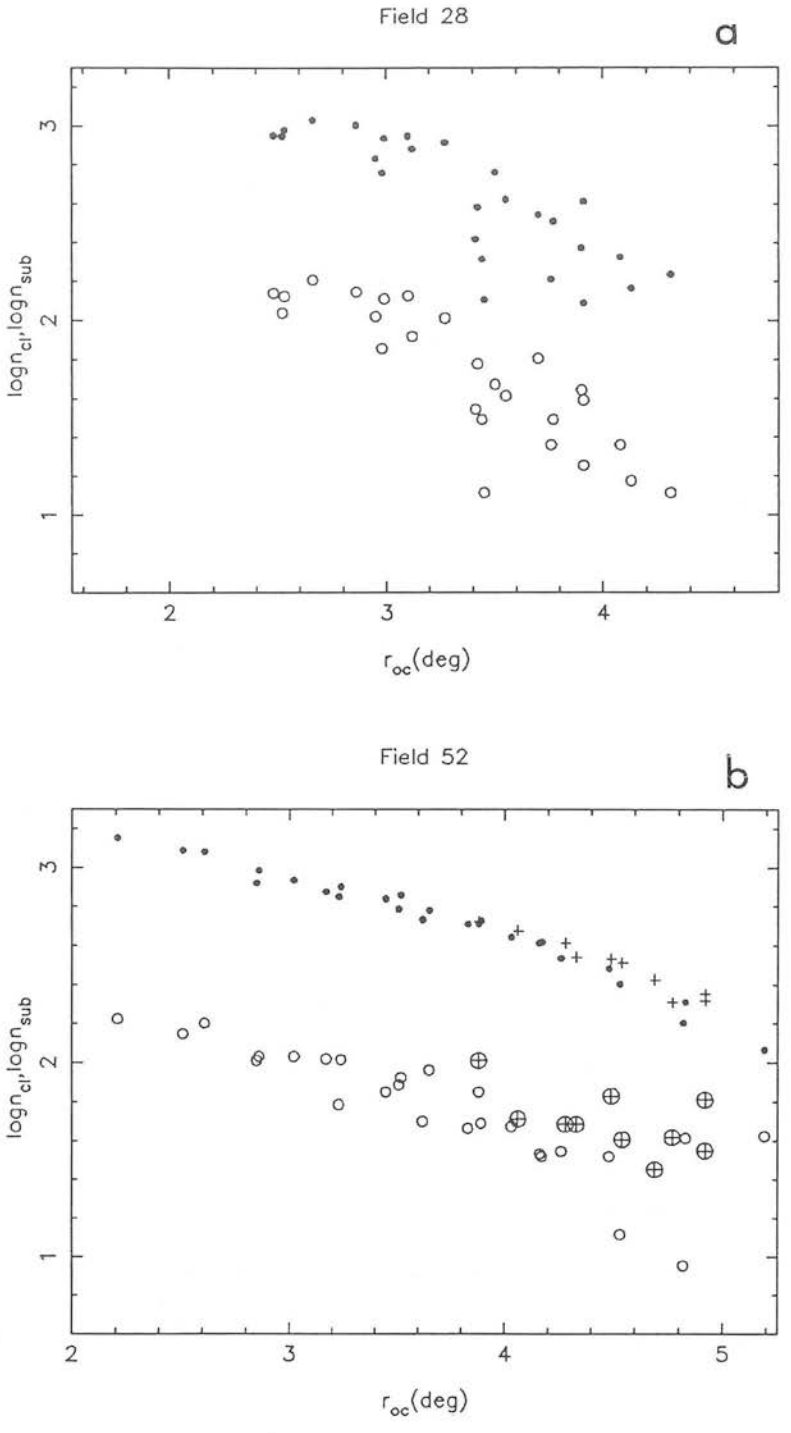

Figure 7: (a) Field 28, (b) Field 52. The radial distribution with respect to the optical centre of the surface number density of clump/HB stars (filled circles) and subgiants (open circles). The different symbols in each case correspond to the group of regions in Field 52 with different d.m. identified in Chapter IX.

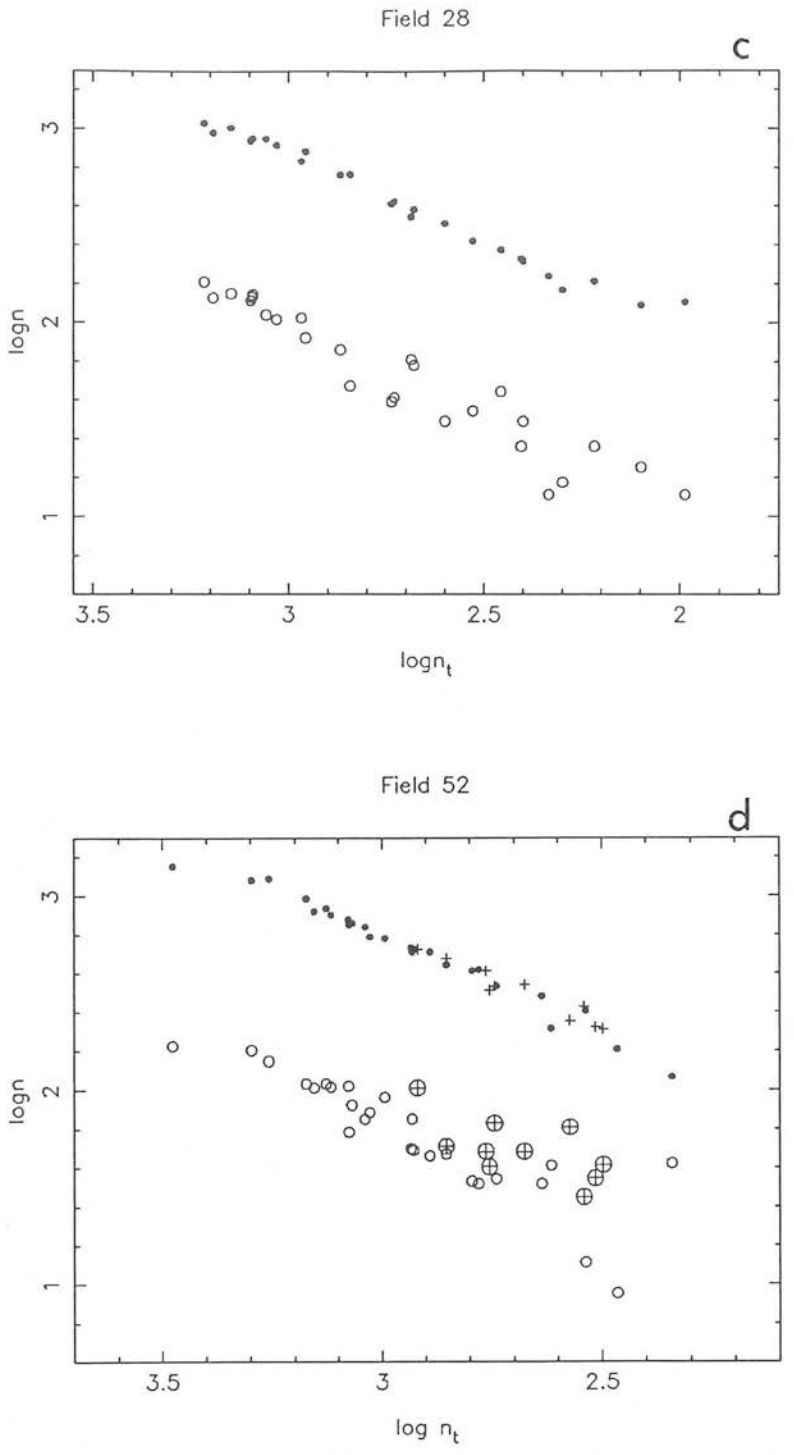

Figure 7: continued. The distribution of the numbers of clump/HB stars and subgiants, as a function of the total number of SMC stars detected; (c) Field 28, (d) Field 52.

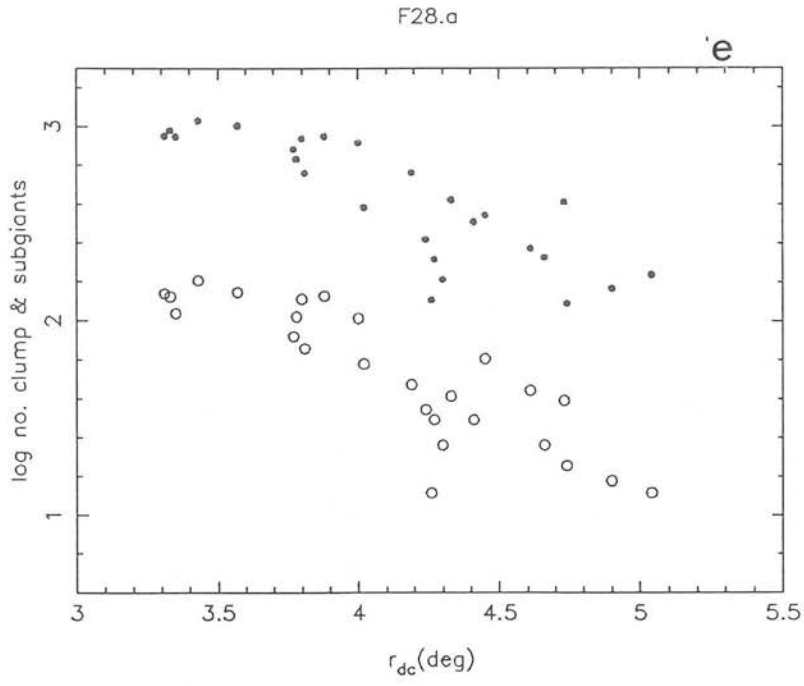

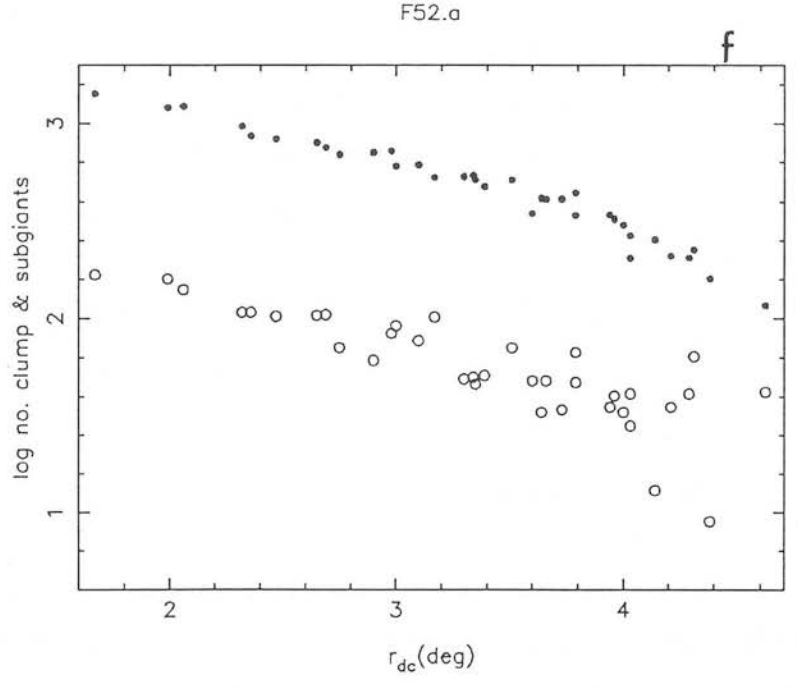

Figure 7: continued. As previously, but with respect to the dynamical centre of the SMC; (e) Field 28, (f) Field 52.

In both cases there is no evidence of a strong central concentration of these predominantly older stars. This was also claimed by Graham (1975; 1984) on the basis of the distribution of RR-Lyrae stars.

The distribution with respect to the dynamical centre of the SMC is shown in Fig.(7e&f). In both fields n_{cl} falls to similar values at $r_{dc} \simeq 5$ kpc; however the density is higher in Field 28 for smaller distances, as was also noticed by Brück (1980). For both centres the approximately exponential decrease of the number of clump stars is marginally steeper in F28 than in F52 (see also Brück 1980). However, it could be caused, in the present case at least, by an overestimate of the back/foreground contribution subtracted from the clump regions (due to the different galactic latitude of the subtracted back/foreground region).

Though the HB/clump giants originate in the whole age range present in the field, they include at least 10 times more stars that are older than 1-2 Gyr. It is interesting to compare the distribution of these prevailingly older populations with that of stars younger than $\sim 1-2$ Gyr derived in the previous section. It is obvious that in the SW the young and intermediate–age populations drop more rapidly with distance than the older stars. In the NE a component of the younger populations appears to follow closely the radial distribution of the older stars, after the disappearance of the youngest component ($\tau < 5 \times 10^8$ yr) at $r_{oc} \sim$ 3kpc. Thus, the way younger populations are mixed with the older ones seems to be different in the SW from the NE outer parts of the SMC. This result will be discussed in Chapter VIII.

3.4 Age distribution from the clump/HB properties

It was shown in Section 3.2 that the observed HB/clump can be attributed almost entirely ($\geq 90\%$, with the exception of the innermost region of Field 52) to populations older than $\sim 1-2 \times 10^9$ yr and with a probably significant component in the 10^{10} yr range (as deduced from the spread in $\log T_{eff}$). The following analysis examines the effective mean age of the clump/HB giants and its change with distance from the SMC centre. In this discussion it will be assumed initially that the effect of populations younger than 1–2 Gyr on the considered HB/clump properties is negligible (with the

exception of the innermost region studied in Field 52). Subsequently, the validity of this assumption will be discussed.

Three different approaches to the problem were attempted:

(i) the blueward displacement of the HB with respect to the RGB locus. Qualitatively, it is expected that clump stars with masses $M_{cl} < 0.9M_{\odot}$ become rapidly hotter (and hence bluer in colour) as the total mass decreases. Thus the age of the corresponding population increases, causing the HB to appear increasingly detached from the RGB. As mentioned in paragraph 3.1, the colour of the core–helium burning stars is not well defined in the theoretical predictions especially for low total mass stars. Thus a quantification of the effect is not feasible at the present stage of the models.

An empirical calibration of the colour difference $\Delta(B-R)_g$ (Table 3), between the short red HB or clump and that of the RGB at the level of the HB, as a function of age, τ, can be achieved using the CMDs of well-observed SMC clusters. The data used for the calibration are shown in Table 4 and the resulting relation in Fig.8. There is a well-defined trend in the predicted sense, with $\Delta(B-R)_g$ increasing with age, from $\sim 0.1^m$ to $\sim 0.3^m$ for ages between 2 and 12 Gyr respectively. Other factors may affect this correlation, such as metallicity, or quantities connected to the second parameter problem in globular clusters. On the basis of the present data it is not possible to evaluate the effect of these potential factors on the calibration. However, it can be assumed that –to first order– metal abundance affects the temperature of both kinds of giants in the same way. This assumption is confirmed by the fact that the two higher metallicity clusters used for the calibration do not deviate from the line defined by the other clusters which have almost identical metallicities ($[Fe/H] \sim -1.35$). In any case, there is no evidence of mean metallicity changes in the regions studied here (Chapter V), and the metallicity range is comparable to the one spanned by the clusters used for the calibration.

An important advantage of this method is its independence from any differential reddening effects or systematic errors in the photometry, since the colour *difference* between $(B-R)_g$ and $(B-R)_{HB}$ is applied. The quantity $(B-R)_g$ was determined in Chapter V. The median colour of the HB/clump stars is given in Table 3. The difference

Field 28	$\overline{B-R}$	$\Delta(B-R)_g$	Field 52	$\overline{B-R}$	$\Delta(B-R)_g$
51	1.29	0.13	11	1.18	0.15
52	1.27	0.11	12	1.14	0.18
41	1.26	0.13	21	1.14	0.18
42	1.26	0.14	22	1.13	0.18
31	1.23	0.14	31	1.13	0.19
32	1.19	0.17	32	1.13	0.19
21	1.23	0.21	13	1.14	0.18
			113	1.17	0.14

Table 3: The median colour ($\overline{B-R}$) of the clump/HB and the age–indicator $\Delta(B-R)_g$, for the coarse–grid CMDs in Fields 28 and 52.

Cluster	age (Gyr)	[Fe/H]	$\Delta(B-R)_g$
L1	10 ± 2	-1.3	0.25
NGC121	12 ± 2	-1.4	0.28
Kron3	8 ± 1.5	-1.3	0.16
47TUC	13.5	-0.65	0.31
L113	5	-1.4	0.2
NGC411	1.8 ± 0.3	-0.9	0.1

Table 4: List of clusters used to calibrate $\Delta(B-R)_g$ as a function of age. Deep CCD CMDs were used for this purpose (references in text).

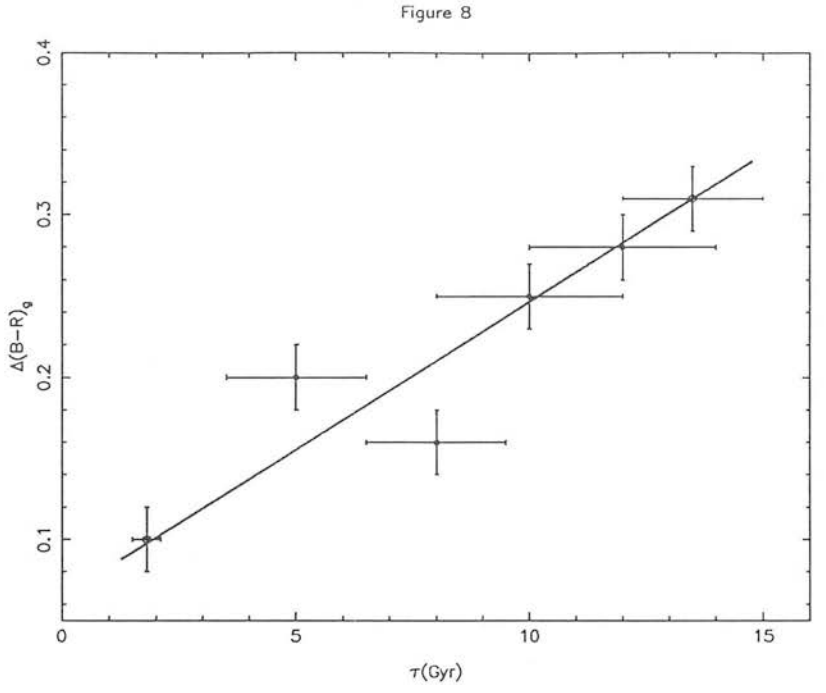

Figure 8: Age calibration of the $\Delta(B-R)_g$ indicator based on the data of Table 4. Filled circles: metallicity $[Fe/H] = -1.35 \pm 0.05$. Open circles: metallicity $[Fe/H] \leq -0.9$ (see Table 4).

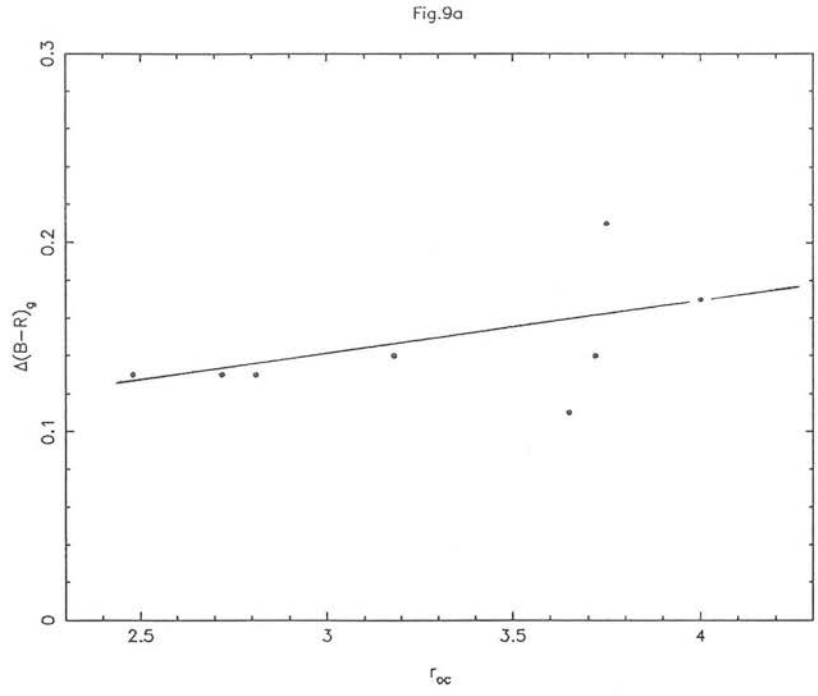

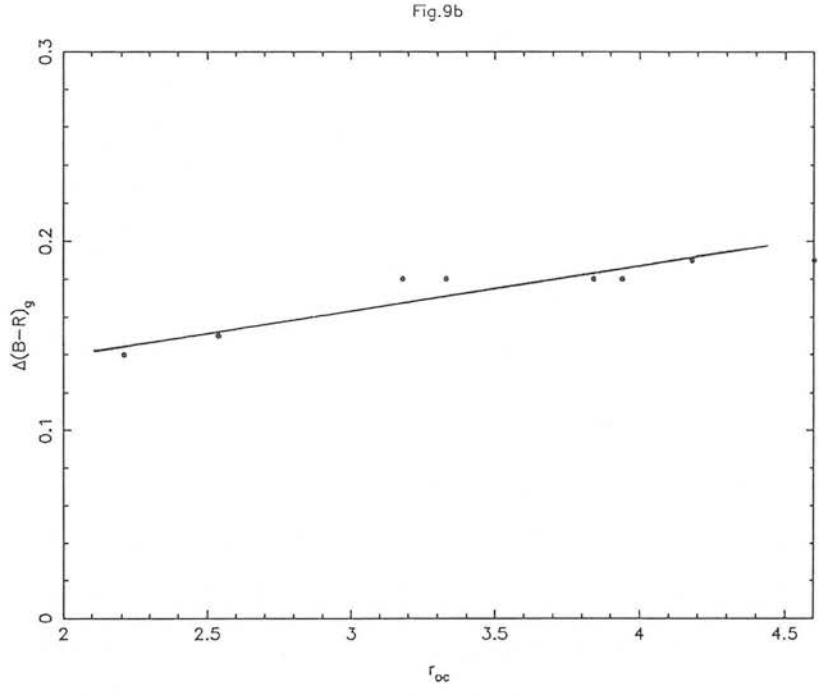

Figure 9: The radial distribution of the $\Delta(B-R)_g$ indicator, evaluated from the coarse-grid CMDs (data from Table 3)

$\Delta(B-R)_g$ as a function of distance r_o from the SMC optical centre is given in Fig.9. For both Fields, there is an increase of $\Delta(B-R)_g$, and therefore an increase of mean age, with increasing r_{oc}. In Field 28, $\Delta(B-R)_g$, lies between 0.10 and 0.22, which corresponds to a change of the mean age from $\sim$ 2 Gyr to $\sim$ 10 Gyr according to the calibration of Fig.8. In Field 52, $\Delta(B-R)_g$ lies between 0.13 and 0.21, indicating a similar range in age. The question that now arises is whether the observed change in $\Delta(B-R)_g$ can be accounted for by the known decreasing contribution of the populations younger than 1–2 Gyr. Let us assume that the contribution of the 1-2 Gyr population is $\sim$10% in the innermost regions (excluding the innermost region in Field 52) and negligible in the outermost ones studied, where older populations prevail. For simplicity an age of 10 Gyr will be assumed for these populations (e.g. Stryker *et al.* 1985). Then the expected value of $\Delta(B-R)_g$ between the inner and outer regions and on the basis of the calibration in Fig.8, would vary from 0.24 to 0.25 which is an order of magnitude smaller than the changes observed. In conclusion, the mixture of populations older than 1–2 Gyr, changes as a function of distance. This has the important implication that there are at least two populations older than 1–2 Gyr, which are distributed differently from the $< 1-2$ Gyr ones and also different from each other, with the older one (or the older ones) progressively prevailing at the outermost regions. Finally, there is some indication of a steeper increase of $\Delta(B-R)_g$ in Field 28 than in Field 52. Although this difference is within the errors, it may be significant, implying the presence of a stronger intermediate age population (but older than $\sim$ 1 Gyr) in Field 52 than in Field 28. These suggestions will be further discussed in Chapter VIII.

(ii) the spread in $\log T_{eff}$ *of the clump/HB stars.* As previously mentioned the colour (temperature) range of the core-helium burning stars depends mainly on age. However, this dependence is not well known either theoretically or empirically. An inspection of Table 3 suggests that there is no implication of a systematic change of the colour spread across the two Fields. This indicates that the presumably 'vertical' clump of the young and intermediate-age populations does not influence significantly the mean size (in colour) of the total clump/HB. This confirms that the young populations do account for only a small percentage of the core-helium burning giants in these outer regions of the SMC.

(iii) The ratio of the numbers of stars occupying the RGB to n_{cl}. Cannon (1983) suggested that the relative 'strength' of the HB or its equivalent clump and the upper giant branch can be used as a crude age indicator, because the lifetime of a star in the double (helium core plus hydrogen shell) energy source phase is only weakly dependent on total mass (and hence on cluster age). On the other hand, the rate of evolution of a giant up the ordinary hydrogen–burning giant branch slows down markedly as the stellar mass decreases. Therefore, one would expect the ratio n_{RGB}/n_{cl} to rise with age. An attempt for an empirical calibration of this quantity as a function of age is shown on Fig.10 (data from well observed Magellanic Cloud clusters; see Table 5). Although there is evidence of a trend in the expected sense, the rate of change of the ratio with age is apparently too small to render a useful age indicator. Mainly two factors reduce the observed rate of change of the ratio: (i) the inclusion of upper RGB stars in n_{cl} due to the broad magnitude limits within which 'clump' stars were counted. The adoption of such broad limits was necessary in order to be able to apply the 'calibration' to the SMC field CMDs of interest here; and (ii) asymptotic giant branch stars could not be separated from first–ascent red giants, thus contaminating n_{RGB}.

For the sake of completeness, this method was applied for the giants in Fields 28 and 52 and Fig.11 shows the resulting radial distribution of the ratio with respect to the SMC optical centre. There is no evidence of a trend towards larger projected distances from the centre. Moreover there is a discrepancy between the values in Field 52 and Field 28. This is believed to be due to the fact that the clump/HB is generally more extended in Field 52, thus contaminating the 'RGB' region more severly than is the case in Field 28. The actual absolute values of the ratios have little meaning, given the different degrees of contamination of the RGB by clump/HB stars in the CMDs and in the calibration ratios. An additional problem is the contribution of the back/foreground stars, which can vary by $\sim 10\%$, the removal of which increases significantly the uncertainty in the determination of the ratio especially affecting n_{RGB}.

Cluster	$age(Gyr)$	n_{RGB}/n_{cl}	Source
SMC			
NGC121	12 ± 2	0.29	Stryker *et al.* 1985
Kron3	8 ± 1.5	0.28	Rich *et al.* 1984
L113	5 ± 0.5	0.20	Mould *et al.* 1984
NGC411	1.8 ± 0.3	0.21	Da Costa & Mould 1986
L1	10 ± 2	0.32	Olszewski *et al.* 1987
LMC			
N1651	2.5 ± 0.5	0.21	Mould *et al.* 1986
N1777	0.9 ± 0.2	0.20	Mateo & Hodge 1985
H4	2.5 ± 0.4	0.19	Mateo & Hodge 1986
N2213	1.6 ± 0.6	0.25	Da Costa *et al.* 1986
N1978	2	0.23	

Table 5: Magellanic Cloud clusters used for the calibration of the ratio n_{RGB}/n_{cl} as a function of age.

Figure 10

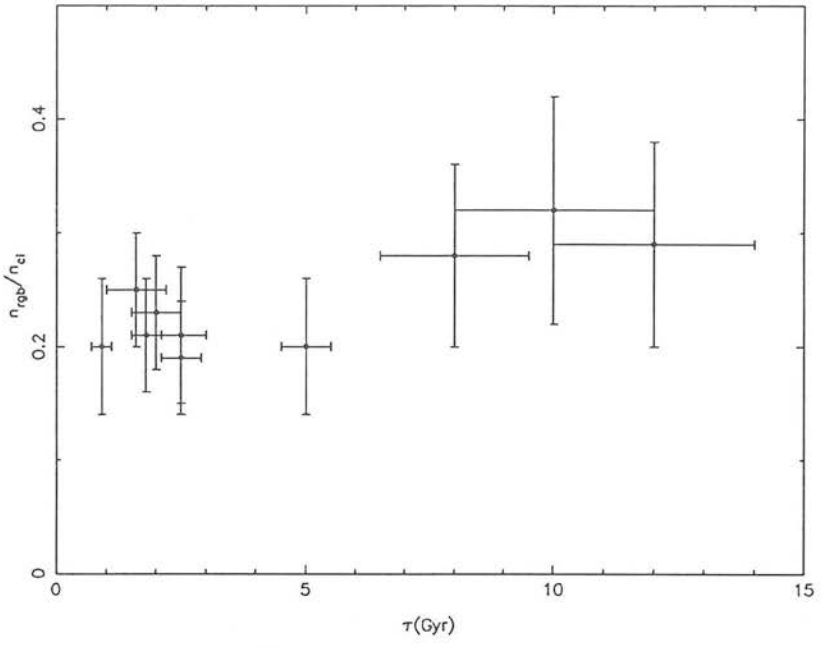

Figure 10: The age calibration of n_{RGB}/n_{cl} for Magellanic Cloud clusters (data from Table 5).

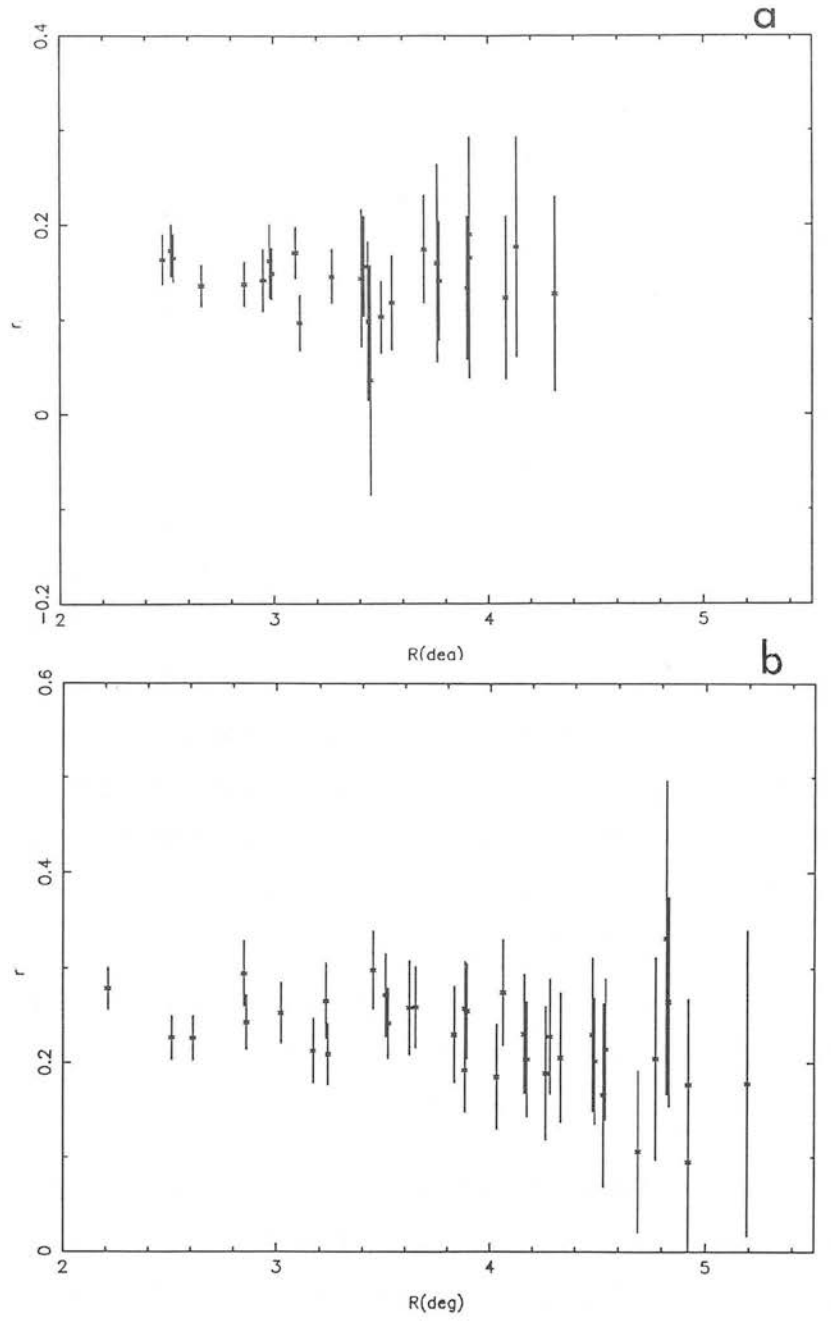

Figure 11: The radial distribution of the ratio of the number of red giant branch stars (n_{RGB}) to clump/HB stars (n_{cl}) in each of the fine-grid CMDs. (a): Field 28, (b): Field 52.

4 The subgiant branch

In the CMD of Appendix A, there is a well defined structure at $R > 19.4$ and $1.0 < B-R < 1.6$, which may be interpreted as a subgiant branch. The existence of subgiants in the SMC field is well established. It was first convincingly demonstrated by Hardy & Durand (1984; hereafter HD) in their study of the population synthesis in the Wing of the SMC. The few existing deep CMDs of SMC field populations (near the clusters Kron3, L113, NGC411 and NGC121) confirm this result. Note that the AAT CMD in Fig.3 also shows a well delineated subgiant branch. Empirical information based on observations in the Galaxy can be used to set limits to the age (or mass) at which subgiants begin to populate the Hertzsprung gap. Inspection of the diagrams of clusters dated by Janes & Demarque (1983) shows that as age increases, the transition to a populated subgiant branch takes place somewhere between the ages of the old Population I galactic clusters NGC2420 ($\tau = 3 \times 10^9$yr) and M67 ($\tau = 4 \times 10^9$ yr), as remarked by HD. Kinahan & Härm (1975) also proved in their theoretical models that the presence or not of subgiants in the HR-diagram is independent of chemical composition. Therefore, the existence of subgiants in the CMD indicates a population at least 3 Gyr old, irrespective of metallicity. In the previous paragraphs the surface distribution of populations younger or older than $\sim$ 1 Gyr was discussed. It was also suggested that the mixture of populations older than 1 Gyr is not uniform. By investigating the behaviour of the subgiant population, one could refine the age grid by effectively isolating the behaviour of tentative populations with ages between $\sim$ 1Gyr and $\sim$ 3 Gyr. The number of subgiants, n_{sub} in the fine-grid CMDs are given in Table 1.

Before proceeding, one should ensure that the contamination of the defined subgiant region with stars from the HB/clump is not large enough to invalidate the proposed effective age separation. Two effects hamper the quantification of this contribution: (i) the increasing incompleteness towards the faint end of the subgiant branch, and (ii) the fact that the dispersion around the mean clump magnitude, as calculated in Chapter IX, includes the subgiant region itself and therefore it can only be used to set an upper limit to the effect. A lower limit can be obtained from the minimum expected dispersion around the mean HB/clump magnitude (see Chapter IX), ± 0.32. However, in each region the contribution of clump/HB stars to the subgiant population

is different, depending on the mean distance modulus and the scatter around this mean in that particular region. Regions 411 in Field 28 and 213 in Field 52 were examined in this respect, as typical examples. The former has a d.m. of 18.98 ± 0.37 and the latter 18.83 ± 0.46. From the number of clump/HB stars within the same colour limits as the subgiant region, and assuming a normal distribution of the magnitudes, it is found that more than 50% of the stars in the subgiant region can be accounted for by high error clump/HB stars, even when the lower limit of the dispersion is applied. Given the small number of stars in the subgiant region and the additional errors introduced by the removal of the back/foreground, the number of stars in the subgiant region is not a very good indicator of the distribution of stars older than 3 Gyr in the SMC outer regions. Fig.7a&b shows the radial distribution (with respect to the optical centre) of the numbers of subgiants in Fields 28 and 52. It can be readily seen that the radial distribution of subgiants follows exactly –within the errors– that of the HB/clump stars. This might be interpreted as indicating that a population between 1–3 Gyr is either negligible with respect to the older populations, or else it is very well mixed with them in the whole of the area studied. However, according to the previous discussion, a significant part of this effect is due to the contamination from HB/clump stars.

5 The absence of blue horizontal branch stars in the SMC 'halo'

The morphology of the horizontal branch (clump, short red HB, bimodal HB, blue HB) depends on age, metallicity and probably on several other parameters like the Z_{CNO}/Z_{Fe} ratio, the helium abundance, rotation and mass loss rates (Stryker, Da Costa & Mould 1985; Rood & Crocker 1988 (IAU 126, 507)).

The oldest known object in the SMC is the cluster NGC121, which possesses a well-populated red HB as well as RR-Lyrae variables, but no blue HB. The age of NGC121 is 12 ± 2 Gyr and comparable to the age of the older stars in the surrounding halo field (Stryker *et al* 1985). No blue HB stars have been identified up to now in any of the studies in the SMC (Stryker 1984).

A blue HB similar to the one found in the LMC cluster H11 (Stryker *et al.* 1984; Andersen *et al.* 1984) would be expected on the SMC field CMDs within the limits $20 > R > 19$ and $B - R < 0.2$. On the basis of the distribution of RR-Lyrae variables (Graham 1975; 1984), as well as of the subgiants and clump stars presented in the previous paragraphs, we do not expect a strong central concentration of the oldest population. However, an inspection of the CMDs in the outer regions, where the ms top is fainter than $\sim 20^m$, does not show any trace of stars in the blue HB area of the CMD. To increase the probability of detection, the most well-populated regions were examined. A blue HB would appear as a 'bump' on the main sequence. There is some evidence of small discontinuities in the main sequence luminosity function in the neighbourhood of $R = 19$ mag, as previously seen, but these can be interpreted equally plausibly as evolutionary effects on the ms itself. With the present data, there is no way of proving that such discontinuities are not due to evolutionary effects among the young populations.

From the number density of stars in the previously defined tentative blue HB region on the CMD for the more remote regions, it is concluded that the blue HB stars, if at all present, have densities smaller than 10-20 stars per square degree, where the red HB star density is of the order of 2000 /per square degree. If this effective absence of blue HB stars is attributed to an age effect, then it can be concluded that the contribution of a population similar to that of H11 in the LMC or of galactic globular clusters ($\tau > 12-14$ Gyr) is at least two orders of magnitude less important than the populations younger than 10–12 Gyr, represented by the short red HB/clump, assuming that both the blue and the red HB are equally populated. However, the relative strength of the two components for a coeval population depends on several factors (second parameter problem) not yet well known. Therefore, even this upper limit is not well-founded.

1 Introduction

A number of recent surveys (Blanco *et al.* 1980; Cohen *et al.* 1981; Russell & Hyland 1985; Westerlund *et al.* 1986) have shown that carbon stars (CS) are abundant in the Small Magellanic Cloud. The CS are considered as belonging to a rather broadly defined intermediate age population and are often used as tracers of the distribution of such populations in nearby galaxies (see e.g. Aaronson & Mould 1980; Mould & Aaronson 1983). The plethora of CS in the SMC field and cluster populations has greatly boosted the theoretical study of these stars, after the breakthrough in the understanding of the basic process of their formation by Iben (1975).

In Section 2, the present status of CS theory will be examined in connection with the significance of CS as age indicators. The properties of the CS in the SMC have played an important role during the past ten years, in promoting the hypothesis of a significant burst of star formation a few Gyr ago in the SMC. However, the current theoretical models can account for these properties without invoking star formation bursts (see Section 4).

Although a lot of work has been done in the past on the properties and space distribution of CS in the SMC general field, no existing survey covers in a satisfactory way the outer periphery of the SMC which is of interest here. Consequently, a separate search was conducted for the detection (Section 3) of carbon stars in Fields 28 and 52. The surface distribution of these CS and their properties are discussed in Section 4.

Notation: In the following, stars with spectral types K and M will be referred to as M stars.

2 The significance of CS as age indicators

The CS are thought to be in the asymptotic-giant-branch (AGB) phase of evolution, alternately burning hydrogen and helium in shells above an e^-–degenerate carbon–oxygen core. The excess of carbon relative to oxygen at the surface of these stars, which gives rise to the CS spectroscopic characteristics, is produced by the 'dredge-up' mechanism, first suggested by Iben (1975): when the helium shell ignites, it does so explosively, pushing the surrounding layers outwards and initiating convective 'dredge-up' of carbon and neutron-rich elements. The helium–shell flash stops the hydrogen burning and the star fades by up to one magnitude till hydrogen reignites. Following this thermal pulse power-down phase, the freshly produced carbon and neutron-rich isotopes are mixed into the He-burning convective envelope. Carbon stars result when dredge-up has increased to beyond unity the ratio of carbon to oxygen in the atmosphere.

Comparative studies of carbon stars in Magellanic Cloud clusters showed that such objects younger than $\sim 8\times10^8$yr, or older than $8-10\times10^9$ yr, do not possess carbon stars (e.g. Iben 1984). The most probable explanation for the lower age limit is the suggestion by Mould & Aaronson (1986) that thermal pulses cannot be established in stars of $5M_\odot$ or more (corresponding to a maximum bolometric magnitude of $M_{bol} = -5.7$), before the stellar envelope is completely eroded away by rapid mass-loss. So younger clusters have the tip of their RGB populated by oxygen rich M giants rather than CS. The upper age limit, on the other hand, is connected with the minimum stellar mass for which the third dredge-up mechanism can occur. This minimum mass depends on the metal abundance of the stellar envelope (Wood 1981), and therefore the upper age limit of CS is not the same for all systems. Another possible explanation is the loss of the stellar envelope before the M-to-CS transition luminosity is reached.

This discussion shows that the presence of carbon stars in a system indicates populations with ages between 0.8 and 8 Gyr.

According to Mould & Aaronson (1980; hereafter MA) *the maximum luminosity of AGB stars*, and hence of CS, is a function of the age of the cluster (or generally of the coeval population) to which they belong. The physical principle is simply that $M_{bol,AGB}$ is a function of the core mass of the red giant which in turn is a function of

the initial mass of the star at the ms-turnoff and hence a function of age. MA derived a theoretical calibration of this dependence, taking also into account the effects of the helium and metal abundances, the mass loss along the RGB phase and the evolution in the RGB. The application of the MA calibration in practice can only yield the maximum age of a cluster, since the observed most luminous star provides only a lower limit to the actual maximum possible luminosity of AGB stars in the particular cluster, because of poor number statistics and the short lifetime ($\sim 7 \times 10^5$yr) of the CS as such. This method of chronology of coeval populations was strongly criticised by Hodge (1983), who found large systematic errors in the ages derived from the AGB luminosity, particularly in the neighbourhood of 1 Gyr. In a more recent publication, Mould & Aaronson (1985) compared their theoretical predictions for the age vs. maximum AGB luminosity relation with observational results, gathered from a number of well–observed Magellanic Cloud clusters. They concluded that for ages of the order of 1 Gyr or less the observational curve flattens away, and the calibration is no longer valid. This effect was interpreted by the authors as stemming from a more rapid mass loss for these more massive stars.

According to the AGB models of Iben (1982), the threshold luminosity for carbon stars is expected to be approximately -4.5 in M_{bol} with a tail extending to -3.7; or, according to Mould & Aaronson (1986), at $M_{bol} \sim -4$ with a tail extending to -3. There are however even fainter CS which seem to require a different mechanism of formation, probably through binary mass transfer.

In conclusion, although the upper and lower limits of the possible ages of CS appear to be well established both observationally and theoretically, the use of their luminosities as age indicators is not –for the moment at least– a good practice.

3 Field carbon stars in the outer parts of the SMC

The most extended –in areal coverage– recent survey of CS in the SMC field was conducted by Blanco & McCarthy (1983, hereafter BMC; also Blanco, McCarthy & Blanco 1980 (BMB); Blanco, Blanco & McCarthy 1978). They found that the SMC carbon stars had magnitudes in the range $14 < R < 17$). Their study was based on low dis-

persion spectroscopy in the near infrared covering a total of 6.8 square degrees on the sky. BMC constructed isopleths of constant surface density for both the central parts and the 'periphery' of the SMC. Their outermost isopleth (10 stars per square degree) only reaches the innermost edge of Field 28, although it penetrates to larger distances in Field 52. On the whole, the BMC survey includes 1.26 square degrees in Field 52 and 0.14 square degrees in the Field 28 part, i.e. less than 3% of the total area of the present study. According to the discussion in the previous section, the CS and their luminosities can serve as age indicators. It was therefore considered important, in the absence of any extended previous study in these regions, to perform an independent search for the detection of carbon stars in Fields 28 and 52. Two different approaches were followed for this purpose: First, CS were identified from their spectra on UKST prism plates and second, from their location on the CMDs.

From UKST prism plates:

The obsevational material used for this search is described in Table 1. The CS were identified on the UKST blue prism plates by the fact that the C_2 band divides the CS spectrum into small blocks which are highly recognisable even in more crowded fields (see Plate 13 in the 'UKST Objective Prisms', Savage *et al.* 1985). Thus the CS detection was straightforward and the CS found are shown on the finding charts of Appendix B. Unfortunately, no prism plate existed for Field 52 and only a small part of it could be searched for CS on the overlapping area with Field 29. The resulting numbers of CS in the coarse grid 'cells' in Fields 28 and 52 are shown in Table 2.

Generally the C_2 strength increases with $(B-R)$ colour (Westerlund, Azzopardi & Breysacher 1986, hereafter WAB). Therefore the bluest CS may have been undersampled in the present survey. Although most of the CS in the SMC seem to fall in this category of 'normal' carbon stars, according to WAB there are also a few CS too red for the strength of their C_2 band, as well as a group of blue CS with strong C_2 (R stars) or with enhanced ^{13}C abundance (J-type stars). Such discriminations were not attempted in the present study. Nevertheless, the above discussion indicates that use of the C_2-band criterion for the detection of CS is actually appropriate, in the sense that its adoption does not seem to be leading to significant biases in the resulting catalogue. Obviously, CS with B magnitudes below the limit of the prism plates ($B_{lim} \sim 19$), such

Field	RA	DEC	Plate	UT	grade	emul.	Filter
28	0^h00^m	-75^o	YJ10373P	13/8/1985	bU	IIIaJ	GG455
SMC	0^h06^m	-75^o	YJ8311p	17/12/1982	aI	IIIaJ	GG455

Table 1: Characteristics of the prism plates used for the carbon-star searches.

Region	$n_{cs,1}$	$n_{cs,2}$	n_{exp}
Field 28			
51	11	6	9
52	0	0	1
41	30	18	(30)
42	2	0	2
31	13	6	10
32	0	2	1
21	2	2	1
Field 52			
11	19	11	33
12	> 6	5	16
13	*	2	8
14	*	0	
21	10	7	(10)
22	*	0	10
23	*	2	3
24	*	0	
31	*	2	4
32	*	0	3
33	*	2	4
34	*	2	

Table 2: Numbers of carbon stars found in Fields 28 and 52; in *Column 1* from method 1 (prism plates) and in *Column 2* from method 2 (CMDs). *Column 3* Number of CS expected on the basis of the number of ms stars in each region (normalisation with respect to region 41 in Field 28v and 21 in Field 52.

Note: (*) regions not covered by the Field 'SMC' plate.

as very red N stars, as well as CS with weak C_2 band, however rare, are not detected.

From the CMD:

As discussed in Section 2, the carbon stars reside on the asymptotic giant branch, beyond the tip of the first-ascent red giant branch. As shown from CS studies in SMC clusters (Bessell, Wood & Lloyd-Evans 1983) CS can be separated effectively from M giants, on the basis of their colour, for $B - R > 3$. Hotter CS also exist, but they apparently occupy the same part of the CMD as M giants. Therefore, a catalogue of CS selected on the basis of their colour from a BR colour-magnitude diagram, is essentially biased in favour of cool CS. As remarked by Russell & Hyland (1985) the existence of a separating zone between carbon and M stars on the CMD depends on the metal abundance. However, the method is worth applying, especially since the first method previously described is not applicable for the greatest part of Field 52. A catalogue of CS candidates was thus created for both Fields 28 and 52, including all detected stars with $14 < R < 17$ (this range adopted according to the results from Blanco, McCarthy & Blanco 1980) and $B - R \geq 2.9$. The original (not corrected for the back/foreground contribution) CMDs were considered. A list of these is presented in Appendix B, along with their coordinates, magnitudes (R) and colours ($B-R$) and bolometric magnitudes; the bolometric corrections (BC) were calculated using the B.C. vs. (B-R) curve shown in Fig.1, which was based on data from Richer (1981). Table 2 presents the numbers of CS candidates identified by this method, in the various 'cells' of the coarse grid of CMD in both Fields 28 and 52.

In addition to the previously mentioned bias of the sample towards cool CS, other factors contribute to increasing the incompleteness of the catalogue. First, the procedure of pairing the photographic plates, may have removed variable carbon stars, or CS with images blended with those of other stars, or stars with randomly erroneous coordinates in any one of the paired plates. Secondly, very red carbon stars, with $B - R > 4 - 7$ (depending on the actual magnitude) are lost due to the limiting magnitude in B. The fact that most of the CS candidates are actually carbon stars is verified by a comparison with a spectroscopically verified sample (see next paragraph). An inspection of the most outlying regions in Field 28 with no CS detected by the first method showed that on the average 1-2 stars per square degree in this region of the CMD are back/foreground

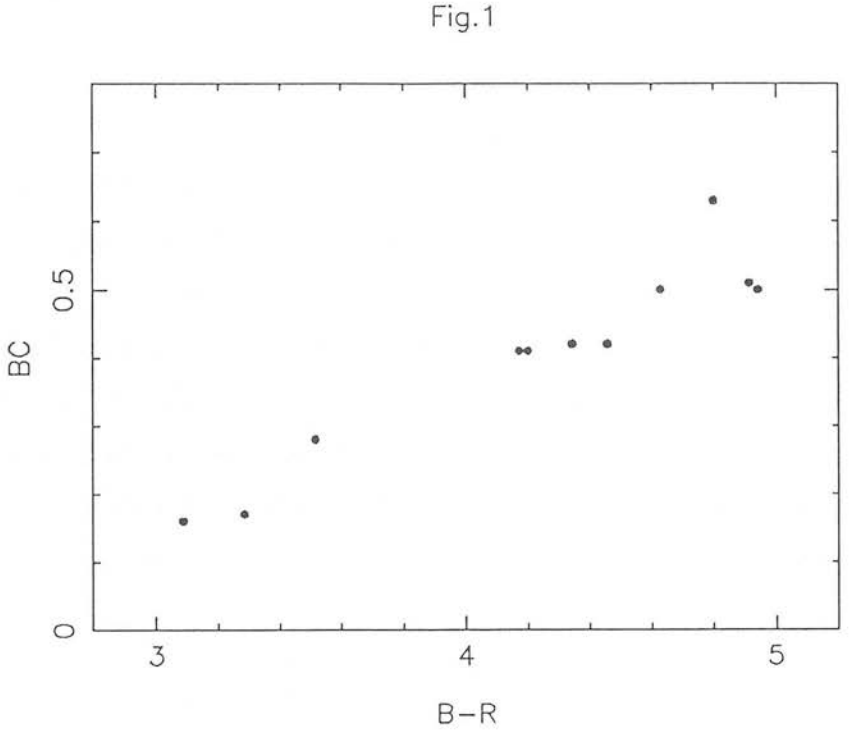

Figure 1: Bolometric correction vs. colour (data from Richer 1981).

objects. The numbers that appear on Table 2, have been corrected for this contribution.

Completeness and comparison of the two catalogues:

A sample of the CS from this study –selected by both methods from Region 4.1 and 3.1 of Field 28– were observed spectroscopically by Lloyd-Evans (private communication) and were all confirmed to be CS of the strong C_2/low CN type, reflecting the low primordial N abundance in the SMC (Lloyd-Evans 1980). The CMD of these carbon stars is shown in Fig 2. The colours and magnitudes were derived from the COSMOS data-set described in Chapter III (see Table 3).

The incompleteness of the second method compared with the first one is obvious in Table 2, from the relative numbers of CS candidates detected by the two procedures. This relative incompleteness of the second method reaches the value of 40% and is mainly due to the large adopted value of the colour limit, which was necessary in order to exclude M stars from the catalogue. The existence of CS bluer than this limit is clearly shown on the CMD of the spectroscopically confirmed CS; the relative numbers of CS bluer and redder than this limit on this CMD are an artifact of the selection criterion for the observations by Lloyd-Evans. On the other hand, a comparison between stars identified with the two methods in these same regions did not yield any star selected on the basis of its colour and not included in the first catalogue, while actually a spectroscopically confirmed CS.

An absolute estimate of the completeness of the first catalogue can be achieved by comparisons with the existing samples of CS detected with infrared techniques. As previously mentioned, the only survey partly overlapping with the present one is that of BMC. They claim a completeness of 95% for their catalogue, at least in the less crowded regions studied (in the central regions however their incompleteness may be as high as 26%, as claimed by Russell & Hyland 1985). The comparison was conducted for region 4.1 in Field 28, in which the number of CS found with the first method is 34 per square degree. By interpolation from the BMC maps, the number predicted by them in the same region is $\sim$ 39 per square degree. Therefore, the deduced completeness of our survey with respect to the BMC infrared survey is 88%, or 84% with respect to the total number of CS expected in the region, according to the BMC estimates.

RA(1950)			DEC(1950)			R	$B-R$
00	20	48	-75	02	40	15.36	2.95
00	21	39	-75	03	01	15.22	2.75
00	17	23	-75	01	02	15.86	3.20
00	14	42	-74	44	07	15.57	2.42
00	12	52	-74	59	24	15.28	2.62
00	13	18	-74	43	31	15.59:	2.73:
00	13	04	-75	12	37	15.40	3.55
00	10	47	-74	34	43	*	*
00	21	03	-74	38	49	*	*
00	12	40	-75	24	11	*	*
00	16	10	-75	25	30	15.65	1.85
00	16	44	-75	11	44	15.92	3.89
00	13	04	-75	11	44	17.10	1.75
00	20	37	-74	47	34	17.11:	1.12:
00	21	34	-74	40	19	13.86:	2.45:

Table 3: Spectroscopically verified carbon stars.

Columns 3,4: the magnitude R and colour B-R are COSMOS estimates (Chapter III).

Note: (*) stars not paired in all J and R plates.

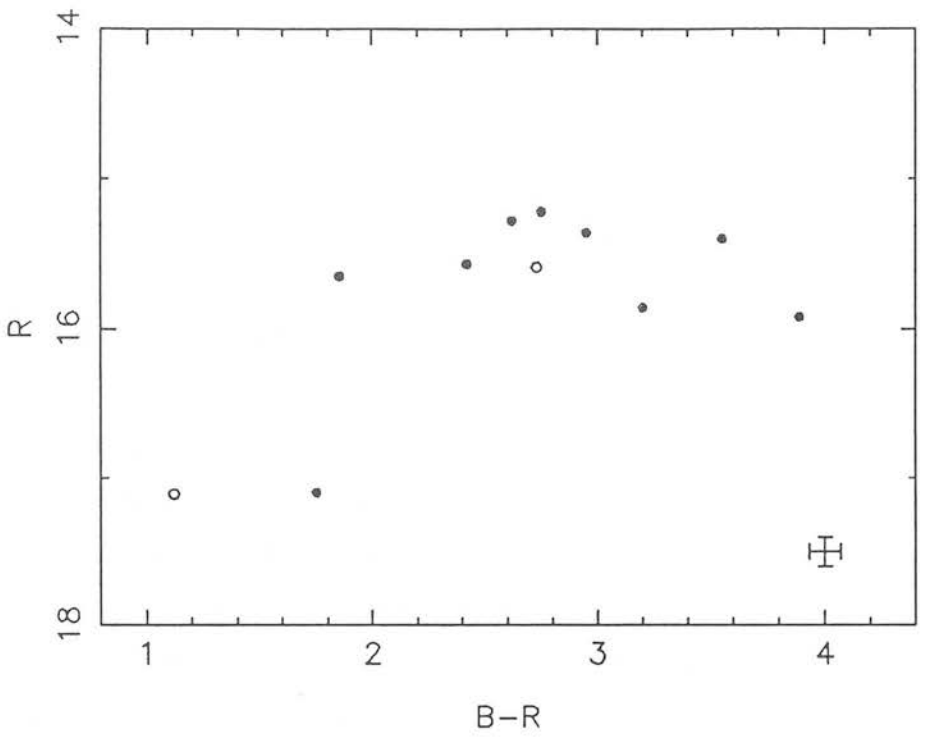

Figure 2: The CMD of the spectroscopically confirmed CS appearing in Table 3.

4 The radial distribution and LF of the CS

The radial distribution of the CS

The CS can be used as tracers of the intermediate populations in a galaxy; the radial distribution of the CS number densities in the NE and SW outer regions of the SMC, with respect to the optical centre are now examined (Fig.3). A first inspection of these distributions shows that they resemble closely the distributions of stars younger than 1-2 Gyr derived in Chapter VI; the corresponding curves are superimposed on Fig.3. In order to confirm qualitatively this similarity, the expected number of CS was calculated in each 'cell' on the basis of the number of main sequence stars younger than 1 Gyr in the same region, the normalisation factor being the ratio of CS to ms stars in the well populated region 4.1 in Field 28. These 'predicted' numbers of CS appear in column 4 of Table 2. In almost all cases the 'predicted' and detected numbers differ by less than 1σ (assuming Poisson number statistics). There is one exception, the relatively low number of CS with respect to the number of ms stars in the region in region 1.1 of Field 52. This however can be understood by the fact that the ms in this region includes a significant number of stars younger than 0.8 Gyr, i.e. populations that do not form CS. It was also noted that the distributions of both samples of CS are similar (at least in Field 28, where such a comparison is feasible), although the more complete catalogue was used for the above analysis whenever possible.

The magnitude distribution of the CS

The second sample was used for this study. It must be kept in mind that the sample is temperature limited, and the magnitude range is preset within $14 < R < 17$ (which –as previously mentioned– is the range of CS magnitudes found by the BMC survey). The magnitude distributions for the whole of Field 28 and Field 52 are shown in Fig.4. The numbers of CS in individual 'cells' are too small to render a comparison of the CS magnitude distribution at various distances from the centre meaningful. However, some conclusions can be derived from the 'global' magnitude distributions shown in Fig.4. In Field 52, CS appear to be systematically brighter by $\sim 0^m.2$ than those in Field 28. Moreover, their magnitude distribution is marginally more dispersed. Both of these differences can be explained by the geometrical effects analysed in Chapter IX: the NE outer regions of the SMC (Field 52) are both nearer in the mean (by $\sim 0^m.2$

Fig.3a

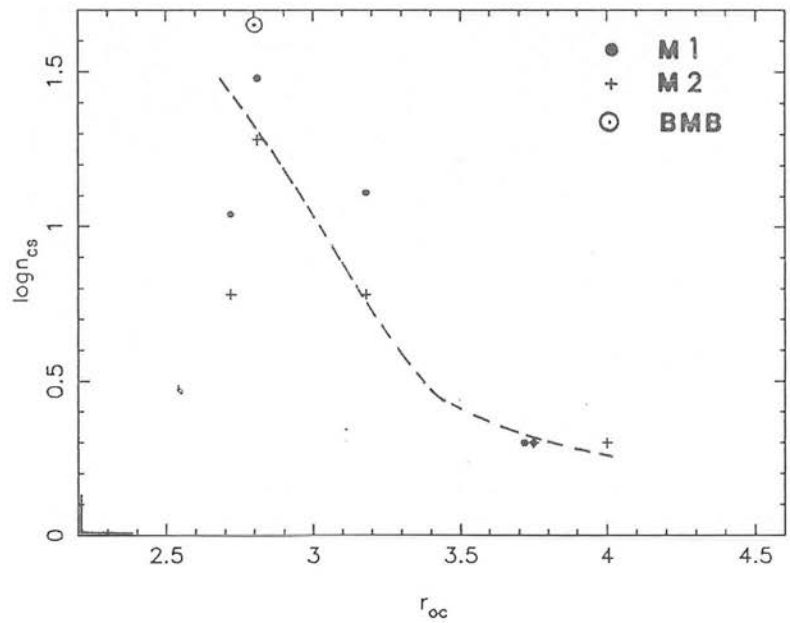

Fig.3b

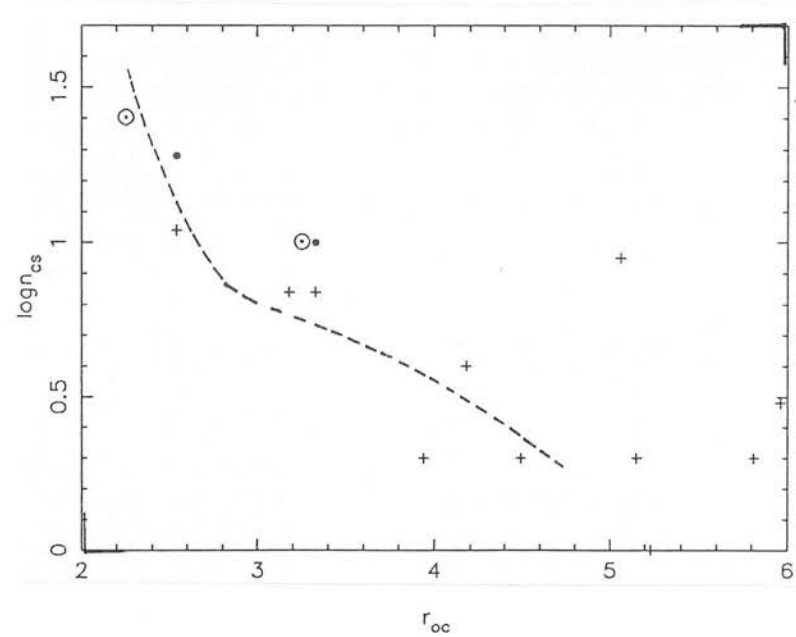

Figure 3: Radial distributions of the numbers of CS (per square degree), with respect to the optical centre; (a) Field 28, (b) Field 52.

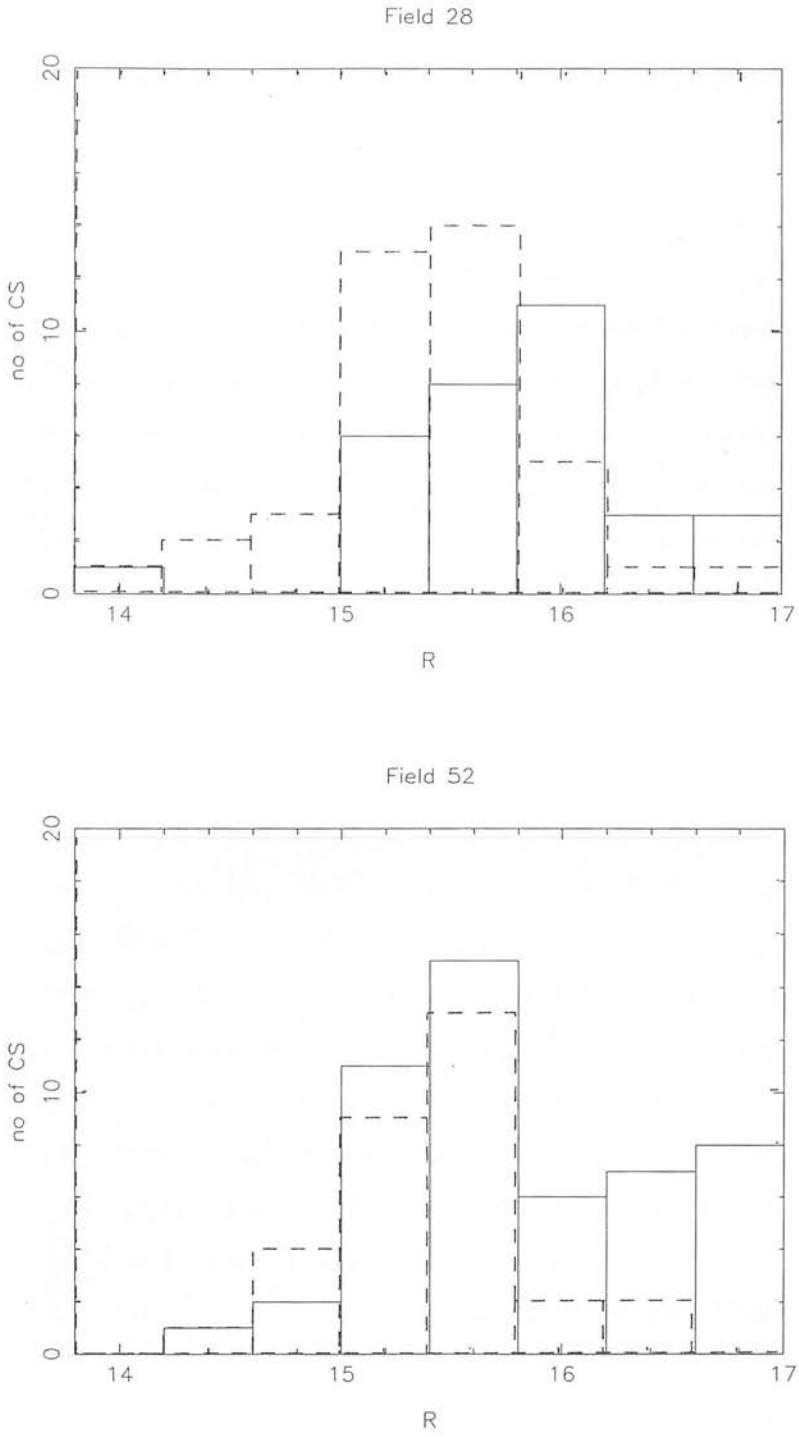

Figure 4: Magnitude distribution of CS (from method 2). The dashed line shows the magnitude distibution of all carbon stars in the BMB catalogue (in the NE).

in distance modulus) and deeper along the line of sight than those in the W/SW (Field 28). However, the same result could be caused by the presence of a group of intrinsically brighter (and presumably younger) CS in Field 52. Although the first interpretation seems satisfactory and entirely consistent with the other results of this study, the second possibility cannot be ruled out.

It is also interesting to compare these magnitude distributions with the ones derived by BMB. As seen on Fig.4 (dashed line histogram), although they differ marginally in shape, they peak around the same magnitudes. This indicates that the CS in the outer and inner regions studied in the two studies originate from the same populations. However, it would be inadvisable to follow up this point any further, in view of the incompleteness of the present samples (especially on the faint end of the CS distribution) and the poor statistics.

Age estimates

By applying the age calibration of the maximum AGB luminosity described in Section 2, an estimate for the (maximum) age of the younger CS in the SMC periphery can be obtained. Taking into account the mean distance modulus difference between the NE and W/SW areas (Chapter IX), the CS bright magnitude cut-off appears to be the same in both Fields, around $R = 15.1$ (reduced to a reference d.m. of 18.7), or $M_{bol} = -4.2$ (according to Fig.1). This corresponds to an age of 9 Gyr according to the Aaronson & Mould calibration. This is of course only an upper limit. There are carbon stars as bright as $R \simeq 14$ in both Fields, corresponding to an age of 0.8-2 Gyr. Assuming that all detected CS originate from this age-range and given that the lifetime of the CS as such is $\sim 10^6$ yr, the probability that the observed brightest star does actually coincide with the upper limit of the AGB luminosity is $\sim 50\%$.

From the BMB distributions, the bright magnitude cut-off occurs at $R = 14.8$, indicating maximum ages between 5-8 Gyr (BMB concluded an age range of 3-5 Gyr, by adopting the long d.m. for the SMC). Given the uncertainties inherent in the calibration, in the determination of the 'bright magnitude cut-off' and in the SMC distance modulus, no firm upper limit can be derived from these arguments on the age of the CS in the SMC periphery. They could well span the whole range of possible ages of CS in the Magellanic Clouds from 0.8 to 8-10 Gyr, although the numerology of the previous

paragraph suggests that many, if not all, of the observed CS are younger than 2 Gyr.

The spatial distribution of the CS examined in the previous subsection is a more useful indicator. The CS follow almost exactly the distribution of the younger populations ($\tau < 1 - 2$Gyr). This can interpreted in the following ways:
(i) Most of the CS detected (at least by the 2nd method) are younger than 1-2 Gyr.
(ii) If they originate from the whole range of possible ages (0.8 to 8-10 Gyr), then all these 'populations' are very well mixed and their distribution is indistinguishable from that of stars in the age range ~ 0.5 to $\sim 1 - 2$ Gyr.
The second suggestion is less conclusive because the efficiency of CS formation depends on age, with all AGB stars becoming CS for the younger populations (see Section 2). Effectively, the first suggestion seems to be valid, although the existence of populations in the 2–8 Gyr range is obviously not excluded.

At this point it is interesting to consider a number of misinterpretations of the properties of carbon stars in the Magellanic Clouds, in the not so distant past:
Firstly, the large number of CS in the SMC (and in the LMC) was initially interpreted as pointing to a star formation burst a few Gyr ago (e.g. Blanco & MacCarthy 1983). However, Bessell and his collaborators (1983; also Bessell 1983) showed that the number of giants that become carbon stars for the same range of initial masses, depends strongly on metallicity. For example, the high metallicity of stars in the galactic centre ($Z \simeq 3 \times Z_{\odot}$) precludes any of them from becoming a carbon star, before their asymptotic giant branch evolution is curtailed by envelope ejection. More recently, Mould (1986) proved that the SFR in the SMC need not have been higher in the past –actually it could have been as low as 1/6 of the present rate– in order to account for the numbers of CS observed in the Cloud.
Secondly, it was noticed by Cohen *et al.* (1981) that there is an apparent sparsity of bright CS with masses greater than 3–5 $M_{\odot}$ in the SMC. The occurence of cepheid variables in the same regions ruled out the possibility of this absence being due to an age effect (Becker 1982). Cohen and her collaborators interpreted the effect as showing either a steeper IMF for intermediate mass stars in the SMC, or a higher SFR in the past than at present, or as the omission of some physical factor in the theory. The latter of these possibilities was actually proved to be the case (see Section 2).

Another important conclusion that can be derived from the CS distribution in Fields 28 and 52 is the confirmation of the asymmetry of the radial distribution of the young-intermediate age populations with respect to the SMC optical centre, which was also noted in Chapter VI. This effect is also indicated by the shape of the outer isopleth given by BMC, although their study is confined to smaller distances from the centre, compared with the present study.

1 Outline of the conclusions on the stellar content of the SMC outer regions

The conclusions from the previous analysis of the stellar content in the NE and SW outer regions of the SMC can be summarised as follows:

(i) There is a mixture of ages present in the field in the outer regions of the SMC studied, ranging from a few 10^8 yr to several 10^9 yr, probably in excess of 10^{10} yr, but apparently not as old as objects in the Galactic halo.

(ii) Different age groups are distributed differently with respect to the SMC centre and in some cases differently in the SW and NE outer parts of the SMC.

Populations younger than 5×10^8 yr are present in the NE at distances between 2 and 3 kpc from the optical centre; these belong to the 'outer arm' population (Brück and Marsoglu 1978; see also Fig.2b in Chapter I).

Populations in the age range of $5 - 6 \times 10^8$ yr to 1–2 Gyr can account for less than 10% of the SMC field populations in the SMC periphery, even at the innermost regions examined. Their radial distribution drops more sharply in the SW than in the NE. In the SW area they display a significantly less extended distribution than the older stars. In the NE, they apparently follow closely the rate of decrease of the older population till they disappear.

Carbon stars with ages between 0.8 and 8 Gyr apparently follow exactly the distribution of the younger than 1–2 Gyr population, at least in Field 28, where the CS survey is complete.

The bulk of the stars in the SMC field belong to populations older than approximately 1–2 Gyr. The mean effective age of the SMC stars increases from $\sim 2-3$ Gyr at $r_o \simeq 2.5$

kpc to ~10 Gyr at $r_o = 4.5$kpc.

(iii) Despite the wide range of ages present in the areas studied and the existing gradient of mean age, the mean metal abundance seems to remain constant throughout both Fields, with the possible exception of the innermost region studied in the NE, which includes a significant younger and more metal-rich population.

(iv) The asymmetry of the stellar population distribution between the NE and SW periphery seems to be less pronounced when the radial distribution is considered with respect to the dynamical centre rather than the optical centre of the SMC, indicating that the bulk of the SMC mass (which determines the position of the dynamical centre) lies in the older populations, which predominate in these outer regions of the SMC.

2 The population synthesis: comparison with previous studies and discussion

The bulk of the populations in the outer regions of the SMC consist of stars older than 1–2 Gyr. The detailed population synthesis of this older component could not be derived from the present data. Supplementary information in this respect can be obtained from a compilation of the results from the few existing deep CMD in the SMC outer regions. Such deep CMD have become available only recently with the extensive use of CCD detectors and are in all cases by-products of the study of SMC clusters or of nearby –in projection– Galactic globular clusters. The CMDs of the field near the clusters NGC411 (Da Costa & Mould 1986) and L113 (Mould *et al.* 1984) in the eastern/northeastern areas and K3 (Rich *et al.* 1984), L1 (Olszewski *et al.* 1987) and NGC121 (Stryker *et al.* 1985) in the West, as well as the deep CMD presented in Chapter VI, and the field regions near the galactic globular clusters NGC362 (Bolte 1987) and 47TUC (Hesser *et al.* 1987) were used. Fig.1 shows the location of these regions with respect to the SMC main body. Most of these CMDs show a steep increase in the numbers of stars at magnitudes fainter than $R = 22.0$. Although all the regions seem to possess younger intermediate-age populations to varying degrees, it appears that this fainter population is dominant. From isochrone fits conducted by the corresponding authors in each case,

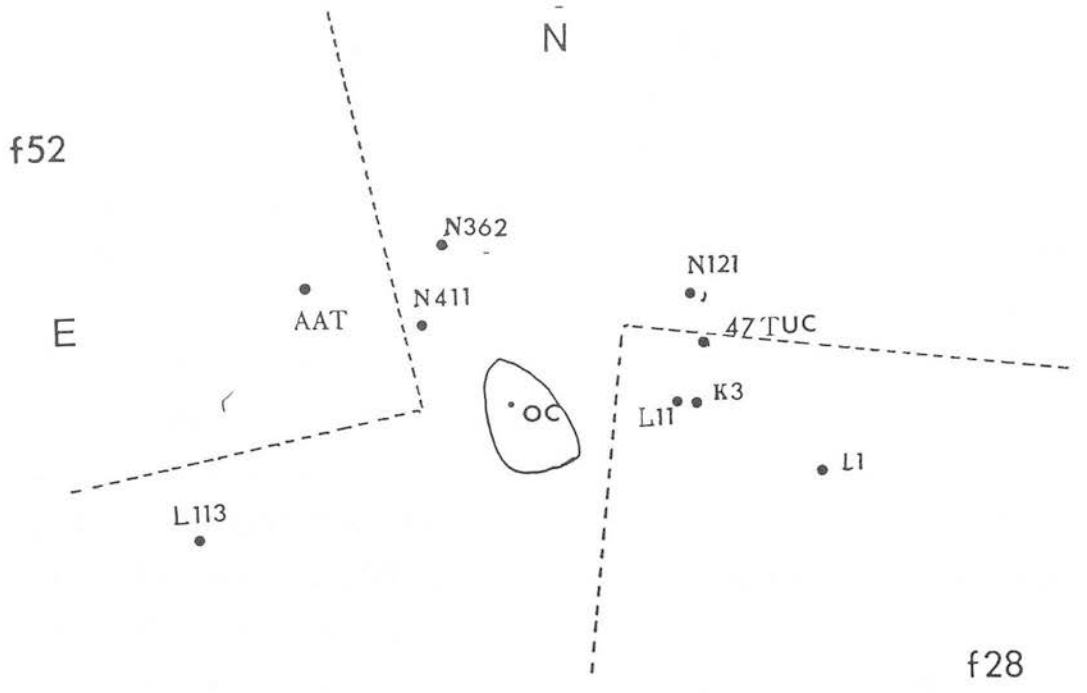

Figure 1: Location of the star clusters near which the SMC field populations have been studied with the use of deep CCD CMDs. The location of the optical centre of the SMC is also indicated, as well as the position of the region studied using the AAT CCD.

it is evident that this population has an age of 10-12 Gyr. The presence of such an old population is also suggested by the existence of RR-Lyrae variables in the SMC field (Graham 1984). However, these variables do not necessarily have ages as old as the Galactic halo (14–16 Gyr): recently Stryker *et al.* (1985) showed that the RR-Lyraes can be as young as 10–12 Gyr.

Returning to the discussion of the CMDs of the SMC field, the main sequence of the younger population reaches magnitudes between 20 and 21 in R (see Table 1). Given the poor statistics and the thinning of the upper ms, it is not clear that different upper limits essentially indicate populations with young components of different ages (1–2 Gyr in the former case and 4–5 Gyr in the latter), as was claimed for example by Stryker *et al.* A construction of faint luminosity functions of the ms from these CMDs was not attempted, because of the different (and basically unknown) degrees of incompleteness of the various studies at faint magnitudes. What can be achieved, however, is a study of the distribution of stars younger than $\sim$ 8 Gyr (i.e. with ms magnitudes brighter than 21.8 in R). The numbers of ms stars with $R < 21.8$ are compared with the total number of stars on the CMD in the same magnitude range, which includes stars of all ages. Table 1 gives the resulting ratios and Fig.2 their radial distribution (with respect to the optical centre) in the eastern and western regions. In all cases considered –with the exception of the region near NGC411– there was no apparent contribution to the ms from stars brighter than $R = 20$. Although the number of points is very small, there is evidence that the populations younger than 8 Gyr appear to have a distribution similar to that of populations younger than 1–2 Gyr examined in Chapter VI, dropping off at radial distances between 3 and 4 kpc from the optical centre and following a less steep decline in the E/NE regions. This result can be interpreted either as showing that stars with ages in the range 1–8 Gyr are well-mixed spatially, or alternatively that the dominant population among these stars is 1-2 Gyr of age. This agrees with the conclusions from the discussion of the carbon-star population (Chapter VII).

Interestingly, the field near clusters L113 and K3 do not appear to possess a dominant contribution from populations of ages similar to those of the clusters themselves, i.e. 4-5 Gyr (L113) and 8 Gyr (K3). Therefore, the second of the previous suggestions seems quite plausible. If this is actually the case then an enhanced SF rate may have

Region	r_{oc}	MS_1	τ_1	MS_2	τ_2	c	Source
	(kpc)		(Gyr)		(Gyr)		
nNGC121	2.5	22	12	21	2-5	0.13	Stryker *et al.* 1985
nKron3	2	22	≥ 10	20.3	2	0.38	Rich *et al.* 1984
nL113	4	22.1	10	20.5	2	0.26	Mould *et al.* 1984
nNGC411	1.6	21.8	5-10	17.	0.3	0.72(1)	Da Costa & Mould 1986
nL1	4	22.3	10	-	-	0.05	Olszewski *et al.* 1987
n47TUC	2	22.1	$\sim$10	20.4	2	(2)	Hesser *et al.* 1987
nNGC362	2	22.3	8–14	18	0.2	(2)	Bolte 1987
AAT	2.2	-	≥ 10	20	2	0.39	Chapters II,VI

Table 1: The stellar content of the SMC general field from deep CMDs obtained with CCD cameras. *Column 1:* the name of the SMC or Galactic cluster near which the field regions were observed. The region observed in Field 52 with the 4m-AAT is identified as 'AAT' in the Table.

Column 2: the radial distance of the centre of each region from the SMC optical centre.

Column 3: The R-magnitude of the ms-turnoff of the 'bulk' of the field stars.

Column 4: the age of the 'bulk' of the field population.

Column 5: the 'apparent' top of the ms of the youngest stars present in the field.

Column 6: the correponding age assigned to these younger populations.

Column 7: the ratio, c, of the ms stars brighter than $R = 21.8$ to the total number of stars in the CMD (with $R > 21.8$).

Notes: (1) includes a significant population younger than 1-2 Gyr . (2) the published data do not allow an evaluation of the ratio.

Fig.2

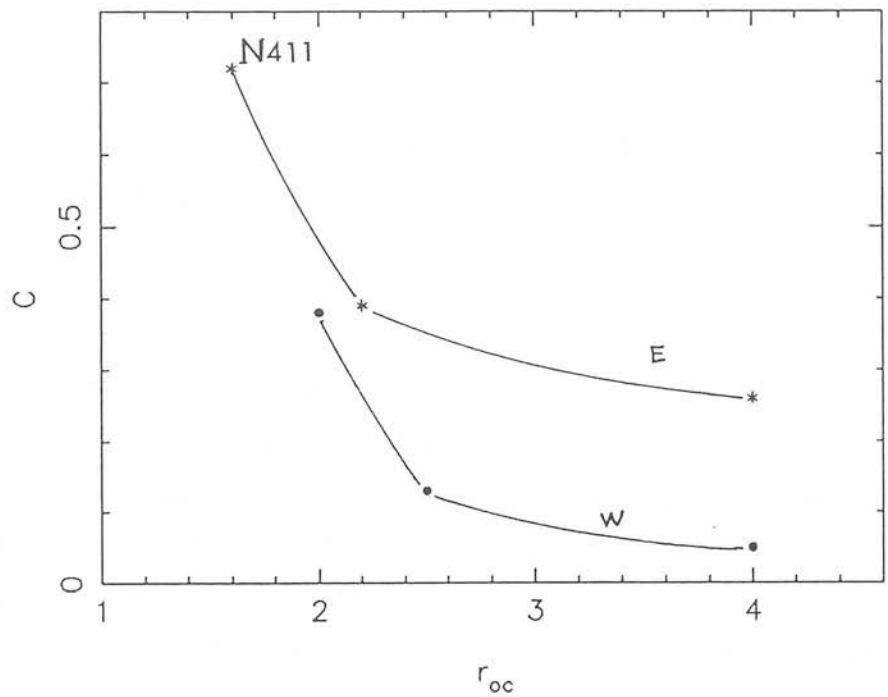

Figure 2: The radial distribution with respect to the SMC optical centre of the contribution of populations roughly between 1 and 8 Gyr to the total stellar content of the SMC field (data compiled from the existing deep CMDs in Table 1). Populations younger than $\sim$ 1 Gyr are negligible in these fields with the exception of the region near NGC411

occurred for a short period of time 1-2 Gyr ago, which may in turn account for the higher rate of chemical enrichment the past 1-2 Gyr of the SMC evolution (Section 3). An extended and faint LF study of the ms is required to gauge such evolutionary effects.

3 The chemical evolution of the SMC

3.1 The age–metallicity relation

Since heavy elements are believed to have been synthesised in massive stars, the metal abundances in present-day galaxies should offer a record through which one may trace the history of star formation within the galaxy. The chemical evolution of a galaxy can be studied on the observational age–metallicity plane.

Fig.3 shows the age–metallicity relation (AMR) for the Small Magellanic Cloud. The circles correspond to well–observed SMC clusters (data from Table 1, Chapter V). The metallicities of young stellar objects (subgiants, cepheids) are represented as one point. The point corresponding to Pop.II RR-Lyraes is placed at the minimum possible age of these variables (10 Gyr), as determined by Stryker *et al.* (1985). Another tentative point can be added on the age–metallicity plane, based on the basis of the remark by Stryker *et al.* that the field population older than 10 Gyr appears to be better fitted with an isochrone of metallicity $[Fe/H] = -1.7$. On the same figure, the shaded region indicates the age and metallicity ranges found in the outer regions of the SMC in the present study (Chapter V). Note that in this case both the age and metal abundances refer to mean (effective) values. A very similar AMR for the SMC was derived by Stryker *et al.* (1985), but was based on fewer data. The form of the AMR is also confirmed by the work of Smith *et al.* (1988) from the integrated spectra of a number of SMC clusters. An important feature of the AMR is the near constancy of metal abundance for ages between 2 and 10 Gyr. Both this constancy in metallicity and the range in age of the effect could be challenged, given the large error bars associated with the observations. Moreover, a significant part of the AMR is defined by the ages and metallicities of clusters; this makes it necessary to hypothesise that the conditions and

Figure 3

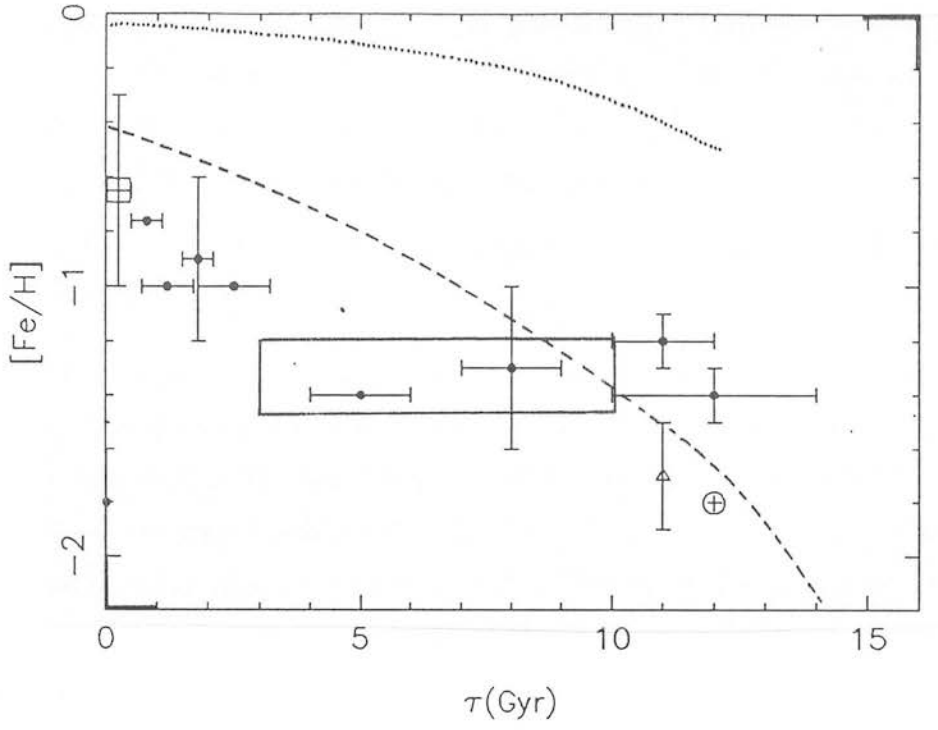

Figure 3: The age–metallicity relation for the SMC. The square sign corresponds to stellar objects younger than a few 10^8 yr (data from Table 1, Chapter V). The rectangle marks the metal abundance limits derived in the present study. The dashed line corresponds to the AMR of the LMC (data from star–clusters metallicities by Smith *et al.* (1988) and Cohen (1982)) and the dotted line to the AMR of the Galactic disk (Twarog 1980).

rate of formation of clusters are the same as that of stars, when interpreting the AMR of Fig.3. It is therefore of particular importance that the present data confirm this near constancy of metal abundance for the same effective range of ages and for a large proportion of the SMC outer regions.

It would appear therefore that no significant chemical enrichment took place in the SMC between $\sim 2-10$ billion years ago. On the other hand, the rate of enrichment has apparently increased substantially during the past 1-2 Gyr. Little can be said about the early stages of the chemical enrichment in the SMC since the only point available is that for the RR-Lyrae variables, which, however, suggests that probably a more rapid initial enrichment took place during the first billion years or so of the chemical life of the SMC. These conclusions are only tentative and the true dispersion in metal abundance for the various age–groups is necessary.

It is interesting to compare the AMR of the SMC with that of the LMC and our own Galaxy. On Fig.3 the AMR of our Galaxy, taken from Aaronson 1986, is shown, along with that for the LMC which was compiled from several sources (Cohen 1982; Mould & Aaronson 1982; Aaronson 1986; Smith *et al.* 1988). In the Galaxy, there has been a rapid initial enrichment between 16 and 14 Gyr ago, followed by a slow steady increase of the metal abundance. In the LMC, the chemical enrichment has proceeded at a more leisurely pace, although faster than in the SMC, at least for a large fraction of its lifetime. The fact that the heavy element enrichment has been relatively slow in the Magellanic Clouds was already foreseen by van den Bergh in 1975. In the next section an attempt is made to interpret the observed AMR of the SMC in terms of a number of standard models of chemical evolution.

3.2 Modelling of the AMR in the SMC

(i) The simple model of chemical evolution:

The so-called simple (one-zone) or closed-box model of chemical evolution is thought to provide –to first order– an adequate description of the enrichment history in isolated Magellanic type irregular galaxies (Pagel 1981; Hunter & Gallagher 1986; Aaronson 1986); it was also found to fit satisfactorily the AMR of the LMC (e.g. Cohen 1982). The simple model was first developed by Searle & Sargent (1972; also Pagel & Patchett 1975). It considers a region in a galaxy ('zone') which can be assumed isolated, with no material entering or leaving it during the period under study. Initially the material is entirely gaseous and free of heavy elements. As stars are formed from the gas, and massive stars explode, heavy elements manufactured in the stars (along with hydrogen) are returned to the interstellar medium (IM). It is assumed that these mix instantaneously with the IM (e.g. through turbulent motions in it), so that the IM remains chemically homogeneous. The supply of the interstellar gas is gradually consumed and the remaining gas becomes steadily more polluted with heavy elements. A further simplification is achieved by assuming that the *nucleosynthetic yield*, p, is the same in each generation of stars. The yield p is the mass of heavy elements ejected from the 'zones' undergoing complete nuclear processing, per unit mass locked up in long–lived stars or remnants. Then the metal abundance Z can be expressed as a function of the ratio of the mass in gas to the mass in stars, μ.

$$Z(t) = pln(\frac{1}{\mu}) \qquad (1)$$

But, Z(t) can be derived as an explicit function of time by assuming a certain star formation law, here the Schmidt law (1959) i.e.

$$\frac{dS}{dt} \propto \mu^n \qquad (2)$$

where S(t) is the total mass of all stars born up to time t. From the law of conservation of mass in the isolated region and eq. (2) Searle & Sargent derive,

$$d(ln(\frac{1}{\mu})/dt = \frac{\mu^{n-1}}{\tau_o}, \qquad (3)$$

where τ_o is a characteristic scale for the 'turnover time' for conversion of gas into stars.

According to Brück (1980), n varies from ~ 0.9 to ~ 1.8 in the SMC central regions. Here three cases will be considered, $n = 0.5, 1.0, 2.0$.

For $n = 1$, the case of constant SF efficiency, eq.(3) becomes $\mu = e^{-t/\tau_o}$ and eq.(1) gives

$$log[Z/Z_\odot] = log[Z_1/Z_\odot] + log(t/t_1), \qquad (4)$$

where Z_1 is the present day metal abundance and t_1 the age of the system; the epoch when the SF began is considered as time zero. Note that in the observational AMR, zero-age is assigned to the present time.

For $n = 2$, eq.(1) & (3) give

$$log[Z/Z_\odot] = log[Z_1/Z_\odot] + log(\frac{ln(1 + t/\tau_o)}{ln(1 + t_1/\tau_o)}), \qquad (5)$$

where $\tau_o = \frac{t_1}{\frac{1}{\mu_1}-1}$ and μ_1 the present day gas-to-total mass ratio.

Finally, for $n = 0.5$, eq.(1) and (2) give

$$log[Z/Z_\odot] = log[Z_1/Z_\odot] + log[ln(1 - \frac{t(1 - \sqrt{\mu_1})}{t_1}] - log[ln(\mu_1/2)] \qquad (6)$$

Adopting the values $t_1 = 12 \times 10^{10}$ yr, $\mu_1 = 0.36$ (Lequeux 1984) and $log[Z_1/Z_\odot] = -0.5$ as plausible estimates for these quantities, the eq.(4)-(6) were applied to provide the predictions of the simple model for the SMC (Table 2). The resulting curves are shown in Fig.4. It must be mentioned at this point that the actual *form* of the resulting age-metallicity curve is not very sensitive on the exact values of t_1 and μ_1. A change in Z_1 results in an almost parallel shift of the curves along the metallicity axis. It can be seen immediately in Fig.4 that the simple model cannot account for the chemical enrichment history of the SMC, at least with the adopted law of SF (eq.2). Aaronson (1986) suggested that if the star formation rate of stars providing the chemical yield is assumed slower in the SMC than in the LMC, the agreement of the simple model with

τ	$\log(Z/Z\odot)_1$	$\log(Z/Z\odot)_2$			$\log(Z/Z\odot)_3$
Gyr		$\mu_1 = 0.36$	$\mu_1 = 0.1$	$\mu_1 = 0.7$	
12	-0.50	-0.50	-0.50	-0.50	-0.50
10	-0.57	-0.54	-0.52	-0.56	-0.59
8	-0.68	-0.60	-0.57	-0.65	-0.69
6	-0.80	-0.69	-0.62	-0.76	-0.83
4	-0.98	-0.83	-0.71	-0.92	-1.01
2	-1.28	-1.09	-0.89	-1.20	-1.32
1	-1.58	-1.37	-1.10	-1.50	-1.62

Table 2: Simple model predictions of chemical evolution of the SMC.

Column 1: the timescale of the evolution, with the present time $\tau_1 = 12 \times 10^9$ yr and $\tau_o = 0$ the time when SF began in the Galaxy.

Column 2: simple model predictions of metal abundance, from eq.(4)

Column 3: same as above, but from eq.(5) and for three different values of μ_1 (the first one being favoured by the observations).

Column 4: same as above, using eq.(6).

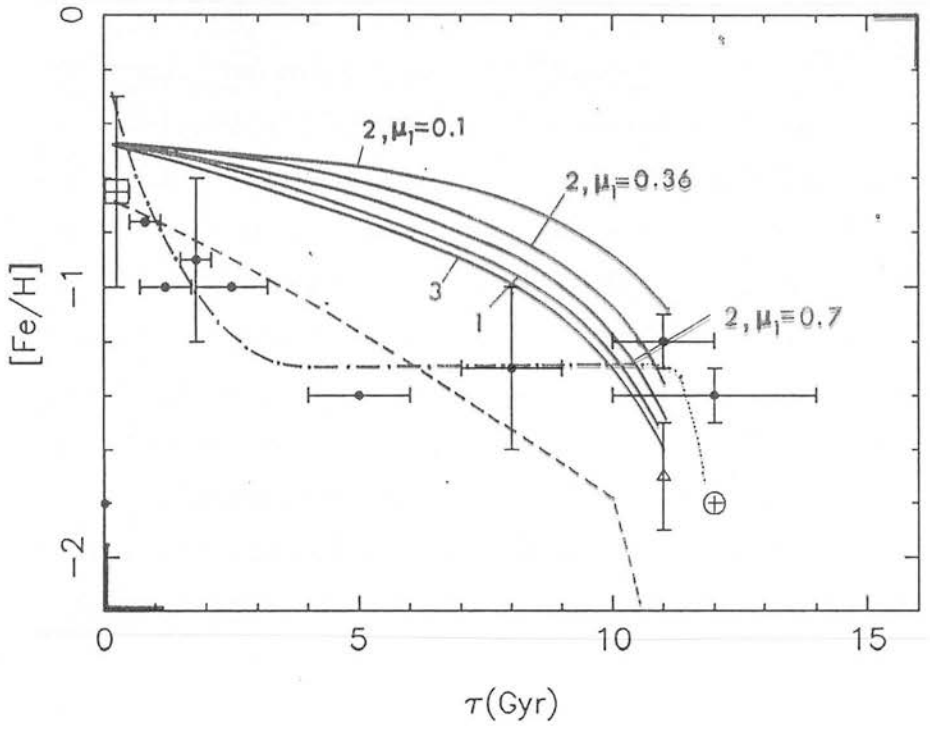

Figure 4: Simple models of chemical evolution for the SMC. *Solid lines*: the simple model of chemical evolution with a Schmidt SF law and the index n=0.5, 1, 2. *Dashed–line:* the Chiosi–Matteucci model, using a SF burst scenario (Matteucci 1984). *Dash–dotted line*: the observational AMR as it appears in Fig.3.

the SMC AMR is improved; however, this possibility is in contrast with the fact that the background stellar sheet in the SMC appears to be older than in the LMC (Hardy & Durand 1984; Brück *et al.* 1985).

In conclusion, one or more of the original assumptions of the simple model do not hold in the SMC, although they apparently do so in the LMC and the majority of Magellanic irregulars.

(ii) The simple model with stochastic SF and SF bursts :

Matteucci & Chiosi (1983) and Matteucci (1984) constructed a chemical evolution model which –while keeping the basic assumptions of the simple model (i.e. single-zone description and complete instantaneous mixing of gas)– takes into account the stochastic mode of SF in the SMC, with the SFR initially assumed continuous but fluctuating. However, they had to invoke a lower SF efficiency in the SMC compared with the LMC; this was no longer essential if, instead of a continuous SF, the SMC was assumed to have undergone several bursts of SF (50-60) during its lifetime. Their proposed AMR is shown on Fig.4. The model agrees with the general trend of the AMR, but it fails to explain –in the same way as the simple model of the previous paragraph– the sharp rise in metallicity among the young objects, or to reproduce the quiescent era between ~ 2 and ~ 10 Gyr. According to this model a change in mean metallicity from ~ -1.3 to ~ -2.0 would be expected in this age range, which does not seem to be the case observationally, even allowing for the large errors.

(iii) Gas infall (accretion) model : The simple closed-box model adopted in the previous paragraphs can be complicated by e.g. gas infall from the outer parts of the galaxy, or by gas that does not actively participate in the chemical evolution of the galaxy. Infall of gas towards the centre of an irregular galaxy has been suggested theoretically in the past and turbulent HI velocities were observed in some Magellanic irregulars, but there is no clear evidence that infall is actually taking place (Hunter & Gallagher 1986).
Here, one of the main assumptions of the simple model –that of the 'closed-box'– will be dropped and metal-free gas will be allowed to enter the disk at some rate. For simplification, this rate is taken as some constant fraction f' of the SFR, which is also assumed to be approximately constant. This *infall* (or *accretion*) chemical model was first devised by Larson (1972) and further developed by Twarog (1980) who used it to

explain the AMR in the galactic disk.

The AMR of the SMC can be at least qualitatively represented by this model, if we assume that in the neighbourhood of 2 Gyr ago there was an abrupt change of the infall rate, without having to change the SF rate. According to Twarog (1980) the infall rate does not affect the SFR in any significant way, while it does dramatically alter the AMR. For a high value of f', there is an initial steep increase of metallicity in a short time, followed by a long period of little or no chemical enrichment. This can account for the observed plateau in the AMR; however it also predicts an abrupt increase of metallicity during the first few Gyr of the SMC life. This cannot be confirmed or rejected by the available observations (although the position of the RR-Lyrae point seems to agree with a sharper trend of the AMR towards lower metallicities in this part of the AMR). A subsequent lowering of the infall rate of metal-free gas would lead to a rapid increase of chemical enrichment.

This assumption of a change of the infall rate appears to be introduced in the above in an *ad hoc* way, without any observational evidence pointing to such a phenomenon. It can be conjectured that this change in infall rate could be caused by an externally imposed (tidal influence of the LMC? See also Chapter IX) change in the gas dynamics in the SMC.

Interestingly, Rocca-Volmerange and her collaborators (1981; also Lequeux 1984) have suggested the possible existence of a large rate of accretion of gas in the SMC, in their attempt to reconcile the conclusion that the SFR appeared to be roughly uniform in the past in the SMC, with the fact that the amount of gas available to form stars has decreased by more than a factor of ten.

3.3 Conclusions

The AMR of the SMC (Fig.3) defies a simple straightforward interpretation in terms of the simplified models usually applied in disk galaxies (such as the Magellanic irregulars) as well as spiral (infall or accretion model) galaxies. Given the multiplicity of the largely unknown factors (like the stellar-mass function, the dynamics of the gas-stars system and the external influence on it, the role of 'passive' gas, the constancy or not of the chemical yield, the possible infall of gas) that can affect the AMR, as pinpointed in the

previous section, it is premature to attribute the form of the AMR as indicating a burst of SF in the SMC 2–3 Gyr ago.

Observationally, it is important to derive the true scatter of the AMR, i.e. how big the abundance spread is at a given age (especially, for the first billion years of the SMC life). Moreover, as remarked by Olszewski (1988), it is questionable whether it is valid to assume that the age–metallicity relation is uniform over the whole of the SMC, in particular since it is possible that the SF propagates stochastically and probably with localised star bursts (for example, the SMC cluster NGC330 has a very low metallicity, although it is very young). However, the present data show that there is uniformity at least in the outer regions studied and within the recorded observational errors.

4 The 'disk' and 'halo' components in the SMC outer regions

As reviewed in Chapter I, the outer regions of the SMC have often been described as consisting of a 'halo' component, mixed to some extent with an 'old disk' component (Brück 1980, 1982). These terms are used in a stellar-evolutionary rather than a dynamical sense. There is no indication that the kinematical or dynamical behaviour of the older ('halo') stars is different from that of the younger 'disk' stars (reference is not made here to the very young stars in the central regions of the SMC, which are known to follow complex kinematic structures, as is as is briefly discussed in the next chapter). Magellanic-type irregulars are generally thought to be disk galaxies (see Chapter I); in the LMC the kinematical study of its cluster system by Freeman *et al.* (1983) showed no spheroidal component even among the oldest clusters. Unfortunately no similar kinematical study exists for the SMC to date.

Although the 'disk' and 'halo' populations do not seem to be distinct in a kinematical sense, the radial distribution of the older and younger stars is different, with the older stars prevailing in the outermost regions. This was pointed out by Brück (1980), and was confirmed in a quantitative way in the present study. It must be mentioned that a similar effect is also suggested –but for regions nearer to the SMC centre– by the

well-known reddening of the integrated colour of the SMC with radial distance from the centre and recently by the work of Blanco and McCarthy (1983), who noticed that the ratio of the numbers of carbon to M stars in the SMC changes with radial distance (while it remains the same all over the LMC).

A similar aging towards the periphery is known to exist in other irregulars (e.g. NGC 5253; Gallagher & Hunter 1986). A possible explanation of the effect lies with the density of gas from which future stars can be condensed. It has been advocated that there is a critical gas density below which star formation cannot take place (Hunter & Gallagher 1986). Therefore one could presume that in the SMC, after the first few generations of stars in the outer periphery, the gas density dropped below the critical value. This conclusion is only conjectural and a lot of both theoretical and observational work is yet required before it could be confirmed or disproved.

1 Introduction

The morphological and kinematic properties of the Small Magellanic Cloud (SMC) have been the subjects of numerous investigations since the publication of the first extended study by de Vaucouleurs (1955). However, the determination and interpretation of the large scale structure of the SMC remains a puzzle.

It is generally accepted that the SMC structure has been strongly influenced during its evolution by the gravitational fields of the Large Magellanic Cloud (LMC) and the Galaxy. Some of the prominent features of the Magellanic System, like the gaseous Bridge connecting the two Clouds, and the Magellanic Stream, are thought to be the products of these interactions; the latter has actually been reproduced quite successfully by the more advanced existing tidal models (Murai & Fujimoto 1980, 1986; Fujimoto & Murai 1984).

One of the principal questions to be addressed is the extent to which the structure of the SMC, as well as its evolution, is determined by the gravitational influence of the LMC and the Galaxy. Detailed modelling and conclusive results on the physical processes involved in the interaction (and consequently, on those in interacting galaxy systems in general) require the imposition of constraints not yet adequately determined by the observations.

There are several observational results which have been interpreted as indicating the tidal effects of the LMC and the Galaxy on the stellar and gaseous components of the SMC: the large line-of-sight depth of the SMC, more pronounced in the northern regions (e.g. Ardeberg & Maurice 1979; Azzopardi 1982; Dubois 1980; Florsch, Marcout & Fleck 1981); the existence of at least four distinct velocity groups of gas and related young objects in the SMC (Torres & Garranza 1987 and references therein); increasing evidence that these velocity groups are stratified along the line-of-sight (Songaila *et al* 1986 and references therein). Actually, Mathewson, Ford & Visvanathan (1986; 1988 hereafter

MFV) interpreted the situation as showing that the SMC is in the process of 'irreversible disintegration'. It must be emphasised that all existing studies on the subject are limited to the gaseous component and the very young and young stars presumably related to it (e.g. blue and red supergiants and cepheid variables), essentially confined in space to the SMC central regions and the Wing (Brück 1982; see also Chapter I). There is virtually no information about the dynamics and kinematics of the intermediate and old populations dominating the outer regions of the SMC, which were studied from the point of view of stellar content in the previous chapters.

In this chapter it is attempted to remedy, at least in part, this incompleteness. The principal aim is to investigate the three-dimensional distribution of the intermediate and old stellar populations in the outlying northeastern and southwestern regions of the SMC, at projected distances larger than ~ 2 kpc from the SMC optical centre and over the total area of 48.5 square degrees of the present study. The luminosity of the red horizontal branch/clump stars are used to probe the distribution along the line of sight of the stellar populations in the regions studied.

In Section 2 the methodology is described, in Section 3 the results on the morphology of the SMC outer regions are presented, while in Section 4 an interpretation of the results in the context of the membership of the SMC to the triple interacting system (the Galaxy-LMC-SMC) is attempted. Finally, in Section 5 the conclusions are summarised.

2 The method

The horizontal branch/clump observed at the base of the red giant branch in the CMDs (Appendix A) of stars in the NE and W/SW outer regions of the SMC was studied extensively in Chapter VI. It was shown that it consists mainly of stars older than 5×10^8yr and therefore according to the discussion in Section 3 of Chapter VI, the mean luminosity of the HB/clump is constant, although it changes considerably for ages younger than the above limit. Consequently, it can be used as an approximate distance indicator.

The mean magnitude of the clump stars, as derived from well-studied SMC clusters older than 0.5 Gyr, is $\overline{R} = 18.92 \pm 0.04$ (Olszewski, Schommer & Aaronson 1987; Olszewski 1988); the recorded error is mostly due to the differences between the distances of the individual clusters used in the calculation. The short distance modulus (d.m.) is adopted for these clusters (see Chapter IV). Thus, the mean absolute magnitude for the clump stars as derived from SMC clusters is $M_R = 0.13 \pm 0.04$ (assuming reddening $A_R = 0.07$ as shown in Chapter IV). From galactic clusters, the value of $\overline{M_V} = 0.7 \pm 0.1$ (Mateo & Hodge 1985) is derived. This value corresponds to $\overline{M_R} = 0.2 \pm 0.1$, which is identical within the errors with the value derived independently from the SMC clusters. However, some uncertainty remains for the mean absolute magnitude of the clump giants derived. This does not hamper the interpretation of the results, since the relative d.m. is mainly of interest in the following.

The range in magnitude of the clump giants plays an important role in what follows. As shown in Chapter VI, there is an intrinsic luminosity range for the clump stars of the order of ± 0.30 mag (or less), which does not display any observable dependence on the age or the metallicity of the stars, at least within the age range of 0.8-10 Gyr.

Using the magnitude distribution of the HB/clump stars, as well as their surface distribution on the plane of the sky, a three-dimensional picture of the outlying NE and SW regions of the SMC is produced.

A first inspection of the CMDs in Appendix A suggests that the magnitude range of the clump stars is larger for the Field 52 CMDs than for the Field 28 ones. In what follows, it is argued that the difference is statistically and physically significant and that it is due to a depth of $\sim$ 16kpc along the line-of-sight of the SMC populations involved; the mean d.m. for the SMC outer regions is also derived from the mean magnitude of the clump stars.

The clump region is studied separately in each of the fine-grid CMDs in both Fields 28 and 52. The clump region was defined so as to include all stars within the following limits: $18.0 \leq R \leq 20.0$ and $0.60 \leq B-R \leq 1.80$. These limits were selected on the basis of the –at least apparently– most extended clump regions in Field 52. Subsequently, the magnitude distribution of the clump giants was examined (Fig.1). In order to

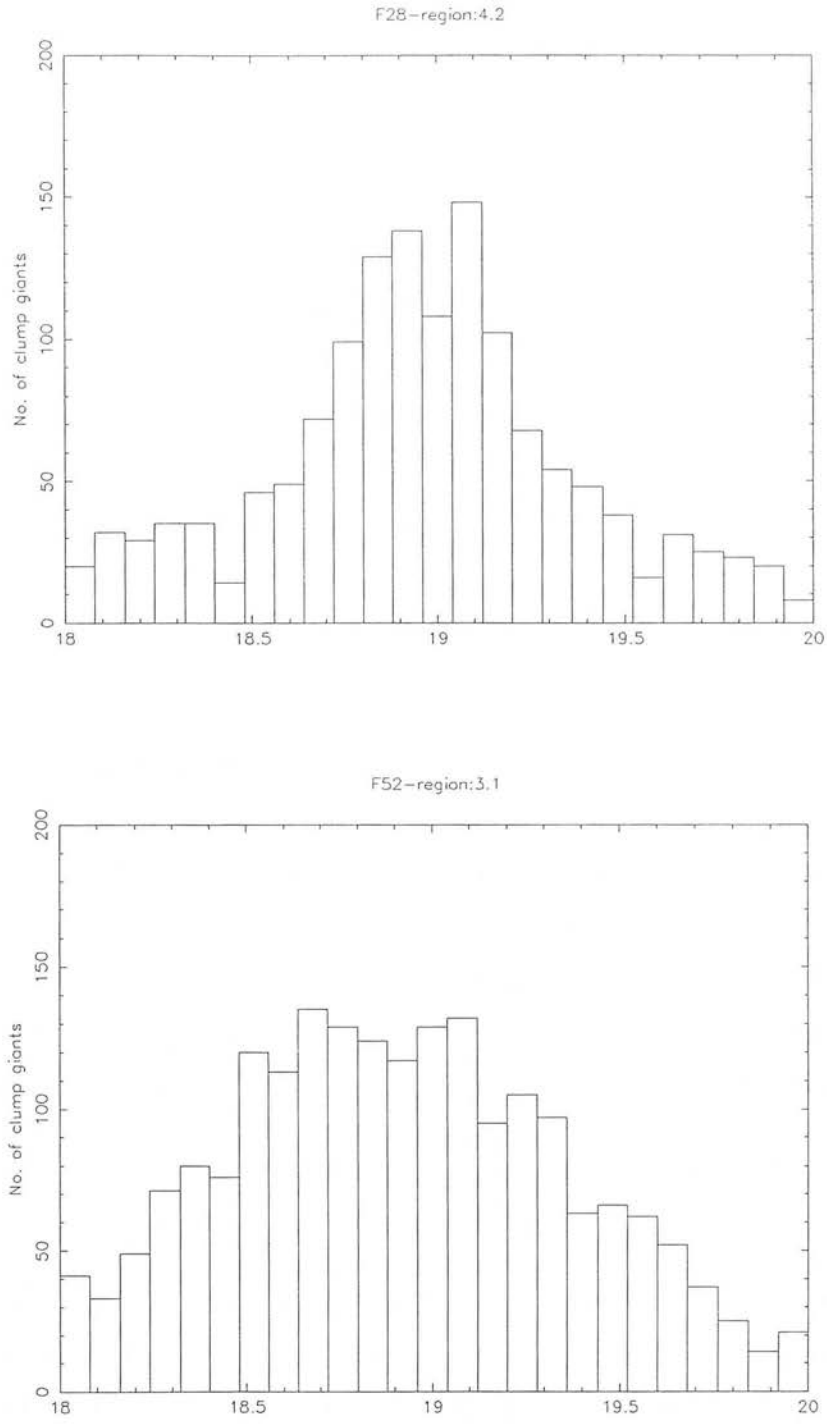

Figure 1: Examples of the distribution in magnitude of the clump stars, in two 0.88-square–degree regions in Field 28(a) and Field 52(b).

estimate the mean and the dispersion around the mean of each distribution, the median method commonly used in such cases was applied; the median was adopted as a location measure, while the dispersion was determined by the range $\pm\Delta$ (after removing the offset), within which 68.3% of the values lie. Only areas with number densities of clump stars per square degree at least twice the mean density of the fore/background in the corresponding area of the CMD have been considered. This choice is justified by the steep increase in the errors of the estimated values of the mean and dispersion of the clump-star magnitudes, for densities lower than the above limit. Table 1(a & b) gives the resulting values of the median and dispersion of the magnitude distribution for the fine-grid CMDs and the corresponding surface number density of clump stars per square degree (after subtracting the back/foreground contribution).

3 The results

3.1 The mean clump magnitude:

As discussed previously, the mean magnitude $\overline{R}_{clump}$ of the clump stars for old enough populations gives a good estimate of the **mean** distance modulus of the stellar populations forming it. The derivation of the distance modulus $(m-M)_o$ in each case is straightforward: $\overline{(m-M)}_o = \overline{R}_{clump} - M_{R,clump} - A_R$, where $A_R = 0.07$. Column 5 in Table 1a&b gives the resulting values of $(m-M)_o$ in Fields 28 and 52 respectively.

Fig.2a and Fig.3a show the dependence of the derived $\overline{(m-M)}_R$ on the projected radial distance from the SMC optical centre r_{oc}, for Fields 28 and 52 respectively.

In **Field 28**, $\overline{R}_{clump}$ varies from 18.95 to 19.07 and $(m-M)_o$ from 18.82 to 18.94 (Table 1a). It appears that there is little dependence of $\overline{R}_{clump}$ on r_{oc}, with the possible exception of the southern-most regions (depicted as encircled crosses on Fig.2a and indicated with asterisks on Table 1a) in the Field, which appear to have a higher mean clump magnitude by ~ 0.07 mag. Although such a difference could be accounted for by some systematic error in the photometry in the region in question it may be a real effect. Disregarding these points, there is still evidence of an ill-defined trend towards greater line-of-sight distances, as r_{oc} increases, corresponding to a total difference of

Region	r_{oc}	$\log d$	$< R >$	$(m-M)_o$	σR	depth
	(kpc)	(deg^{-2})				(kpc)
511	2.48	3.70	18.95	18.82	0.37	10.7
512	2.95	3.58	18.95	18.82	0.38	11.8
513	2.52	3.68	18.92	18.79	0.35	8.4
514	2.98	3.51	18.95	18.82	0.37	10.7
411	2.66	3.78	18.99	18.86	0.36	9.8
412	3.10	3.69	18.98	18.85	0.37	10.9
413	2.53	3.72	18.96	18.83	0.38	11.8
414	2.99	3.68	18.96	18.83	0.39	12.8
311	3.12	3.63	18.95	18.82	0.35	8.6
312	3.50	3.51	18.99	18.86	0.36	9.8
313	2.86	3.74	18.97	18.84	0.37	10.8
314	3.27	3.64	18.97	18.84	0.36	9.7
211*	3.76	3.11	19.04	18.91	0.35	9.0
212*	4.08	3.12	19.07	18.94	0.38	12.4
213*	3.42	3.32	19.05	18.92	0.31	-
214*	3.77	3.26	19.04	18.91	0.37	11.2
521	3.41	3.13	18.92	18.79	0.35	8.4
421	3.55	3.31	18.96	18.83	0.34	7.5
423	3.91	3.31	18.92	18.79	0.34	7.4
321*	3.90	3.18	19.06	18.93	0.38	12.4
323*	3.70	3.29	19.04	18.91	0.38	12.3

Table 1a: Field 28: *Column 3* gives the logarithm of the surface number density d (per square degree) for the fine-grid-division; *Column 3* gives the mean R magnitude of the clump/HB stars; *Column 4*, the corresponding distance modulus $(m-M)_o$; *Column 5* the dispersion around the mean of the clump/HB magnitudes; *Column 6*, the depth along the line-of-sight (in kpc) calculated using columns 5 & 6.

Region	r_{oc}	$\log d$	$< R >$	$(m-M)_o$	σR	depth
		deg^{-2}				(kpc)
111	2.61	3.81	18.89	18.76	0.44	16.2
112	2.86	3.71	18.84	18.71	0.44	15.8
113	2.21	3.87	18.88	18.75	0.42	14.5
114	2.51	3.79	18.88	18.75	0.41	14.0
121	3.17	3.61	18.82	18.69	0.45	16.7
122	3.51	3.52	18.81	18.68	0.47	17.6
123	2.85	3.62	18.81	18.68	0.44	15.7
124	3.23	3.56	18.81	18.68	0.45	16.6
131	3.88	3.43	18.74	18.61	0.49	19.0
132	4.26	3.27	18.75	18.62	0.46	16.7
133	3.62	3.43	18.75	18.62	0.42	13.7
134	4.03	3.36	18.79	18.66	0.43	15.0
211	3.45	3.56	18.83	18.70	0.46	17.3
212	3.65	3.51	18.81	18.68	0.48	18.6
213	3.02	3.66	18.83	18.70	0.46	17.3
214	3.24	3.61	18.80	18.67	0.46	17.0
221	3.89	3.45	18.75	18.62	0.43	14.7
222	4.17	3.34	18.76	18.63	0.45	16.2
223	3.52	3.55	18.74	18.61	0.45	16.0
224	3.83	3.41	18.75	18.62	0.45	16.1
231	4.48	3.21	18.71	18.58	0.45	15.9

Table 1b: Field 52: as in Table 1a.

Region	r_{oc}	$\log d$	$< R >$	$(m-M)_o$	σR	**depth**
		deg^{-2}				(kpc)
232	4.16	3.29	18.70	18.57	0.42	13.4
233	4.53	3.11	18.73	18.60	0.44	15.0
311*	4.33	3.29	18.93	18.80	0.46	18.1
312*	4.49	3.30	18.91	18.78	0.45	17.4
313*	3.88	3.44	18.90	18.77	0.49	20.5
314*	4.06	3.39	18.88	18.75	0.45	17.1
321*	4.69	3.18	18.86	18.73	0.45	17.0
322*	4.92	3.15	18.85	18.72	0.56	24.0
323*	4.28	3.32	18.84	18.71	0.47	17.9
324*	4.54	3.21	18.84	18.71	0.48	18.9
413*	4.77	3.06	18.90	18.77	0.48	19.4
414*	4.92	3.07	18.91	18.78	0.53	22.7

Table 1b: continued.

0.05 mag ($\sim$ 3 kpc). The resulting average d.m. is quite well-defined, around $(m-M)_o$ = 18.83 ± 0.05, excluding the southernmost region mentioned previously, or 18.85 ± 0.06, including it. The errors around the mean value include uncertainties intrinsic in the evaluation method and real trends of the d.m. across the field, such as the suggested increase towards the southernmost areas, as well as the small trend towards larger mean d.m. with increasing projected distance from the SMC centre. For comparison, the corresponding positions for the d.m. (derived by the same method, i.e. from the mean magnitude of the HB/clump) of the field stars near Kron 3 (Rich *et al.* 1984), near 47TUC (Hesser *et al.* 1987) and near L11 (Buttress,Cannon & Griffiths 1988) are also given in Fig.2a. Although all these regions are nearer to the SMC than those considered here, the agreement is good.

In **Field 52**, there is a steeper and better defined dependence of $\overline{R}_{clump}$ –and therefore of the d.m.– on the projected distance from the SMC centre, r_{oc} (Fig.3a). The mean clump magnitude decreases from 18.91 (d.m. $(m - M)_o = 18.78$) in the regions nearest to the SMC centre, to 18.70 (d.m. $(m-M)_o = 18.57$), in the outermost regions, corresponding to a mean decrease of $\sim$ 5 kpc of the line-of-sight distance. For comparison, the positions of two star clusters in the area are also given in Fig.3b (NGC411 and L113, the latter just outside the limits of Field 52, 40 arcmin southwards).

An interesting feature of Fig.3a, is a group of 10 points, systematically more distant from the Sun, by $\sim$ 1.3 mag in d.m., than the others at comparable distances from the SMC centre. All of these points originate in 10 adjacent regions (marked with a star on Table 2b) at the NW of the Field, at a mean radial distance of $r_{oc} \sim 4.5$ deg and with $< RA >= 1^h26^m$ and $< DEC >= -69^o39'.5$. The difference of the d.m. of this group of points from their counterparts is significant at the 3σ level, as can be shown by the application of a two-sample Kolmogorov-Smirnov test. It should also be mentioned that the observed magnitude increase of 1.3 mag is much too large to be accounted for by systematic errors in the photometry (Chapter III).

3.2 The clump size

An inspection of Table 1 (a & b) confirms the systematic difference in dispersion for the clump star distributions in Fields 28 and 52. We define as the clump size the full width 2Δ around the mean. The mean clump size is 0.72 ± 0.03 for the Field 28 regions, while it increases to 0.91 ± 0.04 for the Field 52 areas. There is, therefore, an additional dispersion of $\pm(0.28 \pm 0.05)$, or a rise of 0.56 mag in the full width in Field 52, in comparison with Field 28. The application of the Kolmogorov-Smirnov two-sample test shows that the difference between the two sets of dispersions (i.e. for the Field 28 and 52 regions) is significant at the 0.001 level. In principle, the observational clump-size, as previously defined, can be influenced by a multiplicity of factors:

(i) The random errors in R, which amount to $\sim \pm 0.08$ mag over the whole area of both Fields for the magnitude range of the clump stars (Chapter III).

(ii) As mentioned in Section 2, the clump giants show an intrinsic spread in luminosity corresponding to $\sim \pm 0.3$ mag.

Thus, the clump size expected from (i)&(ii) is $2 \times (0.07^2 + 0.30^2)^{1/2} = 0.62$ mag.

(iii) A range of ages less than $\sim 5 \times 10^8$ yr, superimposed on greater ages, can cause an increase of the clump size toward brighter magnitudes. However, as was established in Section 2, there is no significant contribution from such young populations in the regions of interest. In any case, there is no difference in this respect between the two Fields 28 & 52. Moreover, the regions nearest to the SMC main body in Field 52 which have the largest contribution from younger stars in their CMD (Chapters IV and VI), possess less rather than more dispersed HB/clumps.

(iv) The spread in the line-of-sight distances of the clump stars is an obvious possible source of increase of the clump size.

(v) Inclusion of RGB stars and subgiants, as well as of residual back/foreground objects in the defined 'clump region' of the CMD, can increase our estimate of the clump size; the second factor would be expected to affect especially the less dense regions. Obviously, this effect influences the clump in both Fields in the same way. On the other hand the uncorrected for the back/foreground contribution CMDs show the same effect in the clump size as the corrected CMDs (compare Fig.2 in Chapter IV, and the CMDs in Appendix A).

(vi) Reddening effects –for example if the absorbing cloud is patchy and not well mixed with the stellar populations– can cause an additional spread in R. However, this would affect even more profoundly the colour $B - R$, which is certainly not the case here (see Chapter VI).
(vii) Finally, metallicity is not known to affect the luminosity of the clump stars (Chapter VI). Moreover, as shown in Chapter V, there is no significant metallicity gradient across either Field.

The above analysis indicates that only the depth along the line-of-sight can account for the increased clump size in the Field 52 regions. Actually, some of the dispersion in the Field 28 regions can also be attributed to depth effects. The line-of-sight depth for each region in the Fields 28 & 52 can easily be calculated using the excess dispersion of the magnitudes of the clump stars around the mean, with respect to the expected value of ± 0.31 mag, and the estimated d.m. of each region from the mean clump magnitude. Column 5 in Table 1(a & b), shows the resulting line-of-sight depths. In Field 28 the average depth is 10 ± 2 kpc, while in Field 52 it is 17 ± 2 kpc with a maximum value of 23 kpc.

Fig.2b & 3b show the dependence of the clump size, and Figs.2c & 3c of the line-of-sight depth, on the projected distance r_{oc} from the SMC centre. In Field 28 the clump size appears to be constant throughout the area, while in Field 52 there is a trend towards larger values of the line-of-sight depth as r_{oc} increases.

Interestingly, the areas in the NW of Field 52, which were previously found (Section 3.1) to be at systematically larger mean distances from us than the rest, also display an enhanced line-of-sight depth.
Fig.2d & 3d present the number density profiles of Fields 28 & 52; the NW regions in Field 52 just mentioned also appear to have marginally larger surface number densities than other regions in the field at similar distances r_{oc} from the SMC optical centre.

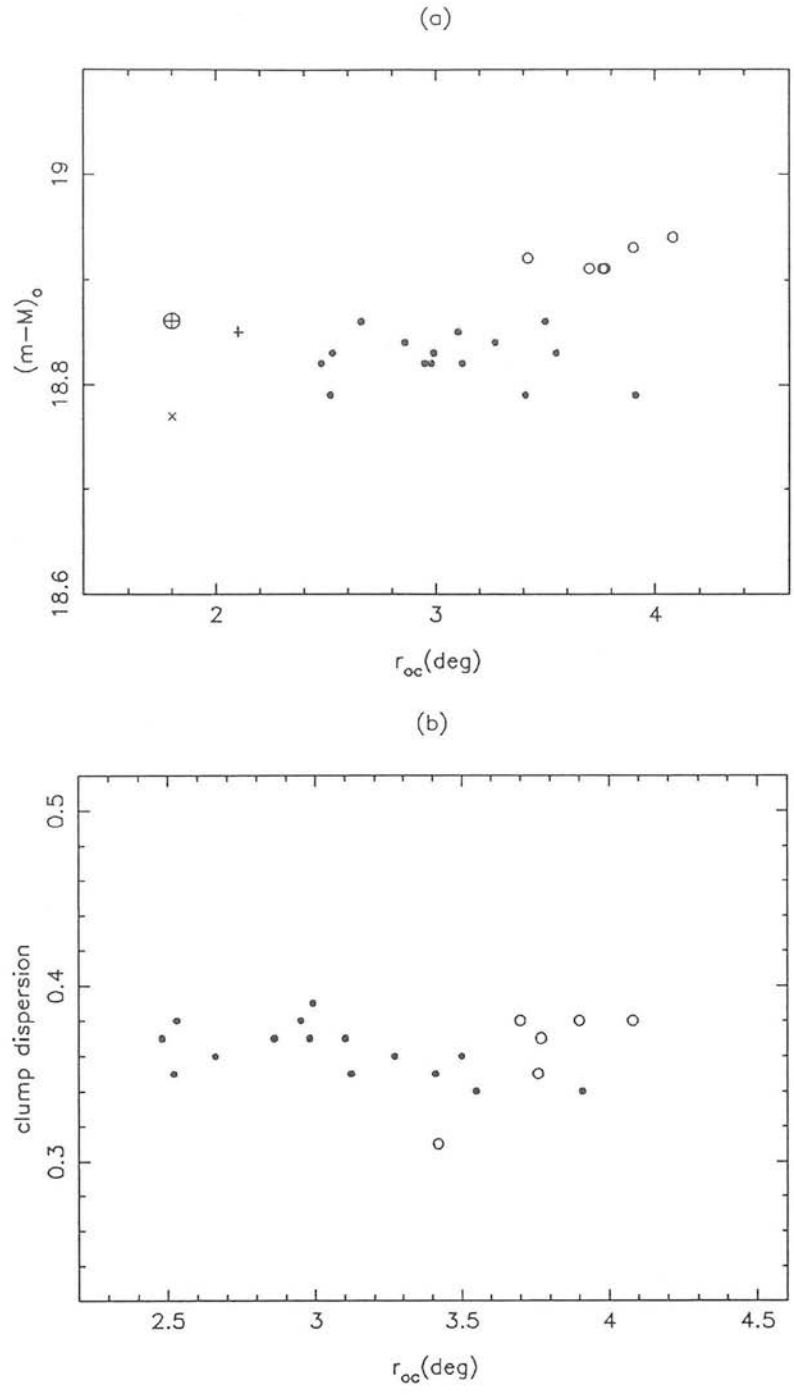

Figure 2: The distribution of the mean clump position (a), the mean apparent d.m. (b), the mean dispersion (c) and the mean number density of the clump stars (d), as functions of the projected radial distance from the SMC centre. The open circles correspond to the regions followed by an asterisk in Table 1a. The sign × corresponds to the clump/HB of the CMD of the field populations near 47 TUC, the + sign to the field near Kron 3, and the ⊕ sign to the L1 field.

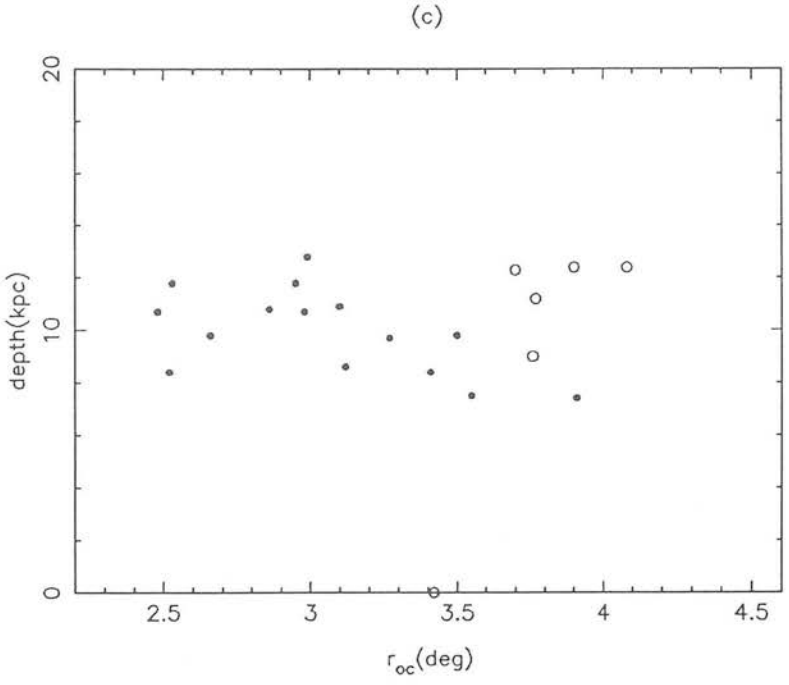

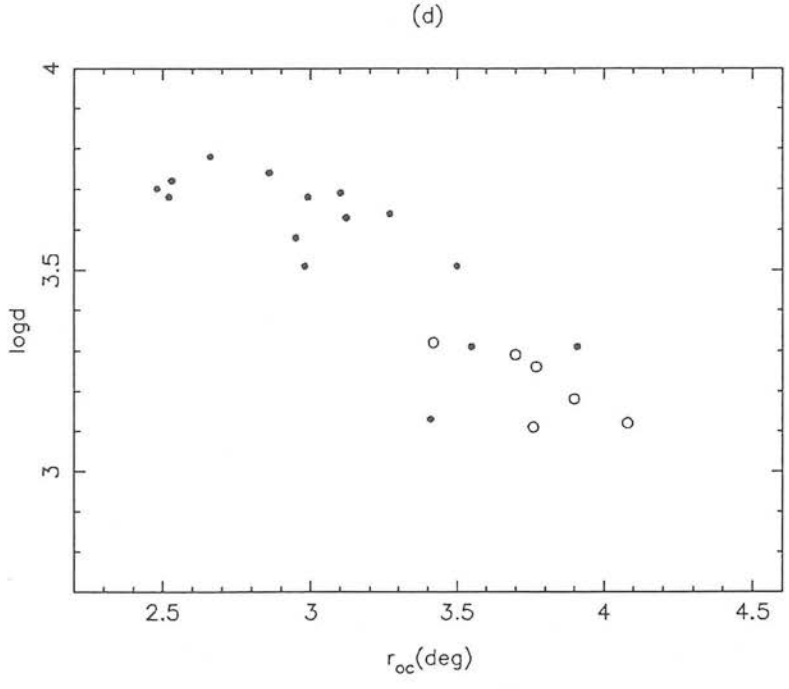

Figure 2: continued.

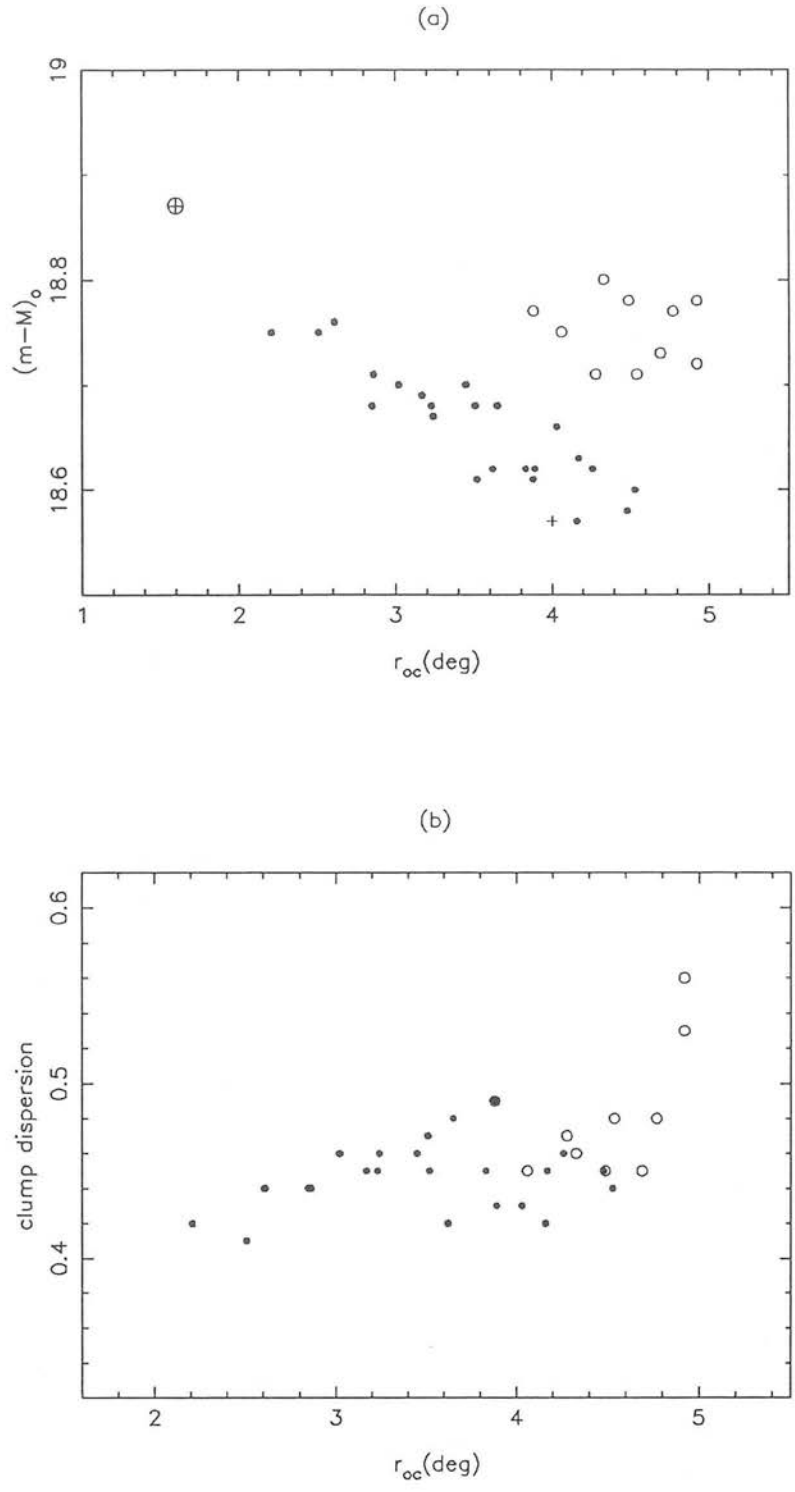

Figure 3: as in Fig.2, for Field 52. The + sign corresponds to L113 and the $\oplus$ sign to NGC411.

(c)

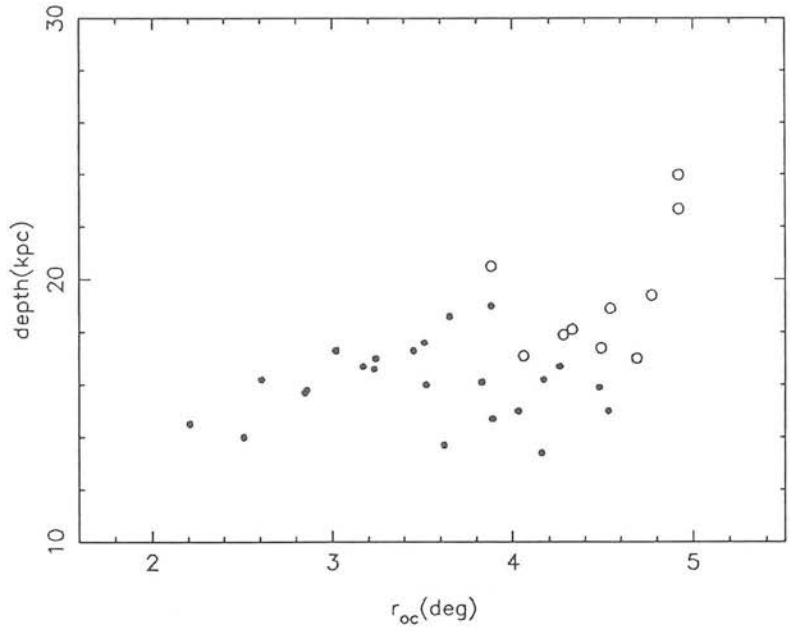

(d)

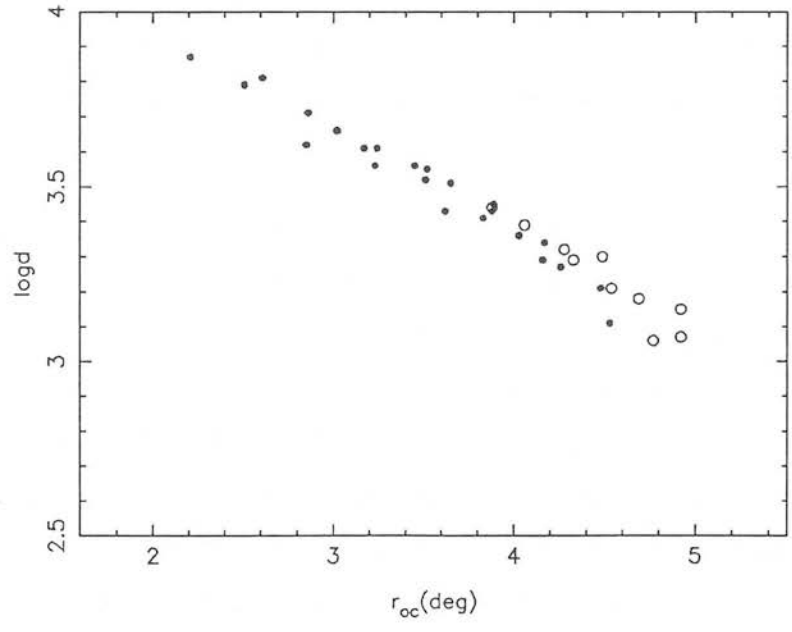

Figure 3: continued.

4 Discussion

It was shown in the previous section that there is a significant increase in the line-of-sight depth of the stellar populations belonging to the NE (Field 52) outer regions of the SMC, compared with the corresponding populations in the SW (Field 28). Although a large line-of-sight depth has been suggested for the SMC central regions in the past, it is the first time that a thorough study over a large area and at large distances from the SMC centre has been undertaken, yielding new results on the three-dimensional structure of the SMC halo regions. In this section, the various geometrical aspects of the phenomenon and its dynamical implications are investigated.

4.1 Interpretation of the observations

The southern and western regions of the SMC (Field 28): according to the results presented in Section 3, there is a depth of a *maximum* value of 10 kpc along the line-of-sight, over the whole of the area studied; this value is compatible with the SMC 'tidal radius' of $\sim$ 5 kpc, as defined by the mass of our Galaxy, at its present distance from the SMC (see e.g. the discussion in Welch *et al.* 1987). Therefore, in these regions there is no evidence of large-scale disruptive dynamical effects.

There is good agreement of these results on the depth of the SW regions of the SMC with the value of 7 ± 3 kpc reported by Azzopardi (1982), for early type supergiants to the south of the SMC Bar (but closer to the SMC centre than the regions considered here). On the other hand the RR-Lyrae stars in the NW of the SMC Bar (near NGC121 and outside the northern limits of Field 28) were found to have a line-of-sight depth of $\sim$ 5 kpc (Graham 1975); taking into account the possible metallicity dependence of the RR-Lyrae luminosity (Sandage 1982) and the expected metallicity spread among field stars, the calculated depth of these stars may be considerably lower than this value (Suntzeff *et al.* 1986).

To complete the three-dimensional picture in the SMC south-western outer regions, it is noted that there may be an overall tilt of the SMC with respect to the line-of-sight (Fig. 2a), corresponding roughly to 50°. However, the scatter involved is too high to

derive any firm conclusions. In addition, each point on Fig.2a corresponds to the average from stars with a range of distances along the line-of-sight as large as 10 kpc. Therefore a total planar inclination of 3 kpc would seem difficult to establish. Finally, there is some evidence in Fig. 2a (see also Section 3.1) of a trend towards larger distance moduli in the southern-most regions in the field. Interestingly, it has been noted in the past, that the extreme southern regions (closer to the Bar than the areas cosidered here) are at systematically larger distances than the rest of the SMC main body (e.g. Azzopardi 1982).

The northeastern outer regions of the SMC (Field 52): the line-of-sight depth reaches a mean of 17 kpc, with a maximum of 23 kpc, which is very high compared with either the projected dimensions of the SMC, or the expected size of its 'tidal radius'. It has been noted in the past that the NE regions of the SMC are particularly dispersed. Florsch *et al.* (1981) find evidence of a 23 kpc depth for the spatial distribution of supergiants and cepheids in the area to the NE of the Bar, but essentially closer to the SMC optical centre than the regions considered here. Their result was confirmed qualitatively by Dubois (1980), and Azzopardi (1982), who actually suggested the presence of at least two stellar systems in the region. The hypothesis of a two-, or possibly multiple-component SMC was first suspected almost three decades ago, by Johnson (1961), but it has been put on a firmer basis only recently by MFV (see also Maurice *et al.* 1987; Torres & Garranza 1987).

Following the basic idea of MFV, the observed large dispersion in d.m. in the northeastern SMC can be interpreted as the result of tidal disruption, caused by the gravitational field of the LMC. A comparison with the predictions of theoretical models on the interaction can be instructive: the most successful tidal models for the triple system LMC-SMC-MW have been developed by Murai & Fujimoto (1980; 1986-MF; see also Fujimoto & Murai 1984) with the initial purpose of reconstructing the gaseous Magellanic Stream (MS). In the earlier version of the model, the SMC and the LMC were assumed to be gravitationally bound to each other for the past 10^{10}yr; in the latest version (1986) this assumption was relaxed, leading to a more satisfactory representation of the MS. In both cases the models predict a close encounter of the SMC and the LMC $\sim 2\times10^{8}$ yr ago. As a result, the SMC 'was severely disturbed, resulting in the formation

of the MS. The outer part of the SMC is now being disrupted' (MF). They also suggested that the close encounter previous to this recent event led to the capture of the SMC by the LMC and happened $\sim 1.7 \times 10^9$yr ago. According to the same models, the present overall line-of-sight extension of the SMC reaches $\sim$ 30 kpc. Although this value is not incompatible with the present results, the models provide no detailed predictions about the nature of the effect, or the direction of maximum disruption; in addition, no discrimination is made between star- and gas-dynamics in the simulations.

Interestingly, both the magnitude distribution of carbon stars in the two Fields (Chapter VII) and the radial distribution of stars younger than $\sim 1 - 2$ Gyr (Chapter VI) show evidence of both the large line-of-sight depth in the NE parts and of the d.m. difference between the NE and the SW. According to the above, the large line-of-sight depth in the SMC northeastern regions can be explained as the effect of one or more of the following factors:

(i) The proposed recent encounter (2×10^8 yr ago) of the SMC with the LMC. Since the stellar populations in the regions of interest are older than 1-2 Gyr, the feature observed would then be due to the tidal effects on the *stellar* component of the SMC NE regions.

(ii) The past encounter, 1-2 Gyrs ago (Murai & Fujimoto 1986), of the LMC and the SMC, probably affecting both the gaseous and the stellar components. It may be suggested that the induced changes in the gas dynamics may have triggered SF activity (see e.g. Fujimoto 1987).

(iii) The cumulative effects of the LMC tidal field on the SMC outer regions.

(iv) According to the Murai & Fujimoto simulations, there has been a recent perigalactic passage of the Magellanic System, about a hundred million years ago. It has been suggested that the resulting tidal forces have enhanced the products of the SMC disruption by the LMC (Fujimoto & Murai 1984; Gingold 1984). However, the processes involved are far from well understood.

In the following, the form of the LMC tidal effect on the SMC old stellar component in the NE outlying areas is investigated, on the basis of the present results.

4.2 The morphology of the tidally disrupted NE area of the SMC

The large line-of-sight depth observed in the NE outer regions of the SMC can be visualised as (i) a tidal extension of the SMC outer regions in the general direction of the LMC, in the sense that stars are pulled out towards the perturber forming a wing-like distortion (Case a) or (ii) two, or even more, distinct entities at different distances from us, but projected along roughly the same line-of-sight of the areas in consideration (Case b). The various aspects of these two possibilities on the basis of the available data will now be examined in detail.

(i) The clump magnitude distribution.

The clump magnitude distribution (typical example in Fig.1b) shows no clear evidence of bimodality in the observed line-of-sight depth of the clump stars, as one would expect in *Case b* for a large enough spatial separation of the two components. This absence does not rule out the second hypothesis, but it sets an upper limit to the possible separation of the two alleged entities. Assuming that both components are of comparable size along the line-of-sight (the dispersion of clump stars distribution is at least ± 0.31 mag according to the analysis in the previous section), they could be distinguished from each other, if the corresponding peaks were at least $\sim 2\sigma$ apart (this estimate naturally depends on the relative numbers of stars in the two components), which is equivalent to $\sim$ 15 kpc, for a mean d.m. of 18.70. It is worth noting at this point that the two separate galaxies –the 'SMC Remnant' and the 'Mini Magellanic Cloud'– proposed by Mathewson (1984) and MFV are 10 kpc apart along the line-of-sight, each of a depth of 5-7 kpc. This suggestion was based on neutral hydrogen velocity maps and distances of young cepheid variables presumably associated with the gas; however, it must be noted that Welch *et al.* (1987) strongly disagree with the large distance ranges reported by MFV for the SMC cepheids. The MFV values for the two components are compatible with the previously estimated upper limits, although it is by no means certain that the entities tentatively identified here are the same objects proposed by Mathewson and his collaborators. The main difference is that the present results refer to the outer regions of the SMC and to stellar populations significantly older. Additionally, Mathewson (1984) suggested that the 'Mini Magellanic Cloud' (NE) is younger than the 'SMC Remnant' (SW). As mentioned Chapters VI and VIII, there is some evidence of a more spatially

extended and probably enhanced population of $\sim$ 1 Gyr of age in the NE regions. No firm conclusions can be reached on the subject at this stage.

(ii) The dependence of the mean clump magnitude and clump size on r.

In *Case a*, one would expect the outermost, more loosely bound, stars to suffer larger displacements due to the tidal field of the perturber (LMC). Therefore, the line-of-sight depth of the stars, as measured by the clump-size, should appear to increase with distance from the SMC, while at the same time, the mean distance modulus of the stars should decrease, as they approach the perturber. Both of these predictions are supported by the observations (Fig.3a, b & c), although the dependence of the dispersion on the projected radial distance r_{oc} is very weak, if at all present, probably masked by the uncertainties of the measurements. It must be emphasised that the rising trend of the clump size (and the line-of-sight depth) with r_{oc} disappears when the northern-most regions in the field are omitted (see also paragraph (iv) below). The interpretation of these points in *Case a* is not straightforward. According to the simple picture drawn above, we would expect these points to have smaller rather than larger line-of-sight depth (given their larger d.m.).

In *Case b*, the observed decrease of the d.m. with r_{oc} (Fig. 3a) can be understood as indicating that the component nearer to us becomes progressively stronger with increasing r_{oc}. The maximum clump size would occur in the region where both components are present in significant numbers. It may be argued that the observed dependence of the d.m. on r_{oc} shown on Fig.3a, is simply the effect of an overall inclination of the SMC with respect to the plane of the sky (total 5 kpc along the line-of-sight, i.e. $i \sim 63^{o}$). However, given the line-of-sight depth of 17 kpc (maximum 23 kpc) for each of the points in Fig.3a, this planar interpretation of the situation is unrealistic. The inapplicability of a planar model for the description of the SMC geometry has also been commented upon most recently by Caldwell & Coulson (1986) and by Laney & Stobie (1986). However, this does not rule out the possibility that one –or both– of the alleged components is tilted with respect to the plane of the sky, in which case the interpretation presented in this paragraph would be too simplistic.

(iii) The surface distribution of the clump stars.

In a further attempt to check the two-component hypothesis against the wing hypothe-

sis, the surface distribution of clump giants –which presumably belongs to the different components– was examined. Clump stars with $R > 18.8$ would be expected to belong preferably to the more distant component (see Fig.1), while those with $R < 18.8$ to the nearer one. The mean x and y coordinates (on the plates) of these two components were calculated for each one of the fine-grid regions in the Field. The differences Δx and Δy between the mean coordinates of the two groups for each subregion are presented in Fig.4a. For the sake of comparison, the same procedure was followed for Field 28 and the corresponding results are shown in Fig.4b. This exercise indicates that there is a small but well defined displacement in the N-S direction, along the y axis, for the clump stars in the two magnitude ranges in Field 52. No systematic effects are observed for the Field 28 clump stars. *It can be deduced from the above that there are actually two components along the line-of-sight*, almost overlapping on the plane of the sky, with the more distant component preferentially located to the north of the nearer one. Interestingly, Mathewson's (1984; MFV) more distant component is also located towards the NE of the nearer component. Although the above argument favours the two-component hypothesis, it cannot show whether the two components are actually separated along the line-of-sight.

In *Case a*, the N-S displacement of the nearer with respect to the farther away stars appears more difficult to account for without introducing some kind of bimodal structure, which would then be indistinguishable from *Case b*. Therefore, this argument favours the 'two-component' hypothesis.

(iv) The Northern 'feature'.

The three-dimensional picture is further complicated by the 2-square-degree region mentioned in the previous section; it lies to the northwest in Field 52 and it is found to consist of populations systematically farther away, in the mean, along the line-of-sight, than their counterparts in the rest of the field. If this feature is related to the two-component structure, it can be interpreted as an area where the more distant of the two components is prevailing. Interestingly, both the dispersion and the number density of stars in this region are marginally enhanced with respect to other areas at similar distances r_{oc}, from the SMC centre. Moreover, according to argument (iii), the more distant 'component' appears to be to the North of the nearer one. The reality of the

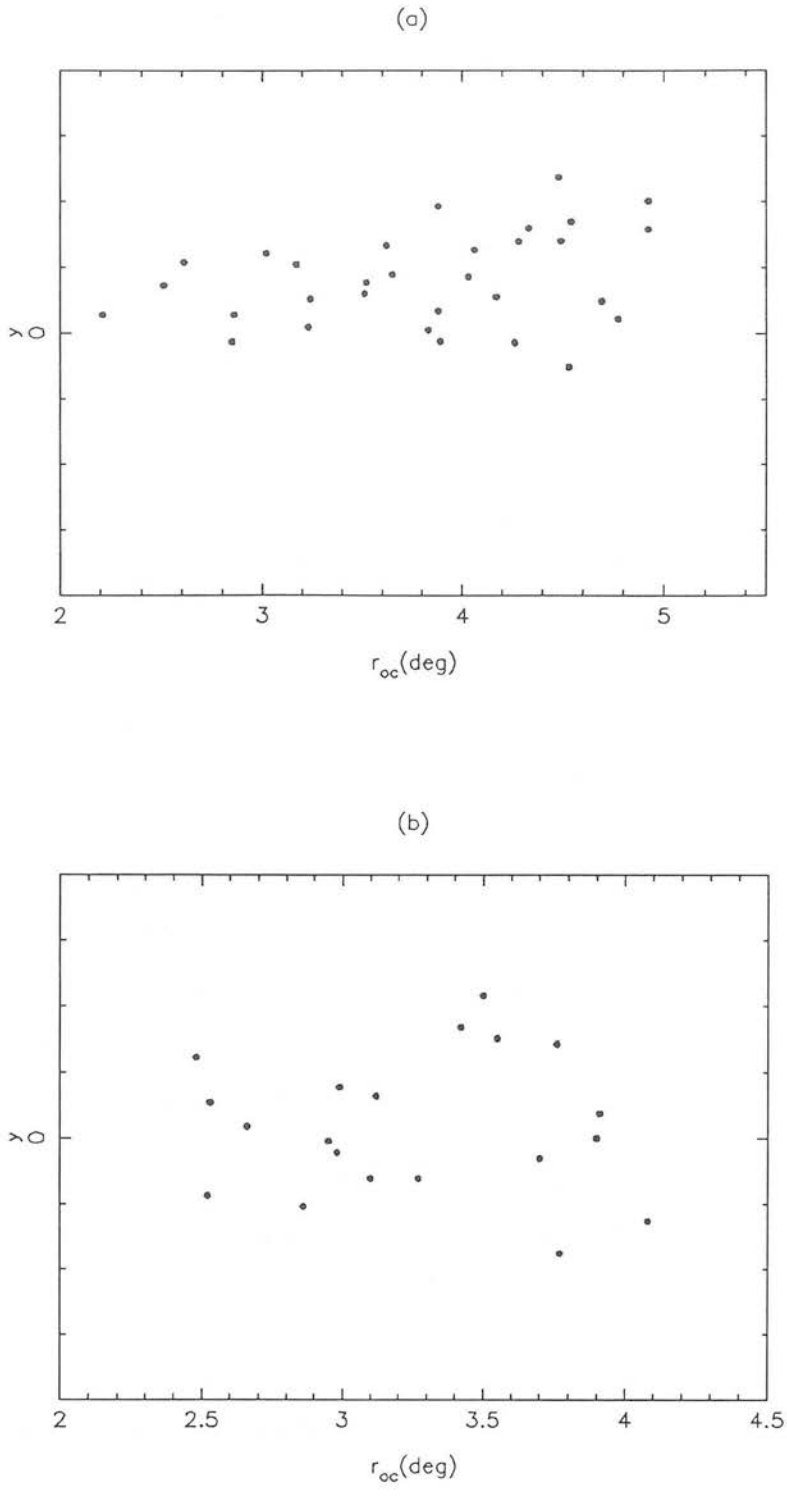

Figure 4: The north-south displacement of the assumed *near* component with respect to the *far* component, in Field 52(a), and for comparison in Field 28(b).

existence of this NW feature is reinforced by the recent work by Albers *et al.* (1987 and private communication), who have noticed a 2σ increase of the surface number density of SMC stars, in roughly the same area in Field 52 as the 'NW feature', which, however, they interpreted as part of a ring structure.

In order to examine the possible relations of this feature with the two-component picture, the dependence of the clump dispersion on the projected distance from the *centre of this region* (without including points from the region itself; Fig.5) was investigated. There is some evidence of an ill-defined trend towards lower values of dispersion as this distance increases. This would be expected in the case of a distinct entity centred in, or near, this area and superimposed on the populations prevailing elsewhere. The 'distinct entity' can be either identified with the more distant component of the two-component model, prevailing in this direction over the near component, or it could indicate the existence of a distinct feature not immediately related to the two components. This last suggestion is probably supported by the fact that the two sets of points appear well separated on Fig.3b. However, all components seem to consist of similar populations (older than 1-2 Gyr), which means that in all regions star formation has proceeded in similar ways and more or less coevally, with no trace of any significant activity for the last 1-2 Gyr or more, in any of the 'components'. Unless the 'NW feature' is unrelated to the general picture in Field 52, it would seem incompatible with the 'wing' hypothesis as described above, while it fits in quite satisfactorily with the two-component picture.

The observations therefore favour the existence of two stellar components along the line-of-sight, in the SMC northeastern outer-disk and halo regions, without ruling out completely the alternative of a wing-like distortion towards the LMC.

5 Summary and Conclusions

The three-dimensional distribution in space of the old disk and halo populations in the SMC northeastern and southwestern outer regions was examined. The study is based on the analysis of the horizontal branch/clump, present on the CMDs examined in the previous chapters.

The observations show a significant line-of-sight depth of 17 kpc in the mean,

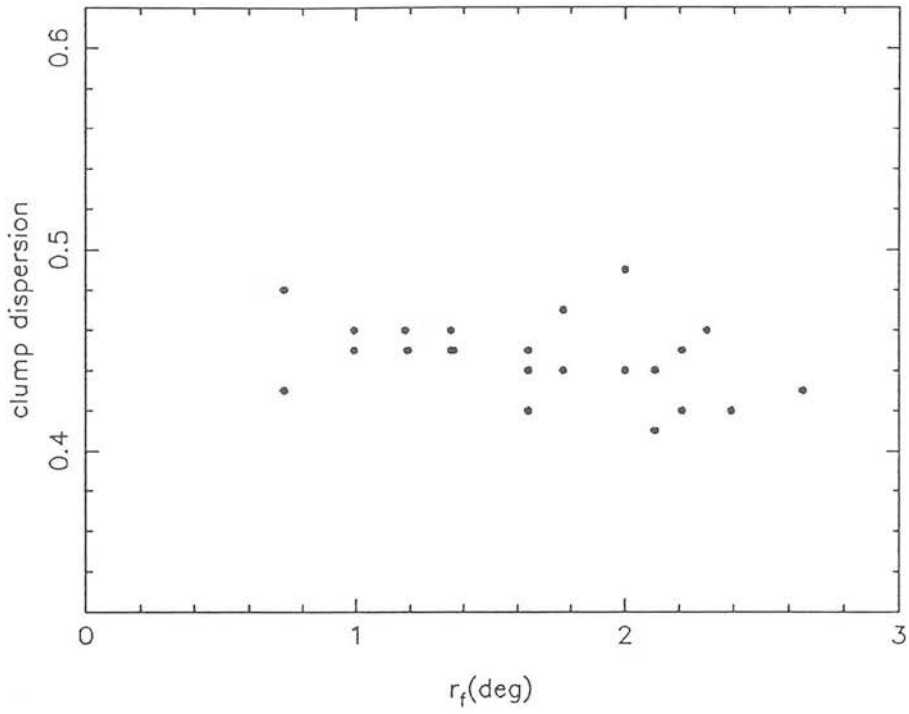

Figure 5: The mean clump dispersion as a function of projected distance from the centre of the NW feature.

reaching a maximum value of 23 kpc, in the NE regions. This can be envisaged as the disruptive effect of the LMC on the SMC. The possibility of the existence of two separate entities along the line-of-sight was examined, in view of these results. The data favour the two-component hypothesis for the SMC, also suggested in the past for the young populations in the SMC central regions. However, an alternative interpretation of a wing-like feature cannot be ruled out.

In the study presented in the previous chapters an attempt was made towards a better and more complete understanding of the structure and evolutionary history of the Small Magellanic Cloud, the second nearest galaxy to our own.

The study was focused on the northeastern and west/southwestern outer parts of the SMC, including populations at projected distances larger than 2.2 kpc from the centre of the SMC. These regions have scarcely been studied in detail in the past.

The observational material consisted of good quality B and R photographic plates taken with the U.K. Schmidt Telescope in Australia, digitised by the COSMOS automatic microdensitometer and calibrated by a series of CCD photometric sequences obtained at the European Southern Observatory (with the 1.5m Danish Telescope) and at the Anglo-Australian Observatory (with the 4m Telescope).

Colour-magnitude diagrams were constructed over the whole of the area measured. The analysis of the properties of these diagrams had the two-fold purpose of (a) establishing the population synthesis in the outer parts of the SMC as a function of position with respect to the centre, and (b) probing the geometrical structure (in three dimensions) of these outlying regions of the SMC.

The general conclusions of this study can be summarised as follows:

The stellar content:

The bulk of the stars in the SMC general field and with projected distances larger than 2.2 kpc from the SMC centre belong to populations older than 1–2 billion years, reaching ages of the order of 10 billion years or more. In spite of the extent of the present study, no convincing evidence was found of a population similar to the Galactic halo (possessing blue horizontal branch stars).

There is a gradual increase of the 'mean' age of the stars in these outer regions of the SMC, even after removing the contribution of the stars younger than 1-2 Gyr, which were shown to have a different distribution from the older populations. This result

was not interpreted as indicating the existence of *discrete* populations, in the sense of discrete star formation events, but rather as the effect of a gradual depletion of 'active' gas, as a function of time. A detailed and deep (down to R=24 mag) luminosity function study is necessary to prove whether or not there was a major SF event 10-12 billion years ago. Some evidence was found of an enhanced mode of SF in the SMC 1-2 Gyr ago, although the interpretation of the data was not unique in this respect.

Interestingly, no significant gradients were detected in the (mean) metal abundance of the field stars in the regions studied, although the mean age appeared to change significantly with distance. This result confirmed –on a larger scale– the suggestion that the chemical evolution of the SMC has been very slow over a large fraction of its lifetime (from $\sim$ 2 to $\sim$ 10 Gyr). More conclusive results must await a detailed and extended metal-abundance study of (individual) field stars of different ages in the SMC.

Another important aspect of the SMC structure revealed by the present study is the fact that stars with ages in the range of 0.5 to 1-2 Gyr have a significantly more extended distribution in the NE outer regions than in the W/SW. This result was also confirmed by the carbon-star distribution in the same regions. This marked asymmetry was tentatively attributed to dynamical factors (the tidal effect of the LMC), especially in view of the results of Chapter IX.

The geometry:
The three-dimensional distribution of the stars comprising the NE and W/SW outer parts of the SMC was examined, using the magnitudes of the horizontal branch stars as distance indicators. The NE–SW 'inclination' of the SMC was confirmed, the NE regions lying closer to us in the mean. Most importantly, a significantly larger line-of-sight depth was detected in the NE regions than in the W/SW. The possible presence of two separate entities along the line-of-sight was advocated. This was interpreted as the disruptive effect of the LMC tidal field on the SMC outer regions 'facing' the LMC. A detailed radial velocity study of the HB/clump stars in the NE would be a most interesting line for future research, as the two entities –if actually existing– would be expected to have different kinematical behaviour.

APPENDIX A

Colour-magnitude diagrams

- **Field 28**

- **Field 52**

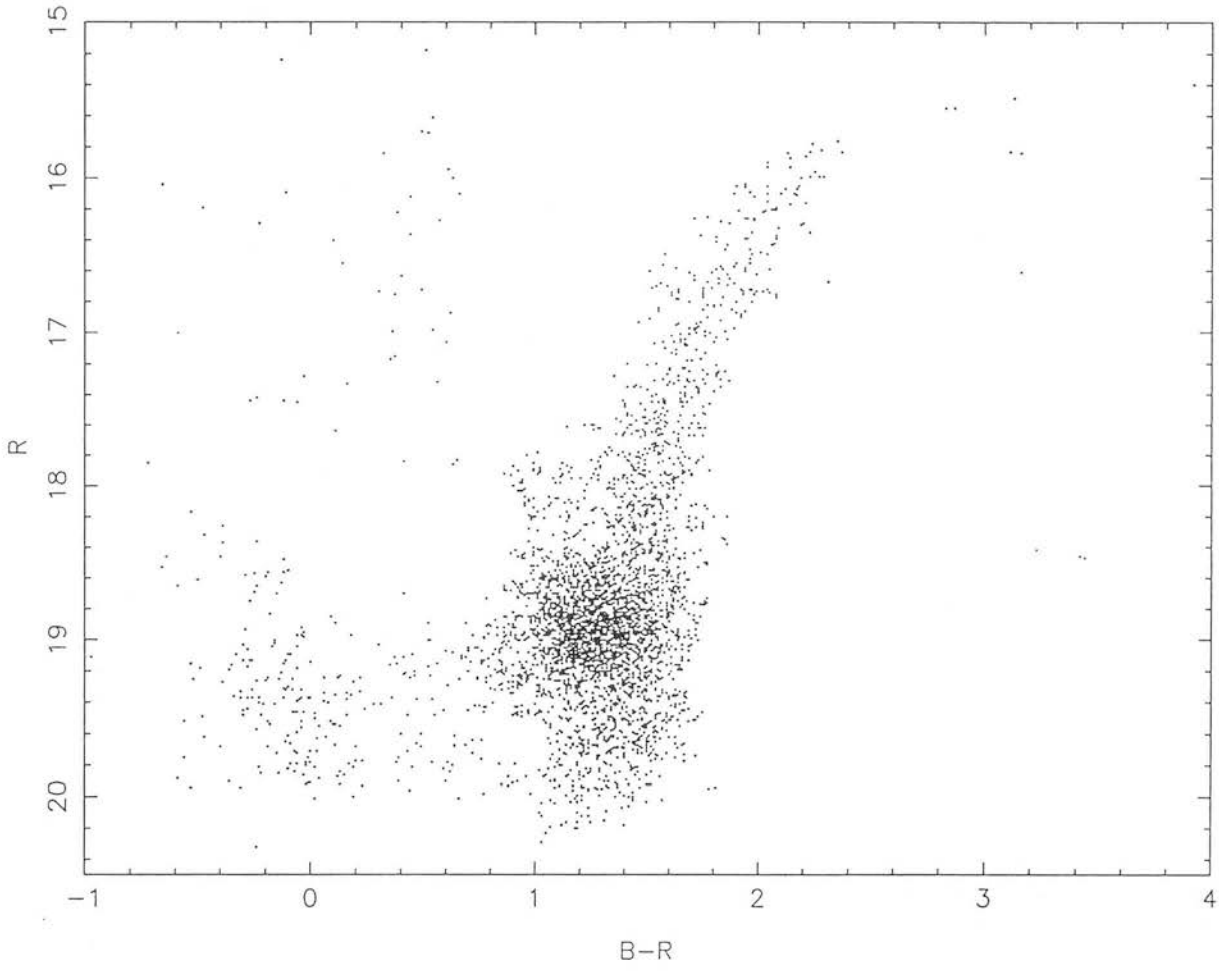

Field 28: Region 5.1

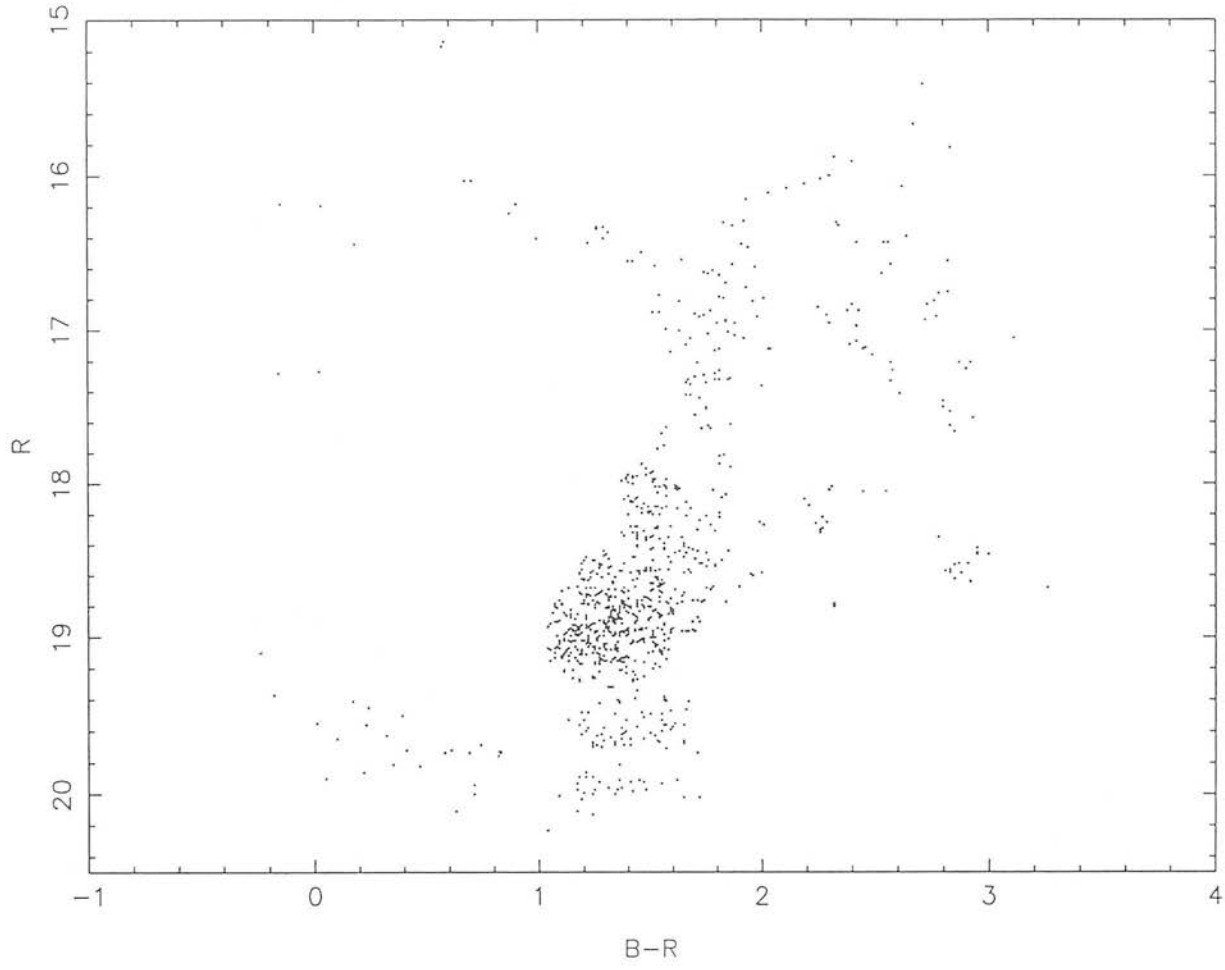

Field 28: Region 5.2

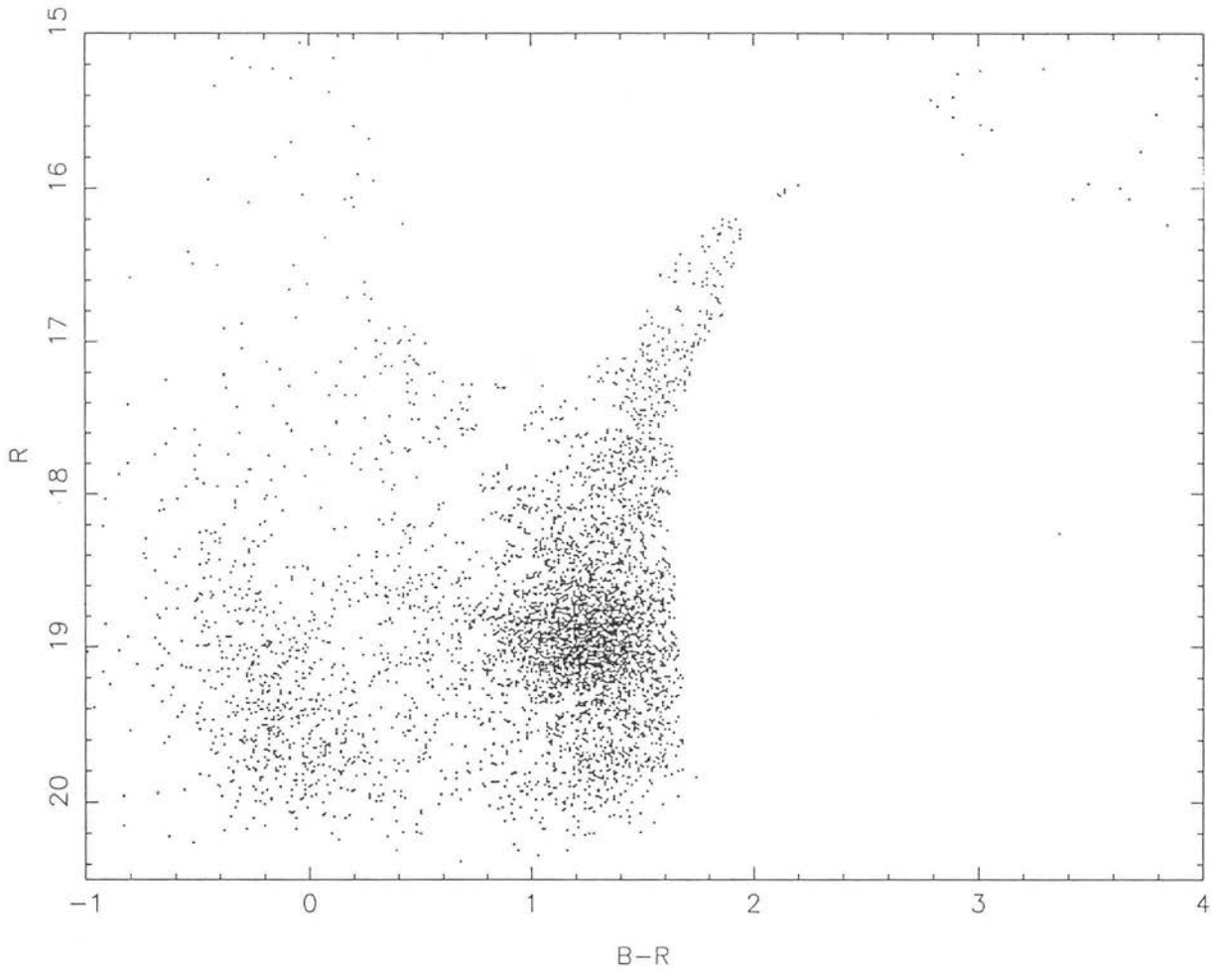

Field 28: Region 4.1

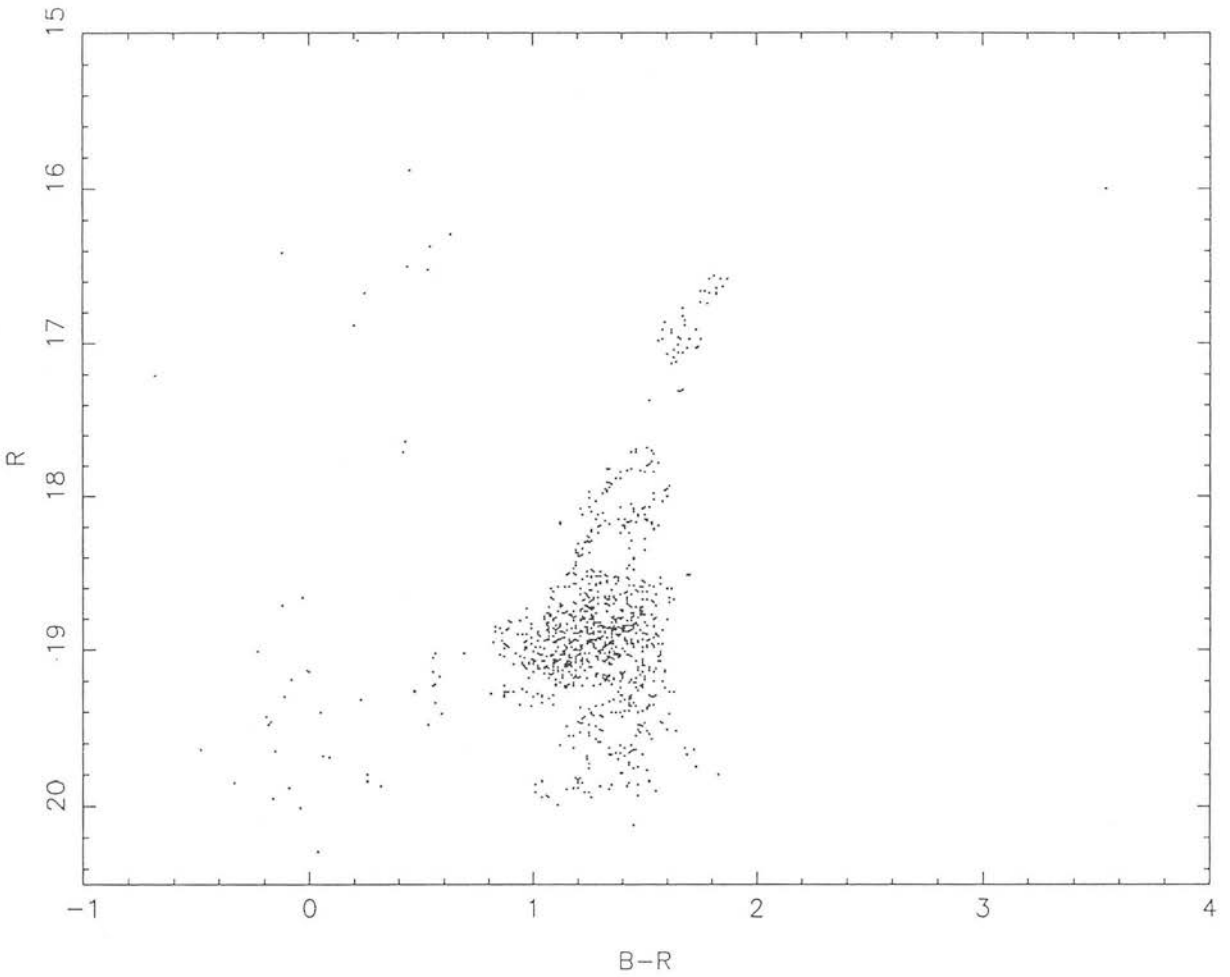

Field 28: Region 4.2

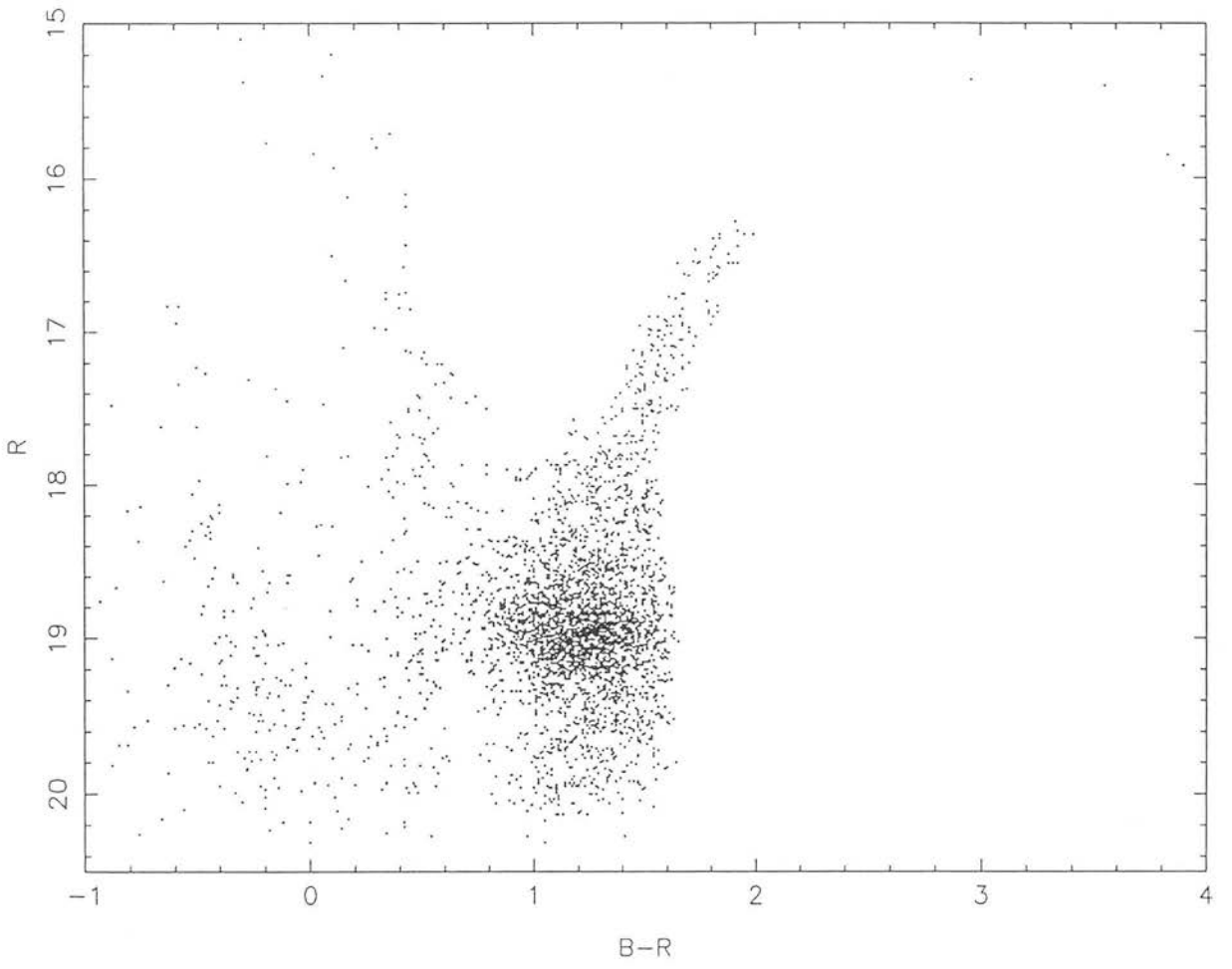

Field 28: Region 3.1

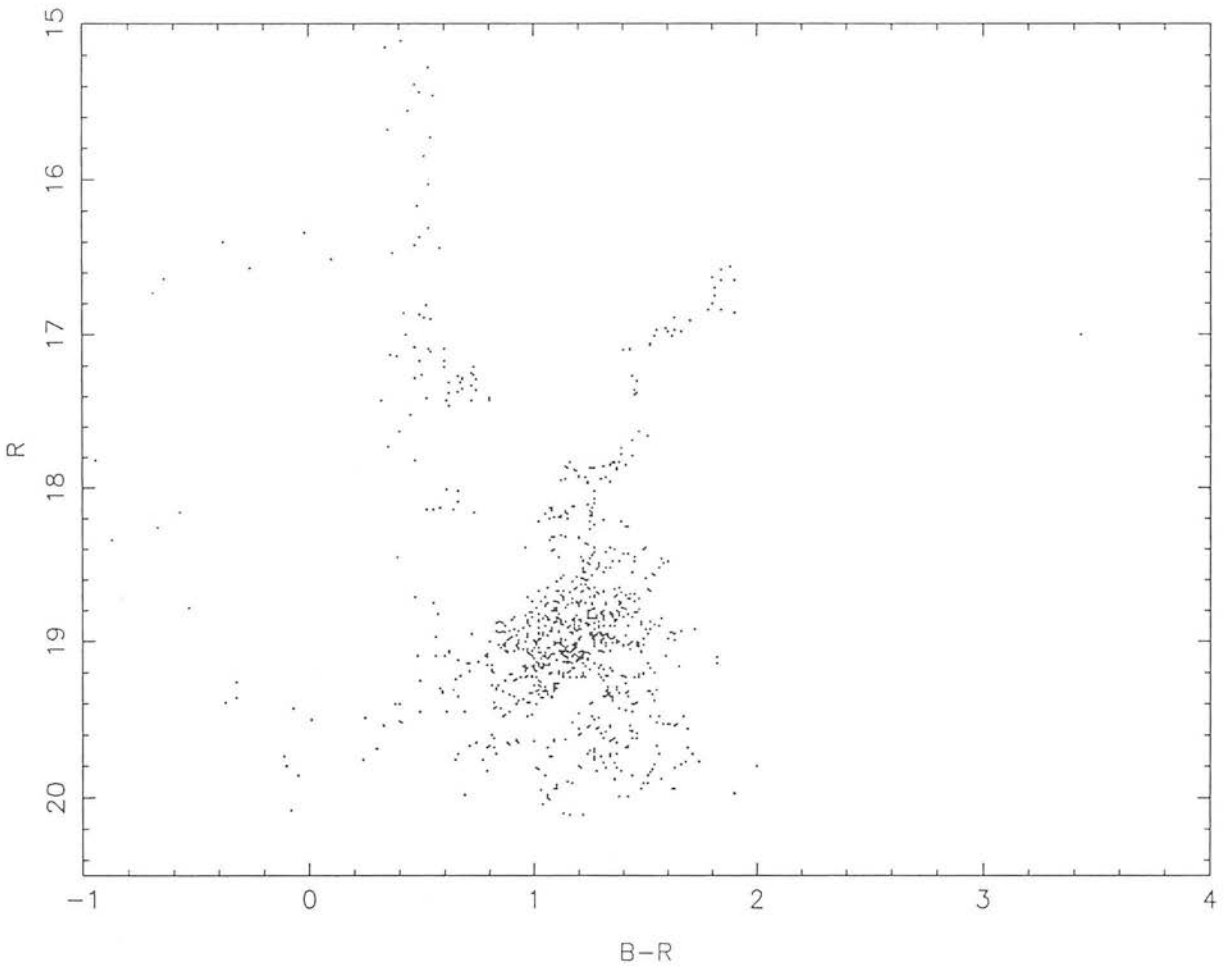

Field 28: Region 3.2

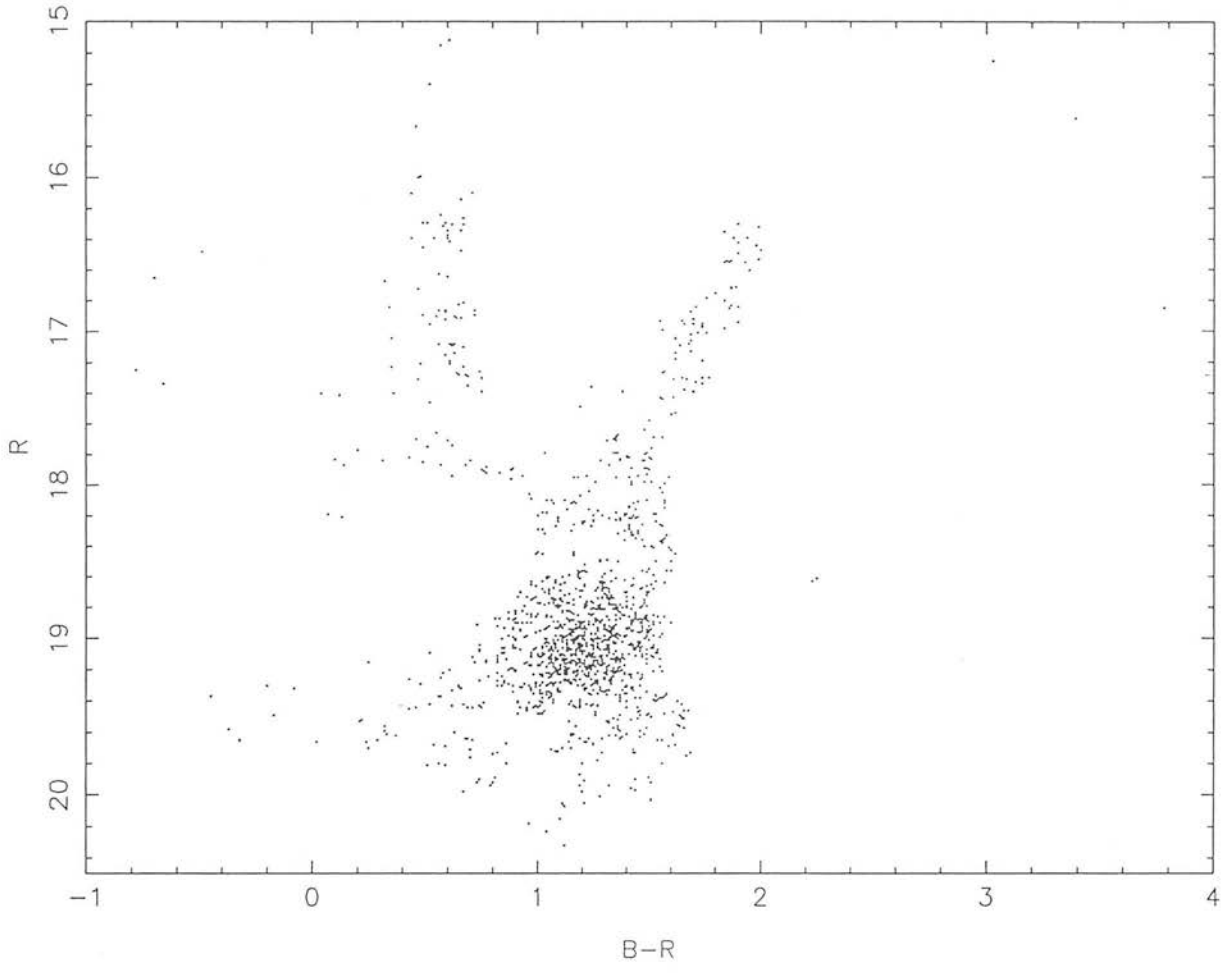

Field 28: Region 2.1

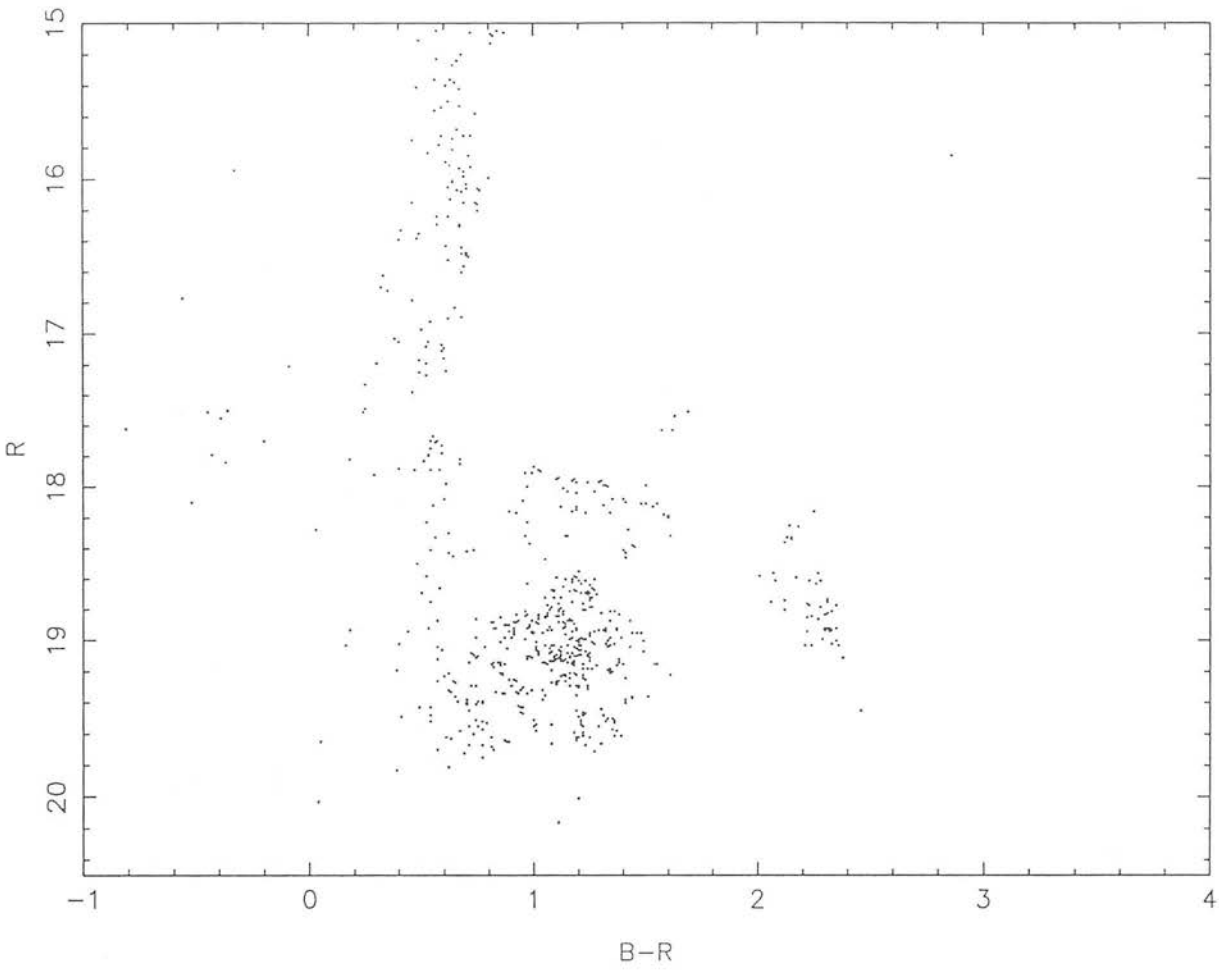

Field 28: Region 2.2

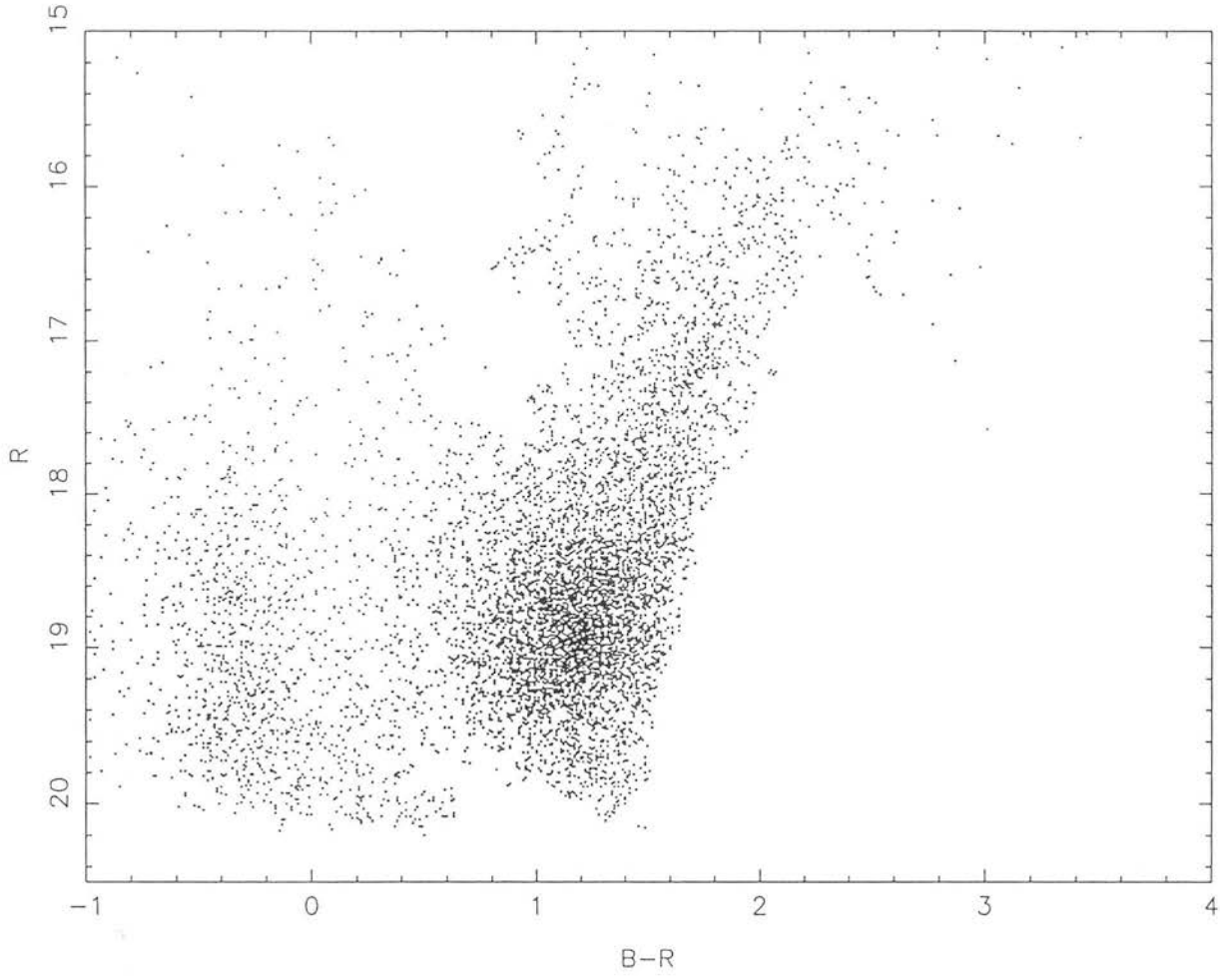

Field 52: Region 1.1

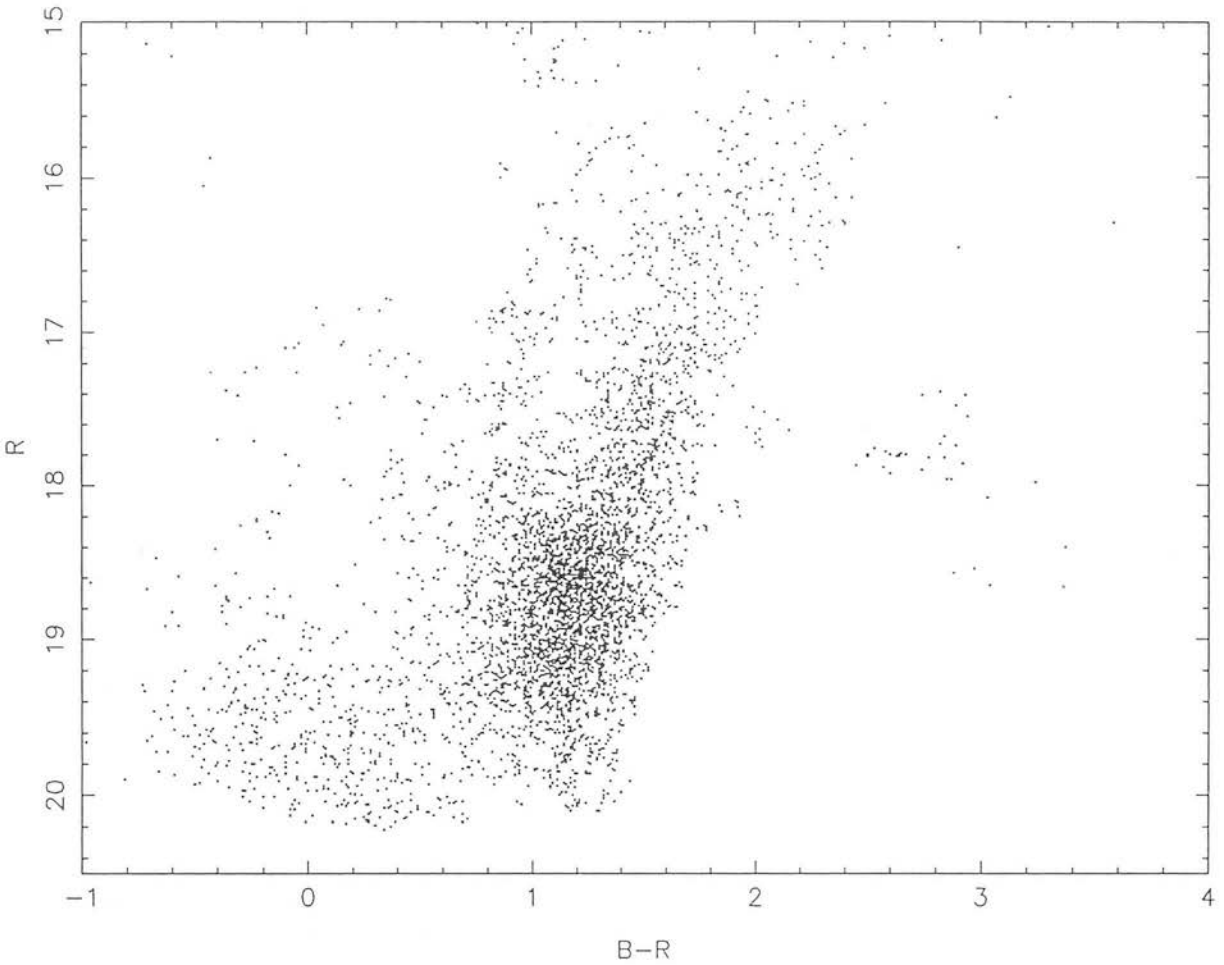

Field 52: Region 1.2

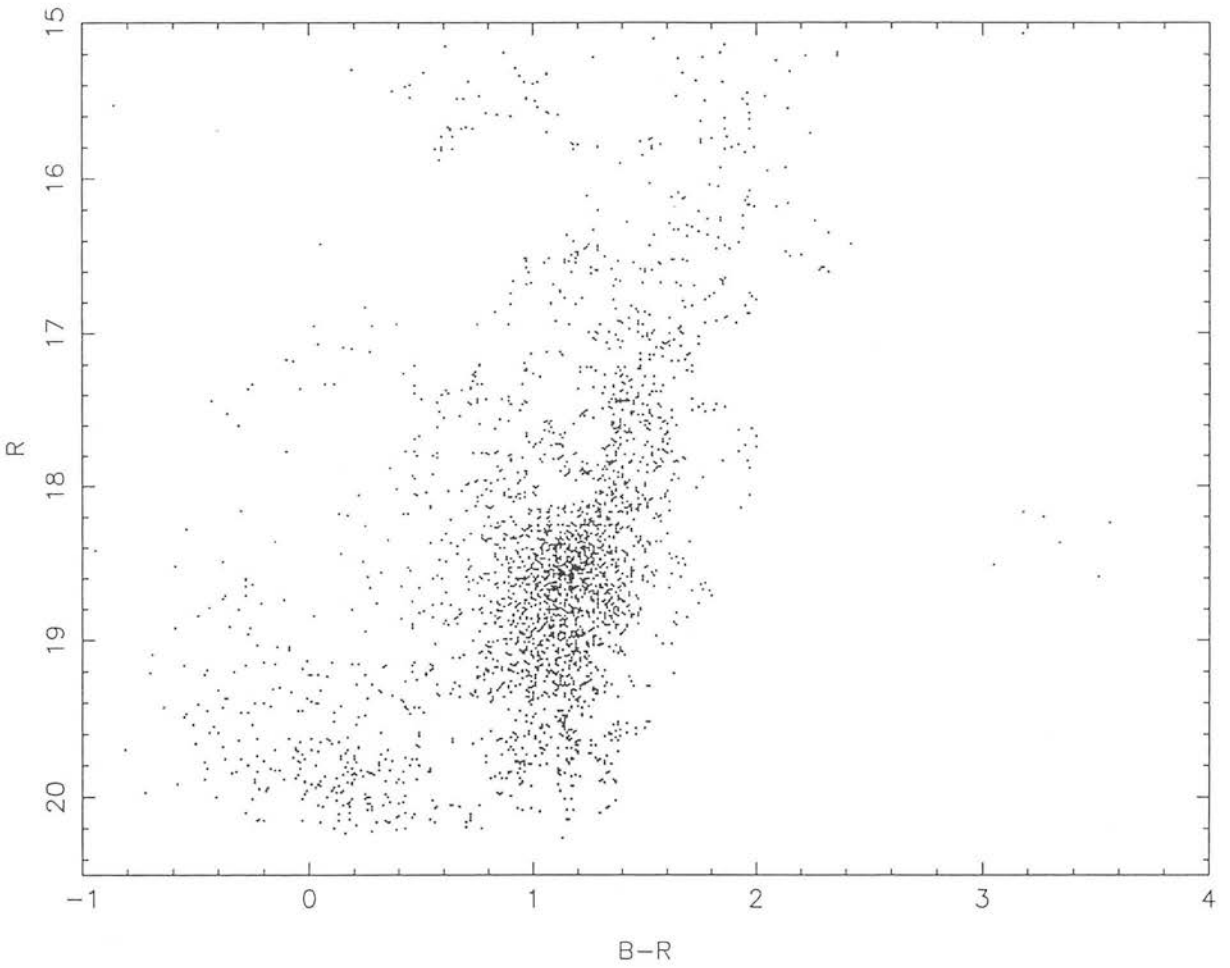

Field 52: Region 1.3

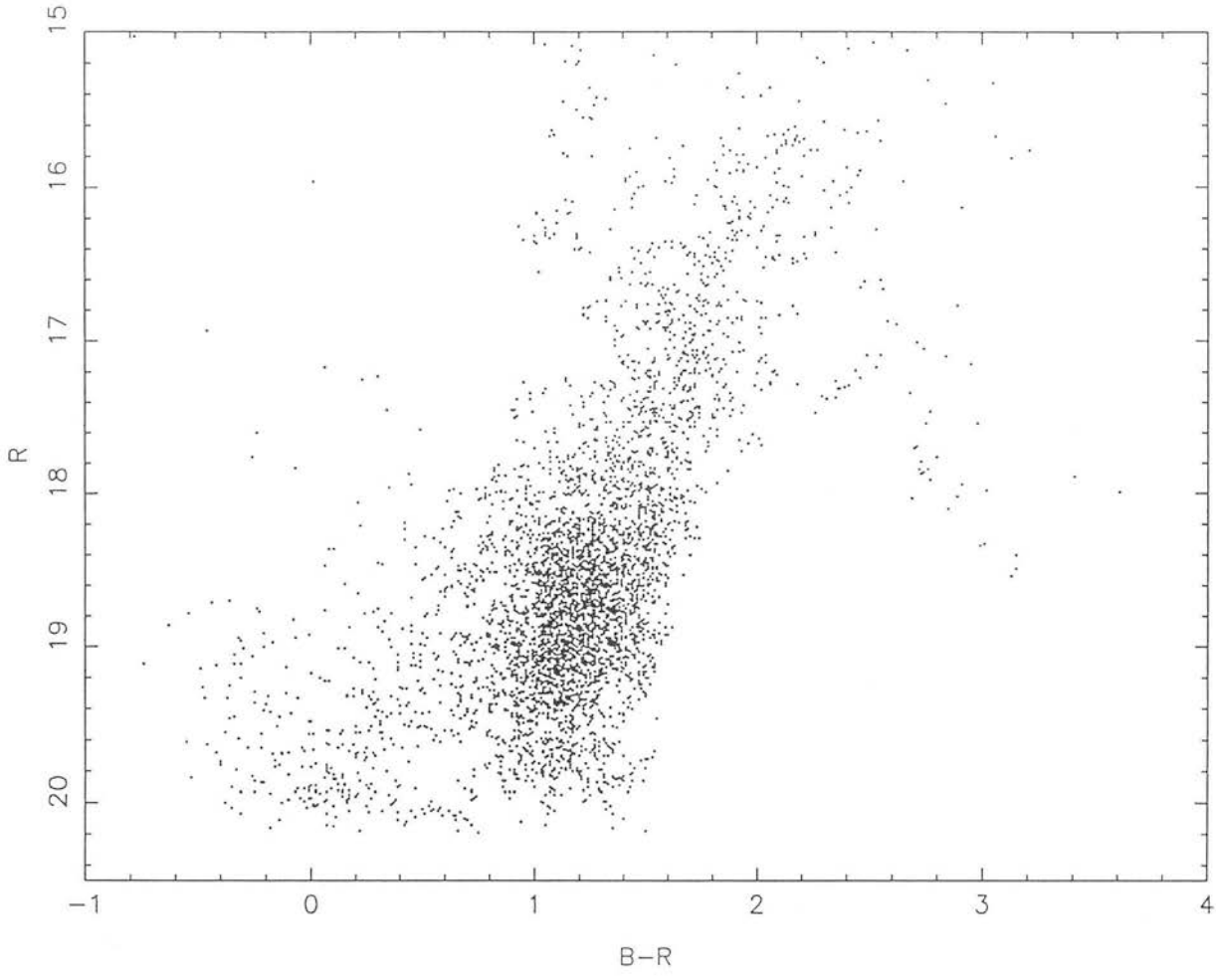

Field 52: Region 2.1

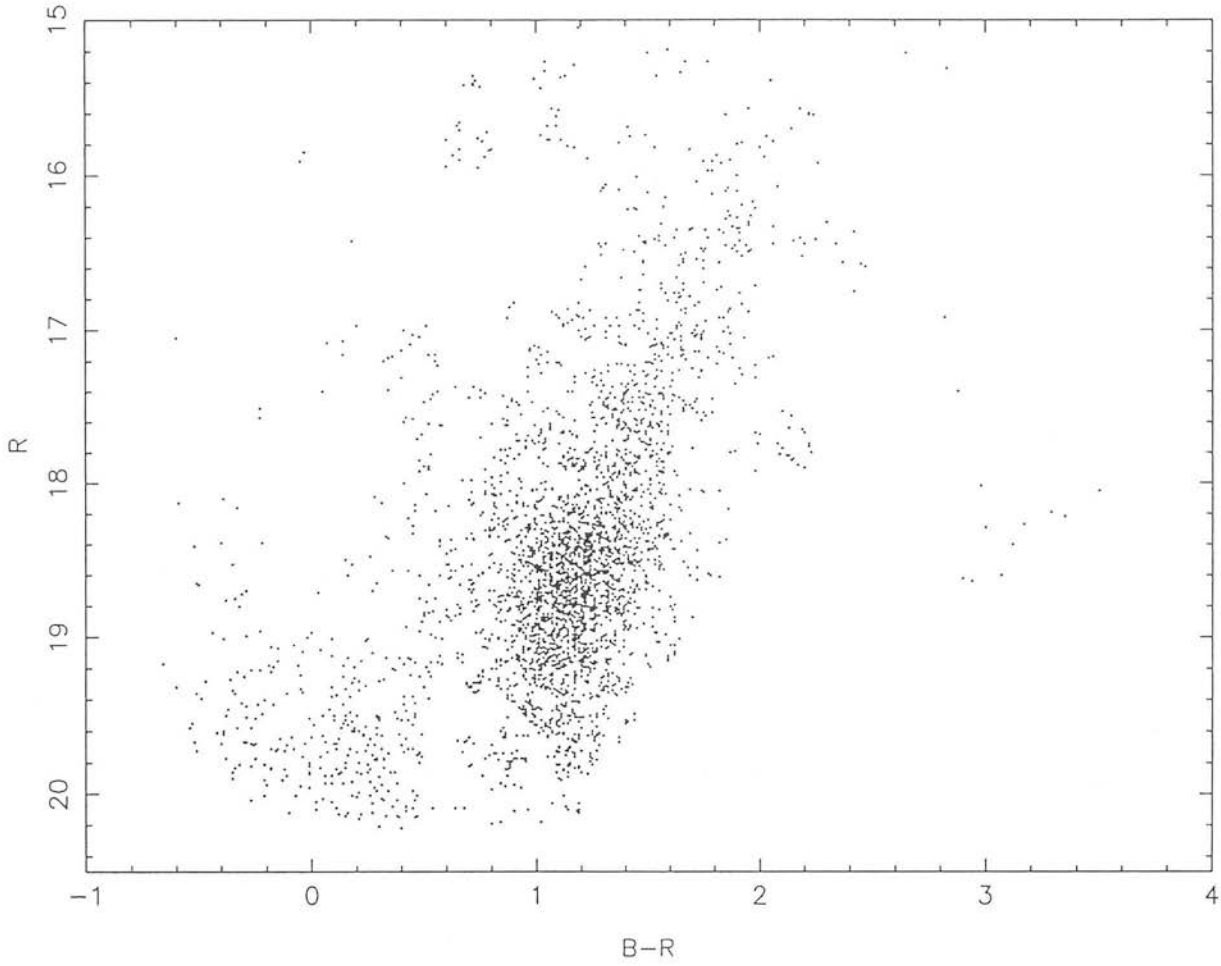

Field 52: Region 2.2

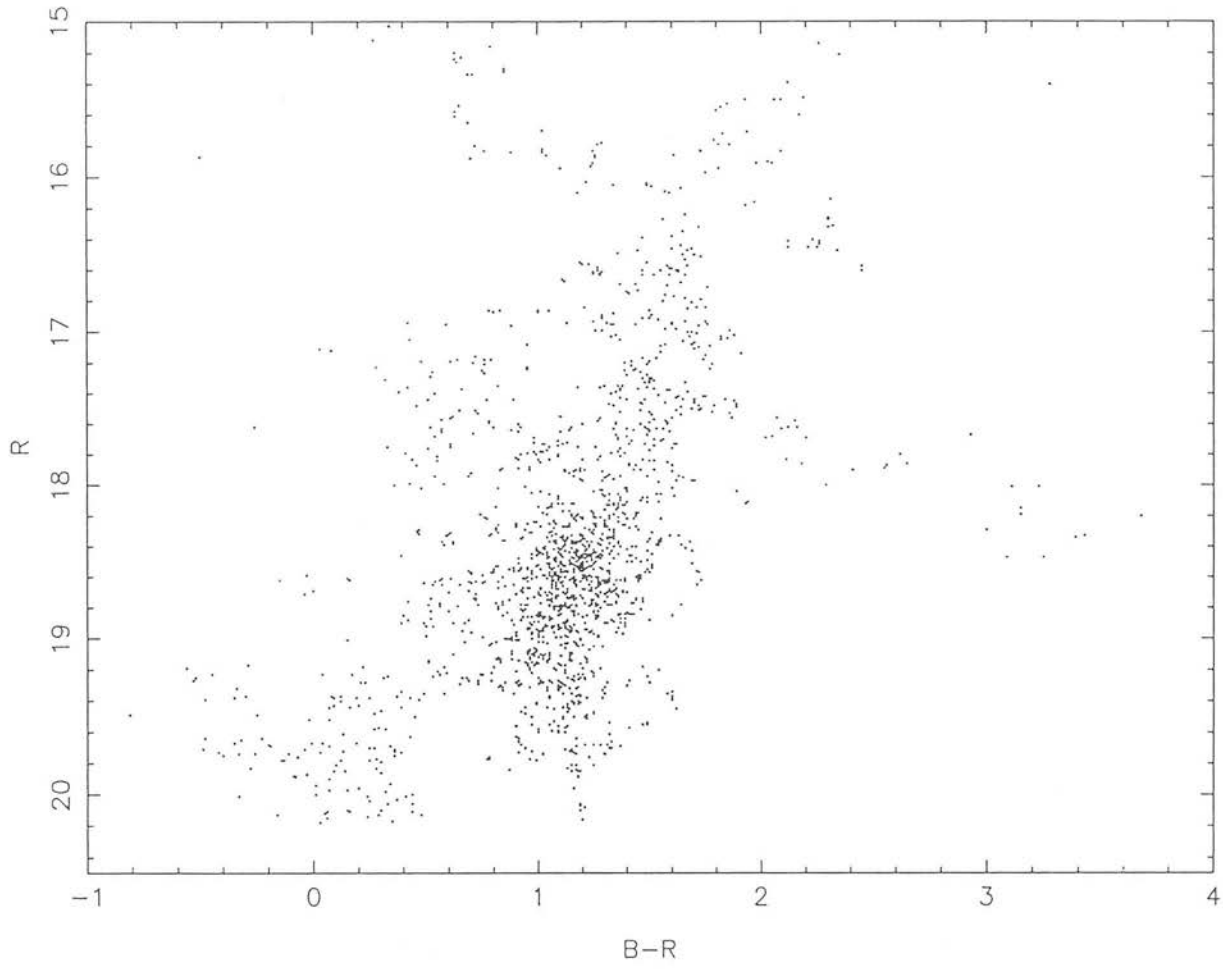

Field 52: Region 2.3

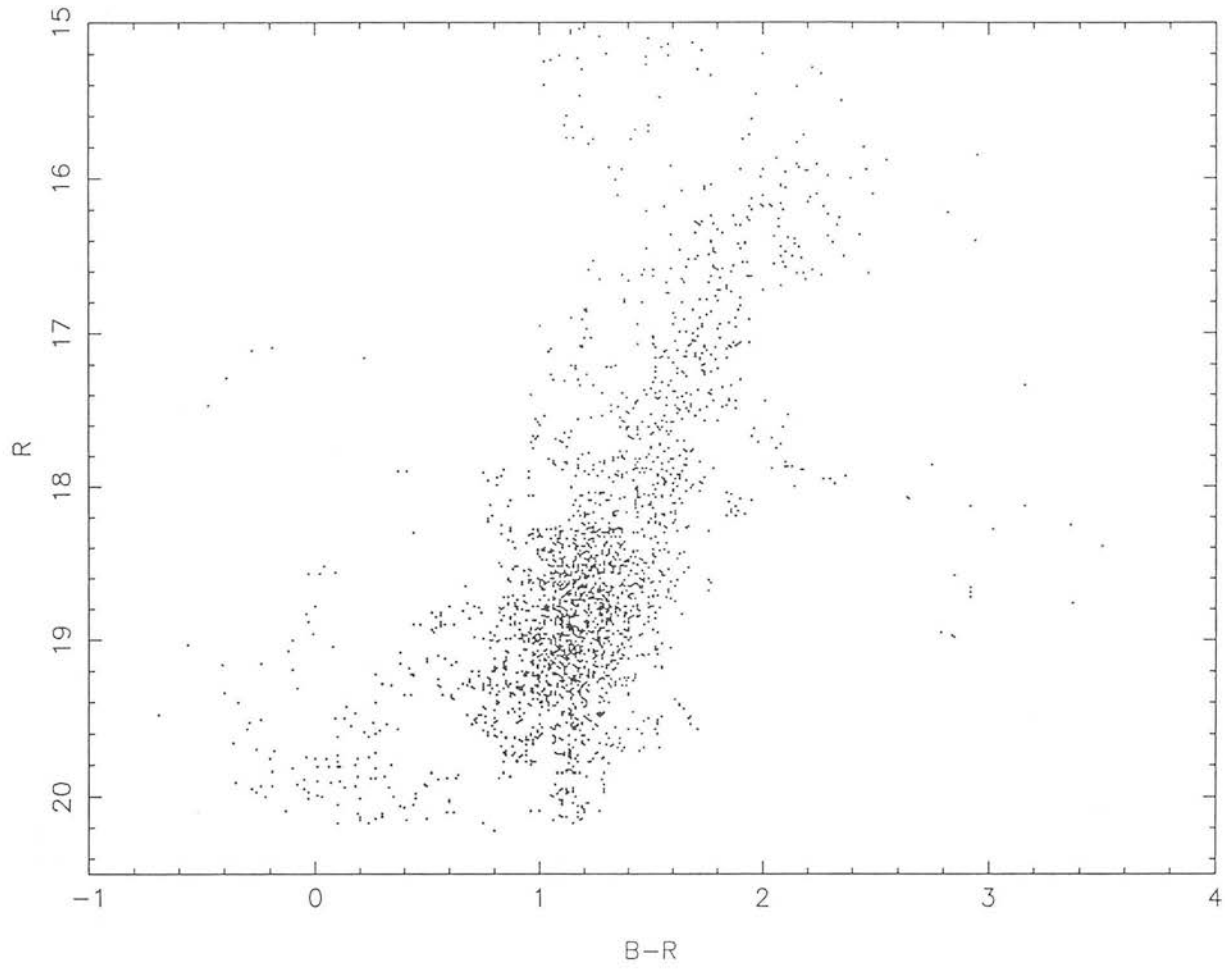

Field 52: Region 3.1

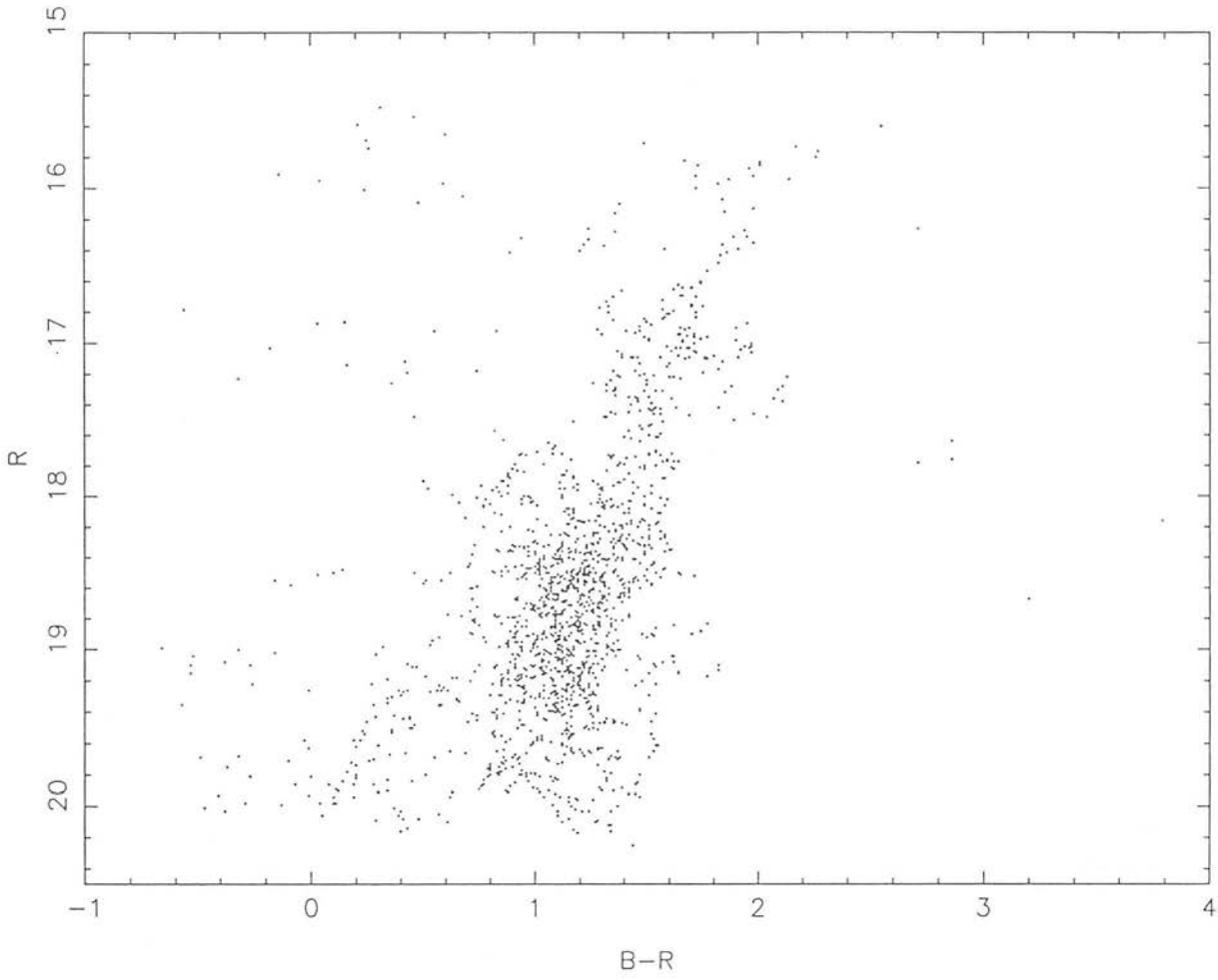

Field 52: Region 3.2

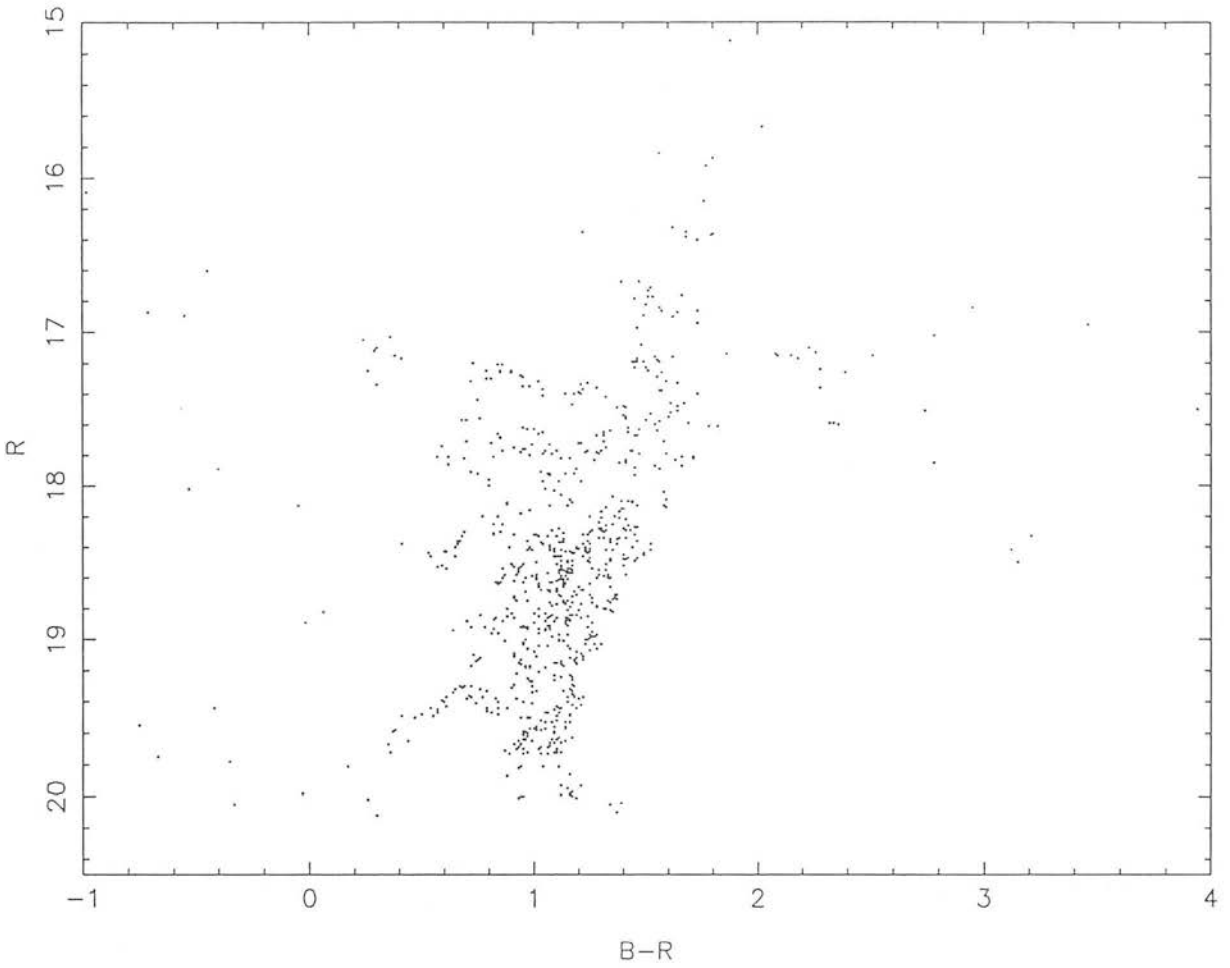

Field 52: Region 3.3

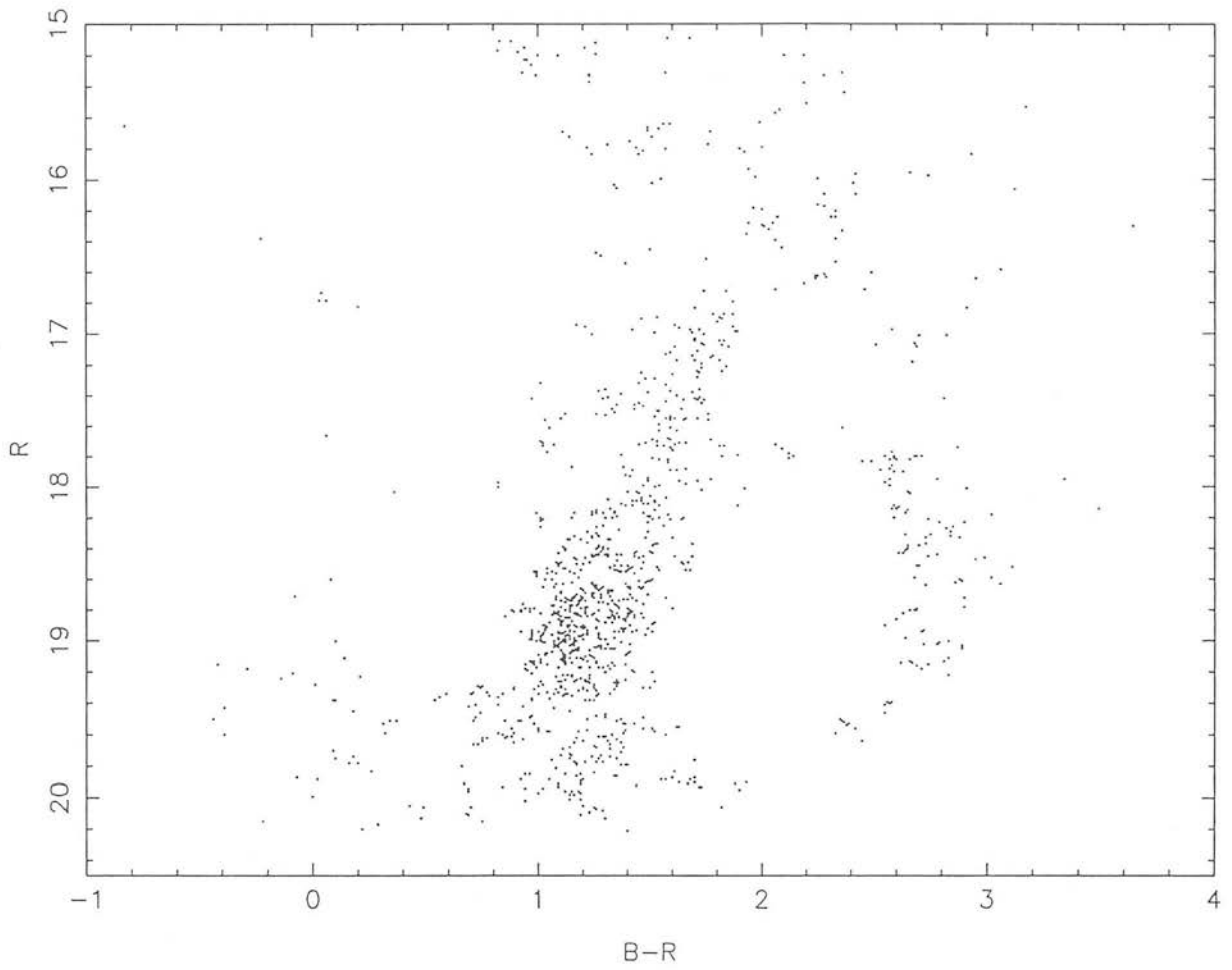

Field 52: Region 4.1

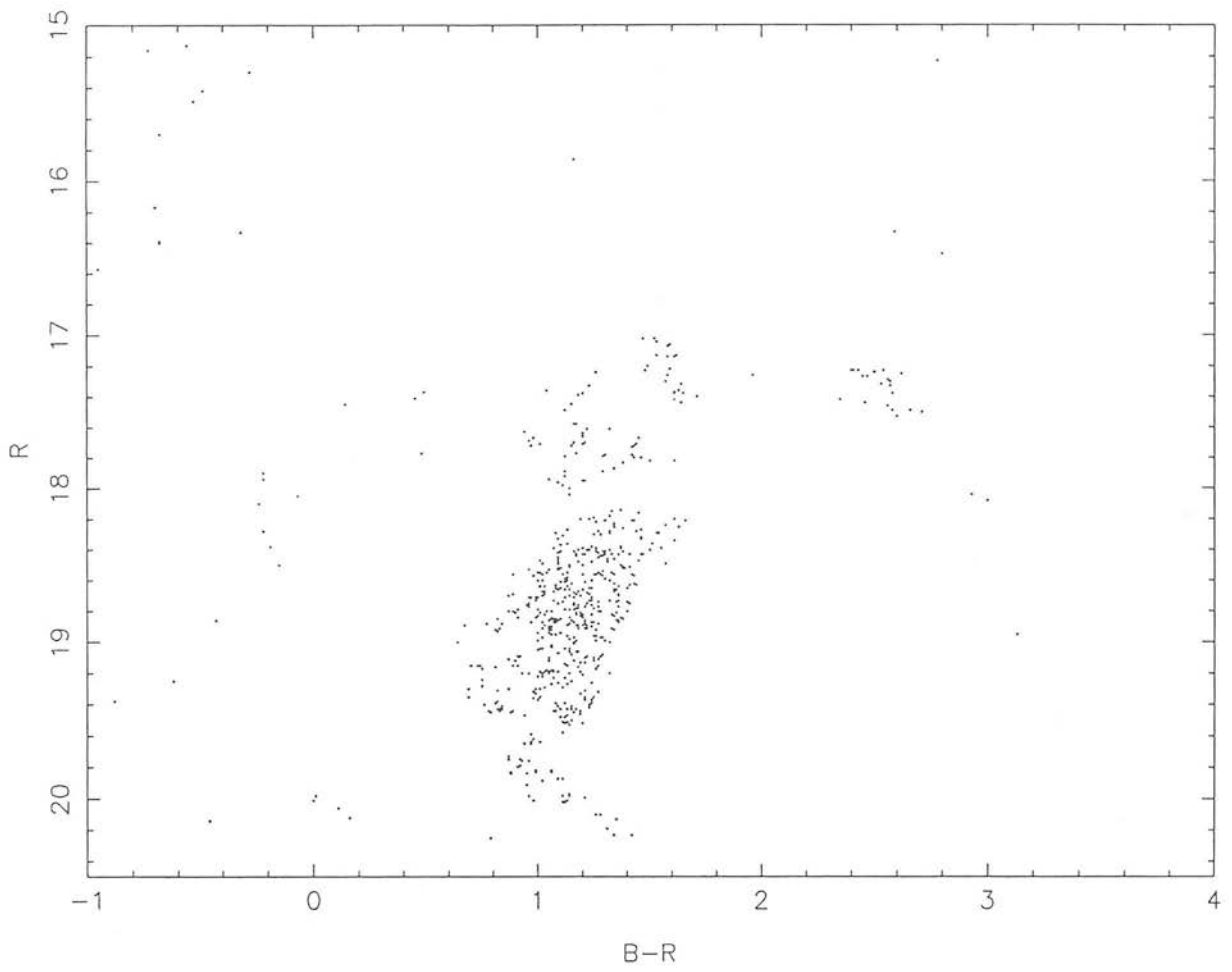

Field 52: Region 4.2

APPENDIX B

- *Finding charts of Carbon star candidates idetified with method 1*
- *Tables of Carbon Star candidates identified with method 2*

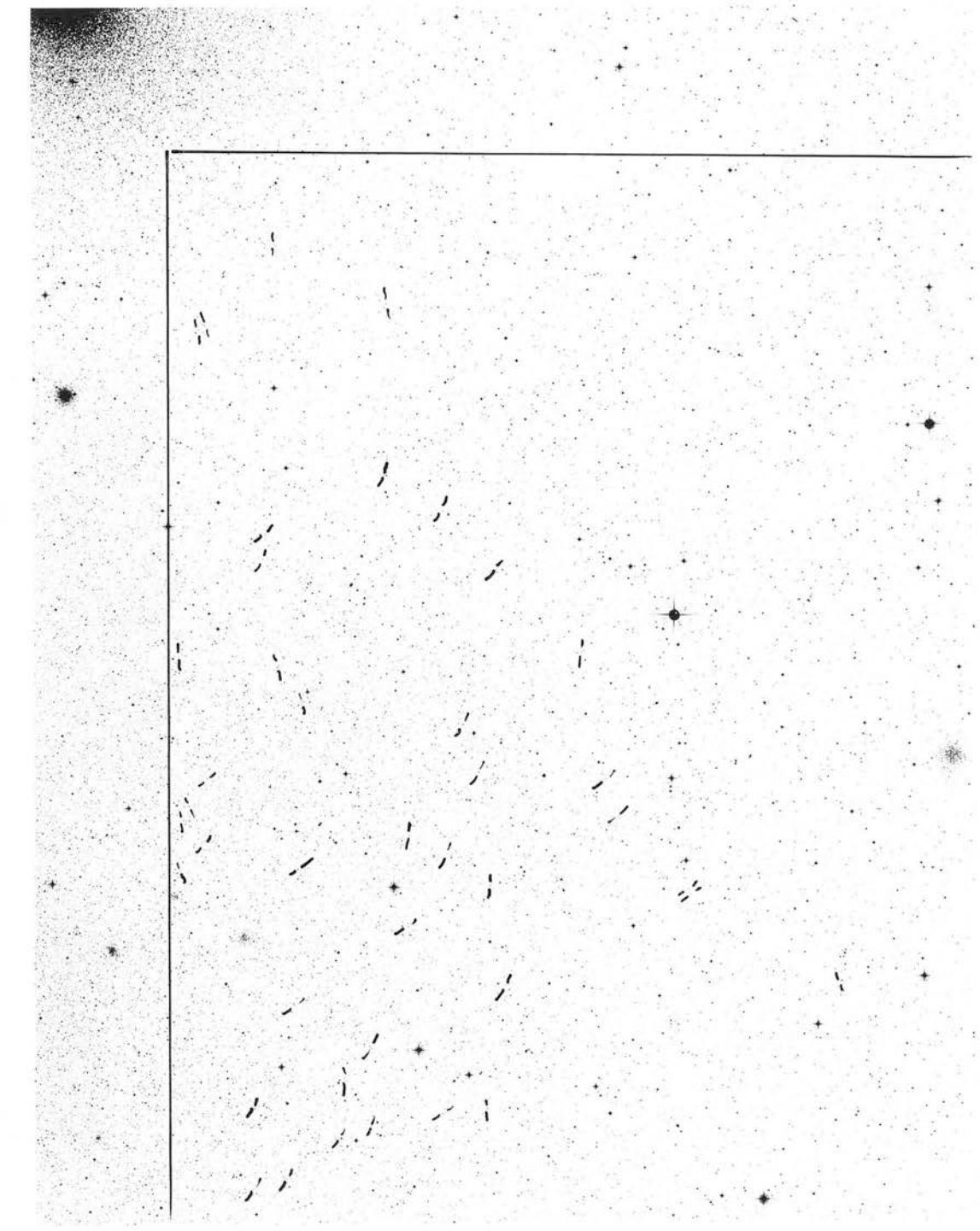

Plate B1: Field 28, NE regions. Finding chart for the carbon star candidates identified with method 1.

Plate B2: Field 28, NW regions.

Plate B3: Field 28, SE regions.

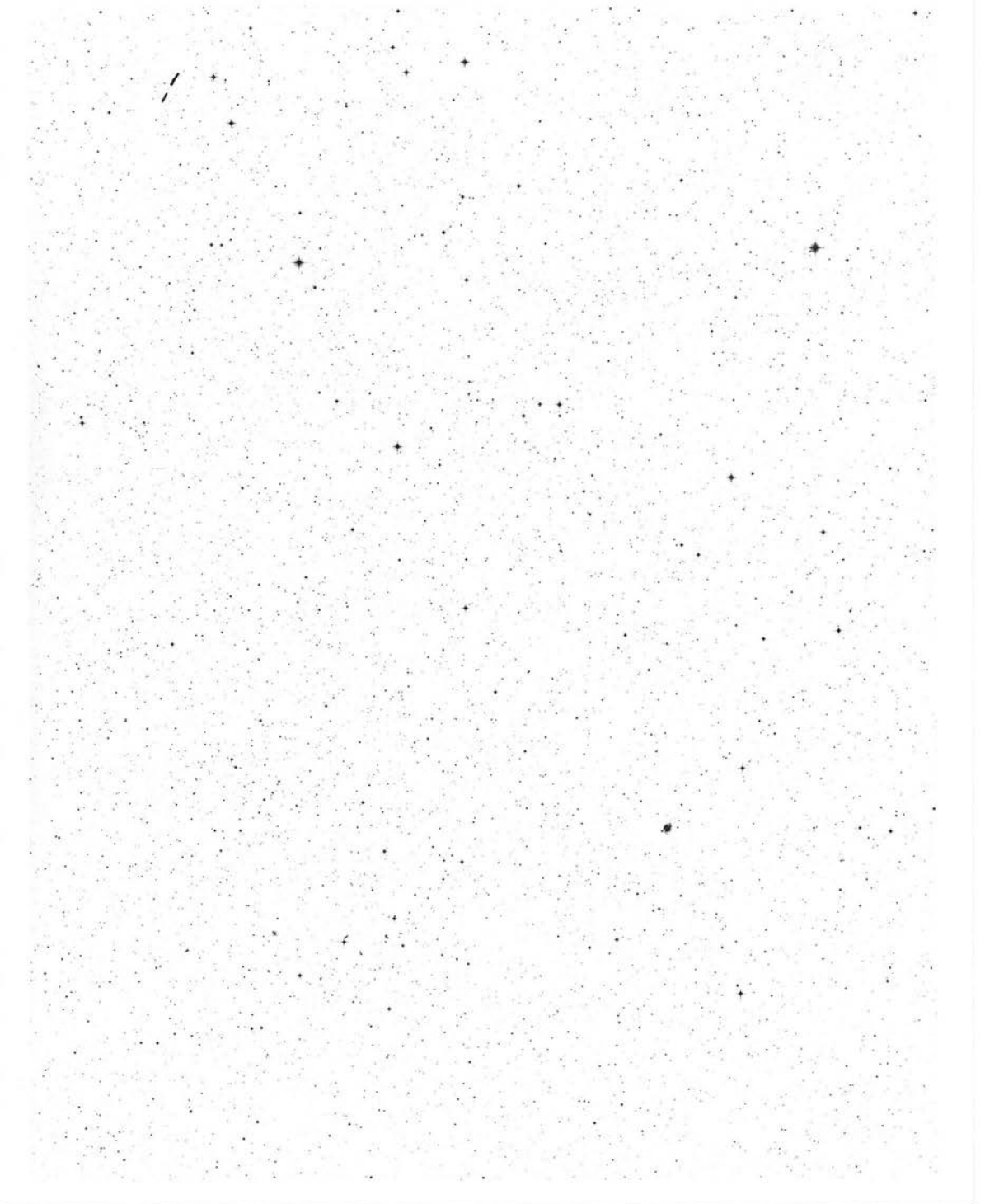

Plate B4: Field 28, SW regions.

Plate B5: Field 29, N regions overlapping with Field 52.

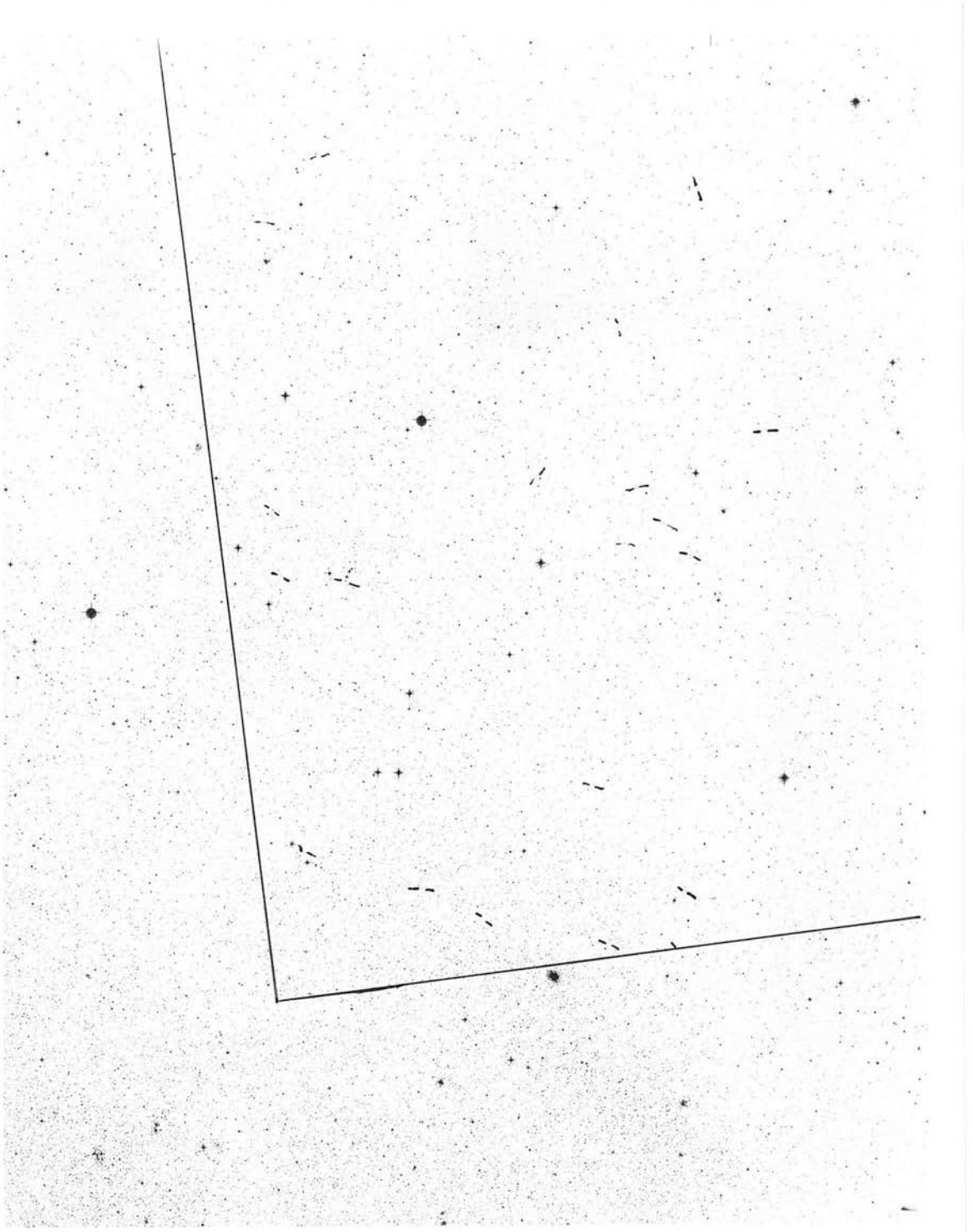

Plate B6: Field 29, S regions overlapping with Field 52.

x_{COSMOS} μ	y_{COSMOS} μ	R	$B-R$
Region 5.1			
1103334	2921248	15.84	3.15
1209609	2918791	16.96	3.02
1256890	2668798	15.40	3.92
1328030	2836028	15.83	3.10
1387421	2539074	15.49	3.12
1423587	2583189	16.61	3.15
1493890	2850558	17.01	3.02
Region 4.1			
1037555	2161387	15.58	4.00
1041293	2417638	15.59	3.00
1039131	2430597	16.24	3.83
1122431	2220696	15.52	3.79
1120096	2264659	16.07	3.67
1127976	2487984	15.97	3.48
1130089	2490086	15.24	3.00
1172282	2141737	15.23	3.29
1170885	2271565	16.46	3.04
1190148	2173397	14.10	3.15

Table B1: Field 28. Carbon Star candidates identified from their position on the CMDs. *Columns 1 & 2*: The COSMOS x and y coordinates of each star on the 'master' photographic plate (see Chapter III). *Column 3 & 4*: the magnitudes (R) and colours (B-R) of the stars.

x_{COSMOS} μ	y_{COSMOS} μ	R	$B-R$
1222675	2099068	16.00	3.63
1236536	2013675	15.78	2.93
1293559	2426861	15.26	2.91
1293582	2476783	16.21	3.07
1318469	2239827	15.29	3.97
1411094	2421751	15.62	3.06
1438906	2033220	16.94	4.76
1492034	2316855	16.07	3.42
Region 3.1			
1066250	1722751	15.36	2.95
1168643	1699915	16.51	4.03
1183231	1746764	15.86	3.20
1216210	1598484	15.92	3.89
1338215	1652990	15.40	3.55
1357104	1550557	15.85	3.83
1387785	1709766	16.14	4.17
Region 3.2			
1663862	1562332	17.00	3.43
Region 2.1			
1157988	1466632	15.62	3.39
1219615	1356680	15.25	3.02
1234800	1003454	16.85	3.78

Table B1: continued.

x_{COSMOS} μ	y_{COSMOS} μ	R	$B-R$
Region 1.1			
508818	2635162	17.08	4.12:
564728	2924823	14.74	3.22
583175	2606764	16.52	2.98
648455	2739348	15.02	3.45
669229	2695888	15.70	3.68
882409	2628971	15.02	3.16
867852	2665233	15.10	3.34
887509	2567389	15.36	3.15
894370	2760841	15.72	3.12
898419	2997863	15.67	3.05
952546	2517895	15.68	3.42
947163	2741175	15.18	3.01
Region 1.2			
1024976	2830977	16.29	3.57
1015618	2834798	16.37	4.60
1074242	2638378	15.46	3.55
1095346	2846463	15.03	3.29
1232082	2953791	15.48	3.12
1284787	2891036	15.61	3.06

Table B2: Field 52 (as in Table A1).

x_{COSMOS} μ	y_{COSMOS} μ	R	$B-R$
Region 1.3			
1740744	2738848	15.07	3.17
1771529	2708638	14.32	3.18
1941459	2965962	15.28	3.70
Region 2.1			
507060	2153459	15.67	3.05
504624	2202241	17.15	2.95:
547458	2351415	15.81	3.12
637538	2286770	15.65	4.44
698741	2060918	16.30	4.12
927051	2383378	15.33	3.05
996539	2325491	16.13	2.91
993629	2467868	15.76	3.20
Region 2.2			
1247551	2249279	14.94	3.05
Region 2.3			
1557130	2482558	15.40	3.28
1731580	2429731	15.45	3.56
1843418	2178713	15.57	3.00

Table B2: continued.

x_{COSMOS} μ	y_{COSMOS} μ	R	$B-R$
Region 3.1			
522889	1658245	16.40	2.94
684785	1805513	17.10	3.98:
984629	1629636	15.85	2.95
Region 3.2			
1233099	1741954	15.66	4.20
Region 3.3			
1540315	1890866	16.84	2.94
1873082	1833640	16.95	3.45
1870504	1842311	17.09	4.64:
Region 3.4			
2184999	1645496	16.89	4.49
2174756	1653058	17.12	3.53:

Table B2: continued.

Aaronson, M., 1986. *Stellar populations*, eds Norman, C.A., Renzini, A. & Tosi, M., p.45, Space Telescope Science Institute Symposium Series, Cambridge University Press.

Aaronson, M. & Mould, J.R., 1980. *Astrophys.J.*, **240**, 804.

Aaronson, M. & Mould, J.R., 1982. *Astrophys.J.Suppl.*, **48**, 161.

Albers, H., MacGillivray, H.T., Beard, S.M. & Chromey, F.R., 1987. *Astr.Astrophys.Lett.*, **182**, L8.

Andersen, J., Blecha, A. & Walker, M.F., 1984. *IAU Symp.No.108*, eds van den Bergh, S. & de Boer, K.S., p.41, Reidel, Dordrecht, Holland.

Ardeberg, A. & Maurice, E., 1979. *Astr.Astrophys.*, **77**, 277.

Arp, H., 1958. *Astron.J.*, **63**, 118.

Arp, H., 1960. *Astron.J.*, **65**, 404.

Azzopardi, M., 1981. *PhD thesis*, l'Université Paul Sabatier de Toulouse.

Azzopardi, M., 1982. *Comptes rendues sur les journées de Strasbourg*, **4**, p.20, Observatoire de Strasbourg.

Azzopardi, M. & Vigneau, J., 1977. *Astron.Astrophys.*, **56**, 15.

Becker, S.A., 1982. *Astrophys.J.*, **260**, 695.

Bell, R.A. & Gustafsson, B., 1975. *Dudley Obs.Report*, **9**, 330.

Bell, R.A. & Gustaffson, B., 1978. *Astr.Astrophys.Suppl.*, **34**, 229.

Bell, R.A. & Gustaffson, B., 1983. *Mon.Not.R.astr.Soc.*, **204**, 249.

Bessell, M.S., 1983. *Mem.Soc.astr.Ital.*, **54**, 47.

Bessell, M.S., Wood, P.R.,& Lloyd Evans, T., 1983. *Mon.Not.R.astr.Soc.*, **202**, 59.

Bhatia, R.K. & Hatzidimitriou, D., 1988. *Mon.Not.R.astr.Soc.*, **230**, 215.

Blanco, V.M. & Blanco, B.M., 1986; *Publs astr.Soc.Pacific*, **98**, 1162.

Blanco, B.M., Blanco, V.M. & McCarthy, M.F., 1978. *Nature*, **271**, 638.

Blanco, V.M & McCarthy, M.F., 1983. *Astron.J.*, **88**, 1442.

Blanco, V.M., McCarthy, M.F. & Blanco, B.M., 1980. *Astrophys.J.*, **242**, 938.

Bok, B.J., 1965. *Publs astr.Soc.Pacific*, **77**, 416.

Bok, B.J., 1966. *Ann.Rev.Astr.Astrophys.*, **4**, 95.

Bolte, M., 1987. *Astrophys.J.*, **315**, 469.

Brück, M.T., 1978. *Astr.Astrophys.*, **68**, 181.

Brück, M.T., 1980. *Astr.Astrophys.*, **87**, 92.

Brück, M.T., 1982. *Compendium in Astronomy*, eds Mariopoulos, E.G., *et al.*, p.297, Reidel, Dordrecht, Holland.

Brück, M.T. & Marsoglu, A., 1978. *Astr.Astrophys.*, **68**, 193.

Brück, M.T., Cannon, R.D. & Hawkins, M.R.S., 1985. *Mon.Not.R. astr.Soc.*, **216**, 165.

Burstein, D. & Heiles, C., 1982. *Astron.J.*, **87**, 1165.

Butcher, H.R., 1977. *Astrophys.J.*, **216**, 372.

Butler, C.J., 1972. *Dunsink Obs.Publs*, **1**, 133.

Butler, D., 1975. *Publs astr.Soc.Pacific*, **87**, 559.

Butler, D., Demarque, P. & Smith, H., 1982. *Astrophys.J.*, **257**, 592.

Buttress, J., Cannon, R.D., & Griffiths, W.K., 1988. *I.A.U. Symposium 126*, eds Grindlay, J.E., & Davis Philip, A.G., p.575, Kluwer Academic Publishers, Doldrecht, Holland.

Caldwell, J.A.R. & Coulson, I.M., 1985. *Mon.Not.R.astr.Soc.*, **212**, 879.

Caldwell, J.A.R. & Coulson, I.M., 1986. *Mon.Not.R.astr.Soc.*, **218**, 223.

Cannon, R.D., 1970. *Mon.Not.R.astr.Soc.*, **150**, 150.

Cannon, R.D., 1983. *Highlights astr.*, **6**, 109.

Carney, B.W., 1980. *Astrophys.J.Suppl.*, **42**, 481.

Carney, B.W., Janes, K.A. & Flower, P.J., 1985. *Astron.J.*, **90**, 1196.

Ciardullo, R. & Demarque, P., 1977; *Trans.astr.Obs., Yale Univ.*, **33**.

Cohen, J.G., 1982. *Astrophys.J.*, **258**, 143.

Cohen, J.G., Frogel, J.A., Persson, S.E. & Elias, J.H., 1981. *Astrophys.J.*, **249**, 481.

Crampton, D. & Greasley, J., 1982. *Publs Astron.Soc.Pacific*, **94**, 31.

Crawford, D.L. & Snowden, M.S., 1975. *Publs Astron.Soc.Pacific*, **87**, 561.

Dachs, J., 1970. *Astron.Astrophys.*, **9**, 95.

Da Costa, G.S. & Mould, J.R., 1986.*Astrophys.J.*, **305**, 214.

Da Costa, G.S., Mould, J.R. & Crawford, M.D., 1985. *Astrophys.J.*, **297**, 582.

Dawe, J.A., Coyte, E. & Metcalfe, N., 1984. *Astronomical Photography*, eds. M.E.Sim & K.Ishida, *Occ.Rep.R.Obs. Edinburgh*, **14**, 59.

Dennefeld, M. & Tammann, G.A., 1980. *Astr.Astrophys.Suppl.*, **83**, 275.

Dickens, R.J. & Sweigart, A.V., 1978. *Bull.Amer.astr.Soc.*, **10**, 693.

Divan, 1976. see de Vaucouleurs 1978.

Dopita, M.A., 1985. *Birth and Evolution of Massive Stars and Stellar Groups*, eds

Boland, W. & van Werden, H., p.269, Reidel Publishing Company.

Dubois, P., 1980. *Ph.D. thesis*, Univ.Louis Pasteur, Strasbourg.

Durand, D., Hardy, E. & Melnick, J., 1984. *Astrophys.J.*, **283**, 552.

Dworak, T.Z., 1974. *Acta Cosmologica*, **2**, 13.

Eggen, O.J., 1977. Astrophys.J.Suppl., **34**, 1.

Ellis, R., 1987. *IAU Symp.No.124*, eds. Hewitt, A., *et al.*, p.367, Reidel, Doldrecht, Holland.

Faulkner, D.J. & Cannon, R.D., 1973. *Astrophys.J.*, **180**, 435.

Faulkner, D.J. & Iben, I., 1966. *Astrophys.J.*, **144**, 995.

Feast, M.W., 1984. *IAU Symp. No.108*, eds van den Bergh, S. & de Boer, K.S., p.157, Reidel, Dordrecht, Holland.

Feast, M.W., & Walker, A.R., 1987. *Ann.Rev.Astr.Astrophys.*, **25**, 345.

Feast, M.W., Thackeray, A.D. & Wesselink, A.J., 1960. *Mon.Not.R.astr. Soc.*, **121**, 337.

Florsch, A., Marcout, J. & Fleck, E., 1981. *Astr.Astrophys.*, **96**, 158.

Flower, P.J., 1984. *Astrophys.J*, **278**, 582.

Flower, P.J., Jones, J.H. & Clemson, U., 1983. *Bull.Amer.astr.Soc.*, **15**, 912.

Flower, P.J., Geisler, D., Hodge, P.W. & Olszewski, E., 1980. *Astrophys.J.*, **235**, 769.

Foy, R., 1981. *Astron.Astrophys.*, **103**, 135.

Frogel, J.A., 1984. *Publs astr.Soc.Pacific*, **96**, 856.

Freeman, K.C., Illingworth, G., & Oemler, A., Jr., 1983. *Astrophys.J.*, **272**, 488.

Fujimoto, M., 1987. *Sci.Rep.Tôhoku Univ.Eighth Ser.*, **7**, 313.

Fujimoto, M. & Murai, T., 1984. *IAU Symp.No.108*, eds van den Bergh, S. & de Boer, K.S., p.115, Reidel, Dordrecht, Holland.

Gallagher, J.S. & Hunter, D.A., 1984. *Ann.Rev.Astr.Astrophys.*, **22**, 37.

Gaposchkin, S., 1970. *Infor.Bull. Variable Stars*, Konkoly Obs., Budapest, no.420.

Garmany, C.D., Conti, P.S. & Massey, P., 1987. *Astron.J.*, **93**, 1070.

Gascoigne, S.C.B., 1969. *Mon.Not.R.astr.Soc.*, **146**, 1.

Gatley, Hyland & Jones, 1982. *Mon.Not.R.astr.Soc.*, **200**, 521.

Geisler, D., 1984. *Astrophys.J.Lett.*, **287**, L85.

Geisler, D., 1986. *Publs astr.Soc.Pacific*, **98**, 762.

Gingold, R.A., 1984. *Proc.astr.Soc.Aust.*, **5**, 469.

Graham, J.A., 1975. *Publs.astr.Soc.Pacif.*, **87**, 641.

Graham, J.A., 1982. *Publs astr.Soc.Pacific*, **94**, 244.

Graham, J.A., 1984. *IAU Symp.No.108*, eds van den Bergh & de Boer, K.S., p.207, Reidel, Dordrecht, Holland.

Green, E.M., Demarque, P. & King, C.R., 1987; *The revised Yale isochrones and luminosity functions*, Yale University Observatory, New Haven.

Gustafsson, B., Bell, R.A. & Hejlesen. P.M., 1977.*Astrophys.J.Lett.*, **216**, L7.

Hardy, E., Buonanno, R., Corsi, C.E., James, K.A. & Schommer, R.A., 1984. *Astrophys.J.*, **278**, 592.

Hardy, E. & Durand, D., 1984. *Astrophys.J.*, **279**, 567.

Harris, H.C., 1981. *Astron.J*, **86**, 1192.

Hartwick, F.D.A, 1968. *Astrophys.J.*, **154**, 475.

Hatzidimitriou, D. & Bhatia, K.B., 1988. *IAU Symp.No.126*, eds Grindlay, J.E. & Davis Philip A.G., p.567, Kluwer Academic Publishers, Dordrecht, Holland.

Hawkins, M.R.S., 1983. *Mon.Not.R.astr.Soc.*, **202**, 571.

Hawkins, M.R.S., 1984. *Mon.Not.R.astr.Soc.*, **206**, 433.

Hawkins, M.R.S & Brück, M.T., 1982. *Mon.Not.R.astr.Soc.*, **198**, 935.

Hawkins, M.R.S & Brück, M.T.,1984. *IAU Symp.No.108*, eds van den Bergh, S. & de Boer, K.S., p.101, Reidel, Dordrecht, Holland.

Hesser, J.E. & Davis-Philip, A.G., 1976. *Publs Astron.Soc.Pacific*, **88**, 89.

Hesser, J.E., Harris, W.E., VandenBergh, D.A., Allwright, J.W.B., Shott, P. & Stetson, P., 1987. *Publ.astr.Soc.Pacif.*, **99**, 739.

Hindman, J.V., 1967. *Austr.J.Physics*, **20**, 147.

Hirshfeld, A.W., 1980. *Astrophys.J.*, **241**, 111.

Hodge, P.W., 1974. *Publs astr.Soc.Pacific*, **86**, 263.

Hodge, P.W., 1981. *Astrophys.J.*, **247**, 894.

Hodge, P.W., 1982. *Astrophys.J.*, **256**, 447.

Hodge, P.W., 1983. *Astrophys.J.*, **264**, 470.

Hodge, P.W. & Wright, F.W., 1969. *Astrophys.J.Suppl.*, **17**, 467.

Hubble, E., 1926. *Asrtophys.J.*, **64**, 321.

Hubble, E., 1936. *The realm of the Nebulae*, p.131, Yale Univ.press, New Haven.

Humphreys, R., 1979. *Astrophys.J.*, **231**, 384.

Hunter, D.A. & Gallagher, J.S., III, 1986. *Publs astr.Soc.Pacific*, **98**, 5.

Iben, I., 1975. *Astrophys.J.*, **196**, 525.

Iben, I., 1982. *Astrophys.J.*, **260**, 821.

Iben, I., 1984. *IAU Symp.No.105*, eds. A.Maeder & A.Renzini, p.3, Reidel, Dordrecht, Holland.

Israel, F.P., 1984. *IAU Symp.No.108*, eds S. van den Bergh & K.S. de Boer, p.319, Reidel, Dordrecht, Holland.

Janes, K.A. & Demarque, P., 1983. *Astrophys.J.*, **264**, 206.

Jarvis, J.F. & Tyson, J.A., 1981.*Astron.J.*, **86**, 476.

Johnson, H., 1961. *Publs.astr.Soc.Pacific*, **73**, 20.

Jørgensen, H.E. & Hansen, L., 1983. *Internal report* no.**5**, Copenhagen University Observatory.

Kennicutt, R.C, & Hodge, P.W., 1986. *Astrophys.J.*, **306**, 130.

Kerr, F.J., 1965. *Mount Stromlo Symp. on the Magellanic Clouds*, p.4.

Kerr, F.J., 1971. *The Magellanic Clouds*, edt Muller, A.B., p.50, Reidel, Dordrecht, Holland.

Kinahan, B.F. & Härm, R., 1975. *Astrophys.J.*, **200**, 330.

Landolt, A.U., 1983. *Astron.J.*, **88**, 439.

Laney, C.D. & Stobie, R.S., 1986. *Mon.Not.R.astr.Soc.*, **222**, 449.

Larson, R.B., 1972. *Nature Phys.Sci.*, **236**, 7.

Leavitt, H.S., 1908. *Harvard Obs.Ann.*, **60**, 87.

Lee, S.W., 1977. *Astron.Astrophys.Suppl.*, **27**, 381.

Leep, E.M., Oki, J.B., & Wallerstein, G., 1987. *Astron.J.*, **92**, 338.

Lequeux, J., 1984. *IAU Symp.No.108*, eds van den Bergh, S. & de Boer, K.S., p.67, Reidel, Dordrecht, Holland.

Lloyd-Evans, T., 1980. *Mon.Not.R.astr.Soc.*, **193**, 97.

MacGillivray, H.T. & Stobie, R.S., 1984. *Vistas Astr.*, **27**, 433.

Mackay, C.D., 1986. *Ann.Rev.Astr.Astrophys.*, **24**, 255.

Madore, B.F., 1982. *Astrophys.J.*, **253**, 575.

Maeder, A. & Mermilliod, J.C., 1981. *Astr.Astrophys.*, **93**, 136.

Mateo, M. & Hodge, P., 1985. *Publs astr.Soc.Pacific*, **97**, 753.

Mateo, M. & Hodge, P., 1986. *Astrophys.J.Suppl.*, **60**, 893.

Mathewson, D.S., 1984. *Mercury*, March-April, 57.

Mathewson, D.S. & Ford, V.L., 1970. *Astron.J.*, **75**, 778.

Mathewson, D.S. & Ford, V.L., 1984. *IAU Symp.No 108*, eds van den Bergh, S. & de Boer, K.S., p.125, Reidel, Doldrecht, Holland.

Mathewson, D.S., Ford, V.L. & Visvanathan, N., 1986. *Astrophys.J.*, **301**, 664.

Mathewson, D.S., Ford, V.L. & Visvanathan, N., 1988. *Astrophys.J.*, **333**, 617.

Matteucci, F. & Chiosi, C., 1983. *Astr.Astrophys.*, **123**, 121.

Matteucci, F., 1984. *IAU Symp.No.108*, eds van den Bergh, S. & de Boer, K.S., p.95, Reidel, Dordrecht, Holland.

Maurice, E., Andersen, J., Ardeberg, J., Bardin, C., Imbert, M., Lindgren, H., Martin, N., Mayor, M., Nordström, B., Prévot, L., Rebeirot, E. & Rousseau, J., 1987. *Astr.Astrophys.Suppl.*, **67**, 423.

McNamara, D.H. & Feltz K.,A., 1980. *Publs Astron.Soc.Pacific*, **92**, 587.

Menzies, J.W., Banfield, R.M. & Laing, J.D., 1980. *South African Astron.Obs.Circ.*, **1**, 149.

Mould, J., 1986. *Spectral evolution of Galaxies*, eds Chiosi, C. & Renzini, A., p.133, Reidel, Dordrecht, Holland.

Mould, J.,& Aaronson, M., 1980. *Astrophys.J.*, **240**, 464.

Mould, J. & Aaronson, M., 1982. *Astrophys.J.*, **263**, 629.

Mould, J. & Aaronson, M., 1983. *Astrophys.J.*, **273**, 530.

Mould, J. & Aaronson, M., 1985. *Astrophys.J.*, **288**, 551.

Mould, J.,& Aaronson, M., 1986. *Astrophys.J.*, **303**, 10.

Mould, J.R., Da Costa, G.S. & Crawford, M.D., 1984. *Astrophys.J.*, **280**, 595.

Mould, J.R., Da Costa, G.S. & Crawford, M.D., 1986. *Astrophys.J.*, **304**, 265.

Murai, T. & Fujimoto, M., 1980. *Publ.Astron.Soc.Japan*, **32**, 581.

Murai, T. & Fujimoto, M., 1986. *Astrophys. and Space Science*, **119**, 169.

Nandy, K., Morgan, D.H. & Carnochan, D.J., 1979. *Mon.Not.R.astr.Soc.*, **186**, 421.

Nandy, K., 1984. *IAU Symp.No.108*, eds van den Bergh, S. & de Boer, K.S., p.341, Reidel, Dordrecht, Holland.

Nissen, P.E., Edvardsson, B. & Gustafsson, B., 1985. *Production and distribution of C, N and O Elements*, eds Danziger, I.J., Matteucci, F. & Kjar, K. ,p.131, München.

Olszewski, E.W., 1988. *I.A.U. symposium 126*, eds. Grindlay, J.E. & Davis Philip,

A.G., p.159, Kluwer Academic Publishers, Doldrecht, Holland.

Olszewski, E.W., Schommer, R.A. & Aaronson, M., 1987. *Astron.J.*, **93**, 565.

Osmer, P.S., 1973. *Astrophys.J.*, **186**, 459.

Pagel, P.E.J., 1981. *Structure and evolution of Normal Galaxies*, eds Fall, S.M. & Lynden–Bell, D., p.211, Cambridge Univ. press, Cambridge.

Pagel, P.E.J. & Patchett, B.E, 1975. *Mon.Not.R.astr.Soc.*, **172**, 13. Parker, Q.A., 1988. *The BDF processing chain* documentation, R.Obs.Edinburgh.

Pel, J.W., 1984. *IAU Symp.No. 108*, eds van den Bergh, S., & de Boer, K.S., p.169, Reidel, Dordrecht, Holland.

Pedersen, H., 1985. *ESO operating manual*, no.**3**.

Przybylski, A., 1972. *Mon.Not.R.astr.Soc.*, **159**, 155.

Ratnatunga, K.U. & Bahcall, J.N., 1985. *Astrophys.J.suppl.*, **59**, 63.

Rich, R.M., Da Costa, G.S. & Mould, J.R., 1984. *Astrophys.J.*, **286**, 517.

Richer, H.B., 1981. *Astrophys.J.*, **243**, 744.

Richtler, T. & Nelles, B., 1983. *Astron.Astrophys.*, **119**, 75.

Richtler, T. & Seggewiss, W., 1987. *ESO Confer.Workshop Proc.*, **27**, 269.

Richtler, T. & Seggewiss, W., 1988. *IAU Symp.No.126*, eds Grindlay, J.E. & Davis Philip, A.G., p.553, Kluwer Academic Publishers, Dordrecht, Holland.

Robertson, J.G., 1987. *Report on the commissioning of new RCA CCD chip for photometry at the AAT prime focus.*

Robertson, J.G. & Stathakis, R., 1987. *AAT-CCD service obsering sheet.*

Rocca-Volmerange, B., Lequeux, J. & Maucherat-Joubert, M., 1981. *Astr. Astrophys.*, **104**, 177.

Rood, R.T., 1972. *Astrophys.J.*, **177**, 681.

Rood, R.T. & Crocker, D.A., 1988. *IAU Symp.No.126*, eds Grindlay, J.E & Davis Philip, A.G. p.507, Kluwer Academic Publishers, Dordrecht, Holland.

Russell, S.C. & Hyland, A.R., 1985. *Proc.astr.Soc.Aust.*, **6**, 52.

Sandage, A.R., 1957. *Astrophys.J.*, **125**, 422.

Sandage, A.R., 1982. *Astron.J.*, **252**, 553.

Sandage, A. & Tammann, G.A., 1981. *A Revised Shapley-Ames Catalogue of Bright Galaxies*, Carnegie Institution of Washington Publ. no. 635.

Sandage, A.R. & Wallerstein, G., 1960. *Astrophys.J.*, **131**, 598.

Savage, A., Waldron, D.J., Fretwell, M., Morgan, D.H., Tritton, S.B., R.D.Cannon, Brück, M.T., Beard, S.M. & Palmer, J.B. 1985. *The UKST Objective Prisms. III. Illustrations of Objective prism spectra*, Royal Observatory, Edinburgh.

Searle, L. & Sargent, W.L.W., 1972. *Astrophys.J.*, **173**, 25.

Searle, L., Wilkinson, A. & Bagnuolo, W.G., 1980. *Astrophys.J.*, **239**, 803.

Seidel, E., Demarque, P. & Weinberg, D., 1987a. *Astrophys.J.suppl.*, **63**, 917.

Seidel, E., Da Costa, G.S., & Demarque, P., 1987b. *Astrophys.J.*, **313**, 192.

Schmidt, M., 1959. *Astrophys.J.*, **129**, 243.

Shanks, T., Stevenson, P.R.F., Fong, R. & MacGillivray, H.T., 1984. *Mon.Not.R.astr.Soc.*, **206**, 767.

Shapley, H., 1956. *American Scientist*, **44**, 73.

Shaw, M., 1988. *PhD thesis*, Univ. of Edinburgh.

Smith, H.A., 1980. *Astron.J.*, **85**, 848.

Smith, H.A., Searle, L., Manduca, A., 1988. *IAU Symp.No. 126*, eds Grindlay, J.E. & Davis Philip, A.G., p.563, Dordrecht, Holland.

Songaila, A., Blades, J.C. & Hu, E.M., 1986. *Astrophys.J.*, **303**, 198.

Spite, F. & Spite, M., 1987. *ESO Confer.Workshop Proc.*, **27**, 233.

Stobie, R.S., 1986. *Pattern Recognition Letters*, **4**, 317.

Stobie, R.S., Sagar, R. & Gilmore, G., 1985. *Astr.Astrophys.Suppl.*, **60**, 503.

Stobie, R.S., Okamura, S., Davenhall, A.C & MacGillivray, H.T., 1984. *Astronomical Photography*, eds M.E.Sim & K.Ishida, *Occ.Rep.R.Obs. Edinburgh*, **14**, 219.

Stryker, L.L., 1984. *IAU Symp.No.108*, eds van den Bergh, S. & de Boer, K.S., p.79, Reidel, Doldrecht, Holland.

Stryker, L.L., Da Costa, G.S. & Mould J.R., 1985. *Astrophys.J.*, **298**, 544.

Stryker, L.L., Nemec, J.M. & McClure, R.D., 1984. *IAU Symp.No.108*, eds van den Bergh, S. & de Boer, K.S., p.43, Reidel, Dordrecht, Holland.

Suntzeff, N.B., Friel, E., Kremola, A., Kraft, R.P. & Graham, J.A., 1986. *Astron.J.*, **91**, 275.

Sweigart, A.V. & Gross, P.G., 1976. *Astrophys.J.Suppl.*, **32**, 367.

Sweigart, A.V. & Gross, P.G., 1978. *Astrophys.J.Suppl.*, **36**, 405.

Thackeray, A.D., 1958. *Spec.Vat.Ric.Astr*, **5**, 195.

Thanisch, P., McNally, B.V. & Robin, A., 1984. *Image and Vision Computing*, **2**, 191.

Théverin, F., 1987. *ESO Confer. Workshop Proc.*, **27**, 243.

Théverin, F. & Foy, R., 1986. *Astron.Astrophys.*, **155**, 145.

Torres, G. & Carranza, G.J., 1987. *Mon.Not.R.astr.Soc.*, **226**, 513.

Twarog, B.A., 1980. *Astrophys.J*, **242**, 242.

U.K.Schmidt Unit handbook, 1983, Royal Observatory, Edinburgh

VandenBergh, D., 1982. *IAU Coll.No.68*, eds A.G.D. Philip & D.S.Hayes, p.357, L.Davis Press, New York.

VandenBergh, D., 1984. *IAU Symp.No.105*, eds Maeder, A. & Renzini, A., p.143, Reidel, Dordrecht, Holland.

VandenBergh, D., 1985. *Astrophys.J.Suppl.*, **58**, 711.

VandenBergh, D. & Bell, R.A., 1985. *Astrophys.J.Suppl*, **58**, 561.

van den Bergh, S., 1975; *Ann.Rev.Astr.Astrophys.*, **13**, 217.

van den Bergh, S., 1984; *IAU Symp.No 108*, eds S. van den Bergh & K.S. de Boer, p.66, Reidel, Dordrecht, Holland.

van den Bergh, S. & Hagan, G.L., 1968. *Astron.J.*, **73**, 569.

van Genderen, A.M., 1983. *Astron.Astrophys.*, **119**, 192.

de Vaucouleurs, G., 1955.*Astron.J.*, **60**, 219.

de Vaucouleurs, G., 1959. *Handb. Phys.*, **53**, 275.

de Vaucouleurs, G., 1978. *Astrophys.J.*, **223**, 730.

de Vaucouleurs, G. & Freeman, K.C., 1972. *Vistas Astr.*, **14**, 163.

Visvanathan, N., 1985. Astrophys.J., **288**, 182.

Walker, A.R., 1984. *Mon.Not.R.astr.Soc.*, **209**, 83.

Walker, A.R., 1985. *Mon.Not.R.astr.Soc.*, **213**, 889.

Walker, A.R. & Mack, P., 1988. *Astron.J.*, **96**, 1362.

Walraven, Th. & Walraven, J.H., 1964. *IAU Sump. No.20*, eds F.J. Kerr & A.W. Rodgers, p.321, Canberra: Australian Academy of Sciences.

Wannier, P. & Wrixon, G.T., 1972. *Astrophys.J.*, **173**, 119.

Welch, D.L., McLaren, R.A., Madore, B.F. & Mc Alary, C.W., 1987. *Astrophys.J.*, **321**, 162.

Westerlund, B.E. & Danziger, I.J., 1985. *Proceedings of the ESO-IRAM-Onsals Workshop on '(Sub)millimeter Astronomy'*, p.107, Aspenäs, Swenden.

Westerlund, B.E., Azzopardi, M. & Breysacher, J., 1986. *Astr.Astrophys.Suppl.*, **65**, 79.

Whitford, A.E., 1958. *Astron.J.*, **63**, 201.

Wolf, B., 1972. *Astron.Astrophys.*, **20**, 275.

Wood, P.R., 1981. *Physical Processes in Red Giants*, eds I.Iben & A.Renzini, p.135, Reidel, Dordrecht, Holland.